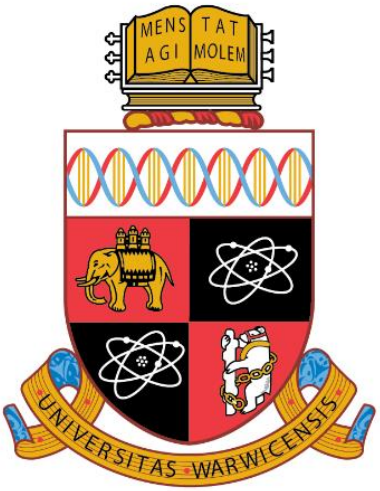

Fluorescent probes for stimuli-responsive polymers

To fluoresce, or not to fluoresce?

Anne Béatrice Marie Mabire

Submitted for the degree of Doctor of Philosophy

Department of Chemistry

July 2017

À mes parents, Marie-Pierre et Marc,

et à “L’échappée belle”…

Table of contents

List of Figures, Schemes, and Tables

Figures

Schemes

Tables

Acknowledgements

Firstly, I would like to thank my supervisor Rachel O'Reilly for her guidance and support during my PhD and Master's projects. I would also like to thank BP for funding this PhD, and especially Emma Chapman for her support.

I would like to thank all the O'Reilly group members both past and present, including Annie, for their support and their patience, even when my English level required guessing games. Thanks for sharing your ideas, your knowledge, and for all the interesting discussions we had these past five years. Thanks also for making the lab (especially bay 2 with Dafni, Alice, Marianne and Becky) a fun place to work. I would also like to thank the Dove group (especially James, Ruairi, Annette, Ed, and Laura), and the Perrier group for making the PhD life a bit more sociable. Special thanks to the Brunchsticles and Guillaume for sharing laughs, thoughts, rants, brunch, coffee, pints and wine with me. Thank you all for making the past five years incredibly fun.

I am particularly grateful to Mat, Helen and Anaïs for patiently teaching me everything and for their guidance throughout my PhD and my Master's projects. Huge thanks to the people who proof-read this thesis; Marianne, Dafni, Tom, Anaïs, Becky, Jon and Charlotte, you have done a wonderful job.

J'aimerais particulièrement remercier ma famille, mes parents Marie-Pierre et Marc, frère et sœur Paul et Alix (L'échappée belle) pour leur compréhension, leur soutien et leurs encouragements sans faille tout au long de ces années, cela n'aurait pas été possible sans vous. Je sais que cette thèse ne vous parle pas beaucoup, mais en résumé, ce sont juste des polymères fluorescents qui s'éteignent quand on les met dans l'eau.

Merci aussi à mes amis berruyers et tout particulièrement Manue, Charlotte, Baudouin et Antoine pour leur bienveillance et pour toutes ces bonnes soirées passées ensemble, me rappelant qu'il y a une vie à l'extérieur de cette bulle universitaire.

Declaration of Authorship

This thesis is submitted to the University of Warwick in support of my application for the degree of Doctor of Philosophy. It has been composed by myself and has not been submitted in any previous application for any degree apart from the background material in Chapter 2, which was previously submitted for a Master's degree at Université du Maine.

The work presented (including data generated and data analysis) was carried out by the author except in the cases which are outlined below, and clearly labelled in the corresponding text.

- The work in Chapter 2 was carried out in collaboration with Dr Mathew Robin (University of Warwick).
- The work in Chapter 3 was carried out in collaboration with Dr Mathew Robin (University of Warwick).
- All SAXS measurements and analysis in Chapter 2 and Chapter 4 were performed by Dr Anaïs Pitto-Barry (Australian Synchrotron facility and University of Warwick).
- Starting materials in Chapter 4 were prepared with the help of Quentin Brouard (University of Warwick).
- The TEM images in Chapter 2, Chapter 4 and Chapter 5 were acquired by Dr Anaïs Pitto-Barry and Dr Kay Doncom (University of Warwick).

Part of this thesis have been published by the author (see list of publications).

List of Publications

1. "Dual effect of thiol addition on fluorescent polymeric micelles: ON-to-OFF emissive switch and morphology transition", Anne B. Mabire, Mathew P. Robin, Helen Willcock, Anaïs Pitto-Barry, Nigel Kirby and Rachel K. O'Reilly, *Chem. Commun*., 2014, **50**, 11492 **(Chapter 2)**.

2. "Aminomaleimide fluorophores: a simple functional group with bright, solvent dependent emission", Anne B. Mabire‡, Mathew P. Robin‡, Wen-Dong Quan, Helen Willcock, Vasilios G. Stavros and Rachel O'Reilly, *Chem. Commun*., 2015, **51**, 9733 **(Chapter 3)**.

3. "CO_2/pH-responsive particles with built-in fluorescence read-out", Anne B. Mabire, Quentin Brouard, Anaïs Pitto-Barry, Rebecca J. Williams, Helen Willcock, Nigel Kirby, Emma Chapman and Rachel K. O'Reilly, *Polym. Chem.*, 2016, **7**, 5943 **(Chapter 4)**.

‡ *denotes equal contribution by authors*

Thesis summary

This thesis explores the use of aminobromomaleimide and dithiomaleimide functionalities to probe their environment. These fluorescent functionalities were incorporated into responsive polymeric nanostructures allowing their behaviour to be read-out upon external stimuli.

Chapter 1 gives a brief introduction on nanoparticles formation and the polymerisation techniques used throughout the thesis. The properties of bromo- and thio-maleimides and their use in protein and polymer chemistry were also introduced.

Chapter 2 describes a morphology transition simultaneously with a fluorescence on-to-off switch as a result of the modification of the dithiomaleimide substituent.

Chapter 3 presents the synthesis of a library of aminomaleimides and explores their fluorescent properties.

In **Chapter 4**, the fluorescent properties of aminobromomaleimide were incorporated into CO_2-responsive polymeric nanoparticles for a built-in read-out of the CO_2-response.

Chapter 5 explores the possibility of using the fluorescent properties of aminobromomaleimide to read-out the behaviour of glutathione-responsive particles.

Abbreviations

ABM	Aminobromomaleimide
ABMMA	Aminobromomaleimide methacrylate
AIBN	2,2'-azobis(isobutyronitrile)
ATRP	Atom transfer radical polymerisation
BAC	N,N-bis(acryloyl) cystamine
BIS	Methylene bis(acrylamide)
CMC	Critic micellar concentration
CTA	Chain transfert agent
d	Doublet
Da	Dalton
DBM	Dibromomaleimide
DBMMA	Dibromomaleimide methacrylate
DEAEMA	*N,N*-diethylaminoethyl methacrylate
DEGMA	Di(ethylene glycol) methyl ether methacrylate
D_h	Hydrodynamic diameter
DLS	Dynamic light scattering
DMAEMA	*N,N*-dimethylaminoethyl methacrylate
DOX	Doxorubicin
DP	Degree of polymerisation
DPAEMA	*N,N*-diisopropylaminoethyl methacrylate
DSDMA	Disulfide-based methacrylate or bis(2-methacryloyl)oxyethyl disulfide.
DTM	Dithiomaleimide
DTT	Dithiothreitol
EGDMA	Ethylene glycol dimethacrylate

em	Emission
EMA	Ethyl methacrylate
eq.	Equivalent(s)
ex	Excitation
FLIM	Fluorescence-lifetime imaging microscopy
FRP	Fluorescent responsive particles
FTIR	Fourier transform infrared spectroscopy
GO	Graphene oxide
GSH	Glutathione
HeLa	Immortal cervical cancer cell line derived from Henrietta Lacks
HEMA	Hydroxyethyl methacrylate
HPLC	High-performance liquid chromatography
HR-MS	High resolution mass spectrometry
J	Coupling constant
KPS	Potassium persulfate
LA	Lactide
LCST	Lower critical solution temperature
m	Multiplet
m/z	Mass-to-charge ratio
MA	Methyl acrylate
MAM	Monoaminomaleimide
MBM	Monobromomaleimide
MMA	Methyl methacrylate
MMAE	Monomethyl auristatin E
M_n	Number average molecular weight

MTM	Monothiomaleimide
M_w	Weight average molecular weight
MWCO	Molecular weight cut off
n	Refractive index
NIPAM	*N*-Isopropylacrylamide
NMR	Nuclear magnetic resonance
OEGMA	Oligo(ethylene glycol) methacrylate or oligo(ethylene glycol) methyl ether
OEGMA2000	Oligo(ethylene glycol) methyl ether methacrylate $M_n \approx 2000$ g·mol^{-1}
OEGMA360	Oligo(ethylene glycol) methacrylate $M_n \approx 360$ g·mol^{-1}
p	Packing parameter
PD	Polydispersity
PDEAEMA	Poly(*N,N*-diethylaminoethyl methacrylate)
PDMAEMA	Poly(*N,N*-dimethylaminoethyl methacrylate)
PEG	Poly(ethylene glycol)
PEGA	Poly(ethylene glycol) acrylate
PEGMA	Poly(ethylene glycol) methacrylate
pet. ether	Petroleum ether
PLA	Polylactide
POEGMA	Poly(oligo(ethylene glycol)methacrylate)
PS	Polystyrene
PTEGA	Poly(triethylene glycol monomethyl ether acrylate)
q	Quartet
q	Scattering vector
RAFT	Reversible addition-fragmentation chain transfer

RDRP	Reversible deactivation radical polymerisation
R_g	Radius of gyration
R_h	Hydrodynamic radius
ROP	Ring opening polymerisation
RP	Responsive particles
rt	Room temperature
s	Singlet
SAXS	Small angle X-ray scattering
SEC	Size exclusion chromatography
SLS	Static light scattering
t	Triplet
tBA	*Tert*-butyl acrylate
TCEP	Tris(2-carboxyethyl)phosphine
TEGA	Triethylene glycol methylether acrylate
TEGMA	Triethylene glycol methyl ether methacrylate
TEM	Transmission electronic microscopy
THF	Tetrahydrofuran
TLC	Thin-layer chromatography
TMS	Tetramethylsilane
UA	Uranyl acetate
UV	Ultraviolet
wt	Weight
δ	Chemical shift
ε	Extinction coefficient
λ	Wavelength
Φ_f	Fluorescent quantum yield

Chapter 1

Introduction

1.1. Abstract

With work in this thesis focusing on the development of fluorescent nanoparticles, this introduction will provide a brief overview first into nanoparticles, focussing on different synthetic methods. Then it will cover maleimide based fluorophores, initially looking at their biological applications, and secondly providing an introduction to their fluorescent properties.

1.2. Polymeric nanoparticles

Polymeric nanoparticles have been widely developed for many applications including nanomedicine, drug/gene delivery, imaging and nanomaterials.[1-9] There are a variety of polymeric particle architectures (Figure 1.1), such as micelles, liposomes, nanoparticles, dendrimers, and latexes, which can be prepared using different techniques.[10-18] In particular, there is a great interest in responsive and fluorescent nanoparticles, especially for nanomedicine and bio-imaging applications.[4,13,19-28]

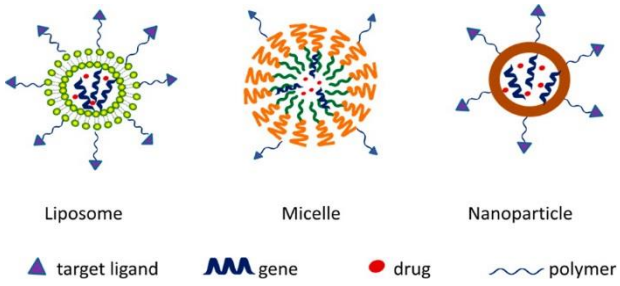

Figure 1.1. Examples of nanostructures developed for drug and gene delivery. Reproduced from reference.[8]

1.2.1. Nanoparticles formation

Different strategies can be used to form nanoparticles. In this thesis, two techniques have been utilised: first, emulsion polymerisation, which is a free radical polymerisation process,[29] and second, the self-assembly of well-defined polymers synthesised *via* controlled polymerisation processes.[17]

1.2.1.1. Emulsion polymerisations

Emulsion polymerisation has several advantages over other methods including the facile nature of the process, the large range of compatible monomers and polymerisations can often be taken to high conversion.[29,30] Moreover, the size of particles synthesised by emulsion polymerisation can be tuned between 0.05-5 μm

in diameter. Most emulsion polymerisations are performed in aqueous media, but inverse emulsion polymerisations are also possible, depending on the solvent used to disperse the insoluble monomer. In the case of an aqueous emulsion polymerisation, the initiator has to be water soluble, and a surfactant is necessary to stabilise the monomer in micelles. Hence, the concentration of the surfactant needs to be above its critical micellar concentration (CMC).

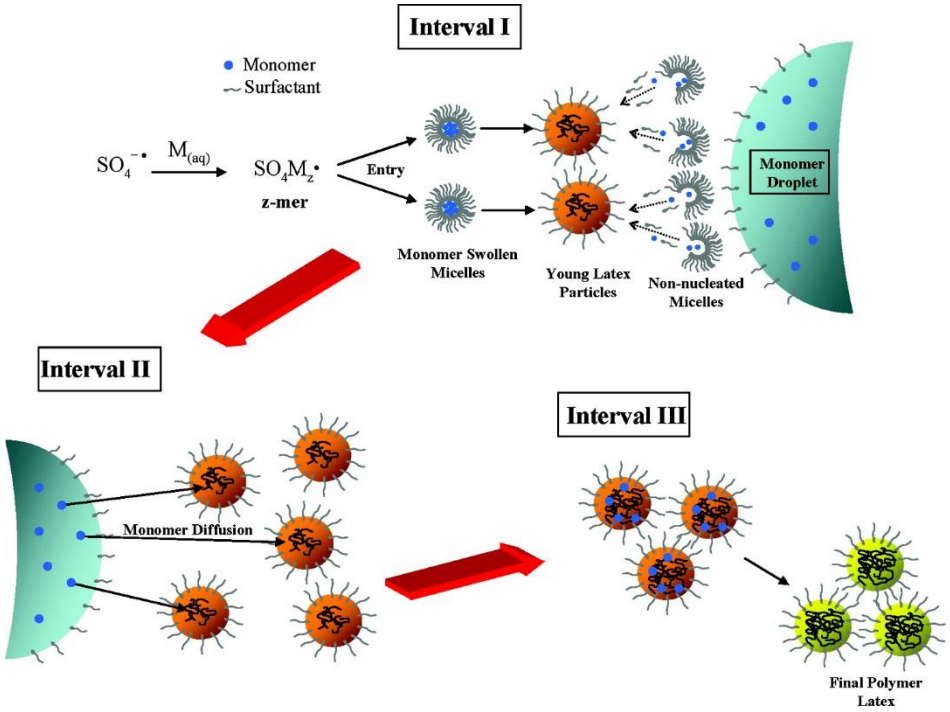

Figure 1.2. Schematic representation of the emulsion polymerisation process. Reproduced from reference.[29]

Firstly during polymerisation, initiation occurs in solution with subsequent reaction with the initiating species and monomer producing an initial growing chain (Figure 1.2, labelled *z-mer*). When the growing chain reaches a critical length, the oligomer becomes insoluble in solution and is stabilised by penetrating a surfactant micelle (Figure 1.2, labelled *monomer swollen micelle*). The propagation of the chains continues inside the micelle consuming the monomer in the droplets. This process continues until all of the growing chains are stabilised, at which point the remaining

surfactant from surfactant stabilised monomer micelles (Figure 1.2, labelled *non-nucleated micelles*) is sequestered to stabilise the growing particles. The propagation ends once all the monomer is consumed and the conversion approaches 100%. Emulsion polymerisation can also be performed with the incorporation of a cross-linker, which "locks" the structure through crosslinking either the core or the shell of the nanoparticles or both. This increases the particle stability to changes in its environment (solvent, temperature, pH or concentration).

The polymerisation process employed in emulsion polymerisation is a free radical process. Free radical polymerisation presents many advantages, with most vinyl monomers able to be used, and it can be carried out in a variety of media: in solution, as a dispersion, as a suspension, in an emulsion or in bulk. The free radical polymerisation mechanism consists of three main stages: initiation, propagation and termination (combination or radical disproportionation) (Scheme 1.1). Owing to termination being significantly faster than propagation ($k_{tc/td} > k_p$), chains terminate before complete monomer conversion. Moreover, as a consequence of the high reactivity of radical species, the rate of initiation is slower than the rate of propagation ($k_i < k_p$) resulting in some chains having grown significantly before other chains have initiated. As a result of these two effects, conventional free radical polymerisation doesn't allow good control over molecular weight or dispersity.

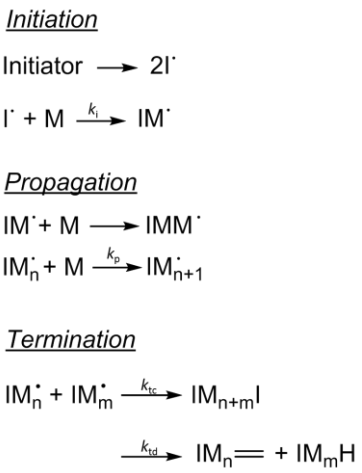

Scheme 1.1. General free radical polymerisation mechanism.

1.2.1.2. Polymer self-assembly

Whilst emulsion polymerisation provides an easy method for the production of spherical nanoparticles, other morphologies can be obtained through copolymer self-assembly. The driving force to form these self-assembled structures depends on the solvophobicity of each block of the copolymer. Indeed, the solvent needs to be a good solvent for one of the blocks and the second block should be insoluble in that solvent. The morphology obtained (spherical micelles, cylindrical micelles or polymersomes, Figure 1.3) depends on the amphiphilic balance between the blocks (represented in red and blue in Figure 1.3), and also on the polymer packing ability and therefore the polymer chain curvature: for higher curvatures, where the packing parameter is < 1/3 (Figure 1.3), smaller structures are obtained. The packing parameter can be determined from the volume (v) and the length of the hydrophobic segment (l_c), and the head group area (a_0).[10,18]

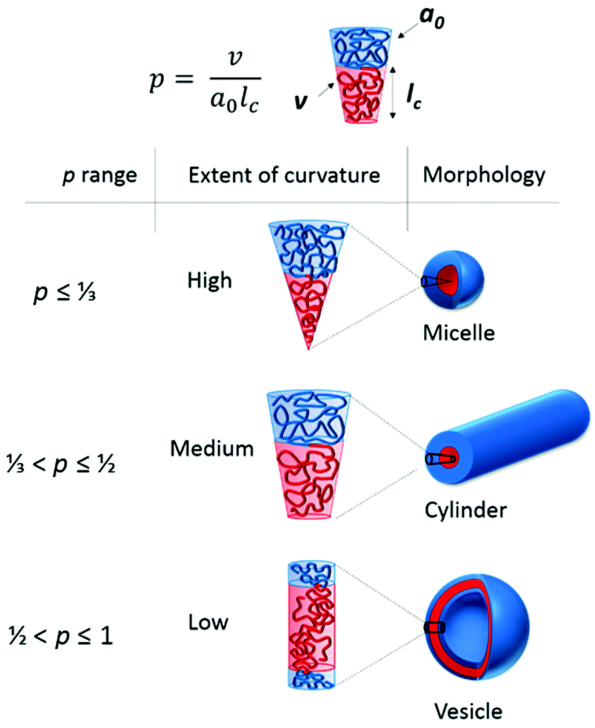

Figure 1.3. Schematic representation of different morphologies adopted in solution depending on the amphiphilic balance of the polymer, where p = packing parameter, v = volume, a_0 = head group area and l_c = the length of the hydrophobic segment. Reproduced from reference.[18]

In order to form these nanostructures, it is necessary to synthesise copolymers in a controlled manner with a low dispersity to ensure a targeted amphiphilic balance and block ratios.[18] In order to produce copolymers in a controlled manner, different polymerisation techniques can be utilised, including reversible addition-fragmentation chain transfer (RAFT) polymerisation, atom-transfer radical-polymerization (ATRP), nitroxide-mediated polymerization (NMP) and ring opening polymerisation (ROP).

1.2.1.2.1. Reversible addition-fragmentation chain transfer (RAFT) polymerisation

RAFT polymerisation is a reversible-deactivation radical polymerisation (RDRP) mechanism, allowing for the synthesis of polymers with control over the molecular weight and therefore with a narrow molecular weight distribution. A large range of monomers can be used for RAFT polymerisation, as RAFT polymerisation is tolerant

of a wide range of functional groups. A RAFT polymerisation is composed of a radical source, a RAFT chain transfer agent (CTA), and a monomer; a solvent is also often used. The RAFT polymerisation mechanism consists of several steps: initiation, reversible chain transfer, reinitiation, chain equilibrium and termination. The RAFT CTA is necessary for exerting control over the polymerisation, producing a dormant form of the polymer chains (Scheme 1.2, compound 4), in equilibrium with the active chains (Scheme 1.2, compound 3), in a process known as chain equilibrium. The rapid exchange between the dormant and growing polymer chains ensures an equal probability for chain growth of any of the polymer chains, therefore resulting in polymers with narrow dispersities. Commonly, the RAFT CTA can be a dithioester, a trithiocarbonate or a dithiocarbamate, with the RAFT CTA chosen depending on the reactivity of monomer class being polymerised.

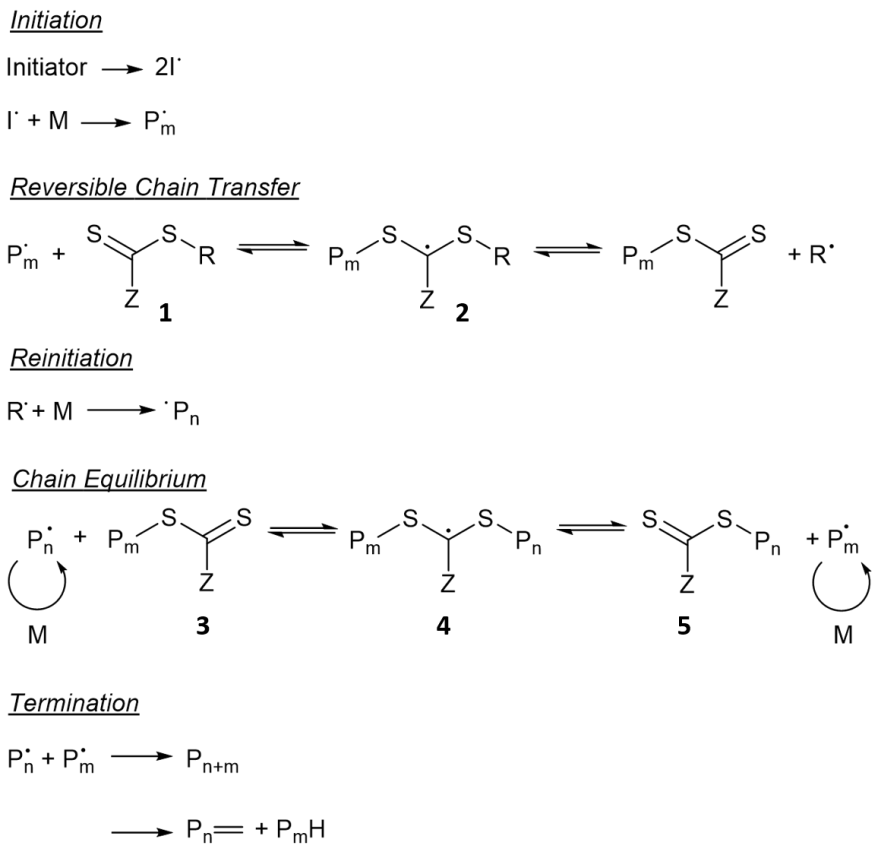

Scheme 1.2. Mechanism of RAFT polymerisation.

1.2.1.2.2. Ring opening polymerisation (ROP)

Ring opening polymerisation consists of the ring opening and polymerisation of a cyclic monomer, catalysed by a metal-based catalyst (*e.g.* Zn, Ca, or Al complexes[31]) or an organocatalyst (*e.g.* thiourea-amine[32], 4-(dimethylamino)pyridine[33], or *N*-heterocyclic carbenes[34]), to obtain a linear polymer. Developments in organic catalysts allowed for the synthesis of well-defined polymers with narrow dispersities.[33-35] A wide range of cyclic monomers can be polymerised by ROP, including lactones,[36,37] lactams,[38] carbonates,[39] and ethers.[40] In the polymerisation of lactide catalysed by a thiourea-amine combination, the lactide carbonyl becomes more electrophilic through the activation from the thiourea, and the alcohol becomes more nucleophilic through the activation by the tertiary amine, (Scheme 1.3). This catalytic system was also shown to be very selective for polymerisation relative to transesterification.

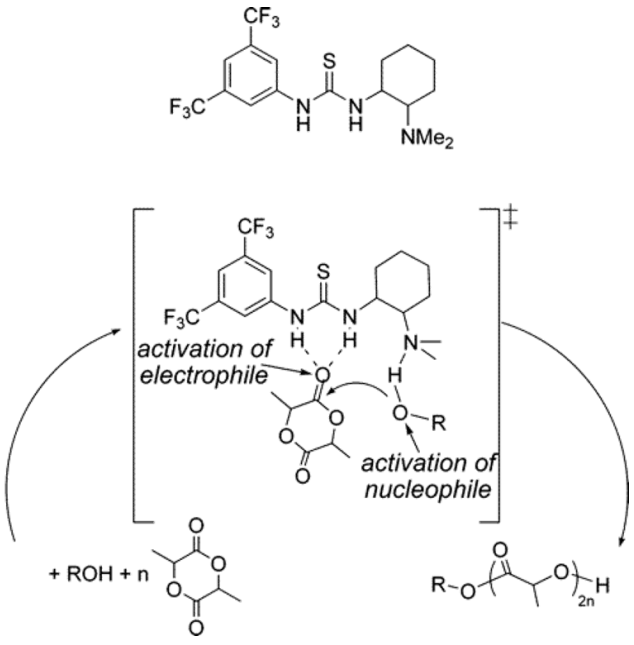

Scheme 1.3. Example of the polymerisation of lactide in the presence of a thiourea-amine catalyst. Adapted from reference.[32]

Pratt *et al.* tested different thiourea-amine catalysts for the polymerisation of lactide.[32] The most efficient catalyst combination to polymerise *rac*-lactide with thiourea was found to be (-)-sparteine (Figure 1.4). The polymerisation reached 99% conversion in only 2 h, which is significantly shorter than polymerisations with other catalytic systems (*e.g.* a in Figure 1.4) that often take 48 to 72 h. Moreover, the polydispersity of the polymer obtained was very low even at high conversion; for example, polymerisation of *rac*-lactide produced a polymer (M_n = 20700 g·mol^{-1}) with a polydispersity of 1.05 at high monomer conversion (99%).

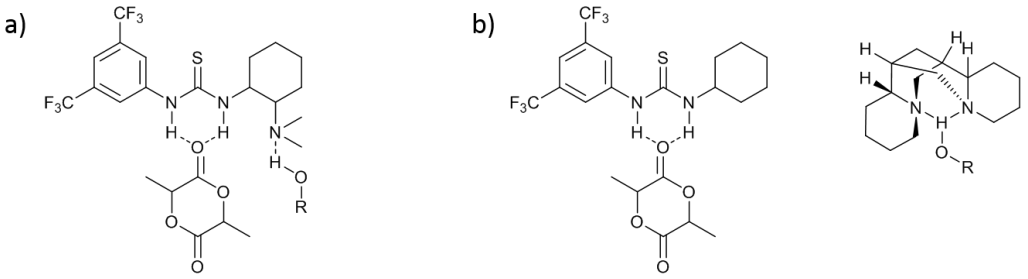

Figure 1.4. Activation of lactide and alcohol initiator with (a) bifunctional thiourea-tertiary amine, *vs.* (b) thiourea and (-)-sparteine.

1.2.2. Responsive polymers and nanoparticles

There is a great interest in responsive polymers, as they are readily employed in a variety of applications such as drug-delivery and sensing.[1,41-47] The key feature of responsive polymers is their ability to respond to their environment, changing their physical or chemical properties in response to a physical, chemical and/or biological stimulus, *e.g.* temperature,[41,48,49] light,[50-52] pH,[53-55] carbon dioxide,[56-58] or a redox reaction.[46,59,60]

The most studied and understood class of responsive polymers are thermoresponsive, the most widely studied of which is poly(*N*-isopropylacrylamide)

(PNIPAM), which exhibits a lower critical solution temperature (LCST). When in solution at a temperature below the LCST, the polymer is hydrophilic as it forms hydrogen bonds with water. However, when in solution at a temperature above the LCST, the polymer becomes hydrophobic and therefore rendered insoluble in water. Such an effect has been reported by Moughton *et al.*, who synthesised a thermoresponsive block copolymer with methyl acrylate (MA) and *N*-isopropylacrylamide (NIPAM), the latter forming the responsive block.[61] The copolymer was synthesised by RAFT polymerisation utilising a quaternary amine functionalised RAFT agent, which formed a permanent hydrophilic 'headgroup'. Below the LCST, the copolymer self-assembled into spherical micelles, but when the temperature was increased above the LCST a morphology transition occurred from spherical micelles to vesicles. The morphology transition was a result of the interfacial curvature variation controlled by the response of the NIPAM segment located between the hydrophilic head and the hydrophobic segment, Figure 1.5.

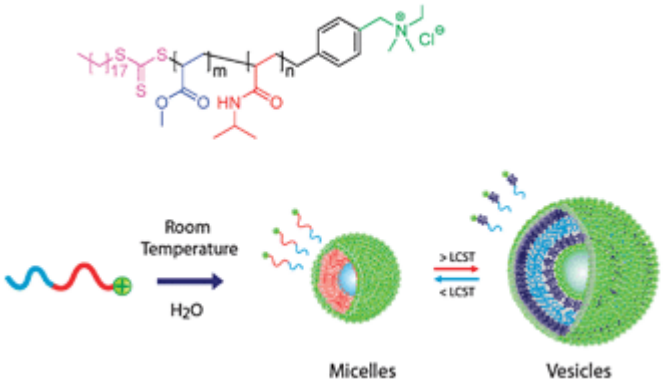

Figure 1.5. Schematic representation of a morphology transition induced by temperature. Reproduced from reference.[61]

Similarly, Feng *et al.* reported a dual-responsive PNIPAM and poly(*N,N'*-(diethylamino)ethyl methacrylate) (PDEAEMA) copolymer, which self-assembled into vesicles (Figure 1.6). PNIPAM was utilised to add thermoresponsive properties

to the copolymer, facilitating a change of the vesicle size and also the reversible self-assembly of the copolymer into spherical micelles. Moreover, with the copolymer second block composed of PDEAEMA, which is pH/CO_2-responsive through the protonation of the amine in acidic environment, a change of the environment triggered a reversible disassembly of the vesicles (Figure 1.6.)

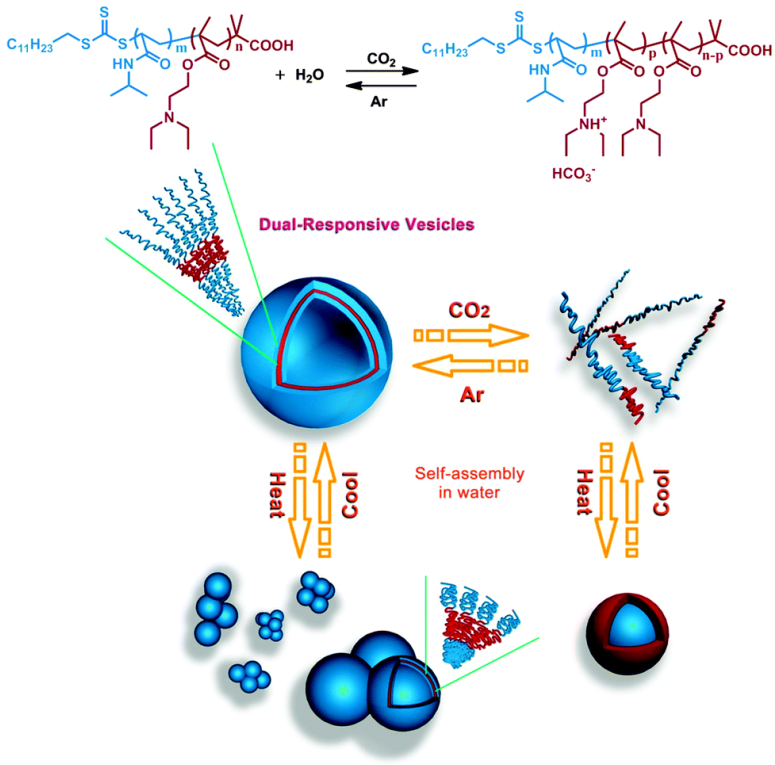

Figure 1.6. Schematic example of dual-responsive vesicles and the transitions upon changes in temperature or pH/CO_2. Reproduced from reference.[62]

As demonstrated in the previous example by Feng *et al.*, pH/CO_2-responsive polymers can be synthesised from amines; however, amidines and guanidines can also be used, see Figure 1.7. Upon pH cycling, these different functionalities can alternate between protonated and non-protonated states. The advantage of utilising CO_2, compared to alternating addition of acid and base, is that it does not contaminate the solution with the formation of salts.

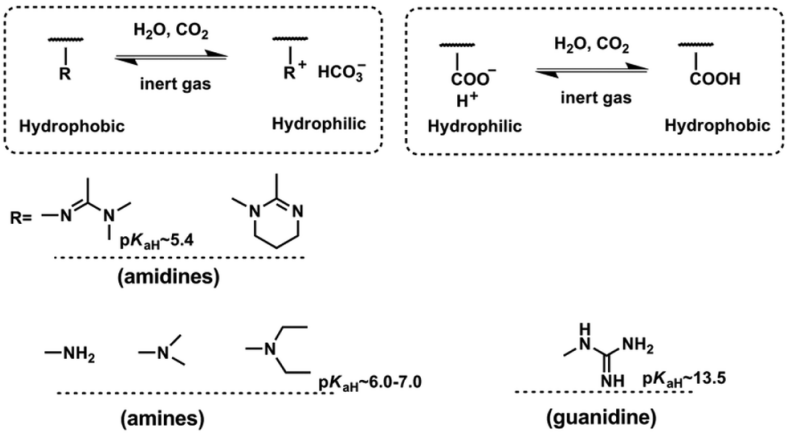

Figure 1.7. pH/CO_2-responsive functionalities and their response to CO_2. Reproduced from reference.[56]

Redox-responsive particles have also received attention, especially for drug-delivery applications.[59,60] The most commonly studied redox system involves the application of glutathione (GSH/GSSH), as it has been shown to be present at higher concentrations intracellularly (*ca.* 1-10 mM) than extracellularly (*ca.* 1-10 μM).[63,64] Moreover, it has been reported that cancer cells have a significantly higher GSH concentration compared to normal cells,[65,66] with the intracellular GSH concentration able to trigger a thiol-disulfide exchange. Indeed, Ryu *et al.* presented the synthesis of an amphiphilic copolymer in which a disulfide bridge links the hydrophobic tail. Depending on the GSH concentration, the micelle disassembled, releasing the drug, see Figure 1.8.[67]

Figure 1.8. Schematic example of drug release through GSH-responsive self-assembled amphiphilic copolymer disassembly. Reproduced from reference.[67]

Li *et al.* reported another example of a glutathione responsive system, involving the crosslinking of nanoparticles upon addition of a catalytic amount of dithiothreitol (DTT), see Figure 1.9. When penetrating the cells, the presence of glutathione induces a disulfide-thiol exchange, resulting in de-crosslinking of the particle core, resulting in the release of doxorubicin.[68]

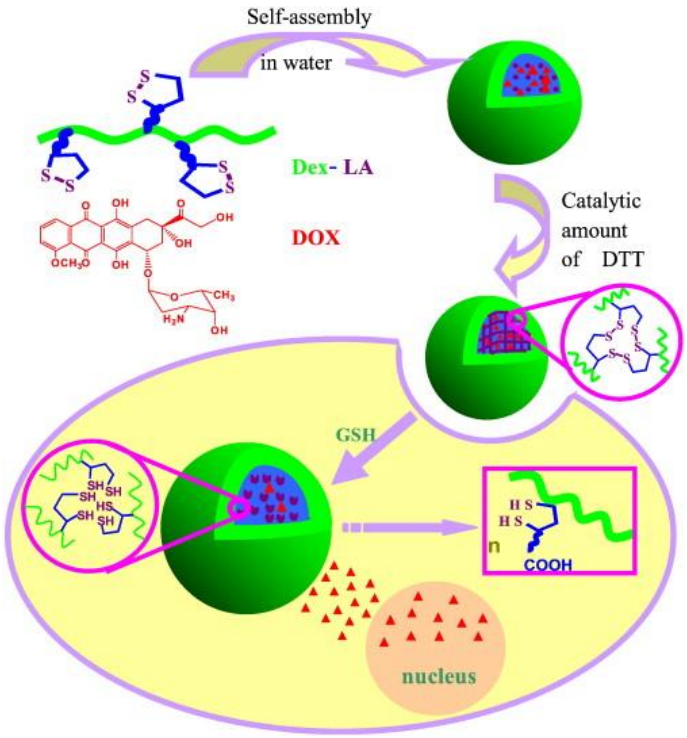

Figure 1.9. Schematic representation of the reversible cross-linking of dextran-lipoic acid anhydride nanoparticles using DTT, and the release of doxorubicin (DOX) in cells. Reproduced from reference.[68]

These different responses can also be combined into one system to produce multi-stimuli responsive materials.[19,51,69-72] The aforementioned dual pH and temperature responsive vesicles by Feng *et al.* is one example of multi-responsive polymer self-assembly.[62] Extending the concept, Klaikherd *et al.* presented the synthesis of a temperature, pH and redox responsive polymer, see Figure 1.10. Consisting of a tetrahydropyran protected poly(2-hydroxyethyl methacrylate) (PHEMA) block, and a PNIPAM block, with the two blocks linked by a disulfide bond.[73] As mentioned

previously, PNIPAM exhibits an LCST, while the deprotection of the HEMA block in acidic conditions will change the block from hydrophobic to hydrophilic. With the disulfide bond sensitive to addition of reducing agents such as DTT, this polymer is triply responsive.

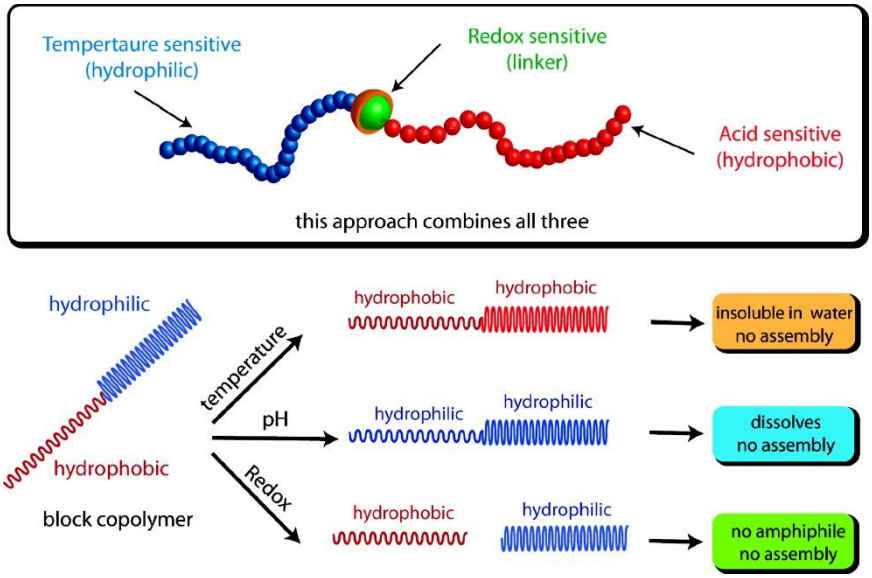

Figure 1.10. Schematic example of a multi-responsive polymer. Reproduced from reference.[73]

1.2.3. Fluorescently labelled nanoparticles

Fluorescent polymer nanoparticles are of great interest for imaging applications.[5,7,24,27] Currently, the most popular fluorescent dyes for polymer functionalisation are small molecules, but these can have problems, for example low emission caused by photobleaching, and/or their toxicity can prevent biomedical applications.[74-76] The incorporation of fluorophores into polymeric particles can overcome these problems, rendering them more applicable for biomedical applications. Different methods to incorporate fluorophores into polymeric particles

have been reported, including direct polymerisation of the fluorophore, and entrapment during self-assembly, emulsion or nanoprecipitation.[7,77,78]

One commonly applied practice is to synthesise a fluorescent monomer from a fluorescent dye;[79] this technique allows the dye to be covalently linked to the polymeric nanostructure. Indeed, Cova *et al.* presented such an approach, synthesising biocompatible fluorescent nanoparticles for bioimaging.[80] In this work, a Rhodamine B functionalised 2-hydroxyethyl methacrylate (HEMA-RhB) was synthesised to form a fluorescent macromonomer. This macromonomer was used to synthesise nanoparticles *via* emulsion polymerisation with methyl methacrylate (MMA). The resultant particles were shown to be successfully internalised by stem cells allowing efficient labelling and tracking of the cells *in vitro* and *in vivo*.

Another technique to obtain fluorescent nanoparticles is to encapsulate an organic dye into polymeric nanoparticles. Indeed, Wang *et al.* showed the synthesis of polymeric nanoparticles using this approach, demonstrating two different routes to incorporate the fluorescent dye into the particles, see Figure 1.11.[81]

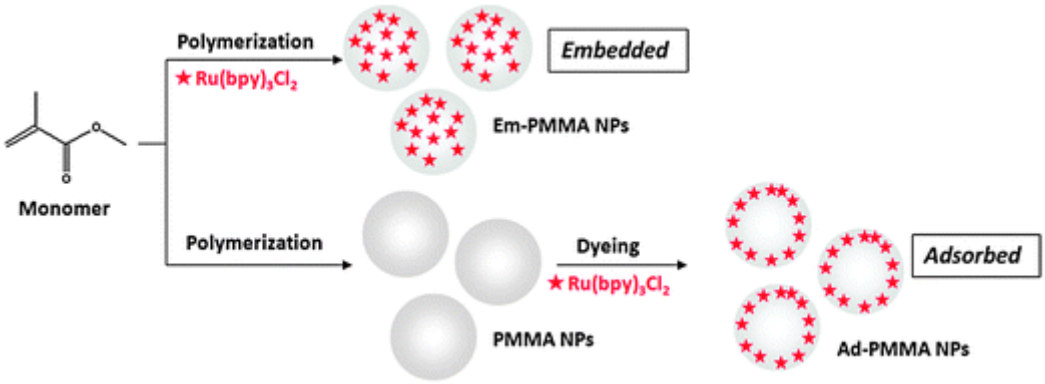

Figure 1.11. Schematic representation for two different routes to encapsulate an organic dye. Reproduced from reference.[81]

These nanoparticles were synthesised *via* emulsion polymerisation; in the first case, the dye was embedded in the particles during the polymerisation, and in the second

case, the dye was adsorbed into the nanoparticles post-polymerisation. It was found that the embedded nanoparticles exhibited higher luminescent properties compared to the adsorbed nanoparticles. It was hypothesised that the difference in luminescence was a consequence of the dye incorporation process. The dye could be incorporated at a higher concentration in the inner core of the embedded nanoparticles, than can be adsorbed into the nanoparticles.

1.3. Dibromomaleimides and dithiomaleimides

Maleimides, important building blocks in synthetic organic chemistry, consist of a cyclic unsaturated imide, of the generic structure indicated in Figure 1.12.

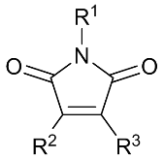

Figure 1.12. Generic structure of maleimides.

1.3.1. For protein modification and disulfide bridging

For many years, there has been a growing interest in maleimides, mainly for protein modification using the amino acid cysteine,[82] but also for thiol detection.[83] The maleimide is often used as it is selective towards cysteine and has a fast rate of the reaction. Moreover, the irreversibility of the modification is also advantageous, though in certain situations may be unwanted. Maleimide has also been utilised as a linker for fluorophores: Baker and co-workers have reported optimised protein modifications and disulfide bridging using dibromomaleimides and dithiomaleimides (Figure 1.12, where R^1 = H, R^2 = R^3 = Br for the former, and R^1 = H, R^2 = R^3 = SR for the latter, respectively).[82,84-86] Indeed, reversible protein modification using bromomaleimide instead of maleimide was demonstrated.[84] By incorporating a leaving group on the maleimide double bond, the reaction with cysteine would produce a thiomaleimide in which the double bond is preserved, see Scheme 1.4 (product **7**).

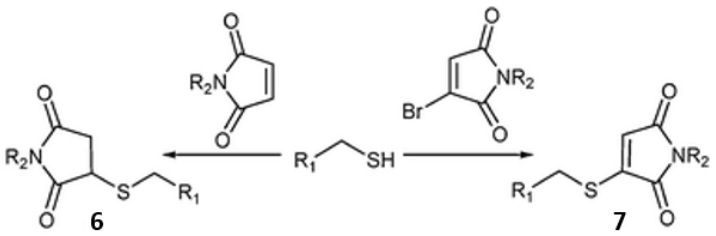

Scheme 1.4. Reaction of thiol with maleimide or bromomaleimide. Adapted from reference.[87]

Furthermore, by reacting both bromomaleimide and maleimide with cysteine, it was confirmed that the reaction of a thiol with bromomaleimide was faster than with unsubstituted maleimide, obtaining a 70:30 mixture of **7** and **6** (Scheme 1.4). Competition between other nucleophiles and cysteine to react with bromomaleimide was also evaluated, by adding propylamine to the mixture of bromomaleimide and cysteine. The results showed a clear selectivity for bromomaleimide towards cysteine over amines. Moreover, the reversibility of the reaction of bromomaleimide with cysteine was demonstrated by reacting the reducing agent tris(2-carboxyethyl)phosphine (TCEP), with the cysteine-maleimide conjugate, which results in the cleavage of the thiomaleimide and release of the cysteine, with a 98% yield, see Scheme 1.5.[84]

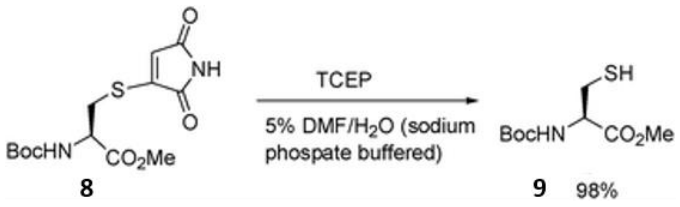

Scheme 1.5. Cleavage of the thiomaleimide with TCEP. Adapted from reference.[84]

The usage of bromomaleimide for protein modification and disulfide bridging was further investigated by the same research group.[82] It was noted that, if dibromomaleimide can be used instead of bromomaleimide, the second bromine

can be substituted by another thiol such as glutathione or thioglucose to obtain a di-substituted maleimide. Moreover, they showed that in the presence of a large excess of another thiol such as mercaptoethanol or glutathione, the free unmodified protein can be fully recovered from either mono-substituted maleimide or di-substituted maleimides, see Scheme 1.6.

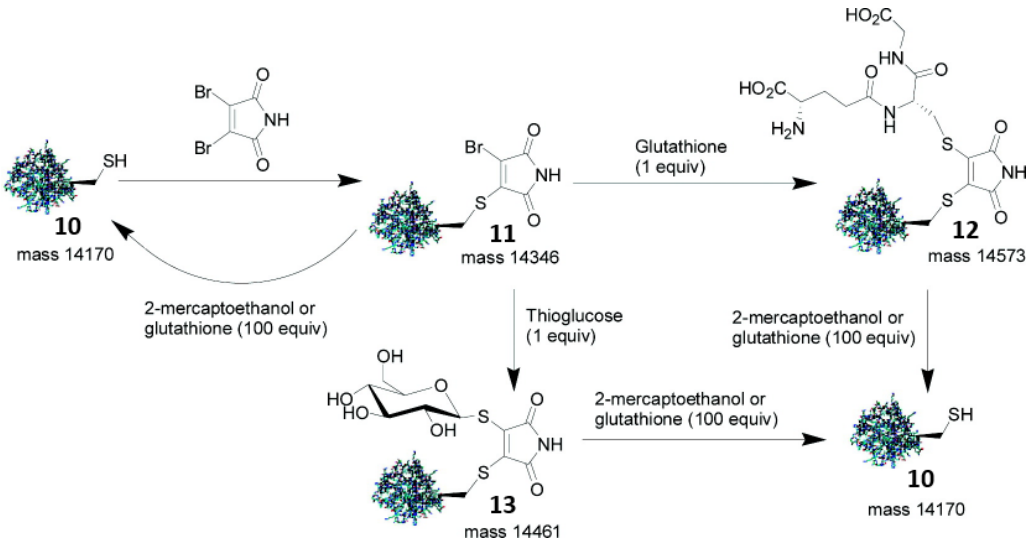

Scheme 1.6. Schematic representation of the reversible modification of cysteine with maleimides. Adapted from reference.[82]

In order to get one step closer to potential drug-delivery applications, the ability of substituted dithiomaleimide (**13** in Scheme 1.6) to be cleaved by glutathione present in the cytoplasm of cells was evaluated. Unmodified free protein **10** (Scheme 1.6) was successfully recovered after treatment of **13** with intracellular-like conditions, confirming cleavage of the maleimide substituted protein.[82] Afterward, cleavability of maleimide conjugates in mammalian cells was tested on different rhodamine-Green Fluorescent Protein-maleimide conjugates. It was found that maleimide conjugates were successfully cleaved *in vitro* at different cleavage rates depending on the structure.[88] The cleavage of the maleimide conjugates was also successful in HeLa cells showing the potential of thiomaleimide in drug-delivery systems.

Baker, Caddick and co-workers also investigated the possibility of using dibromomaleimide to modify disulfide bonds in somatostatin (a disulfide bridge containing peptide playing a role in hormone regulation). The protein was treated with TCEP to break the disulfide bond, which was subsequently reacted with dibromomaleimide, see Scheme 1.7. As previously demonstrated for cysteine (Scheme 1.6), the modification of somatostatin was reversible upon a similar treatment with an excess of mercaptoethanol, see Scheme 1.7. Moreover, it was demonstrated that the modification of somatostatin could be achieved utilising dithiomaleimide instead of dibromomaleimide, preventing some cross reactivity with TCEP.[85]

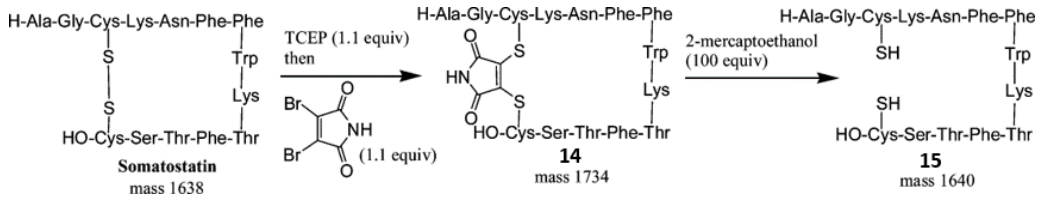

Scheme 1.7. Reversible modification of somatostatin. Adapted from reference.[82]

Inspired from the commercially available fluorescein-maleimide (commonly used in protein labelling), the ability of dibromomaleimide to have three points of attachment was tested through the synthesis of a fluorescently labelled dibromomaleimide, see Scheme 1.8.[82] The reversible modification of somatostatin with fluorescein-dibromomaleimide was performed using the same protocol previously used with dibromomaleimide. Comparison of the emission of the different precursors (fluorescein-dibromomaleimide, fluorescein-amine, and somatostatin) and product of the modification indicated successful labelling of the protein. However, no comparison was made with the maleimide-somatostatin conjugate **14** in Scheme 1.7.

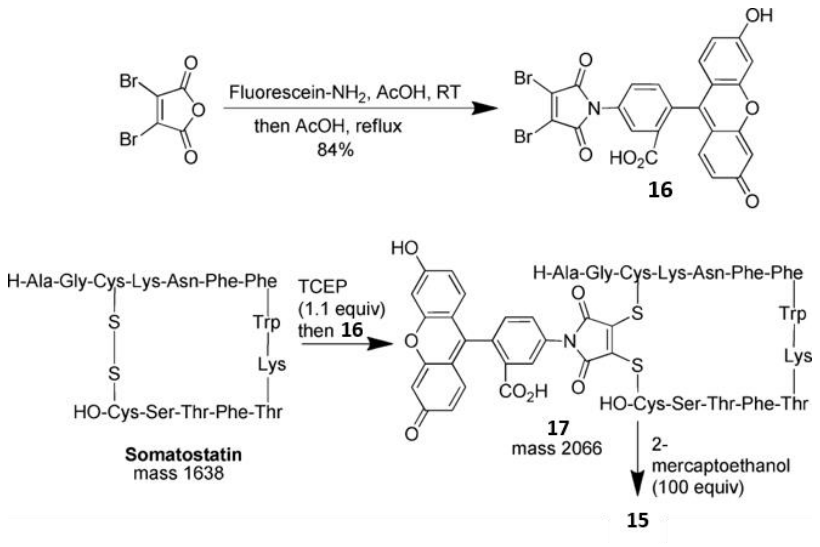

Scheme 1.8. Synthesis of the fluorescein labelled dibromomaleimide, and reversible modification of the somatostatin disulfide bridge with fluorescein-dibromomaleimide. Adapted from reference.[82]

The demonstration of successful three point functionalisation of dibromomaleimide to produce the somatostatin-maleimide-fluorescein conjugate, and the observation that intracellular-like conditions can reduce the disulfide bridge, opened the path to applications in drug-delivery, imaging and detection.

Dibromomaleimide was also functionalized by the attachment of polyethylene glycol (PEG) polymer chains for subsequent conjugation to somatostatin. The PEG-dibromomaleimide and PEG-dithiomaleimide were synthesised *via* a Mitsunobu reaction, with a higher yield obtained when using dithiomaleimide (73%) compared to dibromomaleimide (13%, Scheme 1.6). PEG-dibromomaleimide was tested with sequential addition of TCEP and somatostatin, whereas PEG-dithiophenolmaleimide was tested with *in situ* conditions, see Scheme 1.9.

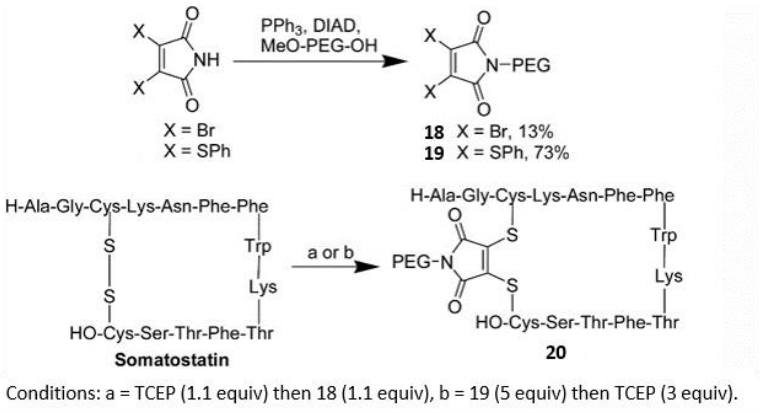

Scheme 1.9. Synthesis of PEG-maleimide and PEGylation of somatostatin *via* a stepwise protocol (**a**) or *in situ* protocol (**b**). Adapted from reference.[85]

1.3.2. For antibody drug conjugation

Following the development of dibromomaleimide/dithiomaleimide disulfide bridging, Caddick and Baker extended the area of study to antibody fragment conjugation.[89-91] PEG-dibromomaleimide and fluorescein-dibromomaleimide antibody conjugates were successfully synthesised *via* similar methods to the ones developed for protein disulfide bridging. The antibody was also labelled with a spin label for EPR-based detection to potentially monitor antibody-antigen interactions (Figure 1.13).[89]

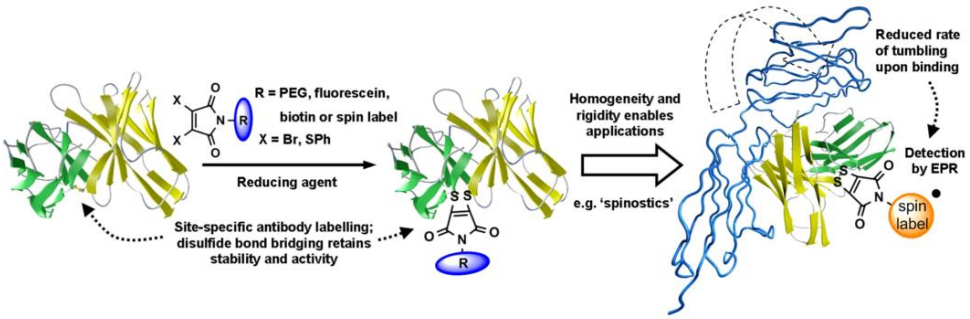

Figure 1.13. Schematic concept of functionalisation of the antibody and the antibody-antigen interaction detection by EPR-sensing. Reproduced from reference.[89]

Further investigations were carried out into the use of dithiomaleimide for antibody drug conjugates. Initially, an anti-cancer drug (monomethyl auristatin E, MMAE)

was coupled to dithiophenolmaleimide. The product was successfully conjugated to an antibody (IgG1 trastuzumab) *via* re-bridging the interchain disulfide bonds (Figure 1.14). Post hydrolysis, the antibody drug conjugate was shown to be stable in blood serum, selectively targeting and killing cancer cells.[90,91]

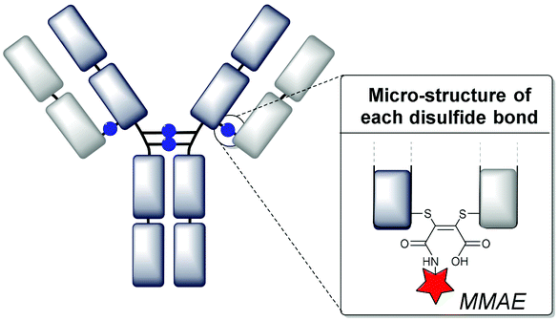

Figure 1.14. Schematic example of an antibody drug conjugate synthesised through utilisation of dithiomaleimide. Reproduced from reference.[91]

1.3.3. For polymers functionalisation

Following their work on the conjugation of PEG and somatostatin with maleimide derivatives, Caddick, Baker and co-workers collaborated with Gibson, Haddleton and co-workers to develop dibromomaleimide functionalised polymers synthesised by atom transfer radical polymerisation (ATRP), a form of reversible-deactivation radical polymerisation, for application in protein disulfide bridging.[92] In this case, salmon calcitonin (a disulfide bridge containing hormone) was targeted for disulfide bridging with the maleimide species. Whilst the same approach as mentioned above (functionalisation of PEG with dibromomaleimide *via* the Mitsunobu reaction, see Scheme 1.9) successfully produced a PEG-dibromomaleimide conjugate, the efficiency and the reaction yield were low, and the product required additional

purification *via* column chromatography. Moreover, the initial test of performing ATRP of oligo(ethylene glycol) methyl ether

Methacrylate (OEGMA) in the presence of dibromomaleimide led to inhibition of the polymerisation under the conditions evaluated. To circumvent this ATRP inhibition, other indirect synthetic routes were tested to obtain dibromomaleimide functionalised PEG. In these alternative routes, dibromomaleimide was successfully added onto PEG *via* post-polymerisation modification. The conjugation of the resulting dibromomaleimide-PEG was evaluated using the disulfide rebridging of the salmon calcitonin, with successful polymer-peptide conjugation reported.

Investigations using a dibromomaleimide functionalised ATRP initiator were further pursued through the synthesis of two dibromomaleimide functionalised ATRP initiators.[93] Both initiators were tested for the ATRP polymerisation of MA and tertbutyl acrylate (tBA). Unlike the earlier results, the polymerisations did not seem to be inhibited, although a loss of control was noticed *via* size exclusion chromatography (SEC) analysis of polymerisation samples, showing bimodal SEC traces. The possibility of using a maleimide ATRP initiator was further investigated. As previously observed, dibromomaleimide was more sensitive to TCEP than dithiomaleimide[85], therefore it was hypothesised that a dithiomaleimide functionalised ATRP initiator would be more tolerant to the reaction conditions. Indeed, oligo(ethylene glycol) methyl ether methacrylates (OEGMA) was successfully polymerised with good control using a dithiomaleimide initiator, and conjugated to salmon calcitonin.[94]

Following the successful polymerisation using a dithiomaleimide ATRP initiator and the conjugation with salmon calcitonin, Haddleton and co-workers developed an oxytocin PEG conjugate *via* disulfide bridging of the oxytocin cysteines and an

α-dithiomaleimide PEG (Scheme 1.10).[95] The formation of this conjugate, reversible *in situ*, significantly reduced the drug degradation.

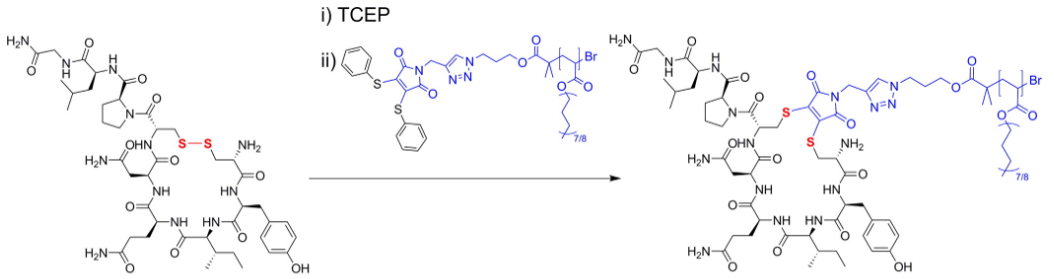

Scheme 1.10. Synthesis of an oxytocin PEG conjugate using a dithiomaleimide functionalised ATRP initiator. Adapted from reference.[95]

The possibility of using RAFT polymerisation was also investigated. Inspired by Caddick, Baker and co-workers, Robin *et al.* synthesised a RAFT CTA containing the dibromomaleimide functionality.[93] The synthesis of the trithiocarbonate-based CTA (**21** in Scheme 1.11) was reported by Petzetakis *et al.*,[96] and the functionalisation with dibromomaleimide was performed following a procedure reported by Weinreb.[97]

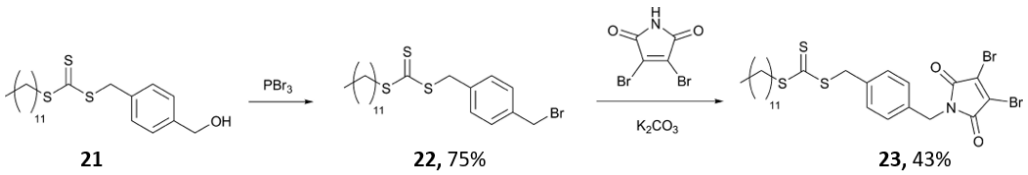

Scheme 1.11. Synthesis of the DBM RAFT agent. Adapted from reference.[93]

Using the dibromomaleimide RAFT CTA, different RAFT polymerisation conditions were tested to polymerise tBA, MA, triethylene glycol acrylate (TEGA), and NIPAM. The resultant polymers were compared to polymers synthesised with the benzylbromine analogue of the dibromomaleimide and its precursor (**22** and **21** in Scheme 1.11, respectively). Polymerisation of tBA, MA and TEGA with CTA **23** proceeded to high conversion with good control (low dispersity); however, a 40

minutes induction period was observed. Moreover, polymerisation of acrylic monomers seemed to be significantly slower than expected. The post polymerisation modification of the dibromomaleimide terminated polymers was also tested and optimised to form monothiomaleimide and dithiomaleimide *via* addition of thiophenol with catalytic imidazole. In the presence of imidazole, the reaction occurred rapidly, achieving high conversion after only 15 minutes (monosubstituted product still present) and total conversion after 60 minutes.[93]

1.3.4. Fluorescent properties

Following the successful RAFT polymerisations, the DBM containing RAFT initiator (**23**) was functionalised with mercaptoethanol (**24** in Scheme 1.12), in order to initiate the polymerisation of *rac*-lactide (LA) *via* ROP, allowing for the synthesis of a block copolymer, see Scheme 1.12.

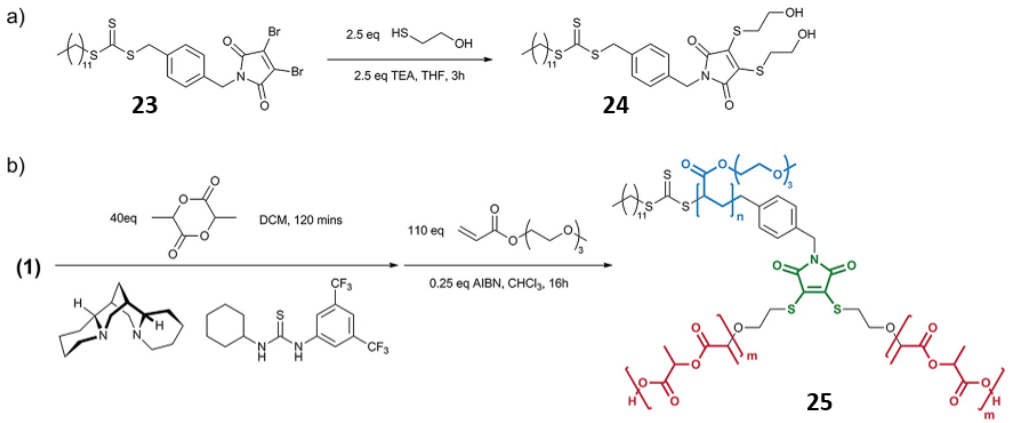

Scheme 1.12. Synthesis of a block copolymer using a novel RAFT/ROP initiator. Adapted from reference.[98]

Interestingly, the block copolymer (**25** in Scheme 1.12) showed luminescent properties, under a UV lamp, see Figure 1.15. It was also noted that the PLA precursor and RAFT/ROP initiator exhibited similar properties.

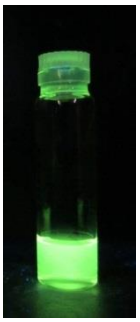

Figure 1.15. Picture of the copolymer **25** at 1mg·mL^{-1} in chloroform under a UV lamp (λ = 345 nm).

To further investigate this phenomenon, Robin *et al.* synthesised a range of dithiomaleimide small molecules *via* the addition-elimination reaction of dibromomaleimide with different thiols, see Scheme 1.13.

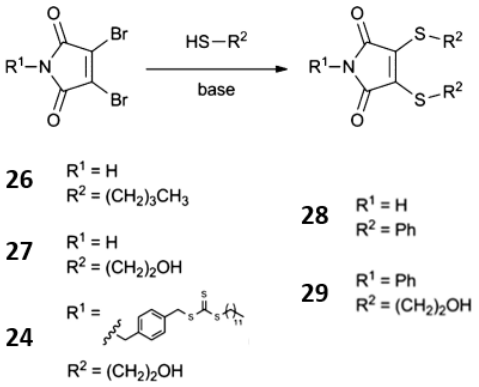

Scheme 1.13. Synthesis of different dithiomaleimide small molecules. Adapted from reference.[99]

Dithiomaleimide **26,** synthesised from dibromomaleimide and butanethiol showed an emission spectrum in chloroform with a maximum at 520 nm, and excitation maxima at 265 nm and 415 nm. Dithiomaleimides **27** (mercaptoethanol substituted) and **24** (*N*-substituted with RAFT agent) showed similar fluorescence spectra. The fluorescence properties of RAFT CTA **24** explained the luminescence observed with the aforementioned block copolymer **25** in Scheme 1.12, the same CTA (**24**) was used to synthesise the copolymer.

These observations are consistent with a patent published in 1987 reporting the use of dibromomaleimide and dichloromaleimide to detect thiol and amine functionalities.[100] The halogenated maleimide stain was used to detect the presence of proteins *via* the direct addition of the stain to the protein sample; fluorescence could be observed within 15 minutes with a UV light source. However, it was observed that when dibromomaleimide was conjugated with an aromatic ring such as **28** (thiophenol substituent) and **29** (*N*-phenyl substituent), the fluorescence emission was drastically decreased, see Figure 1.16.

As a consequence of dithiomaleimides being previously used for cysteine PEGylation, and disulfide re-bridging in somatostatin and salmon calcitonin proteins,[82,84,85] Robin *et al.* tested whether the fluorescent properties of dithiomaleimide were retained when conjugated to proteins. Following a procedure previously developed by Caddick and co-workers, it was successfully demonstrated that dibromomaleimide conjugated with glutathione formed a fluorescent product, as did the dibromomaleimide functionalised cysteine. Similarly, disulfide re-bridging of salmon calcitonin also resulted in the incorporation of fluorescent properties. However, when monocysteine was added to dibromomaleimide, producing a thiobromomaleimide, the product showed fluorescent properties but with considerably reduced intensity, see Figure 1.16.

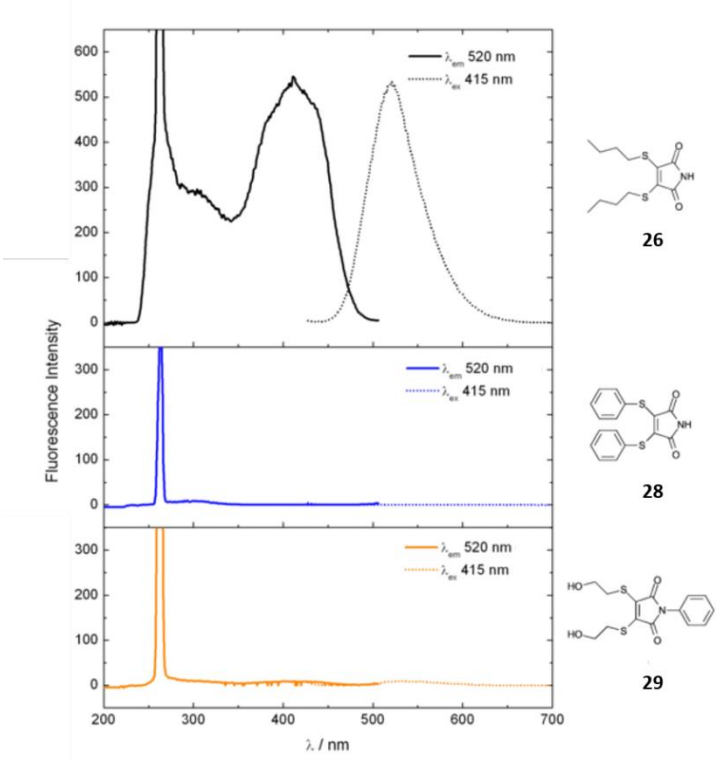

Figure 1.16. Emission and excitation spectra of **26**, **28**, and **29** at 0.1 mM in chloroform. Adapted from reference.[99]

Alongside the study on the fluorescence properties of dithiomaleimides, Robin *et al.* investigated the RAFT polymerisation of different monomers (tBA, TEGA, Styrene and NIPAM) utilising the fluorescent dithiomaleimide RAFT agent (**24** in Scheme 1.13). The polymerisation of these monomers by RAFT polymerisation was previously tested using a dibromomaleimide RAFT agent, where styrene and NIPAM polymerisations were found to be inhibited. However, when using the mercaptoethanol-derived dithiomaleimide RAFT agent (**24** in Scheme 1.13), RAFT polymerisations of the different classes of monomers evaluated were successful, and all the polymers exhibited fluorescent properties similar to the RAFT agent.

As mentioned above, the amphiphilic block copolymer synthesised with the dual RAFT/ROP initiator containing dithiomaleimide (see Scheme 1.12) exhibited luminescent properties, with a fluorescence emission spectrum showing an emission maximum at 522 nm and an excitation maximum at 403 nm in methanol.[98] The

polymer emission intensity also showed a low concentration dependence between 200 nM and 200 μM. It was also found that this amphiphilic block copolymer self-assembled into spherical micelles of 20 nm diameter in water. The small size of the dithiomaleimide functionality presumably located at the hydrophilic/hydrophobic interface did not disrupt the copolymer self-assembly, and the block copolymer appeared to retain fluorescence when self-assembled. The fluorescent behaviour of these fluorescent micelles in *in vitro* conditions was also tested. It was observed that three different forms of micelle and their degraded products could be found in different parts of rat vascular tissue and that these species could be differentiated by their respective fluorescence life-time as determined by fluorescence lifetime imaging microscopy (FLIM), see Figure 1.17.[98] These results showed the potential of dithiomaleimide functional group to be used in self-reporting materials for nanomedicine.

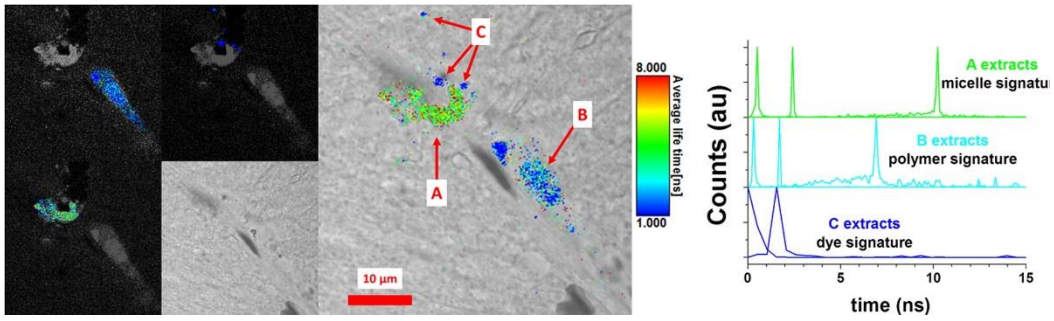

Figure 1.17. Fluorescence lifetime imaging microscopy (FLIM) of fluorescent micelles in a rat hippocampal tissue (A) clotting regions, (B) vascular tissue, (C) blood cells. Reproduced from reference.[98]

The aforementioned copolymer **25** was able to self-assemble into spherical micelles in aqueous media. These micelles were further developed (**RM2**) as a potential nanovehicle for neural stem cells modulation and compared to a fluorescently labelled NIPAM based nanogels (**RM1**).[101] It was reported that both micelles (**RM2**) and nanogels (**RM1**) were successfully internalised by stem cells, which could be observed by fluorescence microscopy, see Figure 1.18. The toxicity of **RM1** and **RM2** was also assessed and it was found that these fluorescent micelles were not toxic at a concentration equal or below 150 μg·mL^{-1}. However, the loading of a drug (retinoic acid) was tested and showed a low loading capacity of the micelles **RM2** as a result of the packed nature of the core.

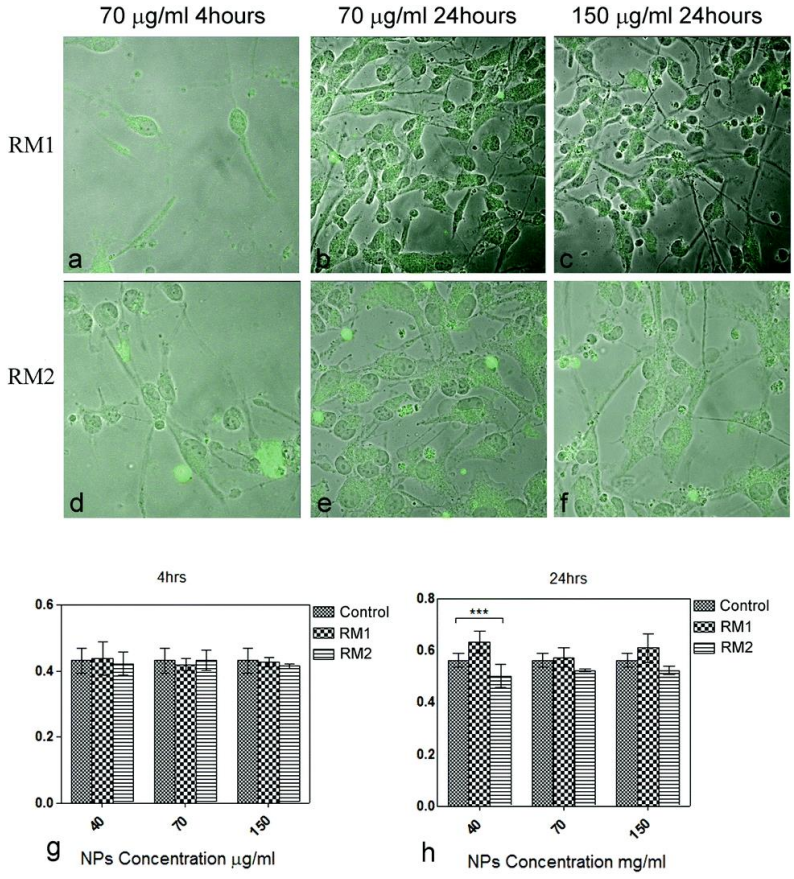

Figure 1.18. Internalisation of nanoparticles **RM1** and **RM2**. (a-f) Confocal microscopy images of cells at 70 and 150 μg·mL^{-1} after 4 h and 24 h. (g-h) Proliferation assays at different concentration. Reproduced from reference.[101]

1.4. Summary

The introduction has mainly been focused, in the first part, on polymeric nanoparticles. There is a large variety of nanoparticles with different properties for a myriad of applications. Specifically, fluorescent responsive particles are of particular interest for biomedical applications, as they can combine drug-delivery, targeting and imaging properties. Concepts involving responsive nanoparticles are utilised in Chapter 2 (self-assembled micelles responsive to an excess of thiophenol), in Chapter 4 (CO_2-responsive fluorescent nanoparticles), and in Chapter 5 (glutathione-responsive fluorescent nanoparticles).

The second part of this introduction has focused on the development of the dibromomaleimide and dithiomaleimide chemistries, which led to the discovery of their fluorescent properties. The dithiomaleimide fluorescent properties introduced have been explored in Chapter 2, with work focussing on a fluorescence emissive on-to-off switch. The fluorescent properties have further been exploited within this Thesis, with the development of another fluorophore derivative in Chapter 3, and subsequent applications in Chapter 4 and 5 allowing for a read-out of the state of the particles, rendering them self-reporting.

1.5. References

1. M. R. Hill, E. J. MacKrell, C. P. Forsthoefel, S. P. Jensen, M. Chen, G. A. Moore, Z. L. He and B. S. Sumerlin, *Biomacromolecules*, 2015, **16**, 1276-1282.

2. M. Elsabahy and K. L. Wooley, *Chem. Soc. Rev.*, 2012, **41**, 2545-2561.

3. Z. L. Tyrrell, Y. Shen and M. Radosz, *Prog. Polym. Sci.*, 2010, **35**, 1128-1143.

4. S. Huang, S. Liu, K. Wang, C. Yang, Y. Luo, Y. Zhang, B. Cao, Y. Kang and M. Wang, *Nanoscale*, 2015, **7**, 889-895.

5. S. M. Janib, A. S. Moses and J. A. MacKay, *Adv. Drug Del. Rev.*, 2010, **62**, 1052-1063.

6. Y. Yang, Y. Li, Q. Lin, C. Bao and L. Zhu, *ACS Macro Lett.*, 2016, **5**, 301-305.

7. K. Li and B. Liu, *Chem. Soc. Rev.*, 2014, **43**, 6570-6597.

8. G. Lin, H. Zhang and L. Huang, *Mol. Pharm.*, 2015, **12**, 314-321.

9. A. Storha, E. A. Mun and V. V. Khutoryanskiy, *RSC Advances*, 2013, **3**, 12275-12279.

10. A. Blanazs, S. P. Armes and A. J. Ryan, *Macromol. Rapid Commun.*, 2009, **30**, 267-277.

11. M. V. Walter and M. Malkoch, *Chem. Soc. Rev.*, 2012, **41**, 4593-4609.

12. C. Chen, R. A. L. Wylie, D. Klinger and L. A. Connal, *Chem. Mater.*, 2017, **29**, 1918-1945.

13. S. Fuchs, H. Otto, S. Jehle, P. Henklein and A. D. Schluter, *Chem. Commun.*, 2005, **14**, 1830-1832.

14. L. Feng, C. Zhu, H. Yuan, L. Liu, F. Lv and S. Wang, *Chem. Soc. Rev.*, 2013, **42**, 6620-6633.

15. N. Sanson and J. Rieger, *Polym. Chem.*, 2010, **1**, 965-977.

16. R. K. O'Reilly, M. J. Joralemon, K. L. Wooley and C. J. Hawker, *Chem. Mater.*, 2005, **17**, 5976-5988.

17. Y. Mai and A. Eisenberg, *Chem. Soc. Rev.*, 2012, **41**, 5969-5985.

18. K. E. B. Doncom, L. D. Blackman, D. B. Wright, M. I. Gibson and R. K. O'Reilly, *Chem. Soc. Rev.*, 2017, DOI: 10.1039/C6CS00818F.

19. E. G. Kelley, J. N. L. Albert, M. O. Sullivan and T. H. Epps, *Chem. Soc. Rev.*, 2013, **42**, 7057-7071.

20. J. Hu, L. Dai and S. Liu, *Macromolecules*, 2011, **44**, 4699-4710.

21. M. C. Baier, J. Huber and S. Mecking, *J. Am. Chem. Soc.*, 2009, **131**, 14267-14273.

22. J. Chen, P. Zhang, G. Fang, P. Yi, X. Yu, X. Li, F. Zeng and S. Wu, *J. Phys. Chem. B*, 2011, **115**, 3354-3362.

23. W. Richtering and A. Pich, *Soft Matter*, 2012, **8**, 11423-11430.

24. G. Sun, M. Y. Berezin, J. Fan, H. Lee, J. Ma, K. Zhang, K. L. Wooley and S. Achilefu, *Nanoscale*, 2010, **2**, 548-558.

25. G. Marcelo, T. J. V. Prazeres, M.-T. Charreyre, J. M. G. Martinho and J. P. S. Farinha, *Macromolecules*, 2010, **43**, 501-510.

26. Y. Yamamoto, K. Yasugi, A. Harada, Y. Nagasaki and K. Kataoka, *J. Control. Release*, 2002, **82**, 359-371.

27. A. Vollrath, S. Schubert and U. S. Schubert, *J. Mater. Chem. B*, 2013, **1**, 1994-2007.

28. X. Zhang, X. Zhang, B. Yang, J. Hui, M. Liu, Z. Chi, S. Liu, J. Xu and Y. Wei, *J. Mater. Chem. C*, 2014, **2**, 816-820.

29. M. J. Monteiro, *Macromolecules*, 2010, **43**, 1159-1168.

30. J. Jennings, G. He, S. M. Howdle and P. B. Zetterlund, *Chem. Soc. Rev.*, 2016, **45**, 5055-5084.

31. M. Bouyahyi and R. Duchateau, *Macromolecules*, 2014, **47**, 517-524.

32. R. C. Pratt, B. G. G. Lohmeijer, D. A. Long, P. N. P. Lundberg, A. P. Dove, H. Li, C. G. Wade, R. M. Waymouth and J. L. Hedrick, *Macromolecules*, 2006, **39**, 7863-7871.

33. F. Nederberg, E. F. Connor, M. Möller, T. Glauser and J. L. Hedrick, *Angew. Chem. Int. Ed.*, 2001, **40**, 2712-2715.

34. A. P. Dove, R. C. Pratt, B. G. G. Lohmeijer, D. A. Culkin, E. C. Hagberg, G. W. Nyce, R. M. Waymouth and J. L. Hedrick, *Polymer*, 2006, **47**, 4018-4025.

35. A. P. Dove, R. C. Pratt, B. G. G. Lohmeijer, R. M. Waymouth and J. L. Hedrick, *J. Am. Chem. Soc.*, 2005, **127**, 13798-13799.

36. O. Dechy-Cabaret, B. Martin-Vaca and D. Bourissou, *Chem. Rev.*, 2004, **104**, 6147-6176.

37. O. Coulembier, L. Mespouille, J. L. Hedrick, R. M. Waymouth and P. Dubois, *Macromolecules*, 2006, **39**, 4001-4008.

38. K. Hashimoto, *Prog. Polym. Sci.*, 2000, **25**, 1411-1462.

39. F. Suriano, O. Coulembier, J. L. Hedrick and P. Dubois, *Polym. Chem.*, 2011, **2**, 528-533.

40. A.-L. Brocas, C. Mantzaridis, D. Tunc and S. Carlotti, *Prog. Polym. Sci.*, 2013, **38**, 845-873.

41. E. Haladjova, N. Toncheva-Moncheva, M. D. Apostolova, B. Trzebicka, A. Dworak, P. Petrov, I. Dimitrov, S. Rangelov and C. B. Tsvetanov, *Biomacromolecules*, 2014, **15**, 4377-4395.

42. K. Nagase and T. Okano, *J. Mater. Chem. B*, 2016, **4**, 6381-6397.

43. Z. Ge and S. Liu, *Chem. Soc. Rev.*, 2013, **42**, 7289-7325.

44. I. Insua, E. Liamas, Z. Zhang, A. F. A. Peacock, A. M. Krachler and F. Fernandez-Trillo, *Polym. Chem.*, 2016, **7**, 2684-2690.

45. M. Kanamala, W. R. Wilson, M. Yang, B. D. Palmer and Z. Wu, *Biomaterials*, 2016, **85**, 152-167.

46. J. Chen, X. Qiu, J. Ouyang, J. Kong, W. Zhong and M. M. Q. Xing, *Biomacromolecules*, 2011, **12**, 3601-3611.

47. M. Wei, Y. Gao, X. Li and M. J. Serpe, *Polym. Chem.*, 2017, **8**, 127-143.

48. M. I. Gibson and R. K. O'Reilly, *Chem. Soc. Rev.*, 2013, **42**, 7204-7213.

49. A. O. Moughton and R. K. O'Reilly, *Chem. Commun.*, 2010, **46**, 1091-1093.

50. J.-F. Gohy and Y. Zhao, *Chem. Soc. Rev.*, 2013, **42**, 7117-7129.

51. F. D. Jochum and P. Theato, *Chem. Soc. Rev.*, 2013, **42**, 7468-7483.

52. O. Bertrand and J.-F. Gohy, *Polym. Chem.*, 2017, **8**, 52-73.

53. J. V. M. Weaver, R. T. Williams, B. J. L. Royles, P. H. Findlay, A. I. Cooper and S. P. Rannard, *Soft Matter*, 2008, **4**, 985-992.

54. A. J. Morse, S. P. Armes, K. L. Thompson, D. Dupin, L. A. Fielding, P. Mills and R. Swart, *Langmuir*, 2013, **29**, 5466-5475.

55. K. E. B. Doncom, C. F. Hansell, P. Theato and R. K. O'Reilly, *Polym. Chem.*, 2012, **3**, 3007-3015.

56. H. Liu, S. Lin, Y. Feng and P. Theato, *Polym. Chem.*, 2017, **8**, 12-23.

57. A. Darabi, P. G. Jessop and M. F. Cunningham, *Chem. Soc. Rev.*, 2016, **45**, 4391-4436.

58. S. Lin and P. Theato, *Macromol. Rapid Commun.*, 2013, **34**, 1118-1133.

59. M. Huo, J. Yuan, L. Tao and Y. Wei, *Polym. Chem.*, 2014, **5**, 1519-1528.

60. Y.-C. Wang, F. Wang, T.-M. Sun and J. Wang, *Bioconj. Chem.*, 2011, **22**, 1939-1945.

61. A. O. Moughton, J. P. Patterson and R. K. O'Reilly, *Chem. Commun.*, 2011, **47**, 355-357.

62. A. Feng, C. Zhan, Q. Yan, B. Liu and J. Yuan, *Chem. Commun.*, 2014, **50**, 8958-8961.

63. J. F. Quinn, M. R. Whittaker and T. P. Davis, *Polym. Chem.*, 2017, **8**, 97-126.

64. C. V. Smith, D. P. Jones, T. M. Guenthner, L. H. Lash and B. H. Lauterburg, *Toxicol. Appl. Pharmacol.*, 1996, **140**, 1-12.

65. G. K. Balendiran, R. Dabur and D. Fraser, *Cell Biochem. Funct.*, 2004, **22**, 343-352.

66. A. Russo, W. DeGraff, N. Friedman and J. B. Mitchell, *Cancer Res.*, 1986, **46**, 2845-2848.

67. J.-H. Ryu, R. Roy, J. Ventura and S. Thayumanavan, *Langmuir*, 2010, **26**, 7086-7092.

68. Y.-L. Li, L. Zhu, Z. Liu, R. Cheng, F. Meng, J.-H. Cui, S.-J. Ji and Z. Zhong, *Angew. Chem. Int. Ed.*, 2009, **48**, 9914-9918.

69. J. Zhuang, M. R. Gordon, J. Ventura, L. Li and S. Thayumanavan, *Chem. Soc. Rev.*, 2013, **42**, 7421-7435.

70. C. Boyer and R. Hoogenboom, *Eur. Polym. J.*, 2015, **69**, 438-440.

71. C.-Y. Chen and H.-L. Wang, *Macromol. Rapid Commun.*, 2014, **35**, 1534-1540.

72. C. Chang, H. Wei, J. Feng, Z.-C. Wang, X.-J. Wu, D.-Q. Wu, S.-X. Cheng, X.-Z. Zhang and R.-X. Zhuo, *Macromolecules*, 2009, **42**, 4838-4844.

73. A. Klaikherd, C. Nagamani and S. Thayumanavan, *J. Am. Chem. Soc.*, 2009, **131**, 4830-4838.

74. X. Fei and Y. Gu, *Prog. Nat. Sci.*, 2009, **19**, 1-7.

75. E. C. Jensen, *Anat. Rec.*, 2012, **295**, 2031-2036.

76. J. Vogelsang, R. Kasper, C. Steinhauer, B. Person, M. Heilemann, M. Sauer and P. Tinnefeld, *Angew. Chem. Int. Ed.*, 2008, **47**, 5465-5469.

77. M. P. Robin and R. K. O'Reilly, *Polym. Int.*, 2015, **64**, 174-182.

78. A. Reisch and A. S. Klymchenko, *Small*, 2016, **12**, 1968-1992.

79. A. M. Breul, M. D. Hager and U. S. Schubert, *Chem. Soc. Rev.*, 2013, **42**, 5366-5407.

80. C. Lidia, B. Paolo, D. Valentina, S. Leopoldo, F. Raffaele, P. Ruggiero Maria, K. Rushd, B. Patrizia, U. Paolo, L. Monica, T. Massimo, C. Laura, G. Daniela, S. Vincenzo, M. Massimo, S. Mario and M. Davide, *Nanotechnology*, 2013, **24**, 245603.

81. X. Wang, S. Xu and W. Xu, *Phys. Chem. Chem. Phys.*, 2011, **13**, 1560-1567.

82. M. E. B. Smith, F. F. Schumacher, C. P. Ryan, L. M. Tedaldi, D. Papaioannou, G. Waksman, S. Caddick and J. R. Baker, *J. Am. Chem. Soc.*, 2010, **132**, 1960-1965.

83. J. R. Winther and C. Thorpe, *Biochim. Biophys. Acta*, 2014, **1840**, 838-846.

84. L. M. Tedaldi, M. E. B. Smith, R. I. Nathani and J. R. Baker, *Chem. Commun.*, 2009, **43**, 6583-6585.

85. F. F. Schumacher, M. Nobles, C. P. Ryan, M. E. B. Smith, A. Tinker, S. Caddick and J. R. Baker, *Bioconj. Chem.*, 2011, **22**, 132-136.

86. C. P. Ryan, M. E. B. Smith, F. F. Schumacher, D. Grohmann, D. Papaioannou, G. Waksman, F. Werner, J. R. Baker and S. Caddick, *Chem. Commun.*, 2011, **47**, 5452-5454.

87. L. M. Tedaldi, A. E. Aliev and J. R. Baker, *Chem. Commun.*, 2012, **48**, 4725-4727.

88. P. Moody, M. E. B. Smith, C. P. Ryan, V. Chudasama, J. R. Baker, J. Molloy and S. Caddick, *ChemBioChem*, 2012, **13**, 39-41.

89. F. F. Schumacher, V. A. Sanchania, B. Tolner, Z. V. F. Wright, C. P. Ryan, M. E. B. Smith, J. M. Ward, S. Caddick, C. W. M. Kay, G. Aeppli, K. A. Chester and J. R. Baker, *Sci. Rep.*, 2013, **3**, 1525.

90. J. P. M. Nunes, M. Morais, V. Vassileva, E. Robinson, V. S. Rajkumar, M. E. B. Smith, R. B. Pedley, S. Caddick, J. R. Baker and V. Chudasama, *Chem. Commun.*, 2015, **51**, 10624-10627.

91. M. Morais, J. P. M. Nunes, K. Karu, N. Forte, I. Benni, M. E. B. Smith, S. Caddick, V. Chudasama and J. R. Baker, *Org. Biomol. Chem.*, 2017, **15**, 2947-2952.

92. M. W. Jones, R. A. Strickland, F. F. Schumacher, S. Caddick, J. R. Baker, M. I. Gibson and D. M. Haddleton, *J. Am. Chem. Soc.*, 2011, **134**, 1847-1852.

93. M. P. Robin, M. W. Jones, D. M. Haddleton and R. K. O'Reilly, *ACS Macro Lett.*, 2011, **1**, 222-226.

94. M. W. Jones, R. A. Strickland, F. F. Schumacher, S. Caddick, J. R. Baker, M. I. Gibson and D. M. Haddleton, *Chem. Commun.*, 2012, **48**, 4064-4066.

95. J. Collins, J. Tanaka, P. Wilson, K. Kempe, T. P. Davis, M. P. McIntosh, M. R. Whittaker and D. M. Haddleton, *Bioconj. Chem.*, 2015, **26**, 633-638.

96. N. Petzetakis, A. P. Dove and R. K. O'Reilly, *Chem. Sci.*, 2011, **2**, 955-960.

97. R. P. Joyce, J. A. Gainor and S. M. Weinreb, *J. Org. Chem.*, 1987, **52**, 1177-1185.

98. M. P. Robin, A. B. Mabire, J. C. Damborsky, E. S. Thom, U. H. Winzer-Serhan, J. E. Raymond and R. K. O'Reilly, *J. Am. Chem. Soc.*, 2013, **135**, 9518-9524.

99. M. P. Robin, P. Wilson, A. B. Mabire, J. K. Kiviaho, J. E. Raymond, D. M. Haddleton and R. K. O'Reilly, *J. Am. Chem. Soc.*, 2013, **135**, 2875-2878.

100. T. L. Smith, *US Pat.,* 4680272, 1987.

101. S. A. Papadimitriou, M. P. Robin, D. Ceric, R. K. O'Reilly, S. Marino and M. Resmini, *Nanoscale*, 2016, **8**, 17340-17349.

Chapter 2

Dithiomaleimide containing polymeric micelles: on-to-off fluorescence emission switch with simultaneous morphology transition

2.1. Abstract

This chapter discusses changes in the morphology and fluorescence of self-assembled polymers containing dithiomaleimide moieties. These changes are shown to be the result of an addition-elimination reaction taking place upon addition of an aromatic thiol that dramatically alters the fluorescence emission properties of dithiomaleimide while the morphology transition is attributed to the change of the polymer polarity. These phenomena are the result of an addition-elimination reaction that occurs on the dithiomaleimide, present at the core-shell interface, in the presence of an excess of an aromatic thiol.*

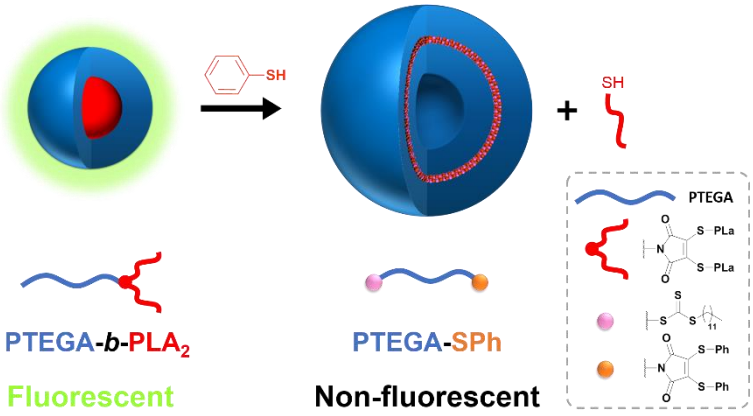

Figure 2.1. Schematic representation summarising the concept of this chapter: morphology transition along with fluorescence intensity decrease, triggered by the addition of thiophenol onto the maleimide and elimination of the PLA-SH. PTEGA-b-PLA_2: poly(triethylene glycol monomethyl ether acrylate)]-*b*-[poly(D,L-lactide)$_2$. Figure reproduced from reference.[1]

* The synthesis of most materials presented in this chapter was carried out by the author in the context of her master's degree however the study of the properties of the materials was mainly carried out during the course of this PhD.

2.2. Introduction

The precise control over self-assembled polymer morphologies in solution is currently of great interest to the research community. Various morphologies such as spherical micelles, cylinders, rods, and vesicles or polymersomes can be formed through the self-assembly of amphiphilic block copolymers in selective solvents.[2] The morphology adopted in solution by the amphiphiles is determined by the block copolymer composition and properties. Conventional self-assembled nanostructures are based on hydrophilic-hydrophobic repulsive interactions,[3] and their morphology can be rationalised with the variation of the packing parameter p, which is defined in terms of optimal interface a_0, volume occupied by the hydrophobic chain v and the maximum length of the amphiphile l_c. Depending on the value of the packing parameter, which is related to the curvature of the amphiphilic polymer: for high curvature or $p \leq ⅓$, the polymer self-assembles into spherical micelles; for medium curvature or $⅓ \leq p \leq ½$, cylindrical micelles are formed; and for low curvature or $½ \leq p \leq 1$, hollow vesicles or polymersomes are formed, see Figure 2.2.[3,4] Self-assembled nanostructures formed from stimuli-responsive polymers are able to undergo morphology transitions induced by external stimuli such as pH, temperature and light.[5-11] The incorporation of a stimuli-responsive polymer into a block copolymer can, upon a specific stimulus, trigger a disruption in the hydrophilic-hydrophobic balance of the copolymer and potentially affect its self-assembly properties to form a different nanostructure. These morphology transition properties can, for example, be utilised for applications in nanotechnology and/or drug delivery.[12-17]

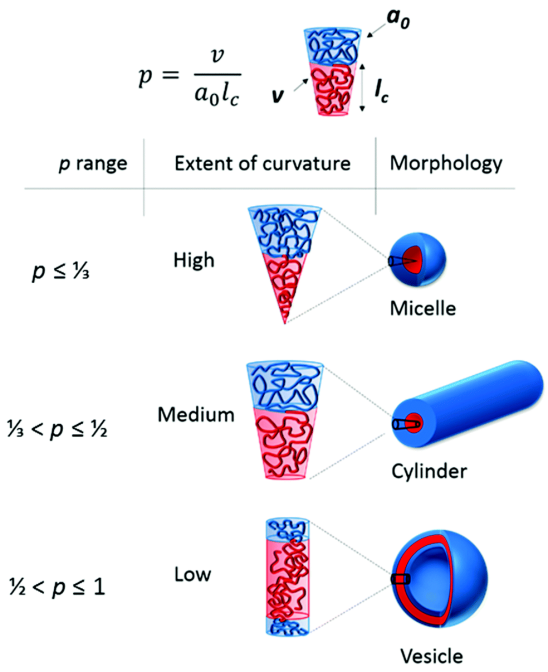

Figure 2.2. Schematic representation of different morphology adopted in solution depending on the amphiphilic balance of the polymer. Figure reproduced from reference.[4]

Previously, Baker *et al*. have shown that the conversion of dibromomaleimide (DBM) to dithiomaleimide (DTM) is highly efficient. They showed that cysteine present in a protein domain can be modified by addition of DBM, which forms a monothiomaleimide (MTM), the addition of 1 equivalent of thioglucose or glutathione can further functionalise the maleimide group to obtain a DTM. Moreover, the addition of a large excess (100 equivalents) of another thiol, in this case 2-mercaptoethanol, glutathione or *tris*(2-carboxyethyl)phosphine (TCEP) can lead to a full recovery of the free unmodified protein.[18]

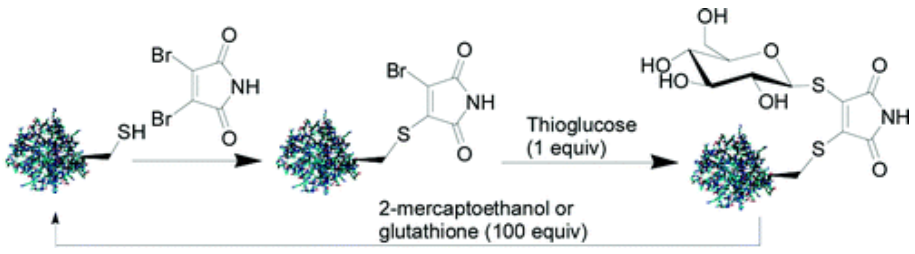

Figure 2.3. Schematic representation of the reversible modification of a protein with DBM. Figure reproduced from reference.[18]

The addition-elimination reaction to obtain a DTM from a DBM or to change the DTM substituents has been shown to be more efficient in the presence of a base catalyst such as triethylamine,[19,20] imidazole [21,22] or sodium acetate. [19,23,24]

When DTMs were found to be fluorescent emissive groups, the investigation of the substituent's nature effect on the DTM's emission led to the conclusions that DTMs functionalised with alkyl thiols are highly fluorescent whilst those with aromatic substituents show a significant decrease in fluorescence emission.[19]

Previously, Robin *et al.* presented the incorporation of the DTM functionality into polymeric self-assembled nanostructure.[20] The DTM functionality was first incorporated into a polymer *via* the synthesis of a DBM containing chain transfer agent (CTA) for reversible addition-fragmentation chain transfer (RAFT) polymerisation followed by a post-polymerisation modification with the addition of thiol.[21] Orthogonal functional groups could be attached on either side of the maleimide group, resulting in a potentially cleavable linkage. Subsequently, the DTM functional group was incorporated into an amphiphilic block copolymer at the hydrophilic-hydrophobic interface *via* a similar method as mentioned above; utilising a DTM labelled dual initiator for ring opening polymerisation (ROP) and RAFT polymerisation.[20] The aqueous solution-state self-assembly of this amphiphilic block copolymer results in the incorporation of the DTM functionality at the core-shell interface of spherical micelles.[20]

Fluorescent labelling functionalities are often large hydrophobic groups that can affect the scaffold size and stability.[17] The small size of the DTM functionality does not affect the micelles' self-assembly as the hydrophilic-hydrophobic balance is not perturb; therefore allows to access fluorescently labelled micelles with very similar properties to the unmodified micelles. Moreover, nanostructures with fluorescence

properties have been of key interest owing their potential use in nanomedicine applications, such as sensing, imaging, and labelling for drug-deliery.[25-27]

2.3. Results and discussion

2.3.1. Synthesis of dithiomaleimide-containing polymers

2.3.1.1. Synthesis of the PTEGA-*b*-PLA$_2$ copolymer (poly(triethylene glycol monomethyl ether acrylate)]-*b*-[poly(D,L-lactide)$_2$)

As mentioned in the previous section, efforts towards stimuli responsive self-assemblies has intensified over the past decade, however only few reports tackle the simultaneous change of morphology and luminescence of such polymer assemblies. Thus, the incorporation of DTM in an amphiphilic polymer was instigated as it would result in highly fluorescent micelles (depending on the polymer chemistry) which would then be tuned through chemical stimulation. Previously, Robin *et al*. reported the preparation of spherical micelles from an amphiphilic dye-containing block copolymer, which was synthesised *via* sequential ROP[28] and RAFT polymerisation[29] utilising a dual RAFT chain transfer agent (CTA)/ROP initiator.[19,20] The design of this species ensured the location of the DTM group between the hydrophobic and the hydrophilic blocks, allowing the addition-elimination reaction to be coupled with a fluorescence emission on-to-off switch simultaneous with a morphology transition as a result of the change in volume fractions of the amphiphile components. The structure and properties of the amphiphilic copolymer were carefully chosen to enable a significant modification of the hydrophilic-hydrophobic balance along with a fluorescence emission decrease by changing the nature of the hydrophobic segment. Being connected to the DTM motif as thiol ligands, the hydrophobic segments were eliminated through subsequent addition-elimination with another thiol.

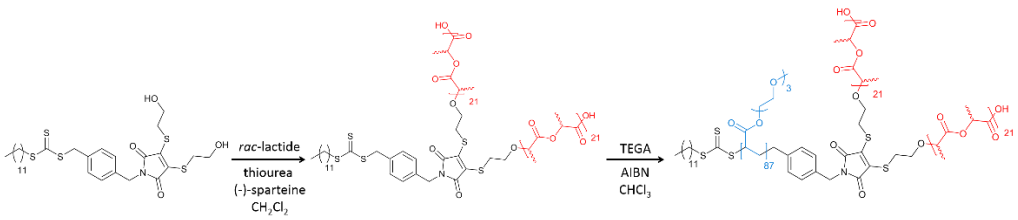

Scheme 2.1. Synthesis of the amphiphilic block copolymer, PTEGA-*b*-PLA_2.
TEGA: triethylene glycol monomethyl ether acrylate ,
AIBN: azobisisobutyronitrile.

The DTM-containing ROP/RAFT dual initiator was synthesised from a 2,3-DBM-functionalised RAFT CTA.[21] Reaction with mercaptoethanol and triethylamine gave a fluorescent DTM-functionalised ROP/RAFT dual initiator with two hydroxyl groups that served as the initiating species for the ROP of *rac*-lactide.[30]

The ROP was chosen to be performed first as it requires dry conditions and it was estimated that the initiator would be easier to dry than the hydrophilic PTEGA. The polymerisation was performed using a thiourea/(-)-sparteine catalyst, which has been reported to allow good control over the polymerisation with narrow molecular weight distribution.[28] The low dispersity expected was confirmed by size exclusion chromatography (SEC) analysis ($Đ$ = 1.13). The resulting polymer was characterised by ^{1}H NMR spectroscopy (see Figure 2.4) and SEC analysis (Figure 2.5), ($M_{n,NMR}$ = 6.7 kg·mol^{-1}, $M_{n,SEC}$ = 8.1 kg·mol^{-1}).† Fluorescence spectroscopy confirmed the presence of the DTM functional group in the PLA_2 polymer, by showing a similar emission spectrum as for the initiator, see Figure 2.6. The shift in emission could be attributed to the difference in polarity of the solvents utilised for the measurements.

† Synthesis and characterisation of materials previously reported during Master's degree project are marked with this symbol (†).

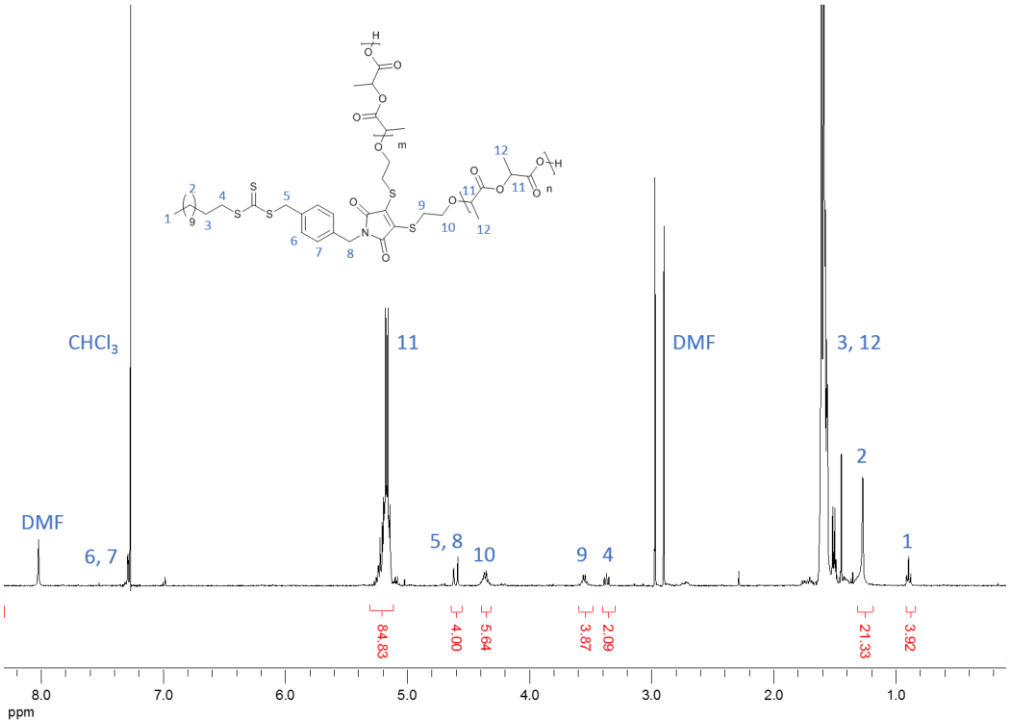

Figure 2.4. ^{1}H NMR ($CDCl_3$, 400 MHz) spectrum of PLA_2.†

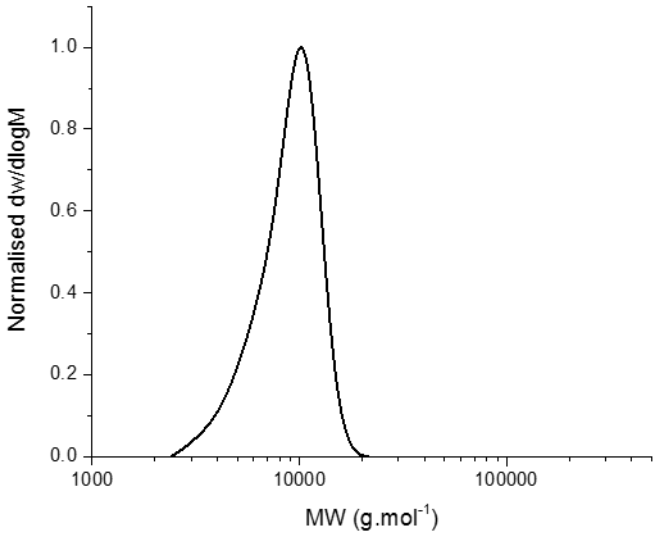

Figure 2.5. Molecular weight distribution of PLA_2. SEC in THF, PS calibration. †

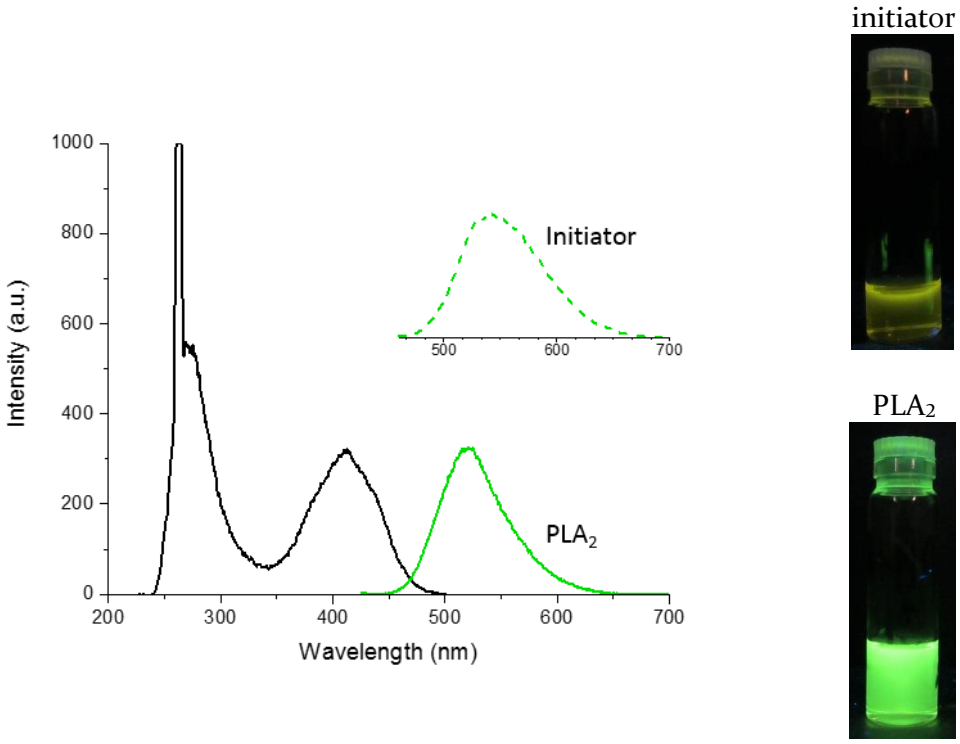

Figure 2.6. Fluorescence emission (green) and excitation (black) spectra of PLA_2 in chloroform at 1 mg·mL^{-1} (λ_{ex} = 410 nm and λ_{em} = 520 nm); insert: emission spectrum of the initiator in methanol (λ_{ex} = 450 nm); pictures of initiator and PLA_2 under UV lamp. †

The PLA_2 polymer was then chain-extended to afford the diblock copolymer [poly(triethylene glycol monomethyl ether acrylate)]-*b*-[poly(*rac*-lactide)]$_2$, PTEGA-*b*-PLA_2, see Scheme 2.1. The polymerisation was performed utilising 1 equivalent of initiator for 0.25 equivalents of AIBN, 110 equivalents of TEGA in chloroform for 16 hours. The product was purified by dialysis against water. ^{1}H NMR (Figure 2.7) and SEC analysis (Figure 2.8) confirmed the chain extension by showing the presence of both PLA and PTEGA characteristic chemical shifts, the increased molecular weight compare to the PLA_2 precursor, and the low dispersity of the copolymer ($M_{n,NMR}$ = 25.7 kg·mol^{-1}, $M_{n,SEC}$ = 19.5 kg·mol^{-1}, $Đ$ = 1.21). †

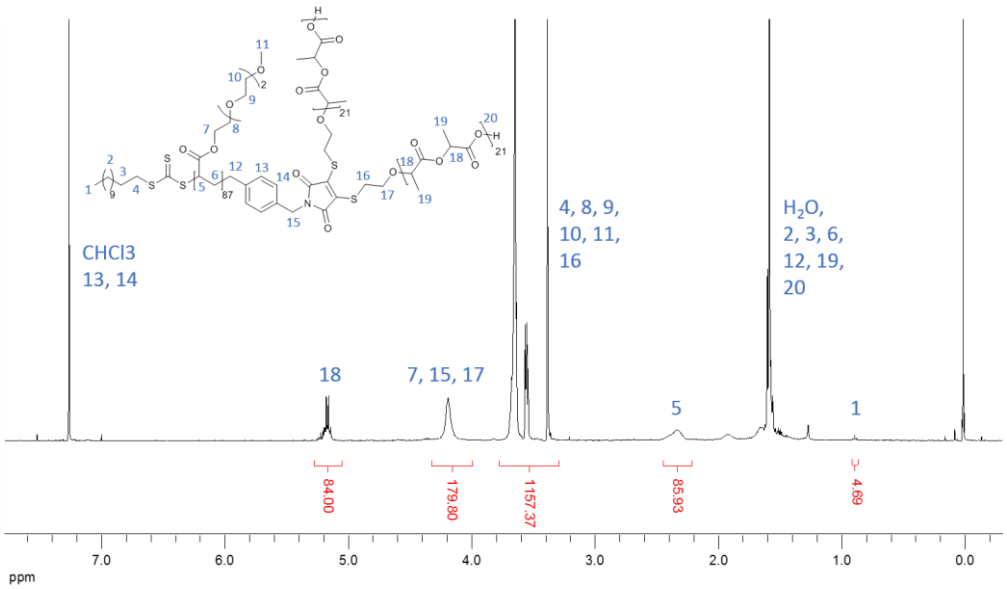

Figure 2.7. ^{1}H NMR ($CDCl_3$, 400 MHz) spectrum of PTEGA-*b*-PLA_2.†

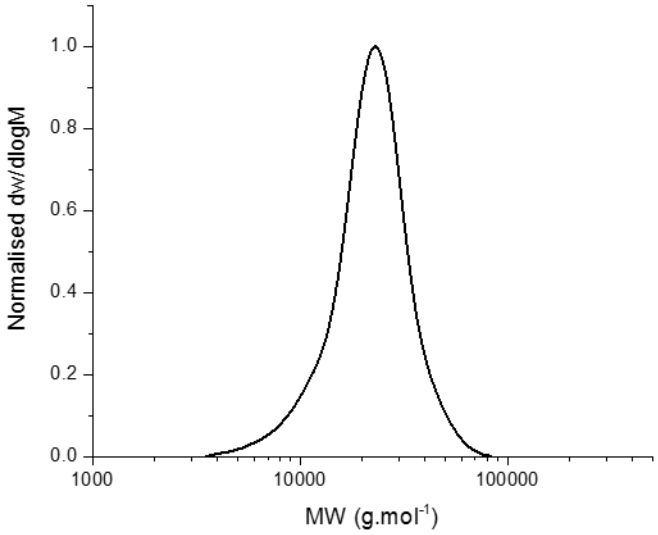

Figure 2.8. Molecular weight distribution of PTEGA-*b*-PLA_2. SEC in THF, PS calibration. †

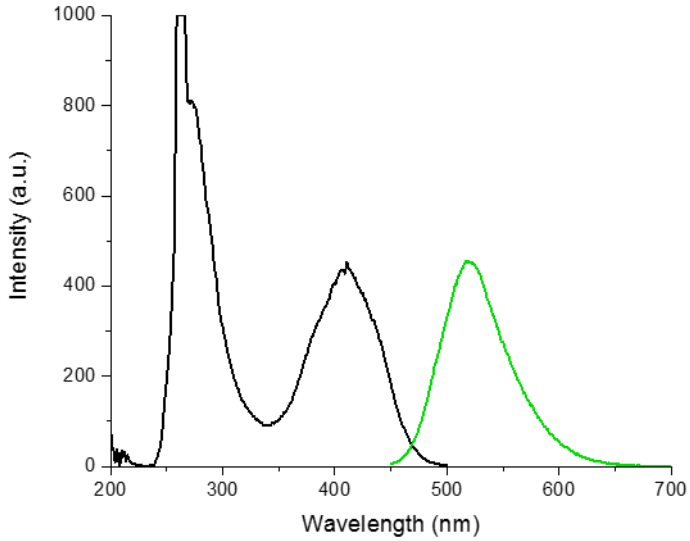

Figure 2.9. Fluorescence emission (green) and excitation (black) spectra of PTEGA-*b*-PLA_2 in chloroform at 1 mg·mL^{-1}; λ_{ex} = 410 nm and λ_{em} = 520 nm. †

The presence of a fluorescence emission peak in the same region as the initiator further confirmed the presence of the DTM moiety in the polymer.

2.3.1.2. Synthesis of the PTEGA homopolymer

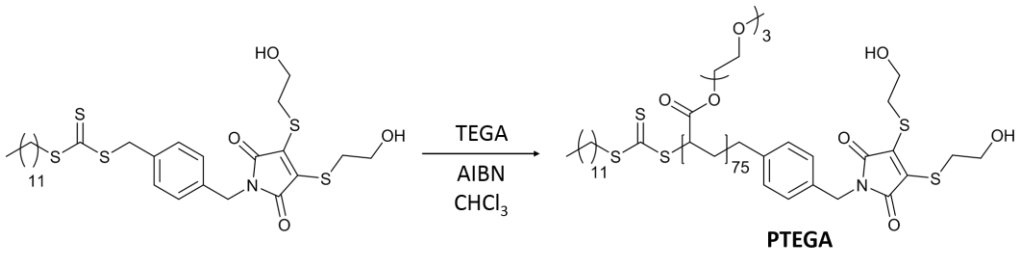

Scheme 2.2. Synthesis of the PTEGA homopolymer

A PTEGA homopolymer was synthesised for the comparison of the addition-elimination reaction on both PTEGA-*b*-PLA_2 block copolymer and PTEGA homopolymer, and the comparison of the properties of the respective products. The initiator of the block copolymer synthesis was also utilised to synthesise a PTEGA

homopolymer by RAFT polymerisation with 0.1 equivalent of AIBN for 1 equivalent of initiator and 110 equivalents of TEGA. The resulting polymer was purified by dialysis against water and analysed by ^{1}H NMR (Figure 2.10), and SEC (Figure 2.11). The polymer was found to be of a similar DP = 75 as the PTEGA block in the block copolymer presented above (DP = 87), and of a low molecular weight dispersity ($Đ$ = 1.19). $M_{n,NMR}$ = 16.2 kg·mol^{-1}, $M_{n,SEC}$ = 13.5 kg·mol^{-1}.†

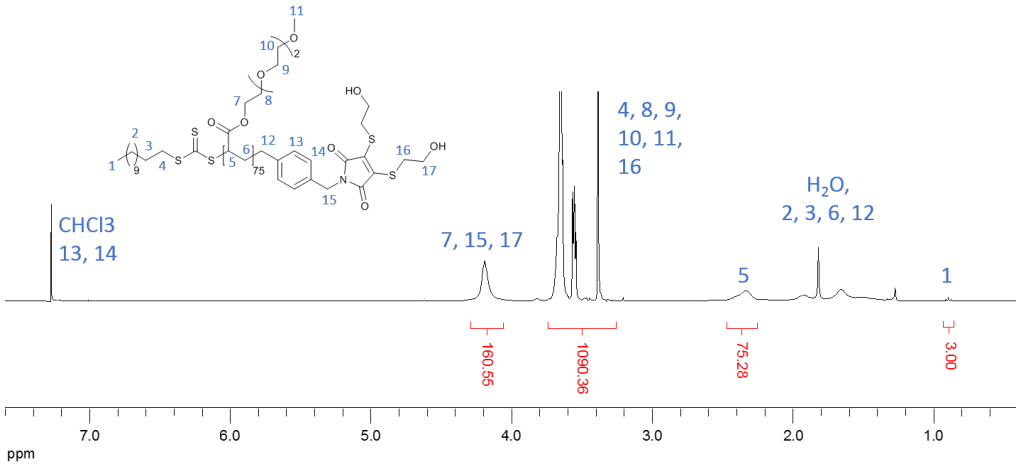

Figure 2.10. ^{1}H NMR spectrum of PTEGA ($CDCl_3$, 400 MHz).

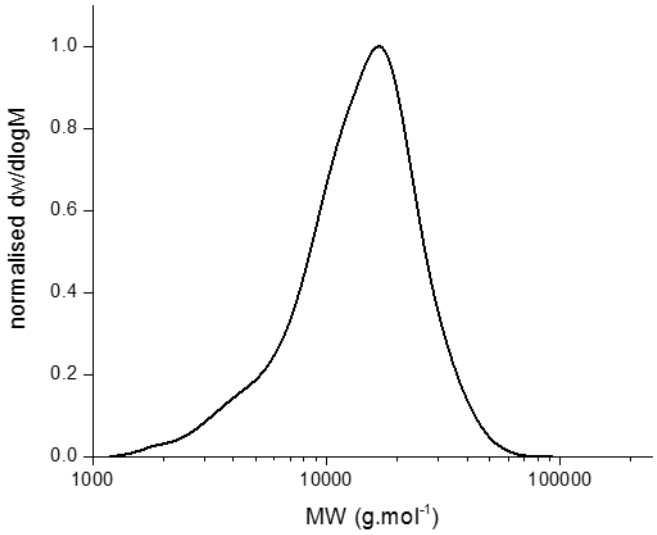

Figure 2.11. Molecular weight distribution of PTEGA. SEC in THF, PS calibration.

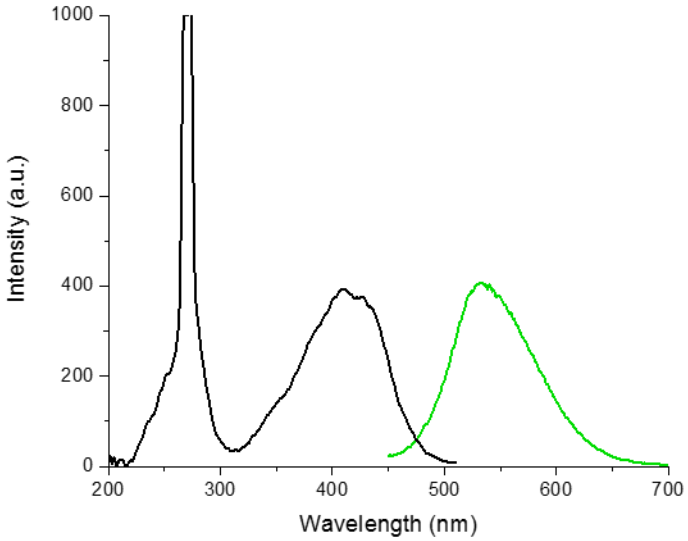

Figure 2.12. Fluorescence emission and excitation spectra of PTEGA in water at 1 mg·mL;
λ_{ex} = 415 nm and λ_{em} = 535 nm.

The comparative PTEGA was successfully synthesised with a similar DP as the PTEGA block in block copolymer PTEGA-*b*-PLA_2. The emission spectrum confirmed the presence of the DTM moiety with an emission maximum at 535 nm, which is similar to the initiator emission maximum (see insert in Figure 2.6). However, the emission intensity was low, in order to detect the emission the sensitivity of the instrument was increased (intensities of different fluorescence emission spectra cannot be compared unless the instrument parameters are kept constant).

2.3.1.3. Self-assembly of PTEGA-*b*-PLA_2

After confirming that the polymers were successfully synthesised with the DTM intact in between the two blocks, we instigated its self-assembly in water, as the polymer was composed of a hydrophilic PTEGA and two hydrophobic PLAs. It was anticipated that the DTM would reside at the interface of the hydrophilic and hydrophobic regions of the self-assembly. The copolymer self-assembly was

achieved *via* direct dissolution of the copolymer in 18.2 MΩ.cm water at a concentration of 1 mg·mL^{-1}, see Scheme 2.3.

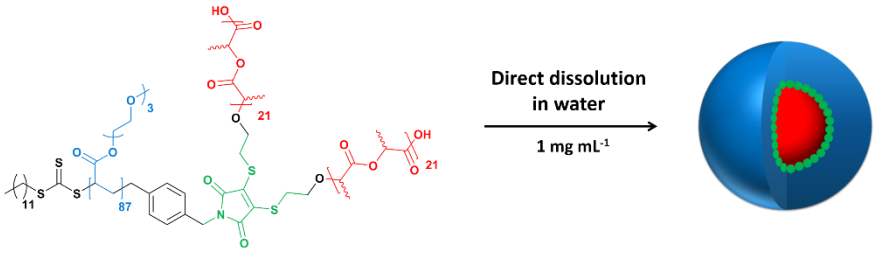

Scheme 2.3. Self-assembly of the PTEGA-*b*-PLA$_2$ amphiphilic block copolymer in water at 1 mg·mL^{-1}.

2.3.1.3.1. Fluorescence characterisation

The fluorescence excitation spectrum of the self-assembled polymer in 18.2 MΩ·cm water showed an excitation maximum at 405 nm, and an emission maximum at 510 nm as shown in Figure 2.13, these are similar to previously reported DTM polymer systems.

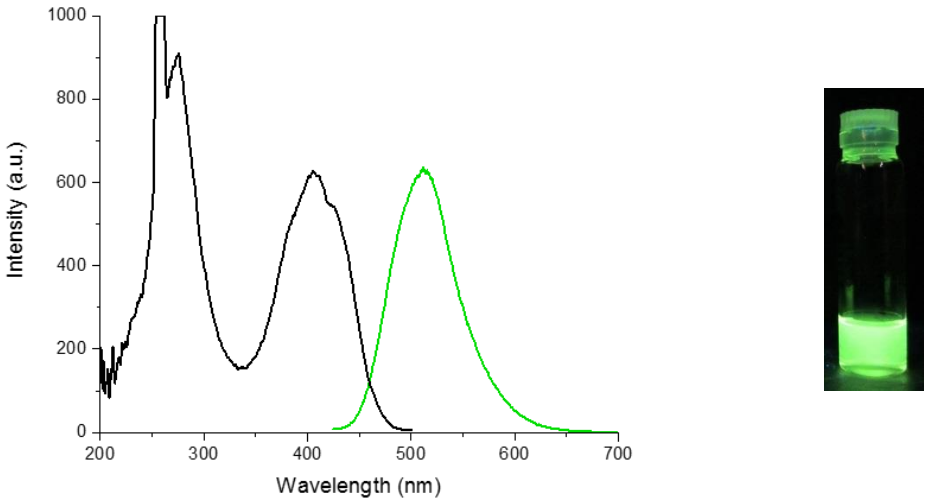

Figure 2.13. (left) Fluorescence emission and excitation spectra of micelles in water at 1 mg·mL^{-1}, λ_{ex} = 405 nm and λ_{em} = 510 nm; (right) picture of a solution of micelles in water at 1 mg·mL^{-1}, λ_{lamp} = 365 nm.

The presence of a fluorescence emission peak at a wavelength that corresponds to the emission wavelength of the copolymer confirmed the fluorescence properties of the self-assembly in water.

2.3.1.3.2. Size and morphology characterisation

The size and morphology of the self-assembled polymers in water was investigated by light scattering and microscopy analysis. Initially, DLS measurements were performed at angles from 80° to 140° for a sample of PTEGA-*b*-PLA_2 micelles at 1 mg·mL^{-1} to evaluate the angular dependence of the apparent diffusion coefficient D_{app}, see Figure 2.14. From the slope of the plot τ^{-1} vs. q^2 (Figure 2.14) D_{app} was calculated and found to be 6.13×10^{-15} m^2ms^{-1}, a value that according to the Stokes-Einstein equation (section 2.5.1) corresponds to a hard sphere with a hydrodynamic radius of 26 nm.

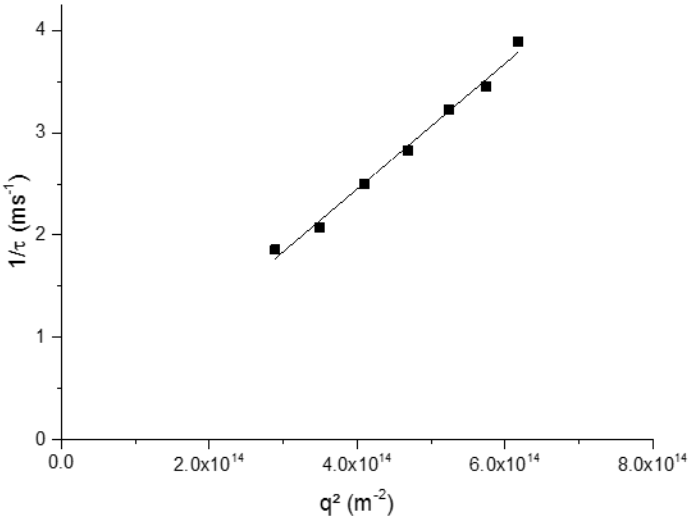

Figure 2.14. Light scattering results from the self-assembly of PTEGA-*b*-PLA_2 in water at 1 mg·mL^{-1}; Plot of τ^{-1} vs. q^2.

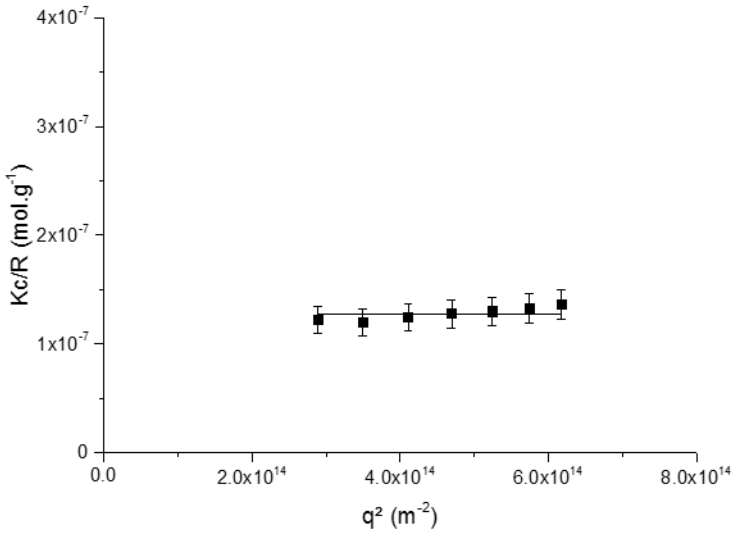

Figure 2.15. Light scattering results from the self-assembly of PTEGA-*b*-PLA_2 in water at 1 mg·mL^{-1}; Plot of $\tau^{-1}q^{-2}$ vs. q^2.

The same sample was then subjected to SLS measurements to further characterise the self-assembled polymer. The plot of Kc/R_θ vs. q^2 (Figure 2.15), showed an angular independence of Kc/R_θ within the 10% error applied to laser light scattering measurements.[31] A slight slope could be observed which was attributed to the fact that the size of the particles is close to the detection limits of the setup: for spherical particles with a radius smaller than $\lambda/20$ (*i.e.* 30 nm) there is a negligible phase difference between light emitted from various scattering centres within the particle. Thus, the scattering intensity is independent of the angle of observation, and is only dependent on the mass of the particle; in this case, a reliable radius of gyration could not be determined.

The spherical morphology of the micelles was further analysed *via* synchrotron small angle X-ray scattering (SAXS) experiments.‡ Analysis of the SAXS curves were fitted to a Guinier-Porod plot (Figure 2.16) confirmed the spherical morphology with an R_g value of 10.2 nm, such a difference with light scattering results could be explained

‡ SAXS experiment and analysis performed by Dr Anaïs Pitto-Barry.

by the hydration of the PTEGA shell, and thus the radius visible by SAXS would correspond to the radius of the core and a partial layer of the shell, the one which is denser and near the core.

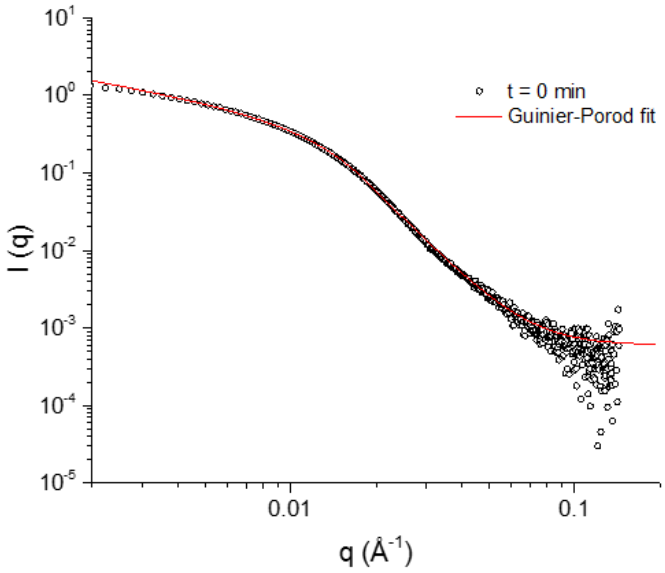

Figure 2.16. SAXS profile and Guinier-Porod fit of the solution of micelles in water at 1 mg·mL^{-1}.

Transmission electron microscopy (TEM) was also employed to determine the morphology of the assembled polymers. To achieve this, a droplet of the solution used for light scattering measurements was allowed to dry on a graphene oxide TEM grid, which owing to its low thickness allows stain-free observation of the sample (Figure 2.17).[32]

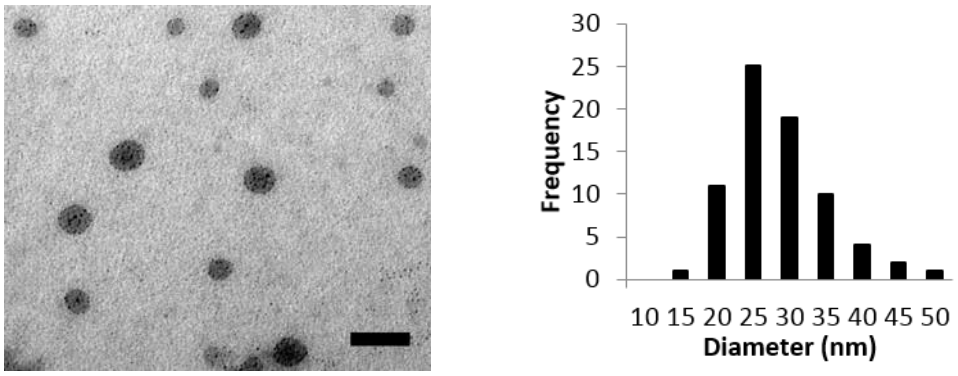

Figure 2.17. Representative TEM image of the self-assembled polymer PTEGA-*b*-PLA_2 on GO grids (scale bar = 50 nm) and size distribution of the observed particles. [§]

The average diameter of the observed particles (*ca*. 26 nm) was smaller than the hydrodynamic diameter determined from dynamic light scattering (*ca.* 52 nm). This could be attributed to fact that in dry conditions, the volume of the hydrophilic layer is reduced by the absence of water, which in DLS analysis contributes to the size of the self-assembly.

2.3.2. Reactions of the dithiomaleimide-containing polymers with thiophenol

2.3.2.1. Optimisation of the reaction

Depending on the nature of the thiol conjugated to the maleimide, the resulting DTM can be highly emissive or not, *e.g.* the fluorescence emission is drastically decreased when maleimides are directly conjugated to an aromatic ring.[19] In order to induce a dual response through one stimulus for the polymer self-assemblies, thiophenol was chosen as the chemical stimulus, as upon thiol exchange with the thio-poly(lactide) hydrophobic segment, the fluorescence was expected to be

[§] TEM image was acquired by Dr Anaïs Pitto-Barry.

reduced and the amphiphilic character of the polymer changed. The reaction conditions were first optimised utilising an analogous small molecule model system: di(thioethanol)maleimide in lieu of the polymer. The first conditions tested for this reaction were inspired from the DTM syntheses presented by Muus *et al.*[22] and Robin *et al.* [21] The first conditions utilised were 1:2:2 (DTM, thiophenol, imidazole) in THF but no conversion was observed over the 15 hours of monitoring by TLC, which could be attributed to the lack of excess of reagents. Then, the ratio were increased (1:5:5, 1:10:10) to push the reaction toward the product, but even with 1:10:10, no conversion was observed. Since the polymer was self-assembled in water, the reaction was also tested in water with a 1:10:10 ratio, some product was observed by HPLC but the conversion was too low to be isolated. The same reaction was tested without the imidazole catalyst to confirm its effect and the product was obtained with the same conversion, so the following attempts were performed without the imidazole catalyst. The ratios were further increased to 1:20 and 1:50 (DTM: thiophenol), and a drastic increase in conversion was observed.

The conclusions of these optimisation experiments were that the reaction can occur in the absence of imidazole, water seems to be a good solvent for the reaction and the optimum number of molar equivalents of thiophenol is 20 for 1 equivalent of DTM. Moreover, the reaction was monitored by HPLC and a complete consumption of the starting material (**1**) was observed 10 min after the addition. The different peaks were identified utilising purified solution of each compound, the starting material was also detectable by the HPLC fluorescence detector.

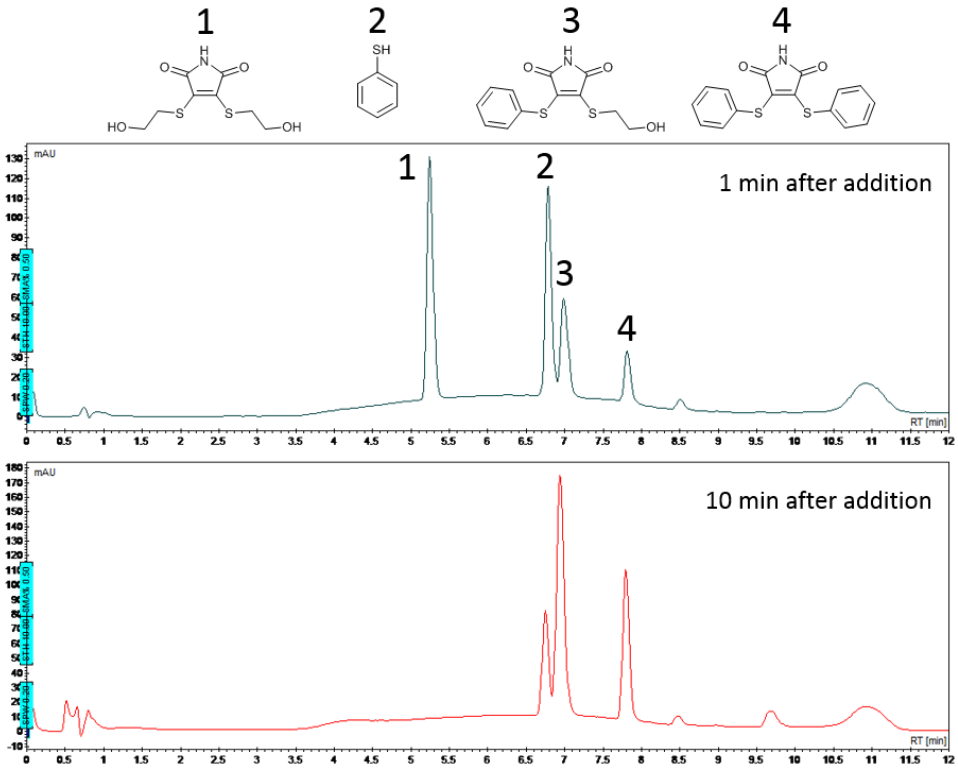

Figure 2.18. HPLC traces of the reaction mixture before the reaction and 10 min later; 1 is the starting material, 2 is thiophenol, 3 is the mono-substituted product, and 4 is the di-substituted product.†

2.3.2.2. Reaction of PTEGA-*b*-PLA$_2$ micelles with thiophenol

Based on the results obtained from the reaction of thiophenol with the small DTM model compound it was hypothesised that the optimised conditions, i.e. water, 20 equivalents of thiophenol, were suitable for the reaction of thiophenol with the DTM derivative of the micelles. The PTEGA-*b*-PLA$_2$ micelle solution was treated with 20 equivalents of thiophenol, and then purified by exhaustive dialysis (MWCO = 1 kDa) against water. It was anticipated that the addition of thiophenol to the micelle solution would result in the addition of thiophenol to the maleimide and synchronous elimination of two thiol terminated PLAs.

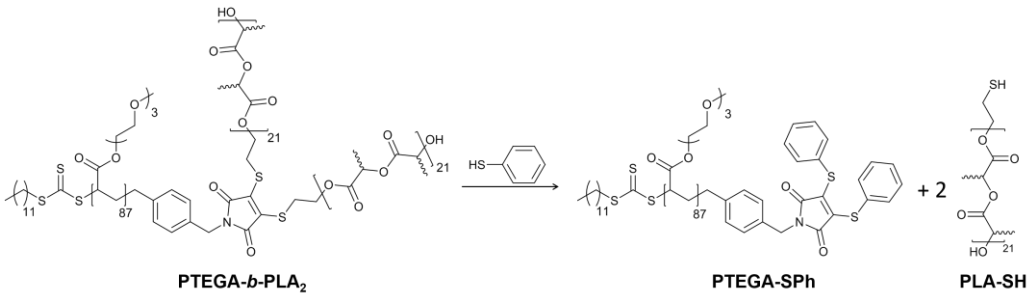

Scheme 2.4. Reaction of PTEGA-*b*-PLA_2 copolymer in water at 1 mg·mL^{-1} with thiophenol.

When the reaction was performed in water, a precipitate was observed; it was assumed this precipitate is the water-insoluble PLA. Despite the results observed with the model reaction (section 2.3.2.1), a small amount of organic solvent (dioxane, THF) was added in an attempt to improve the solubility of the detached PLA in the reaction mixture. The percentage of organic solvent in water was increased up to 20 vol%, but in all cases the PLA-SH residue was found to be insoluble in the reaction mixture. Further increase of the organic solvent ratio was found to interfere with the formation of micelles as a consequence of the increased solubility of the two blocks in the medium, thus preventing segregation and subsequent self-assembly. Therefore, the reaction was performed in water and the resultant heterogeneous solution was centrifuged to remove the precipitate which was confirmed by ^{1}H NMR spectroscopy to be mainly composed of PLA (Figure 2.19).

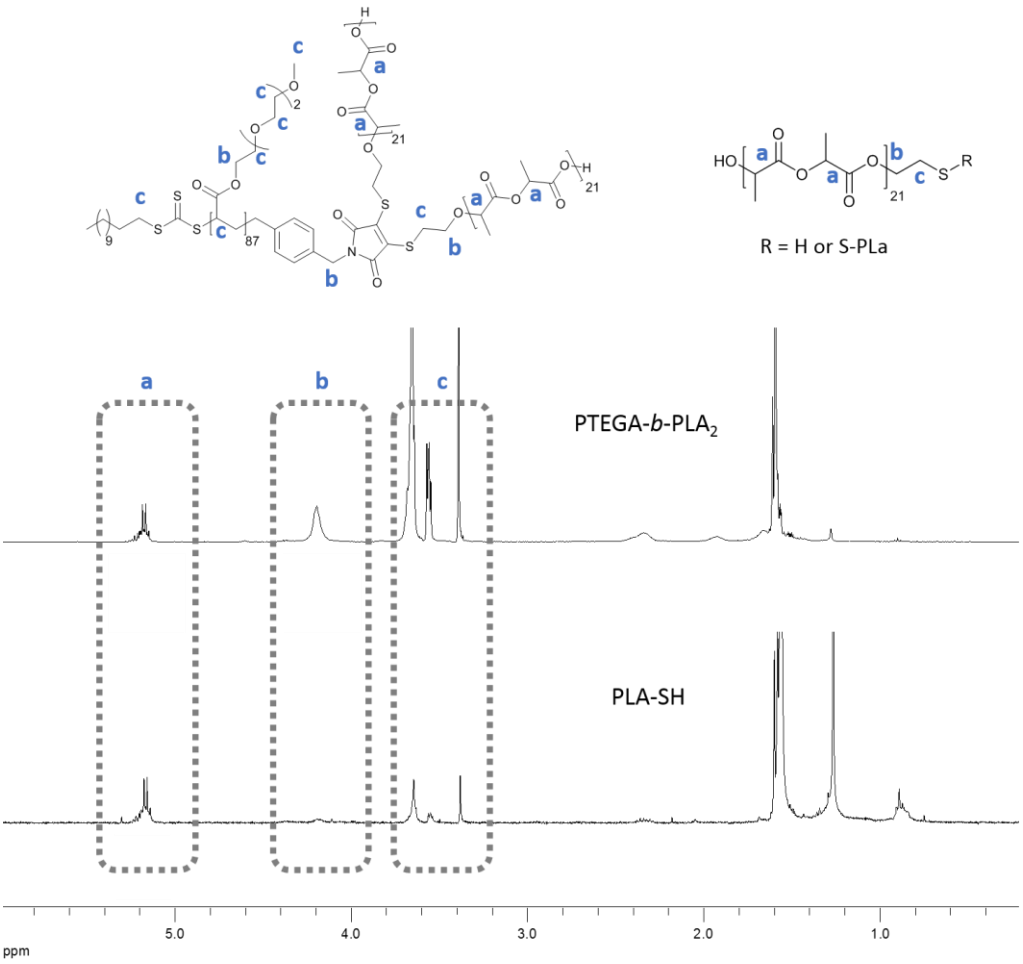

Figure 2.19. ^{1}H NMR (400 MHz, $CDCl_3$) spectrum of the PLA-SH, obtained after separation following the addition-elimination reaction compared to ^{1}H NMR spectrum of the starting block copolymer PTEGA-*b*-PLA_2. The characteristic signal of the PLA protons is highlighted at 5.2 ppm while the absence of the characteristic TEGA proton signals at 4.2 ppm is also indicated.

In order to further confirm the successful scission of the block copolymer into the corresponding homopolymers, SEC characterisation was employed to compare the chromatograms of the parent copolymer with the two isolated polymers, i.e. the dissolved polymer and the precipitate.

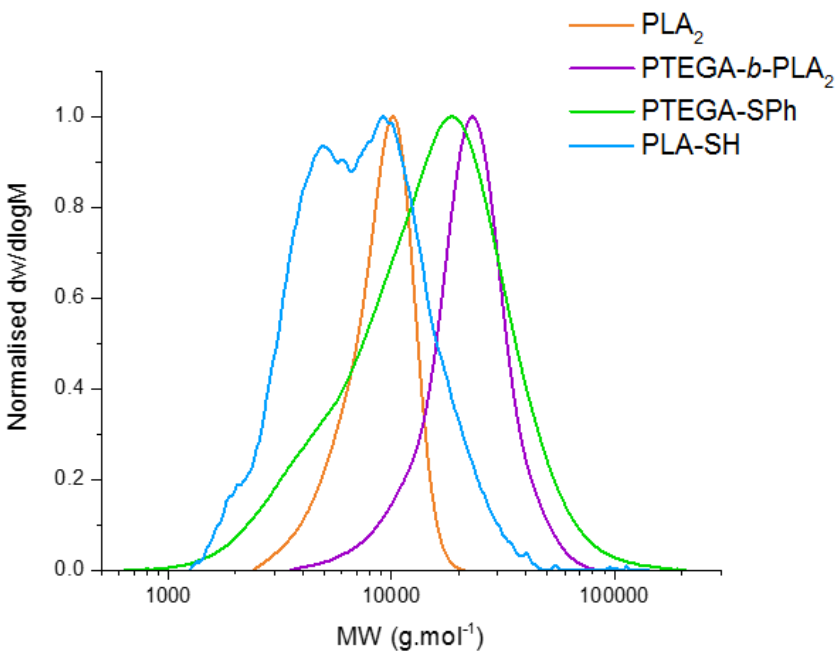

Figure 2.20. Molecular weight distributions of PLA_2, PTEGA-*b*-PLA_2, PTEGA-SPh, and PLA-SH. SEC in THF, PS calibration.

Sample	$M_{n,SEC}$ **(kg·mol^{-1})**
PLA_2	8.1
PTEGA-*b*-PLA_2	19.5
PTEGA-SPh	10

The SEC chromatograms showed a clear decrease of the molecular weight upon exposure to thiophenol (PTEGA-*b*-PLA_2 vs. PTEGA-SPh). The SEC chromatogram of the PTEGA-SPh exhibiting a tailing could correspond to residual cleaved PLA-SH. The trace of the isolated PLA precipitate showed a double peak, corresponding to half of the PLA_2 molecular weight and also an equivalent molecular weight of PLA_2, these could be attributed to the cleaved PLA-SH and possibly a disulfide bridging between two PLA-SH chains.

It was shown that the reaction of thiophenol with the DTM moiety present at the interface between the PTEGA block and the PLA_2 block was successful and the majority of the PLA residue could be removed from the reaction mixture.

2.3.2.2.1. Characterisation of the fluorescence emission upon exposure to thiophenol

Along with a structure modification, the purpose of the addition of thiophenol was also to alter the fluorescence emission of the polymer. The fluorescence emission was monitored *via* steady state fluorescence spectroscopy and time-resolved fluorescence spectroscopy.

The examination of the emission spectrum of the resultant solution of PTEGA-SPh indicated a drastic decrease of the fluorescence as a result of the modification at the DTM reactive centre. At the same excitation wavelength, the comparison of the emission spectra of the solution before and after the reaction (measured at the same concentration) showed a decrease in the intensity of the maxima (510 nm) from 730 to 30 a.u, see Figure 2.21.

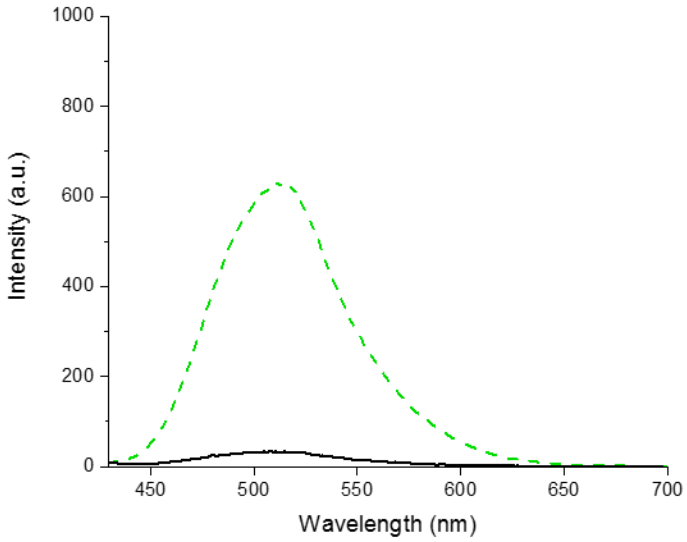

Figure 2.21. Fluorescence emission spectra before (dash line) and after the reaction (solid line) in water at 1 mg·mL^{-1}, with an excitation wavelength of 405 nm.

The decrease in fluorescence emission intensity was also monitored over time, after the addition of thiophenol, a drastic intensity decrease can be observed in less than 10 min, see Figure 2.22.

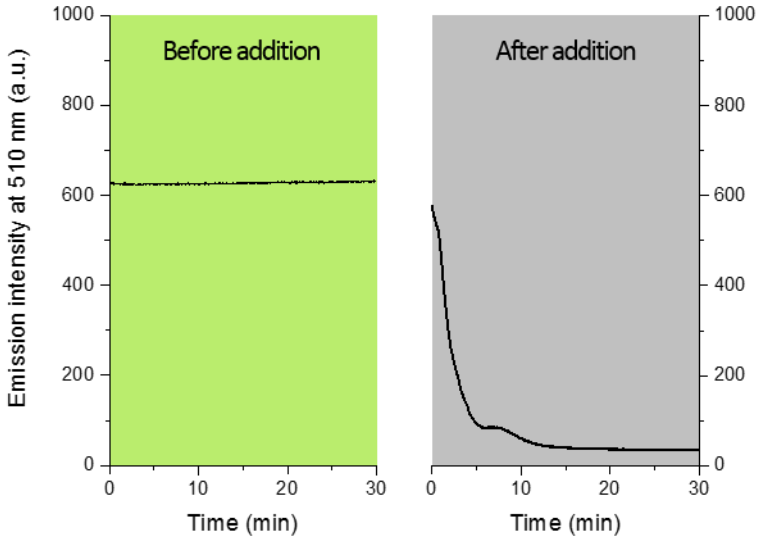

Figure 2.22. Variation of fluorescence emission maxima at 510 nm over time before and after addition of thiophenol to micelles in water at 1 mg·mL^{-1}; excitation wavelength 405nm.

The results obtained confirmed the expectation of a quick fluorescence switch off upon reaction of the copolymer PTEGA-*b*-PLA$_2$ with thiophenol.

2.3.2.2.2. Morphology transition characterisation

The expected result of the reaction was to simultaneously quench the fluorescence emission and induce the micelles' disassembly as a result of the disruption of the hydrophilic/hydrophobic balance of the self-assembled nanostructure. Instead of the expected disassembled micelles, another nanostructure was observed. This nanostructure appeared to be of a larger diameter than the starting spherical micelles. Although the structural modification was not expected, the fluorescence emission switch off occurred simultaneously.

(i) Analysis by DLS/SLS

The morphology of the assemblies obtained following the reaction of micelles with thiophenol was characterised *via* multi-angle laser light scattering.

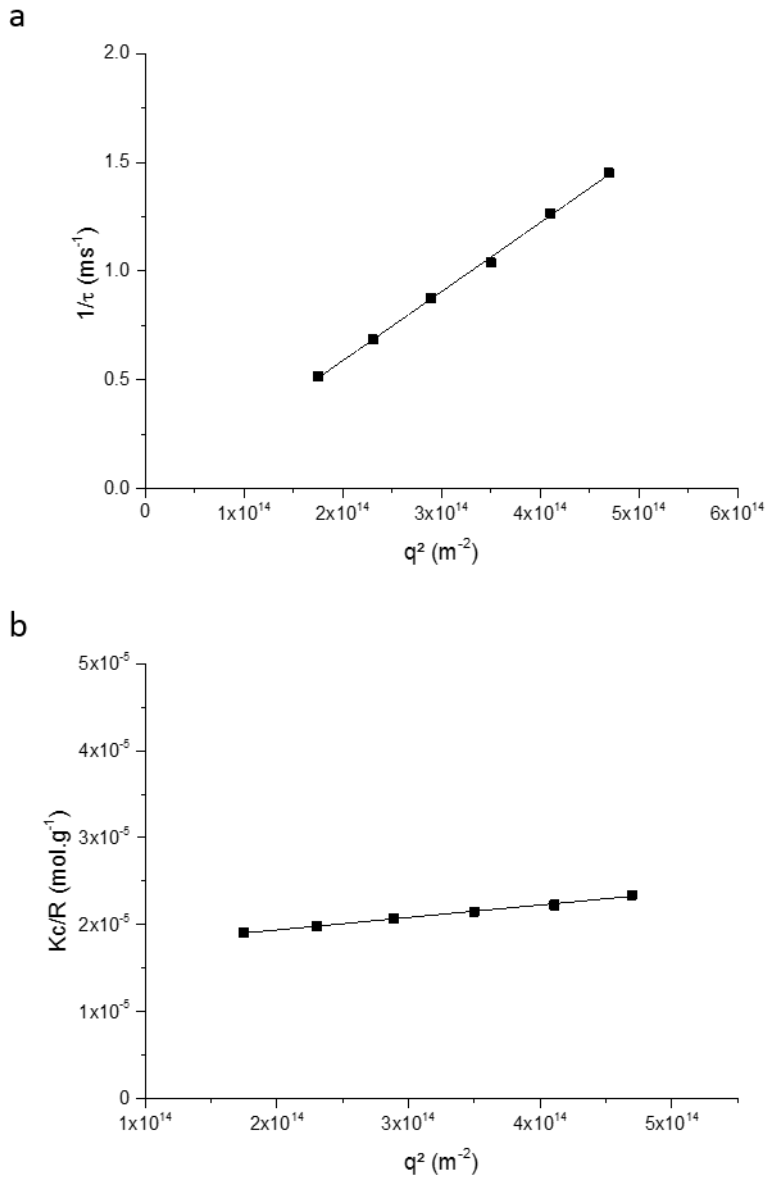

Figure 2.23. Light scattering results from the self-assembly of PTEGA-SPh in water at 2 mg·mL^{-1}; (a) Plot of τ^{-1} vs. q^2; (b) Plot of Kc/R_θ vs. q^2.

From the DLS data, the hydrodynamic radius R_h was found to be 56 nm, see Figure 2.23.c. The angular independence of the apparent diffusion coefficient showed in Figure 2.23 (a, b).

Interpretation of the data collected in static light scattering (SLS) mode, using CONTIN analysis, allowed to plot Kc/R_θ vs. q^2 (see Figure 2.23.d), which showed an angular dependence of Kc/R_θ. The radius of gyration R_g can be determined from the slope (a) of the linear regression of this plot, according to the Zimm equation:

$R_g = \sqrt{a3M_W}$ and it was found to be 51 nm.

As previously mentioned, the ratio of R_g/R_h can give an indication on the nanostructure morphology, 0.775 indicating a solid spherical micelle and 1 indicating a hollow vesicular structure.[33] In this case, R_g/R_h was calculated to be 0.91, suggesting the formation of hollow vesicular nanostructures.

It was proposed that the vesicles hydrophobic layer could be composed of both the substituted maleimide group (containing the –SPh ligands) and dodecyl end group (the RAFT agent Z-group). This was consistent with previous reports which have shown that hydrophilic polymers with hydrophobic aromatic and aliphatic end-groups can self-assemble into nanoparticles, including vesicles.[34-37]

(ii) Analysis by SAXS[**]

To further probe the proposed micelle-to-vesicle transition upon thiophenol addition, synchrotron SAXS experiments were performed. The reaction was performed in the beamline and the *in situ* kinetics of the morphology transition were examined. Analysis of the SAXS curves over a 20 minutes time period indicated a change of morphology, see Figure 2.24. An increase in the size of the morphologies in solution happened promptly (less than 10 min) and after 18 minutes, the form factor fit indicated the formation of vesicles as well as the presence of random chains in solution (PLA in solution).

[**] All SAXS experiments and analyses were performed by Dr Anaïs Pitto-Barry.

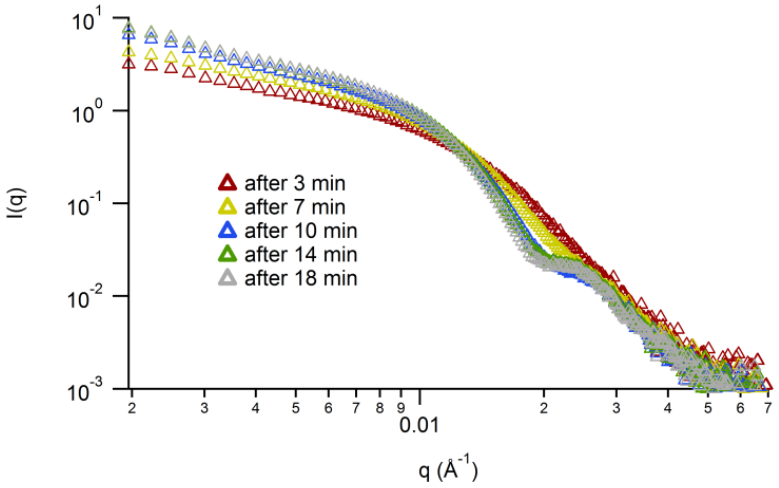

Figure 2.24. SAXS profiles for the *in situ* micelle-to-vesicle transition in water at 1 mg·mL^{-1}.

At the beginning, a spherical morphology was observed, see Figure 2.25. The Guinier-Porod fit gave an R_g value of 12 nm, and the PolyCoreForm function†† [38,39] used for this fit was considered as a uniform micelle with some dispersity (PD = 0.3), a radius of 14 nm was obtained, which fitted well with the R_g obtained with the Guinier-Porod plot. The scattering length density of the micelle was found slightly higher than usual for lactide, which suggested the incorporation of some PTEGA in this layer.

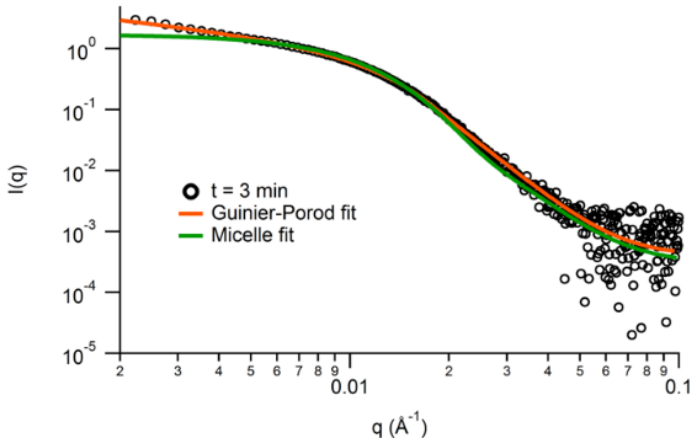

Figure 2.25. SAXS profile and fits of the reaction mixture (in water at 1 mg·mL^{-1}) at t = 3 min.

†† This function is used to calculate the form factor of polydisperse spherical particles with a core-shell scaffold.

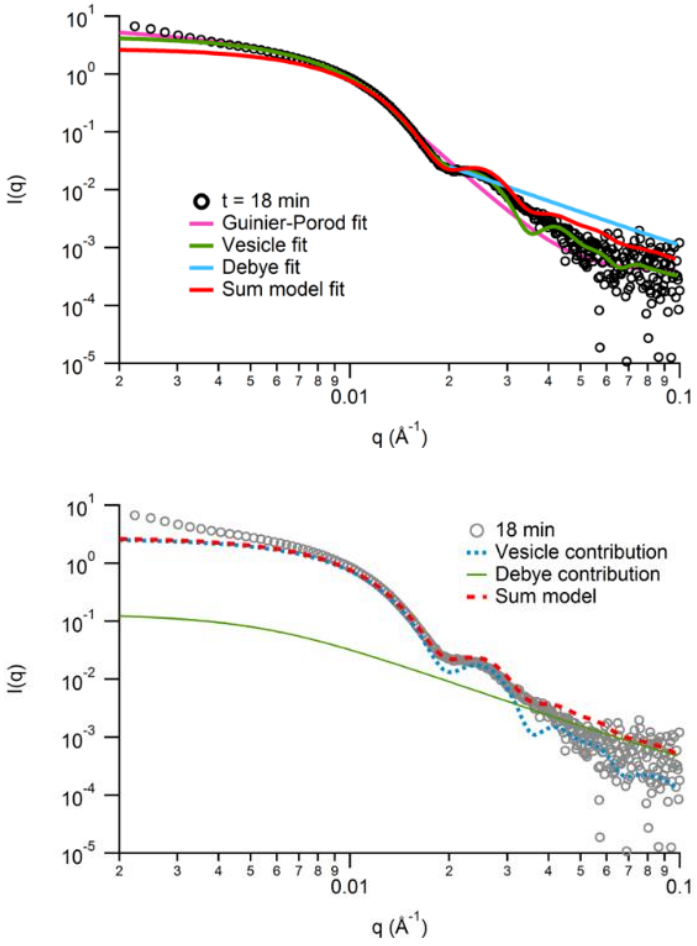

Figure 2.26. (top) SAXS profile and fits of the reaction mixture (in water at 1 mg·mL^{-1}) at t = 18 min; (bottom) SAXS data after 18 min showing the Sum model and the different contributions.

After 18 minutes, the Guinier-Porod fit gave an R_g value of 20 nm (see Figure 2.26), which was lower than the value determined by LS. Again, the hydration of PTEGA does not allow for the polymer to be entirely visible by SAXS. A PolyCoreForm function with a core-shell structure was fitted to the experimental curve for q values below 0.025 Å^{-1}, which suggested the presence of another morphology with poorly-defined form factor in the solution. This correlates well with the presence of polylactide in solution. Polylactide being hydrophobic, it tends to form collapsed coils in water, which was confirmed by a Debye fit. To further confirm the presence of these two structures in solution, a linear combination of the PolyCoreForm function with a core-shell structure and Debye fits was performed. This Sum model

confirmed the structure of vesicles with a large dispersity on the core. These vesicles seemed to have a core full of water with a radius of 4 nm and a shell of PTEGA with a thickness of 19 nm. These values were similar to the ones obtained with the PolyCoreForm function for vesicle alone, and were in good agreement with the Guinier-Porod fit. The addition of random coil polymer allowed for a better fit for *q* values above 0.025 $Å^{-1}$. The vesicle contribution was much more important at low q than the Debye one, for q above 0.015 Å, the two models contributed more equally, see Figure 2.26 (bottom). The evolution of SAXS curves and their fit at different times showed the transition, see Figure 2.27. A Guinier-Porod used for each curve provided general information on the shape and size of the sample in solution (see values in Table). The values followed a trend: bigger particles were obtained after the reaction, and they were more spherical than at the beginning of the reaction. A transition from spherical micelle to vesicle was confirmed by the change of shape of the raw data curves and the incorrect fit provided by the micelle model after 7 min.

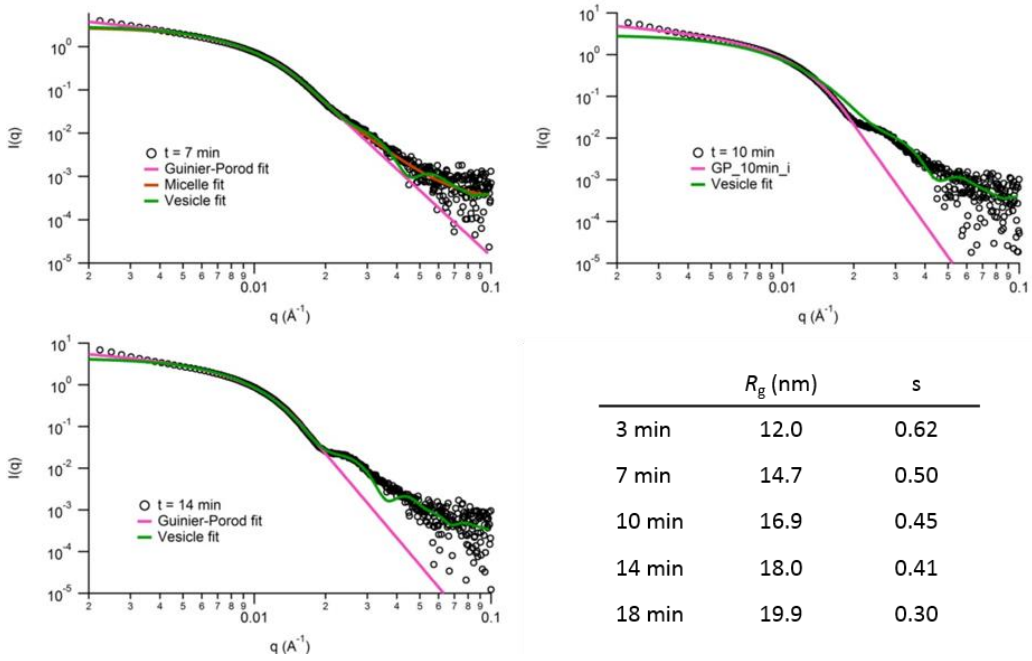

	R_g (nm)	s
3 min	12.0	0.62
7 min	14.7	0.50
10 min	16.9	0.45
14 min	18.0	0.41
18 min	19.9	0.30

Figure 2.27. SAXS curves and fit at different time points during the reaction in water at 1 mg·mL^{-1}.

(iii) TEM imaging

Unfortunately, attempts to image the vesicles by dry-state TEM, were not possible as the nanostructures were not stable to dehydration and hence no structure were observed upon drying and TEM analysis.

2.3.2.3. Model thiophenol-functional PTEGA

To further probe the vesicle formation which was observed in the micelle-to-vesicle transition (see Scheme 2.5), the addition-elimination reaction was performed on a model homopolymer.

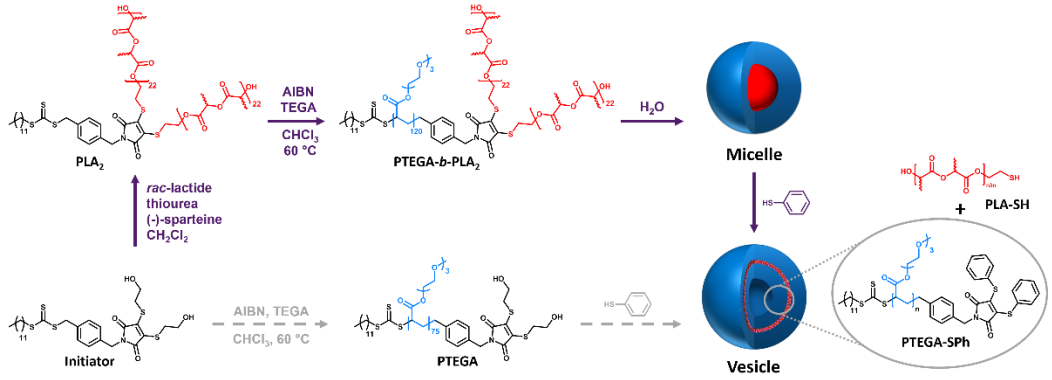

Scheme 2.5. Schematic representation of the two different routes to obtain PTEGA vesicles.

2.3.2.3.1. Characterisation of the fluorescence emission intensity decrease

The reaction of PTEGA with thiophenol would be expected to induce a fluorescence emission decrease. Indeed, the comparison of the emission spectra before and after the reaction showed the clear decrease in intensity, see Figure 2.28.

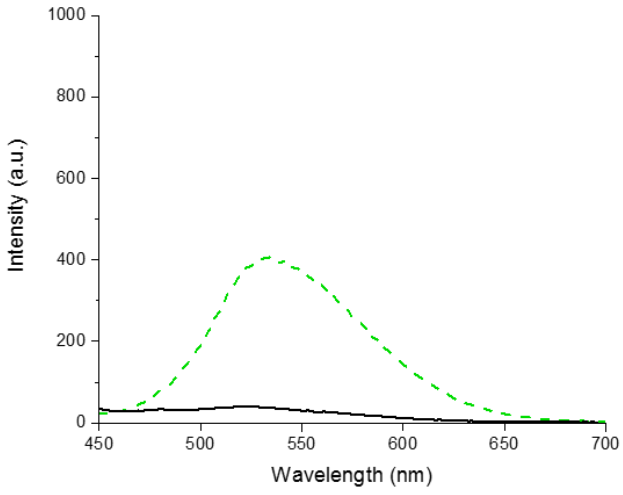

Figure 2.28. Fluorescence emission spectra before (dash line) and after the reaction (solid line) in water at 1 mg·mL^{-1}, excitation wavelength at 415 nm.

As observed for the addition-elimination reaction with the micelles, the fluorescence emission of the homopolymer solution again underwent a fast on-to-off switch (15 min by analysis of the 535 nm emission) during the reaction with thiophenol, see Figure 2.29.

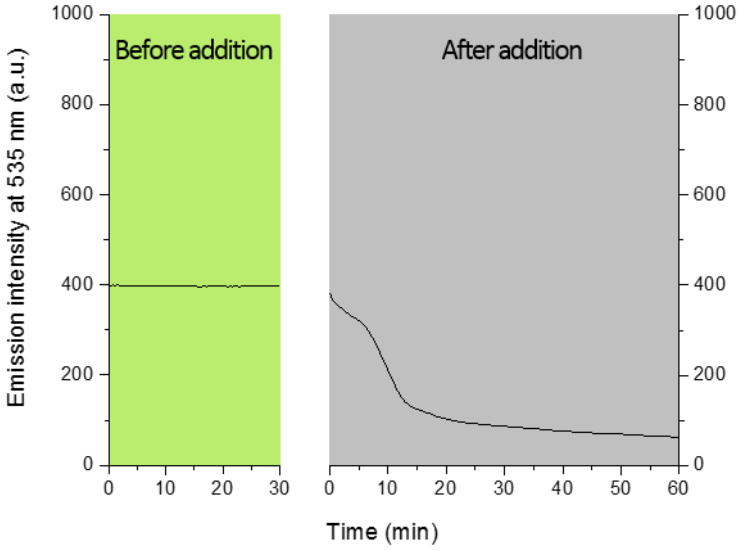

Figure 2.29. Variation of the fluorescence emission maxima at 535 nm over time before and after the reaction in water at 1 mg·mL^{-1}; excitation wavelength 415 nm.

Similarly to the reaction of PTEGA-*b*-PLA$_2$ micelles with thiophenol, the reaction of the PTEGA homopolymer with thiophenol resulted in the same fluorescence emission decrease.

2.3.2.3.2. Characterisation of the self-assembly

The product of the reaction of PTEGA and thiophenol being the same as the product of the reaction of PTEGA-*b*-PLA$_2$ with thiophenol, the potential formation of a nanostructure was also investigated. DLS analysis of aqueous solutions of the initial PTEGA homopolymer (which possesses α-diol and ω-dodecyl end-groups), indicated the presence of unimers in solution. However, after the addition-elimination reaction between PTEGA and an excess of thiophenol, well-defined

nanostructures were observed, MA-LLS was performed, and values of R_g and R_h were extracted from the results.

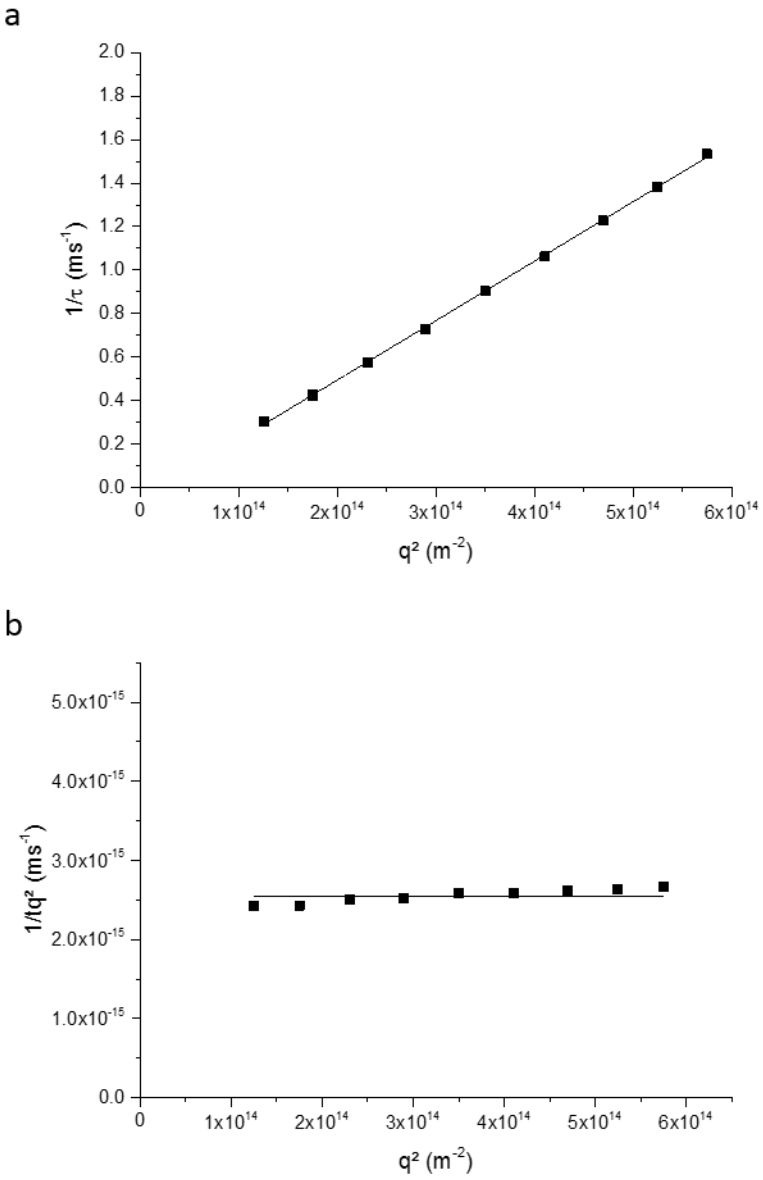

Figure 2.30. Light scattering results from the self-assembly of PTEGA-SPh in water at 1 mg·mL^{-1}; (a) Plot of τ^{-1} vs. q^2, (b) Plot of Kc/R_θ vs. q^2.

By interpreting the data collected in SLS mode (see Figure 2.30), R_g was found to be 63 nm. From the DLS data, R_h was calculated utilising the Zimm equation and found to be 68 nm. Hence the R_g/R_h obtained was 0.93, which once again suggested that the nanostructures formed in this reaction were vesicles. Similarly to the vesicles previously observed, resulting from the reaction of the PTEGA-*b*-PLA$_2$ micelles with

thiophenol, the reaction of the PTEGA homopolymer with thiophenol formed self-assemblies of a similar size and morphology. This is understandable as the addition-elimination reaction of PTEGA-*b*-PLA_2 and PTEGA would be expected to give the same resultant homopolymer, namely PTEGA-SPh homopolymer with α-SPh and ω-dodecyl end-groups, which would be expected to assembly into similar morphologies, as showed in Scheme 2.5.

2.4. Conclusions

A fluorescence on-to-off emission switch simultaneously with a fast micelle-to-vesicle morphology transition were presented. The transition's triggering reaction was an addition-elimination: an excess of thiophenol reacting with the DTM present at the hydrophilic/hydrophobic interface; eliminating the hydrophobic block. The suggested driving force for the formation of vesicles was the combination of both end-groups hydrophobicity. A unimer-to-vesicle transition also occurred for a DTM group-containing homopolymer as the end-group was modified *via* the same triggering reaction. These experiments highlighted the high reactivity of the DTM functional group toward thiols present in its environment and the ability to switch the fluorescence emission depending on the DTM substituents. This versatile system could be tuned for utilisation of different aromatic thiol and could be used for release monitoring in self-assembled systems. Further investigation into tuning the system to obtain a fluorescence emission switch-on simultaneously with the disassembly of the vesicle could extend the potential of the system.

2.5. Experimental

2.5.1. Materials and methods

Chemicals were used as received from Aldrich, Fluka and Acros. Dry solvents were obtained by passing over a column of activated alumina using an Innovative Technologies solvent purification system. TEGA was synthesised by Mathew Robin as previously reported and stored below 4 °C.[40]

^{1}H and ^{13}C NMR spectra were recorded on a Bruker DPX-400 spectrometer in $CDCl_3$. Chemical shifts are given in ppm downfield from the internal standard tetramethylsilane (TMS).

Size exclusion chromatography (SEC) measurements were conducted using a Varian 390-LC-Multi detector suite fitted with differential refractive index (DRI), light scattering (LS) and photodiode array (PDA) detectors equipped with a guard column (Varian Polymer Laboratories PLGel 5 μm, 50×7.5 mm) and two mixed D columns (Varian Polymer Laboratories PLGel 5 μm, 300×7.5 mm). The mobile phase was either tetrahydrofuran (THF) with 2% triethylamine (TEA) at 40 °C operating at a flow rate of 1.0 ml·min^{-1} and data was analysed using Cirrus v3.3 with calibration curves produced using Varian Polymer laboratories Easi-Vials linear poly(styrene) or poly(methyl)methacrylate standards.

Multi-angle Laser Light Scattering (MA-LLS) measurements were performed at angles of observation ranging from 30° up to 150° with an ALV CGS3 setup operating at λ_0 = 632 nm and at 25 ± 1 °C, the data was collected with 100 s run time in duplicate unless otherwise specified. Calibration was achieved with filtered toluene and the background was measured with 18.2 MΩ.cm water. Electric field autocorrelation functions (g_1 (q,t)) were fitted with CONTIN. In DLS mode, the apparent diffusion coefficient of the particles (D_{app}) is determined from the relaxation time (τ) for a

specific concentration (see equation 2.1). The hydrodynamic diameter R_h is calculated using the Stokes-Einstein equation (2.2), in which k_B is the Boltzmann constant, T the temperature and η the viscosity. In SLS mode, the Zimm equation (2.3) allows determination of different parameters: the radius of gyration (R_g), the particle's molecular weight (M_w) and the second virial coefficient (A_2).

$$\tau^{-1} = D_{app}q^2 \tag{2.1}$$

$$R_h = \frac{k_B T}{6\pi\eta D_0} \tag{2.2}$$

$$\frac{Kc}{R_\theta} = \frac{q^2 {R_g}^2}{3M_W} + \frac{1}{M_W} + 2A_2c \tag{2.3}$$

Synchrotron small-angle X-ray scattering (SAXS) measurements were carried on the SAXS/WAXS beamline at the Australian Synchrotron facility at a photon energy of 11 keV. The samples in solution were run by using a 1.5 mm diameter quartz capillary. Temperature was held at 25 °C and controlled *via* a water bath connected to a brass block which is part of the sample holder. The measurements were collected at a sample to detector distance of 7.323 m to give a q range of 0.02 to 0.14 $Å^{-1}$. All patterns were normalised to fixed transmitted flux using a quantitative beamstop detector. The scattering from a blank was measured in the same capillary and was subtracted for each measurement. The two-dimensional SAXS images were converted into one-dimensional SAXS profile (*I(q)* versus q) by circular averaging, where *I(q)* is the scattering intensity. The functions used for the fitting from the NIST SANS analysis package were "Guinier-Porod",[41,42] "Debye"[43] and "PolyCoreForm".[38] ScatterBrain[44] and Igor[45] were used to plot and analyse the data. The scattering length density of the solvent and the monomers were calculated using

the "Scattering Length Density Calculator"[46] provided by NIST Centre for Neutron Research. Limits for *q* range were applied for the fittings from 0.002 to 0.1 Å $^{-1}$.

Solutions of graphene oxide were synthesised as reported previously. Aqueous solutions of graphene oxide (0.10 mg.mL^{-1}) were sonicated for 30 s prior to use. Lacey carbon grids (400 Mesh, Cu) (Agar Scientific) were cleaned using air plasma from a glow-discharge system (2 min, 20 mA). The TEM grids were placed on a filter paper and one drop (≈ 0.08 mL) of the sonicated GO solution was deposited onto each grid from a height of ≈ 1 cm, allowing the filter paper to absorb the excess solution, and the grids were left to air-dry in a dessicator cabinet for ≈ 60 min. 4 µL of the nanoparticle dispersion (~20 ppm) was pipetted onto a GO grid and left to air-dry in a dessicator cabinet for ≈ 60 min. Bright field TEM images were captured with a transmission electron microscope (JEOL TEM-2011), operating at 200 kV.

Fluorescence spectra were recorded using a Perkin-Elmer LS 55 Fluorescence Spectrometer.

2.5.2. Specific safety procedures

All work with thiols was carried out in an efficient fume cupboard and on the smallest scale possible. Disposable gloves were used, changed regularly. All materials (gloves, paper towels, glassware) utilised to work with thiol were decontaminated with the thiol killing solution.[47-49]

Sulfide Oxidiser (thiol killing solution):

% by weight: 3% cyclohexane, 82% water, 5% sodium dodecyl sulfate, 10% butan-1-ol, 1 ml of sulfide in 15 ml of microemulsion. Add 5% aqueous sodium hypochlorite solution (undiluted bleach) in 2-fold excess. Takes approximately 15 seconds to kill smell.

2.5.3. Synthetic procedures

2.5.3.1. Dual RAFT/ROP initiator synthesis

The synthesis of the initiator was concluded in four steps, the three first steps are based on procedures from the literature.[19,21,50]

2.5.3.1.1. First step

Synthesised as reported by Petzetakis *et al.*[50]

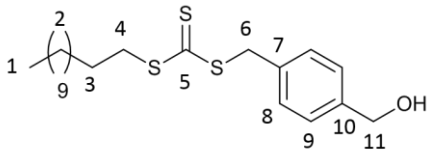

For the first step, potassium phosphate (3.725 g, 17.5 mmol) was dissolved in acetone (300 mL) with carbon disulphide (3 mL, 49.5 mmol) and dodecanethiol (3.8 mL, 15.9 mmol) and the reaction was stirred for 2 hours at room temperature. Then, 4-(chloromethyl)benzyl alcohol (2.5 g, 15.9 mmol) was added to the mixture and stirred for 24 h at room temperature. The solvent was removed under vacuum and the solid was dissolved in DCM (200 mL). The organic layer wash washed with HCl (1M, 150 mL x 2), water (3 x 150 mL), brine (150 mL), dried with $MgSO_4$ and filtered. The solvent was evaporated under vacuum. The crude product was a yellow solid which was washed with hexanes (200 mL x 3). The pure product is a yellow solid (3.49 g, 55 %). ^{1}H NMR (400 MHz, $CDCl_3$) δ 7.35-7.30 (4H, m, H8 & H9), 4.67 (2H, s, H11), 4.61 (2H, s, H6), 3.36 (2H, t, J = 7.5 Hz, H4), 1.73-1.66 (3H, m, H3 & H12), 1.43-1.26 (18H, m, H2), 0.88 (3H, t, J = 7.0 Hz, H1).

2.5.3.1.2. Second step

Synthesised as reported by Robin *et al.*[21]

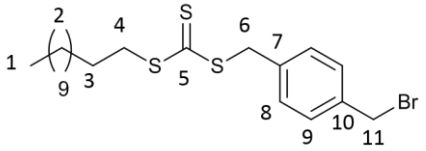

For the second step, the yellow solid (3.4 g, 8.53 mmol) was dissolved in dry diethyl ether (75mL) and dry dimethylformamide (15mL) at 0 °C, then was added phosphorous tribromide (0.8 mL, 8.53 mmol). The reaction was stirred under inert N_2 atmosphere at room temperature for 3 hours. The crude product was added to diethyl ether (100 mL) and washed with sodium hydrocarbonate (3 x 100 mL), water (2 x 100 mL) and brine (100 mL). The organic layer was dried with $MgSO_4$ and the solvent was removed in under vacuum. The crude product was purified *via* column chromatography (30:1 pet. ether : ethyl acetate). The pure product is a yellow solid (2.81 g, 71 %). Rf = 0.77. ^{1}H NMR (300 MHz, $CDCl_3$) δ 7.35-7.30 (4H, m, H8 & H9), 4.60 (2H, s, H6), 4.47 (2H, s, H11), 3.37 (2H, t, ^2J = 7.5 Hz, H4), 1.75-1.65 (2H, quin., ^2J = 7.5 Hz, H3), 1.43-1.26 (18H, m, H2), 0.88 (3H, t, J = 7.0 Hz, H1).

2.5.3.1.3. Third step

Synthesised as reported by Robin *et al.*[21]

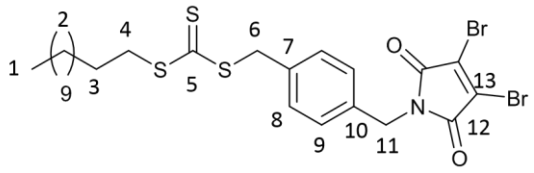

For the third step, the yellow solid from the second step (2.8 g, 6.1 mmol) was dissolved in acetone (45 mL), 2,3-dibromomaleimide (1.7 g, 6.7 mmol) and crushed anhydrous potassium carbonate (0.92 g, 6.7 mmol) were added to the mixture. The reaction was stirred at room temperature for 24 hours. The solvent was removed

under vacuum. The crude product was added to DCM (100 mL) and washed with water (3 x 100 mL) and brine (2 x 100 mL). The organic layer was dried with $MgSO_4$ and the solvent was removed under vacuum. The crude product was purified *via* a column chromatography (gradient 1:2 DCM: pet. ether then 2:3 DCM: pet. ether and finally 1:1 DCM: pet. ether). The pure product is a yellow solid (1.36 g, 35 %). ^{1}H NMR (400 MHz, $CDCl_3$) δ 7.33-7.28 (4H, m, H8 & H9), 4.72 (2H, s, H11), 4.58 (2H, s, H6), 3.36 (2H, t, ^2J = 7.5 Hz, H4), 1.73-1.65 (2H, quin., ^2J = 7.5 Hz, H3), 1.41-1.26 (18H, m, H2), 0.88 (3H, t, J = 7.0 Hz, H1).

2.5.3.1.4. Fourth step

Synthesis as reported by Robin *et al.*[19]

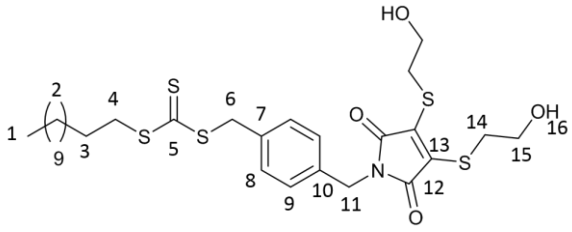

For the last step, the yellow solid from the third step (0.7 g, 1.1 mmol) was dissolved in THF (10 mL) and cooled to 0 °C. TEA (0.38 mL, 2.75 mmol) and mercaptoethanol (0.19 mL, 2.75 mmol) were added to the mixture. The reaction was stirred for 3 hours, allowing to warm to room temperature. The solvent was removed under vacuum, the crude product was dissolved in DCM (150 mL) and washed with water (2 x 100 mL) and brine (100 mL). The product was purified *via* a column chromatography (1:2 pet. ether: ethyl acetate). The pure product is a yellow solid (0.25 g, 35 %). Rf = 0.47. ^{1}H NMR (400 MHz, $CDCl_3$) δ 7.30-7.28 (4H, m, H8 & H9), 4.63 (2H, s, H11), 4.58 (2H, s, H6), 3.83 (4H, t, ^2J = 6.0 Hz, H15), 3.47 (4H, t, ^2J = 6.0 Hz, H14), 3.36 (2H, t, ^2J = 7.5 Hz, H4), 1.73-1.65 (2H, quin., ^2J = 7.5 Hz, H3), 1.59 (2H, m, H16), 1.41-1.26 (18H, m, H2), 0.88 (3H, t, J = 7.0 Hz, H1) ; ^{13}C NMR δ223.6 (C5),

166.2 (C12), 136.4 (C13), 135.4 (C7), 135.1 (C10), 129.6 (C8), 128.7 (C9), 62.1 (C15), 41.9 (C11), 40.8 (C6), 37.1 (C4), 34.7 (C14), 32-22 (C2-3), 14.1 (C1) ; (MaXis) m/z found 652.1688, calc. 652.1688 (M+Na, 100 %) ; FTIR ν3258 cm^{-1} (alcohol), 1763 cm^{-1} (maleimide), 1700 cm^{-1} (maleimide), 1524 cm^{-1} (aromatic), 1466cm^{-1} (aromatic) ; Fluorescence in methanol λ_{em} = 545 nm, λ_{ex} = 450 and 370 nm.

2.5.3.2. Polymer syntheses

2.5.3.2.1. Polylactide block, PLA_2

The PLA was synthesised by ring opening polymerisation (ROP), this reaction has been set up in the glove-box to be free of water. A thiourea/sparteine co-catalyst system was used as previously reported.[28]

The dual RAFT/ROP initiator (70 mg, 0.11 mmol) dissolved in dry DCM (2 mL) was added to a mixture of *rac*-lactide (0.641 g, 4.4 mmol) and thiourea catalyst (82.3 mg, 0.22 mmol) in dry DCM (4.41 mL). Then (-)-sparteine (25.5 µL, 0.11 mmol) was added and the reaction was stirred at room temperature for 2 hours to a monomer conversion > 99%. Out of the glove-box, the resultant polymer was precipitated in hexane (200 mL) and filtered. The crude polymer was dissolved in CH_2Cl_2 and precipitated in hexane (200 mL). The polymer was purified *via* a prep GPC column (Bio-beads). The pure polymer is a yellow solid (0.5293 g, 74 %). $M_{n,SEC}$ = 8.1 g·mol^{-1} ; $M_{n,NMR}$ = 6.7 kg·mol^{-1}; $Đ$ = 1.13, see Table 2.1 for the details. Fluorescence in $CHCl_3$ λ_{em} = 520 nm, λ_{ex} = 410 and 275 nm. ^{1}H NMR spectrum shown in Figure 2.4, molecular weight distribution shown in Figure 2.5 and fluorescence spectra shown in Figure 2.6.

2.5.3.2.2. PTEGA-b-PLA_2 block copolymer

PLA_2 (25 mg, 3.7 µmol, 1 eq.), TEGA (79.9 µL, 0.4 mmol, 110 eq.), AIBN (261 µg, 0.1 eq.), $CDCl_3$ (240 µL) were added to a polymerisation ampoule. The solution was degassed by three freeze-pump-thaw cycles, the ampoule was sealed under N_2 and the reaction was stirred at 60 °C. A conversion sample was taken at the end of the reaction. The product as purified by dialysis (MWCO 6-8000 Da) against distilled water and dried by lyophilisation. The pure polymer is a yellow oil. $M_{n,NMR}$ = 25.7 kg·mol^{-1}, $M_{n,SEC}$ = 19.5 kg·mol^{-1}, $Đ$ = 1.21, see Table 2.1 for the details. ^{1}H NMR spectrum shown in Figure 2.7, molecular weight distribution shown in Figure 2.8 and fluorescence spectra shown in Figure 2.9.

2.5.3.2.3. PTEGA homopolymer

The initiator (10 mg, 1 eq.), TEGA (0,343 mL, 110 eq.), AIBN (261 µg, 0.1 eq.) were dissolved in $CHCl_3$ and added to a polymerisation ampoule. The solution was degassed by three freeze-pump-thaw cycles, then sealed under N_2 and the reaction was stirred at 60 °C for 16 hours. The polymer was purified by dialysis (MWCO 6,000-8,000 Da) against DI water and dried by lyophilisation. The pure polymer is a yellow oil. $M_{n,NMR}$ = 16.2 kg·mol^{-1}, $M_{n,SEC}$ = 13.5 kg·mol^{-1}, $Đ$ = 1.19, see Table 2.1 for the details. ^{1}H NMR spectrum shown in Figure 2.10, molecular weight distribution shown in Figure 2.11 and fluorescence spectra shown in Figure 2.12.

Table 2.1. Characteristic of the different polymers synthesised.

polymer	Conv.	M_{th} (kg·mol^{-1})	$M_{n,NMR}$ (kg·mol^{-1})	$M_{n,SEC}$ (kg·mol^{-1})	$Đ$	DP
PLA_2	>99%	6.4	6.7	8.1	1.13	42
PTEGA-*b*-PLA_2	82%	33.1	25.7	19.5	1.21	87-42
PTEGA	95%	24.6	16.2	13.5	1.19	75

2.5.3.3. Reaction of the self-assembled PTEGA-*b*-PLA_2 with thiophenol

20 Equivalents of thiophenol were added to the solution of self-assembled PTEGA-*b*-PLA_2. The reaction was stirred at room temperature for 1 h. The mixture was purified *via* exhaustive dialysis (MWCO = 1000 Da) against 18.2 MΩ.cm water to remove the excess thiophenol, centrifuged to separate the precipitate PLA-SH and freeze-dried. The resultant solid PTEGA-SPh was re-suspended at 1 $mg{\cdot}mL^{-1}$ to give a solution of vesicles.

2.5.3.4. Reaction of the PTEGA homopolymer with thiophenol

The PTEGA homopolymer was dissolved in 18.2 MΩ.cm water at 1 $mg{\cdot}mL^{-1}$ and 20 equivalents of thiophenol were added to the solution. The reaction was stirred at room temperature for 1 h. The mixture was purified *via* exhaustive dialysis (MWCO = 1,000 Da) against 18.2 MΩ.cm water to remove the excess of thiophenol and freeze-dried. The resultant solid PTEGA-SPh was re-suspended at 1 $mg{\cdot}mL^{-1}$ to give a solution of vesicles.

2.6. Notes

† This symbol was used to tag materials synthesised and characterised during Master's degree project.

2.7. References

1. A. B. Mabire, M. P. Robin, H. Willcock, A. Pitto-Barry, N. Kirby and R. K. O'Reilly, *Chem. Commun.*, 2014, **50**, 11492-11495.

2. Y. Mai and A. Eisenberg, *Chem. Soc. Rev.*, 2012, **41**, 5969-5985.

3. A. Blanazs, S. P. Armes and A. J. Ryan, *Macromol. Rapid Commun.*, 2009, **30**, 267-277.

4. K. E. B. Doncom, L. D. Blackman, D. B. Wright, M. I. Gibson and R. K. O'Reilly, *Chem. Soc. Rev.*, 2017, **46**, 4119-4134.

5. A. O. Moughton and R. K. O'Reilly, *Chem. Commun.*, 2010, **46**, 1091-1093.

6. J.-Z. Du, H.-Y. Long, Y.-Y. Yuan, M.-M. Song, L. Chen, H. Bi and J. Wang, *Chem. Commun.*, 2012, **48**, 1257-1259.

7. A. Klaikherd, C. Nagamani and S. Thayumanavan, *J. Am. Chem. Soc.*, 2009, **131**, 4830-4838.

8. C. L. McCormick, B. S. Sumerlin, B. S. Lokitz and J. E. Stempka, *Soft Matter*, 2008, **4**, 1760-1773.

9. F. Chécot, S. Lecommandoux, Y. Gnanou and H.-A. Klok, *Angew. Chem. Int. Ed.*, 2002, **41**, 1339-1343.

10. C. Chang, H. Wei, J. Feng, Z.-C. Wang, X.-J. Wu, D.-Q. Wu, S.-X. Cheng, X.-Z. Zhang and R.-X. Zhuo, *Macromolecules*, 2009, **42**, 4838-4844.

11. W. Kim, J. Thévenot, E. Ibarboure, S. Lecommandoux and E. L. Chaikof, *Angew. Chem. Int. Ed.*, 2010, **49**, 4257-4260.

12. M. Lazzari and M. A. López-Quintela, *Adv. Mater.*, 2003, **15**, 1583-1594.

13. G. Gaucher, M.-H. Dufresne, V. P. Sant, N. Kang, D. Maysinger and J.-C. Leroux, *J. Control. Release*, 2005, **109**, 169-188.

14. Z. L. Tyrrell, Y. Shen and M. Radosz, *Prog. Polym. Sci.*, 2010, **35**, 1128-1143.

15. K. Miyata, R. J. Christie and K. Kataoka, *React. Funct. Polym.*, 2011, **71**, 227-234.

16. E. G. Kelley, J. N. L. Albert, M. O. Sullivan and T. H. Epps, *Chem. Soc. Rev.*, 2013, **42**, 7057-7071.

17. M. Elsabahy and K. L. Wooley, *Chem. Soc. Rev.*, 2012, **41**, 2545-2561.

18. M. E. B. Smith, F. F. Schumacher, C. P. Ryan, L. M. Tedaldi, D. Papaioannou, G. Waksman, S. Caddick and J. R. Baker, *J. Am. Chem. Soc.*, 2010, **132**, 1960-1965.

19. M. P. Robin, P. Wilson, A. B. Mabire, J. K. Kiviaho, J. E. Raymond, D. M. Haddleton and R. K. O'Reilly, *J. Am. Chem. Soc.*, 2013, **135**, 2875-2878.

20. M. P. Robin, A. B. Mabire, J. C. Damborsky, E. S. Thom, U. H. Winzer-Serhan, J. E. Raymond and R. K. O'Reilly, *J. Am. Chem. Soc.*, 2013, **135**, 9518-9524.

21. M. P. Robin, M. W. Jones, D. M. Haddleton and R. K. O'Reilly, *ACS Macro Lett.*, 2011, **1**, 222-226.

22. U. Muus, C. Hose, W. Yao, T. Kosakowska-Cholody, D. Farnsworth, M. Dyba, G. T. Lountos, D. S. Waugh, A. Monks, T. R. Burke Jr and C. J. Michejda, *Biorg. Med. Chem.*, 2010, **18**, 4535-4541.

23. L. M. Tedaldi, A. E. Aliev and J. R. Baker, *Chem. Commun.*, 2012, **48**, 4725-4727.

24. L. M. Tedaldi, M. E. B. Smith, R. I. Nathani and J. R. Baker, *Chem. Commun.*, 2009, **43**, 6583-6585.

25. M. J. Ruedas-Rama, J. D. Walters, A. Orte and E. A. H. Hall, *Anal. Chim. Acta*, 2012, **751**, 1-23.

26. F. Canfarotta, M. J. Whitcombe and S. A. Piletsky, *Biotechnol. Adv.*, 2013, **31**, 1585-1599.

27. S. M. Janib, A. S. Moses and J. A. MacKay, *Adv. Drug Del. Rev.*, 2010, **62**, 1052-1063.

28. R. C. Pratt, B. G. G. Lohmeijer, D. A. Long, P. N. P. Lundberg, A. P. Dove, H. Li, C. G. Wade, R. M. Waymouth and J. L. Hedrick, *Macromolecules*, 2006, **39**, 7863-7871.

29. G. Moad, E. Rizzardo and S. H. Thang, *Aust. J. Chem.*, 2009, **62**, 1402-1472.

30. A. P. Dove, *ACS Macro Lett.*, 2012, **1**, 1409-1412.

31. O. Colombani, M. Ruppel, M. Burkhardt, M. Drechsler, M. Schumacher, M. Gradzielski, R. Schweins and A. H. E. Müller, *Macromolecules*, 2007, **40**, 4351-4362.

32. J. P. Patterson, A. M. Sanchez, N. Petzetakis, T. P. Smart, T. H. Epps, I. Portman, N. R. Wilson and R. K. O'Reilly, *Soft Matter*, 2012, **8**, 3322-3328.

33. J. P. Patterson, M. P. Robin, C. Chassenieux, O. Colombani and R. K. O'Reilly, *Chem. Soc. Rev.*, 2014, **43**, 2412-2425.

34. T. Liu, W. Tian, Y. Zhu, Y. Bai, H. Yan and J. Du, *Polym. Chem.*, 2014, **5**, 5077-5088.

35. J. Du, H. Willcock, J. P. Patterson, I. Portman and R. K. O'Reilly, *Small*, 2011, **7**, 2070-2080.

36. J. P. Patterson, E. G. Kelley, R. P. Murphy, A. O. Moughton, M. P. Robin, A. Lu, O. Colombani, C. Chassenieux, D. Cheung, M. O. Sullivan, T. H. Epps and R. K. O'Reilly, *Macromolecules*, 2013, **46**, 6319-6325.

37. J. Xu, L. Tao, C. Boyer, A. B. Lowe and T. P. Davis, *Macromolecules*, 2010, **44**, 299-312.

38. P. Bartlett and R. H. Ottewill, *J. Chem. Phys.*, 1992, **96**, 3306-3318.

39. NIST, Center for Neutron Research, SANS Model Function Documentation, ftp://ftp.ncnr.nist.gov/pub/sans/kline/Download/SANS_Model_Docs_v4.10.pdf.

40. F. Hua, X. Jiang, D. Li and B. Zhao, *J. Polym. Sci., Part A: Polym. Chem.*, 2006, **44**, 2454-2467.

41. A. Guinier and G. Fournet, *Small-angle scattering of X-rays*, John Wiley & Sons, New York, 1955.

42. O. Glatter and O. Kratky, *Small-Angle X-Ray Scattering*, Academic Press, 1982.

43. R.-J. Roe, *Methods of X-ray and Neutron Scattering in Polymer Science*, Oxford University Press, New York, 2000.

44. S. T. Mudie, *scatterBrain*, Australian Synchrotron, (v1.15), 2013

45. S. Kline, *J. Appl. Crystallogr.*, 2006, **39**, 895-900.

46. NIST, Center for Neutron Research, SLD calculator, www.ncnr.nist.gov/resources/sldcalc.html.

47. University of Warwick, Department of Chemistry, Handbook 2016, www2.warwick.ac.uk/fac/sci/chemistry/chemintra/safety/handbook/.

48. F. M. Menger and M. J. Rourk, *Langmuir*, 1999, **15**, 309-313.

49. F. M. Menger and A. R. Elrington, *J. Am. Chem. Soc.*, 1991, **113**, 9621-9624.

50. N. Petzetakis, A. P. Dove and R. K. O'Reilly, *Chem. Sci.*, 2011, **2**, 955-960.

Chapter 3

Aminomaleimide fluorophores

3.1. Abstract

This chapter presents the synthesis of a library of amino-substituted maleimides: a new class of highly emissive compounds, with large Stokes shifts (>100 nm) and high fluorescence quantum yields (up to ~60%). The emission of this dye is responsive to its environment with both a red-shift, and quenching, observed in protic polar solvents. These compounds can easily be functionalised and provide a versatile fluorescent probe. This new class of fluorophore can be divided in two main subcategories, the monoaminomaleimides (MAMs) and the aminobromomaleimides (ABMs), depending on the precursor utilised, see Figure 3.1.*

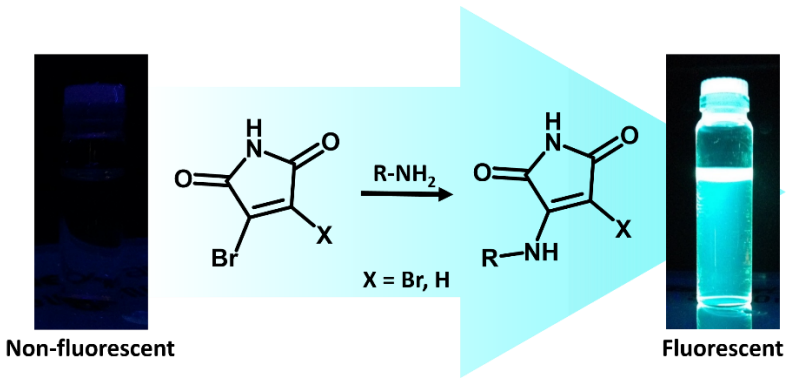

Figure 3.1. Schematic representation of the synthesis of aminomaleimide and pictures of the reagent and product.[1]

* MAMs were synthesised and analysed by Dr Mathew Robin.

3.2. Introduction

Fluorophores play an important role as probes in biological systems, for imaging, and for the study of dynamic processes.[2-8] These choices of application result from the high sensitivity and ease of measurement for fluorescence emission, and the responsiveness of dyes to the physical nature of their environment – for example solvatochromism. A solvatochromic shift is observed when the absorption and emission wavelengths shift depending on the solvent polarity.[9] The response of fluorophores to chemical stimuli is also highly desirable, and is frequently utilised in the study of conjugation to biological macromolecules.[10] One mechanism for response is the conversion of a latent quenched fluorophore to an emissive fluorophore upon the application of the desired chemical stimulus.[11,12] Quenching occurs both with direct conjugation of maleimide to fluorophore (as a consequence of maleimide's low lying nπ* state providing a non-radiative pathway for excited state decay[13-15]) and also where maleimide and fluorophore are joined by a spacer group (as a consequence of photo-induced electron transfer (PET) to the C=C double bond).[16-18] By this process, *N*-fluorophore maleimides have been used as fluorescent probes for the detection of thiols such as cysteine, homocysteine and glutathione. Bis-maleimides have been used to allow detection of bis-thiols (including reduced disulfides),[19-21] and maleimide-functional probes have been used for protein labelling[22] and both single and two-photon imaging of cells where they allow detection of thiol functional peptides.[19,21,23-26] Response to chemical stimuli can also be achieved when the reaction of two non-fluorescent species leads to the generation of a fluorophore. For example the highly efficient tetrazole-alkene/azirine-alkene cycloaddition results in an emissive pyrazoline product.[27] This cycloaddition reaction has been used to fluorescently label proteins both *in vitro* and

within live cells,[28-30] and for the construction of labelled polymer conjugates with silicon and cellulose surfaces,[31-33] and with proteins (PEGylation).[34]

An alternative fluorophore-generating reaction was previously reported in our group, whereby the addition of two equivalents of an alkyl thiol to 2,3-dibromomaleimide (DBM) generates the dithiomaleimide (DTM) fluorophore, see Scheme 3.1.[35] In these compounds rather than quenching emission, the maleimide forms the fluorophoric centre. This off-to-on emission switch upon thiol addition has been used in protein labelling (including disulfide bridging),[35] polymer and polymer nanoparticle labelling,[35-39] and the formation of polymer-protein conjugates.[35] Furthermore, as a consequence of the reversibility of thiol addition to DBM[40] the alkyl thiols of emissive DTMs can be replaced with aromatic thiols, the result being the formation of a non-emissive DTM. This on-to-off switch has been used as an indicator of polymer nanostructure morphology transition.[37]

Previous reports have shown that incorporation of the maleimide group into extended π-systems gives a range of dyes with fluorescence quantum yields (Φ_f) of up to 100%, emission maxima ranging from 460-680 nm, and often large Stokes shifts (> 100 nm).[41-46] There are also scattered reports of emissive maleimides with heteroatom substitutions,[47-49] although a thorough investigation has been lacking.

The ability to form a fluorophore by amino-substitution of a bromomaleimide is of particular interest as a consequence of the prevalence and availability of amine groups in biological substrates.

3.3. Results and discussion

3.3.1. Synthesis of aminomaleimides

A library of monoaminomaleimides (MAMs) and aminobromomaleimides (ABMs) was constructed. These compounds were synthesised through an addition-elimination reaction with monobromomaleimide (MBM) or 2,3-dibromomaleimide (DBM), see Scheme 3.1.

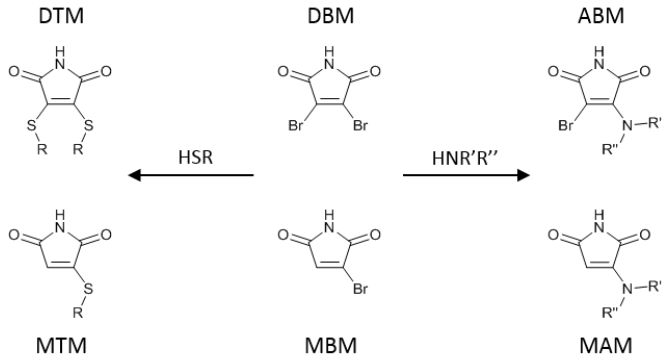

Scheme 3.1. Reaction of DBM or MTM with thiols or amines to obtain DTM, MTM, ABM, or MAM.

The first objective was to compare the previously reported dithiomaleimide fluorophore with the novel aminomaleimide compounds. The thiomaleimides used for the purpose of this comparison were dithiobutylmaleimide (**DTM-1**) and monothiobutylmaleimide (**MTM-1**), see Figure 3.2 for structures. Four model compounds were synthesised with different substituents, including butylamine (**ABM-1** and **MAM-1**), which allowed a direct comparison with the DTM compounds; and diethylamine, (**ABM-2** and **MAM-2**), to observe the difference between a secondary amine and a tertiary amine product (see Figure 3.2 for structures).

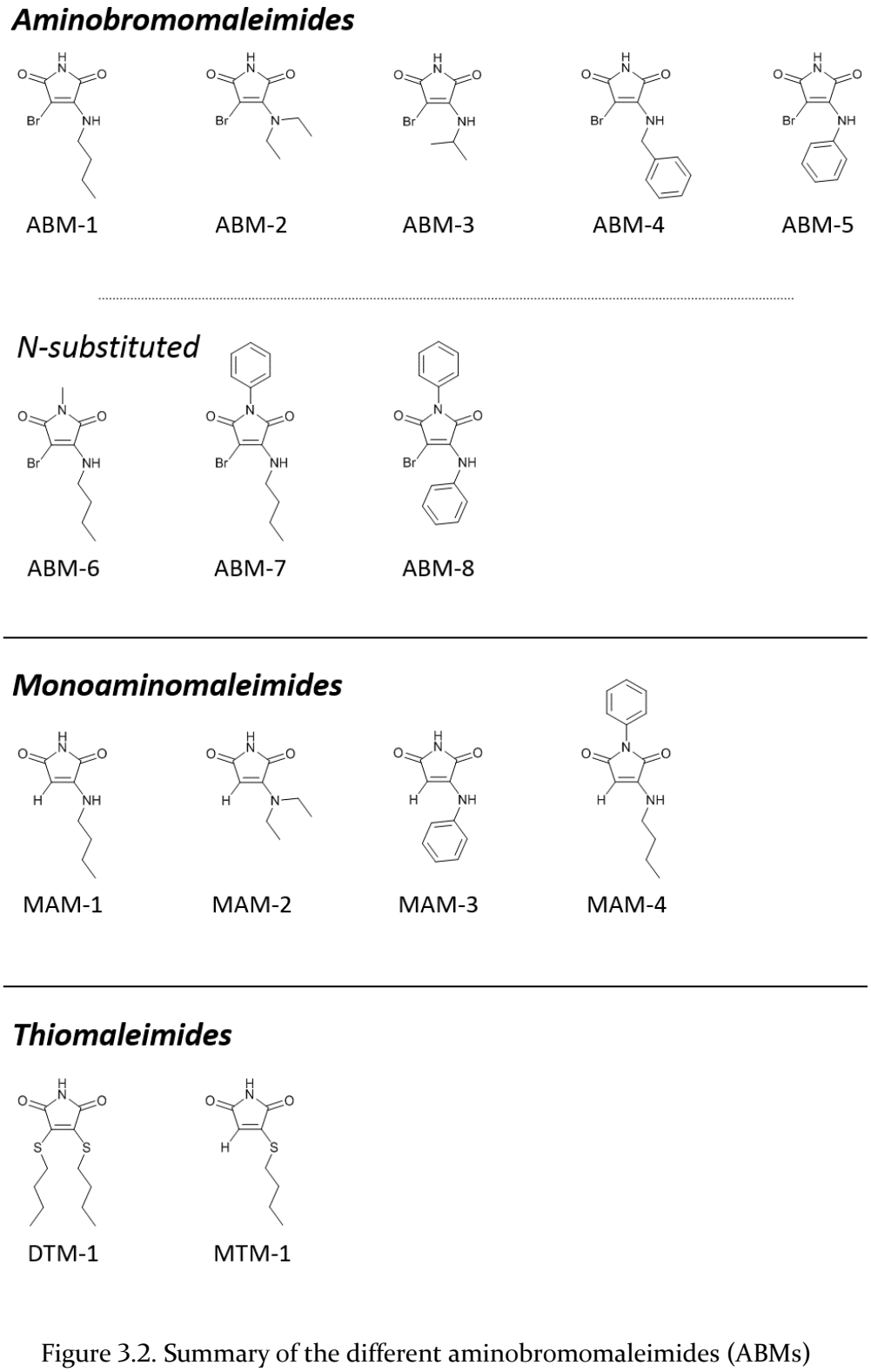

Figure 3.2. Summary of the different aminobromomaleimides (ABMs) synthesised, their monoaminomaleimide (MAM) homologues, and thiomaleimides (dithiomaleimide (DTM), and monothiomaleimide (MTM)).

Awuah and Capretta developed a method to synthesise a library of substituted maleimides including amino-substituted maleimides.[50] They demonstrated that under mild conditions with an excess of amine, only the monoaminated maleimide can be formed (with microwave irradiation required to achieve a second substitution). Therefore, as the maleimide undergoes a single amine substitution only, the second substituent of the C=C double bond can be retained; bromine or hydrogen depending on the reactant used (DBM or MBM), see Scheme 3.1, and Scheme 3.2 for an example mechanism.

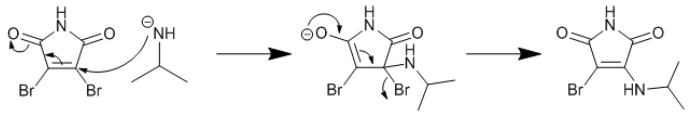

Scheme 3.2. Example of an ABM synthesis mechanism (DBM and isopropylamine) to obtain **ABM-3**.

All reactions were performed in tetrahydrofuran at room temperature with a small excess of amine, and sodium carbonate as a base. Reactions were completed within 0.5-2 hours. The resultant mixture was washed and purified *via* column chromatography on silica gel. The product was obtained with a yield ranging from 11% to 79%. The structures were confirmed by ^{1}H NMR spectroscopy, ^{13}C NMR spectroscopy, mass spectrometry and IR spectroscopy, see Experimental, section 3.5.3.

3.3.2. Spectroscopic properties of aminomaleimides compared to thiomaleimides

In order to compare spectroscopic properties, absorption, excitation and emission spectra were recorded, the extinction coefficient and the fluorescence quantum yield were calculated, and the brightness (being a function of both fluorescence quantum yield and extinction coefficient: $B = \Phi_f \times \varepsilon$) was then deduced.

The fluorescence quantum yield (Φ_f) is one of the most important parameters to compare fluorophores. It allows calculation of the efficiency of the conversion of absorbed photons into emitted photons. The quantum yields quoted below were determined following the protocol presented by Resch-Genger and co-workers.[51] The use of a standard, which has a known quantum yield under specific conditions, is necessary to determine fluorescent quantum yields. The standard is chosen depending on its absorption and emission wavelength range, which should respectively correspond to the sample's absorption and emission wavelengths. In the case of aminomaleimides and thiomaleimides, the most appropriate standard was quinine sulfate dihydrate in solution in 0.105 M perchloric acid, with a quantum yield of 59%.

3.3.2.1. Thiomaleimide models

The thiomaleimides **DTM-1** and **MTM-1** (see Figure 3.2 for structures) had different spectroscopic properties. **DTM-1** showed an emission maximum at 504 nm for excitation maxima at 262 nm and 405 nm in 1,4-dioxane, see Figure 3.3. Peaks at $\lambda_{ex} = \lambda_{em}$ are the result of Rayleigh scattering from the sample solution. An increase of the solvent polarity also generated a red-shifting of the fluorescence emission maximum, from 486 nm in cyclohexane to 504 nm in 1,4-dioxane and 546 nm in methanol.

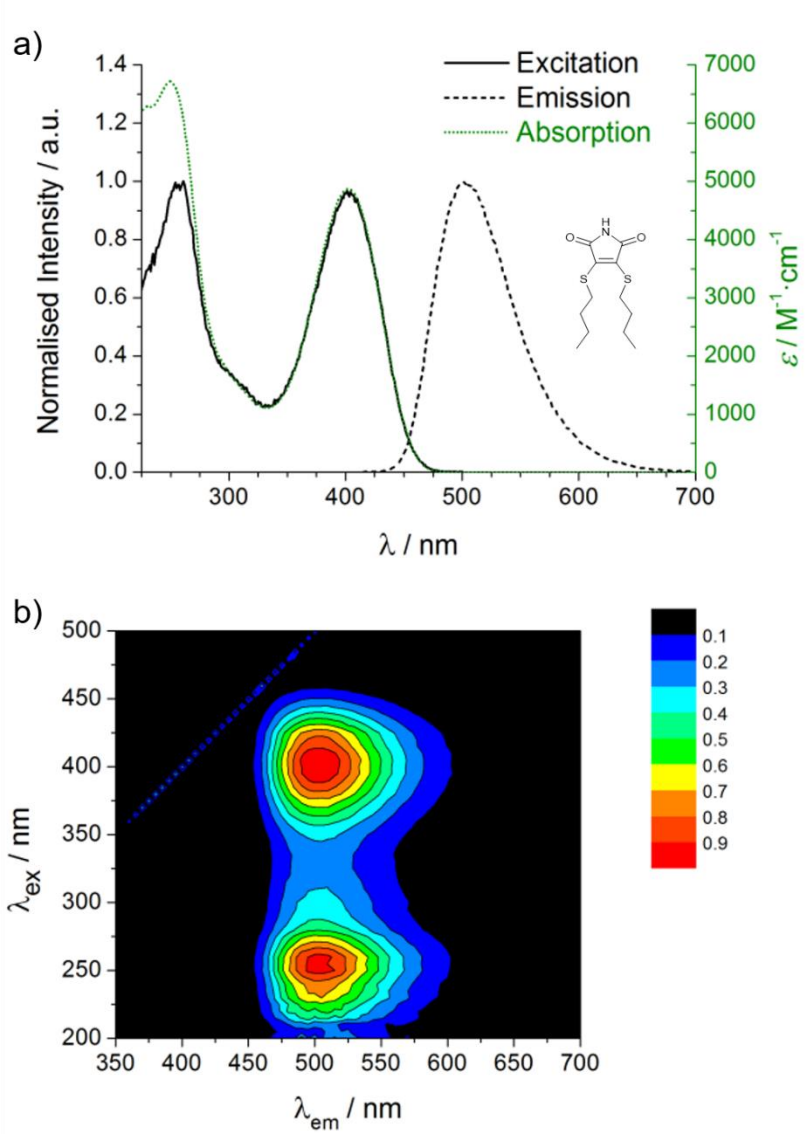

Figure 3.3. a) Excitation, emission and absorption spectra of **DTM-1** in 1,4-dioxane at 10 μM; b) 3D excitation-emission spectra (with a 5 nm step) of **DTM-1** in 1,4-dioxane at 10 μM.

The polarity of the solvent had an effect on the fluorescence of **DTM-1**: a decrease in fluorescent quantum yield could be observed for solvents with a higher polarity. Φ_f was calculated to be 28% in cyclohexane, 10% in 1,4-dioxane and 0.4% in methanol. The molar extinction coefficient (ε_{max}) varied less significantly with solvent: between 4900-5500 $M^{-1}\cdot cm^{-1}$.

Interestingly, while **DTM-1** is emissive with a Φ_f of 10% in 1,4-dioxane, **MTM-1** is non-emissive, having a $\Phi_f < 0.05\%$ in both 1,4-dioxane and methanol.

3.3.2.1. Aminomaleimide models

Spectroscopic properties were investigated first for four model compounds **ABM-1**, **ABM-2**, **MAM-1** and **MAM-2**, the measurements were performed in cyclohexane, 1,4-dioxane, methanol and water (where solubility allowed) to examine the effect of solvent polarity on the emission.

3.3.2.1.1. Aminobromomaleimides

In 1,4-dioxane, **ABM-1** showed excitation maxima at 233 nm and 363 nm, with both excitation wavelengths corresponding to the same emission maximum at 469 nm, see Figure 3.4. Stokes shifts for these excitation wavelengths were respectively 236 nm and 106 nm. This good spectral separation of excitation and emission is important for potential application in FRET experiments.[52] **ABM-1** also showed a solvatochromic emission with a red-shift upon increasing solvent polarity, see Figure 3.5.

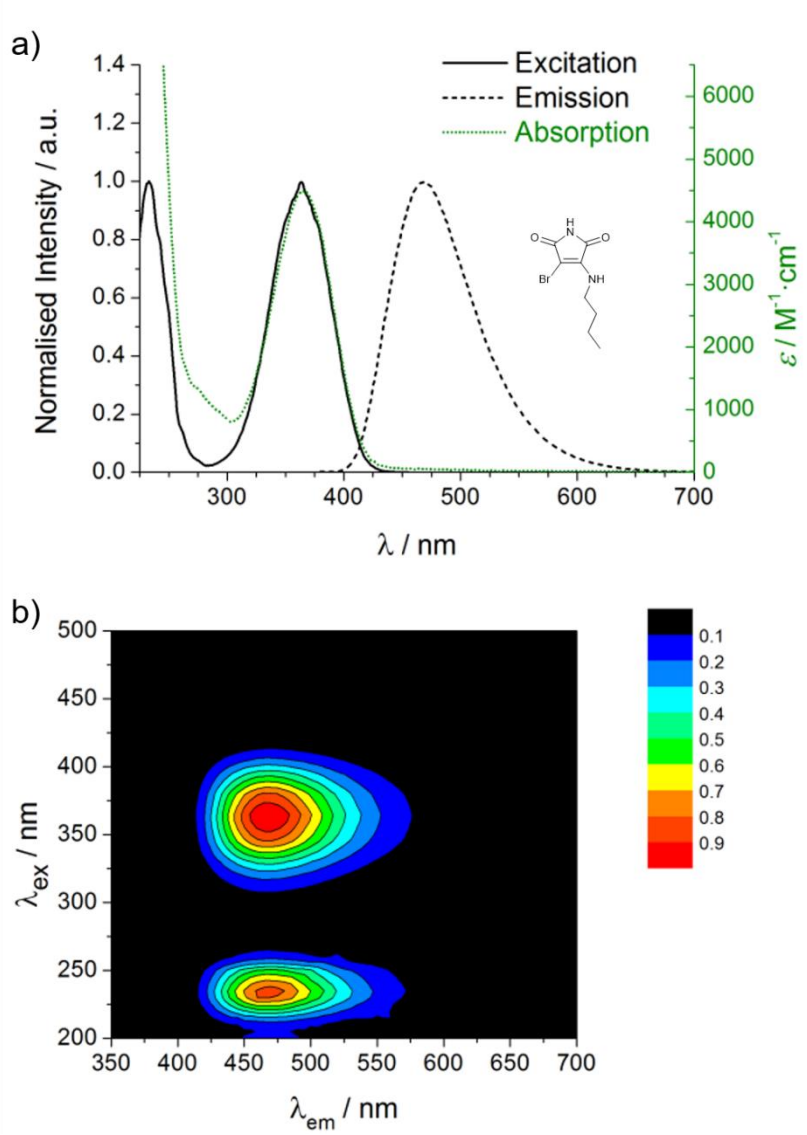

Figure 3.4. a) Excitation, emission and absorption spectra of **ABM-1** in 1,4-dioxane at 10 μM, b) 3D excitation-emission spectra (with a 5 nm step) of **ABM-1** in 1,4-dioxane at 10 μM.

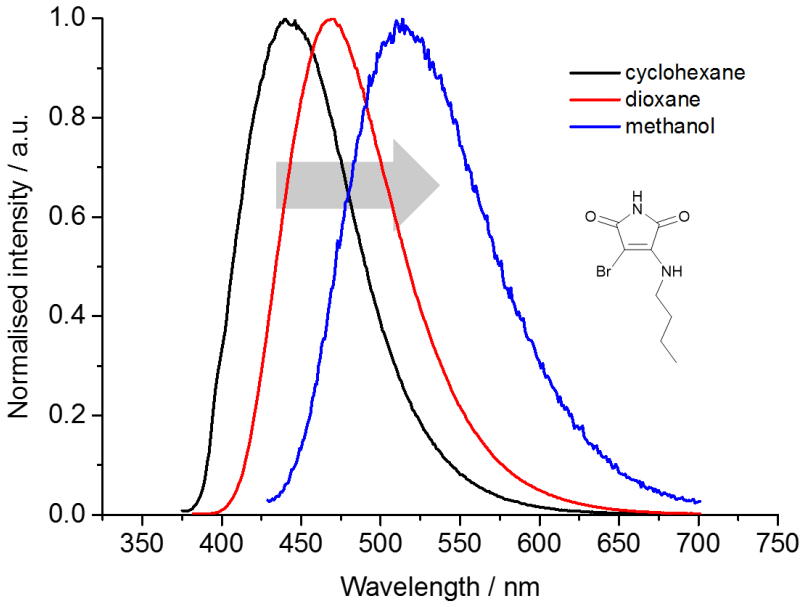

Figure 3.5. Emission spectra of **ABM-1** at 10 μM in cyclohexane (λ_{ex} = 354 nm), dioxane (λ_{ex} = 363 nm), and methanol (λ_{ex} = 370 nm). These spectra were normalised to their maxima to help the wavelength maxima comparison.

The fluorescent quantum yield for **ABM-1** was calculated to be 31% in cyclohexane, 38% in 1,4-dioxane, and 1.1% in methanol, see Figure 3.6. A significant decrease in Φ_f was observed in the protic polar solvents methanol and water. The molar extinction coefficient in 1,4-dioxane was found to be 4500 $M^{-1}{\cdot}cm^{-1}$ and the brightness was calculated to be 1700 $M^{-1}{\cdot}cm^{-1}$. In comparison with quinine, a well-known fluorophore emitting in a similar region (and the standard used for the fluorescent quantum yield), exhibiting a brightness of 3000 $M^{-1}{\cdot}cm^{-1}$,[53] **ABM-1** has a lower brightness. However, these measurements illustrated that the aminomaleimide fluorophores were significantly brighter than the previously reported DTM fluorophores.[39] A further advantage for the aminobromomaleimides is that these fluorophores were generated by single substitution of the maleimide, whereas for thiomaleimide fluorophores intense emission is only observed for di-substitution.[35]

This property would be particularly beneficial for sterically demanding substituted products.

Interestingly, ABM synthesised with a secondary amine produced a non-emissive compound (**ABM-2**), with $\Phi_f < 0.2\%$ in all solvents (see Figure 3.6), suggesting perhaps that the inductive effects of the diethylamine perturbs the electronic structure.

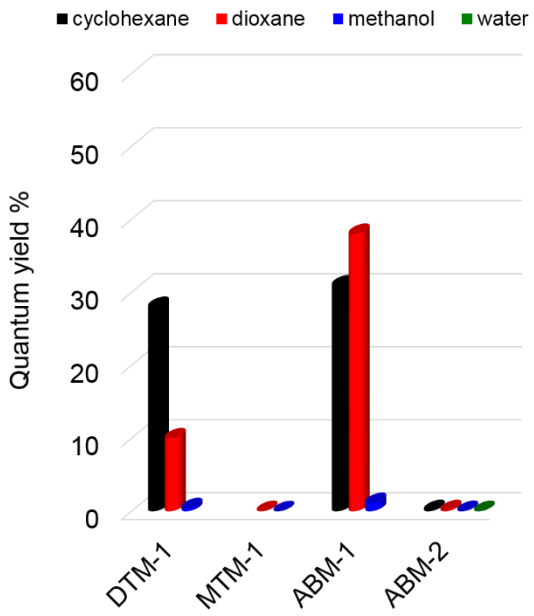

Figure 3.6. Relative fluorescence quantum yield for the ABM models in different solvents compared to DTM, MTM models.

3.3.2.1.2. Monoaminomaleimides

The MAM with an *n*-butylamine substituent (**MAM-1**) showed a very similar excitation and emission spectral profile to the corresponding ABM (**ABM-1**). For example in 1,4-dioxane **MAM-1** displayed a slight blue shift in the absorption (233 nm, 346 nm), excitation (236 nm, 346 nm) and emission (450 nm) maxima relative to **ABM-1**, see Figure 3.7, and Figure 3.8 for the comparison of emission spectra of **MAM-1**, **ABM-1** with **DTM-1**. Similarly to **DTM-1** and **ABM-1**, **MAM-1**

showed a solvatochromic emission with a red-shift upon increasing solvent polarity, see Figure 3.9.

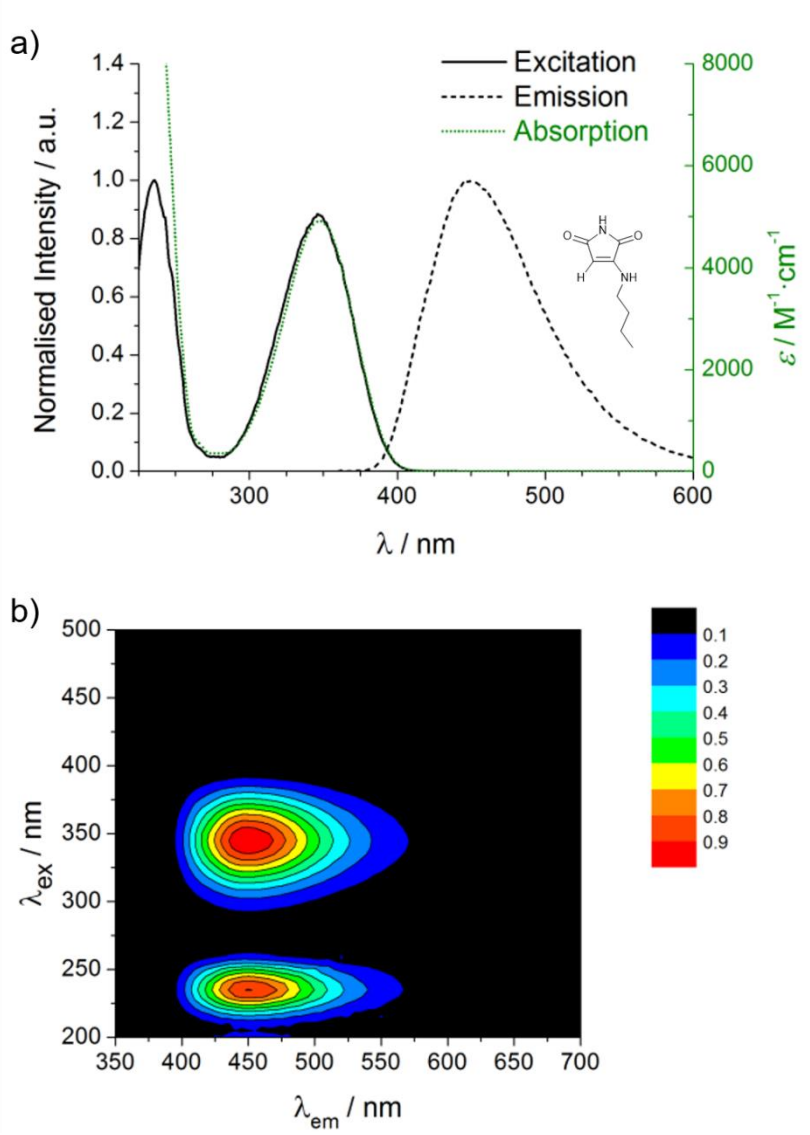

Figure 3.7. a) Excitation, emission and absorption spectra of **MAM-1** in 1,4-dioxane at 10 μM; b) 3D excitation-emission spectra (with a 5 nm step) of **MAM-1** in 1,4-dioxane at 10 μM.

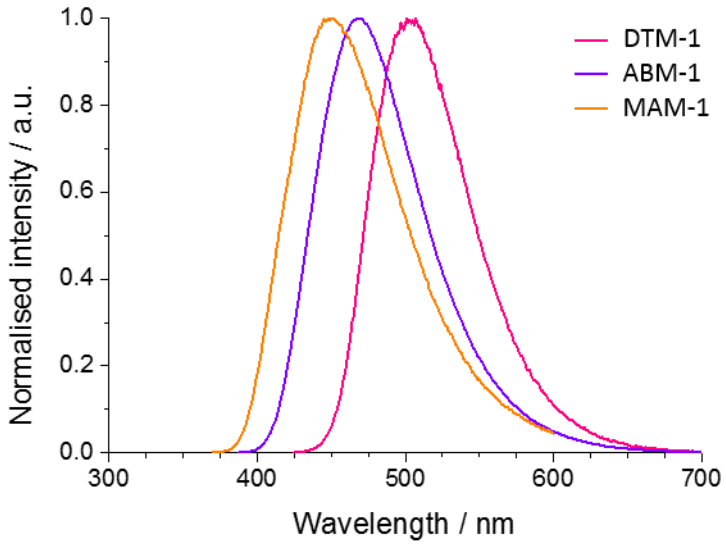

Figure 3.8. Emission spectra of **ABM-1** (λ_{ex} = 363 nm) and **MAM-1** (λ_{ex} = 346 nm) compared to **DTM-1** (λ_{ex} = 405 nm). All spectra were recorded in 1,4-dioxane at 10 μM.

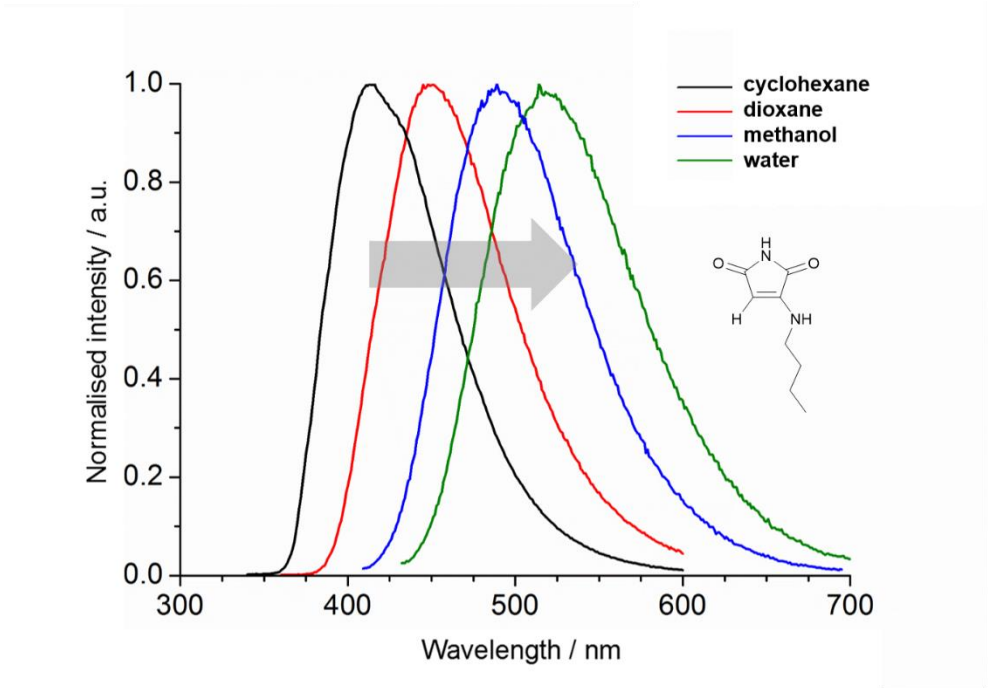

Figure 3.9. Emission spectra of **MAM-1** at 10 μM in cyclohexane (λ_{ex} = 334 nm), dioxane (λ_{ex} = 346 nm), methanol (λ_{ex} = 355 nm) and water (λ_{ex} = 365 nm).

The extinction coefficient for **MAM-1** (4900 $M^{-1}{\cdot}cm^{-1}$) was comparable to **ABM-1**, while Φ_f, and therefore the brightness ($\Phi_f \times \varepsilon_{max}$), were significantly higher at 59%

and 2900 $M^{-1}\cdot cm^{-1}$ respectively, see Figure 3.10. A significant decrease in Φ_f was also observed in the protic polar solvents methanol and water.

Similarly to the non-emissive tertiary **ABM-2**, the equivalent **MAM-2** with a diethylamine substituent displayed $\Phi_f < 0.5\%$ in all solvents, see Figure 3.10.

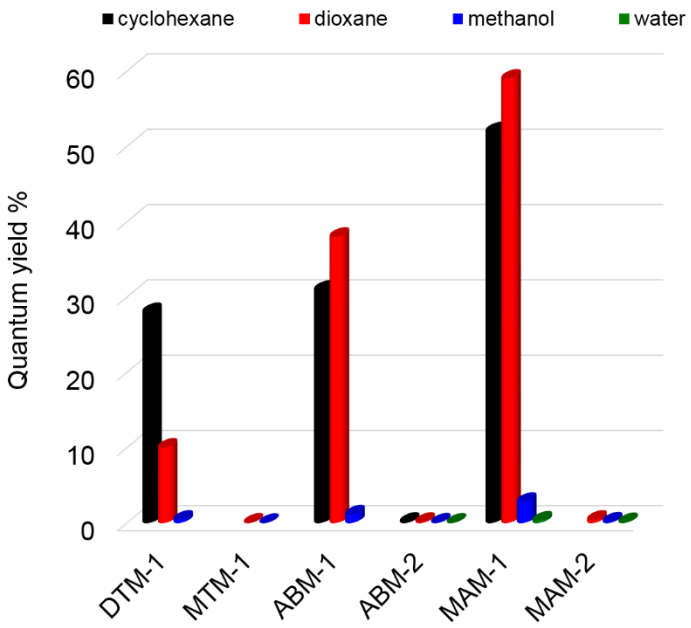

Figure 3.10. Relative fluorescence quantum yield for the MAM models in different solvents compared to DTM, MTM and ABM models.

3.3.2.2. Additional aminomaleimides

In order to compare the effect of amino-substituents on fluorescence emission, a range of amines were selected for the addition-elimination reaction with 2,3-dibromomaleimide in addition to the six model systems studied. Different primary amines were utilised; isopropylamine, benzylamine and aniline, see Figure 3.2, the latter aromatic amine being included to illustrate the effect of conjugation of the maleimide with an aromatic ring. All further spectroscopy measurements were performed in 1,4-dioxane. This solvent was chosen for giving the brightest emission for one of the model compounds (**MAM-1**), and the better solubility of aminomaleimides in 1,4-dioxane than in cyclohexane.

Interestingly, DBM substituted with different primary amines such as isopropylamine (**ABM-3**) and benzylamine (**ABM-4**) showed similar fluorescence properties to **ABM-1** (*n*-butylamine substituent) in 1,4-dioxane with absorption maxima at 233 nm and 364 nm and emission maxima at 467 nm, see Figure 3.11 for **ABM-3** and Figure 3.12 for **ABM-4**. Fluorescent quantum yields for **ABM-3** and **ABM-4** in 1,4-dioxane were calculated to be respectively 35% and 34%, which are similar to **ABM-1** with Φ_f = 38%.

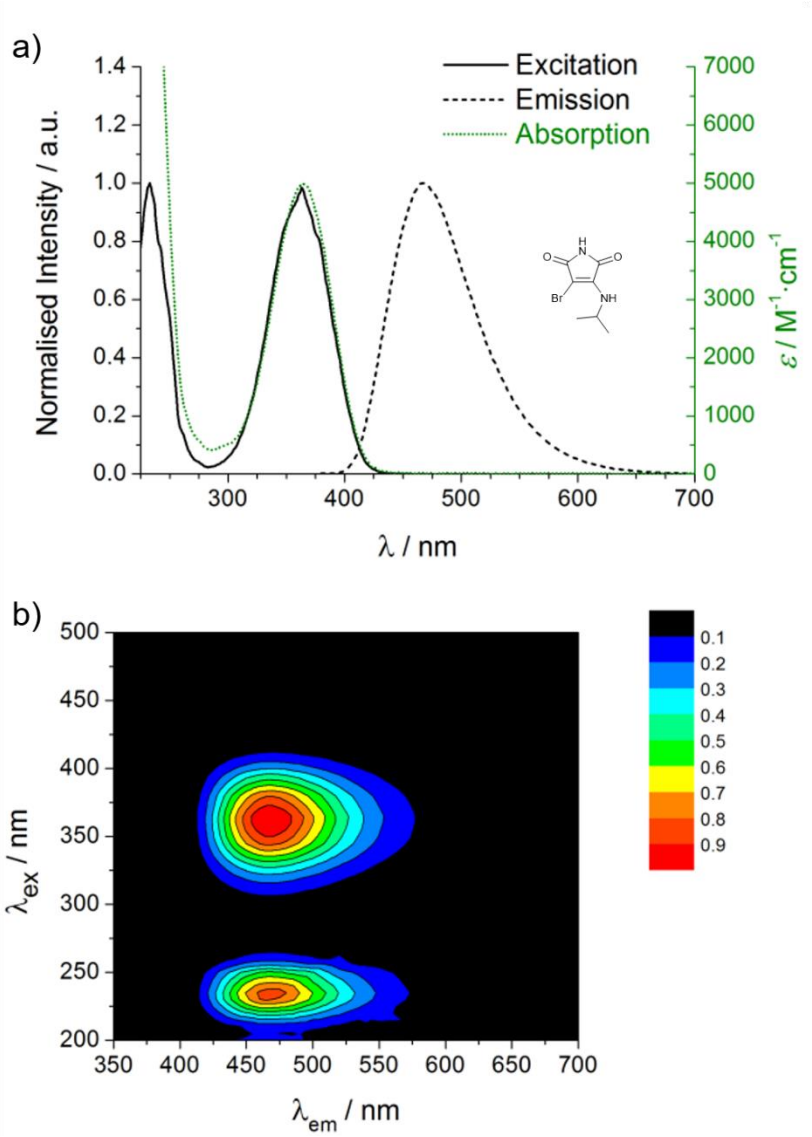

Figure 3.11. a) Excitation, emission and absorption spectra of **ABM-3** in 1,4-dioxane at 10 μM; b) 3D excitation-emission spectra (with a 5 nm step) of **ABM-3** in 1,4-dioxane at 10 μM.

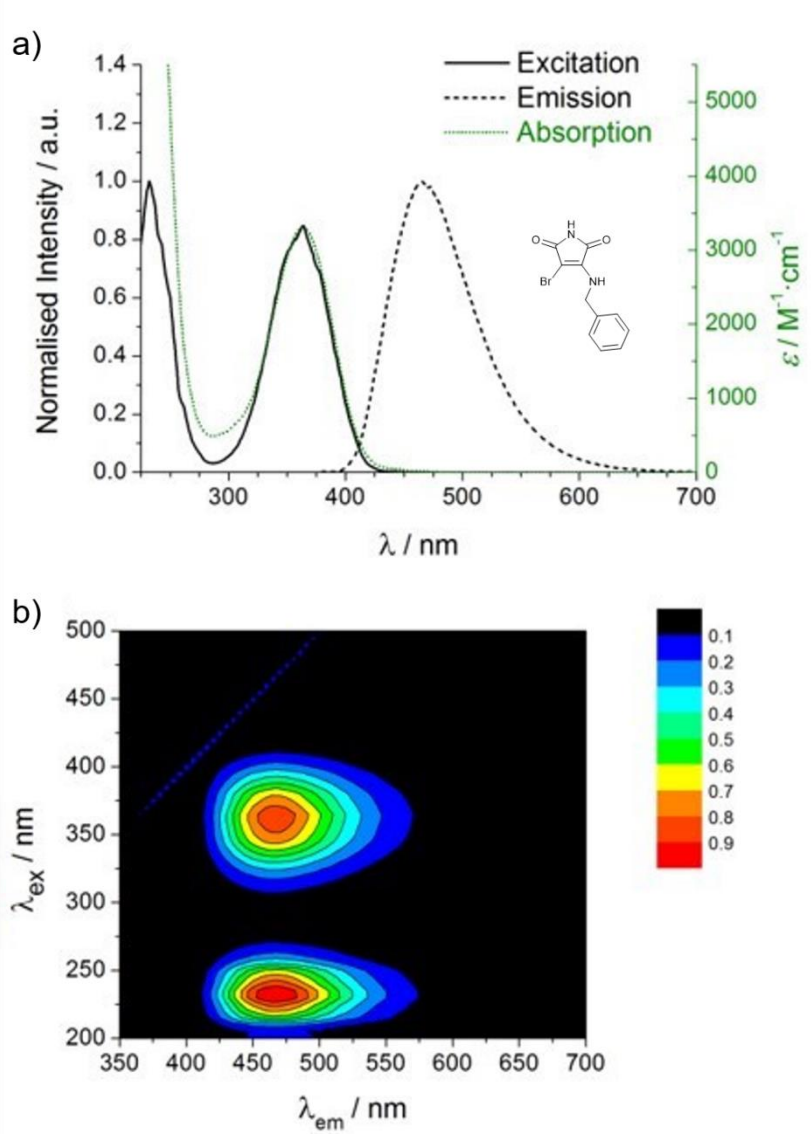

Figure 3.12. a) Excitation, emission and absorption spectra of **ABM-4** in 1,4-dioxane at 10 μM; b) 3D excitation-emission spectra (with a 5 nm step) of **ABM-4** in 1,4-dioxane at 10 μM.

The possibility of using different primary amines as substituents demonstrated the versatility of the ABM fluorophores to further functionalisation, as the emission was invariant to the groups attached to the primary amine. However, when the maleimide was directly conjugated with a phenyl group (**ABM-5**) the product was non-emissive with Φ_f = 0.05%. This result was consistent with our previous reports of emission quenching where DTM was directly conjugated to aromatic rings.[35,37,38] A similar result was obtained for MAM with an aniline substituent (**MAM-3**), which was also quenched, having Φ_f = 0.02%.

In addition to the introduction of functionality to these aminomaleimide fluorophores through choice of the amine substituent, further functionality can also be easily incorporated at the maleimide nitrogen.[54,55] The effect on emission of *N*-functionalisation of the maleimide was investigated by synthesising an *N*-methyl ABM with an *n*-butylamine substituent (**ABM-6**). Incorporation of an alkyl group at the maleimide nitrogen produced a fluorescent compound (**ABM-6**) with an emission maximum at 486 nm for the excitation maxima at 244 nm and 374 nm, see Figure 3.13. However, a reduction in fluorescent quantum yield was observed: 20% for **ABM-6** compared to a similar compound that did not have an *N*-substituent (see Figure 3.2 for structures), **ABM-1** with Φ_f = 38%.

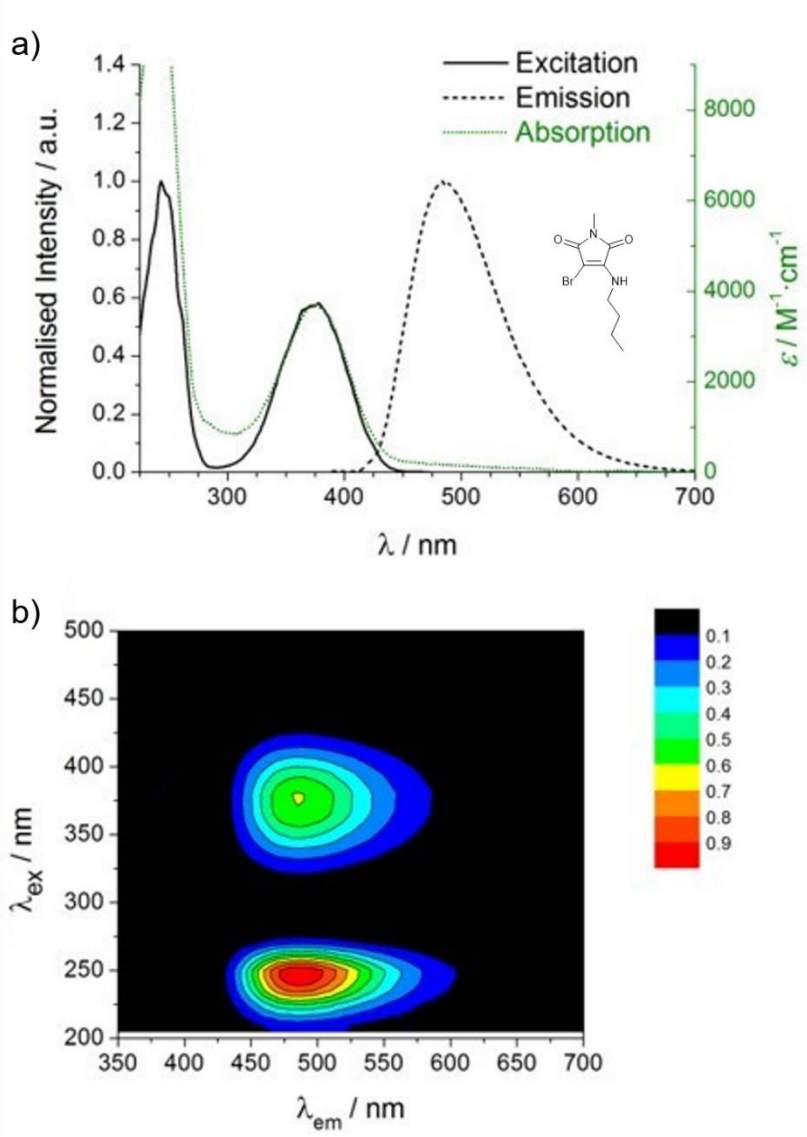

Figure 3.13. a) Excitation, emission and absorption spectra of **ABM-6** in 1,4-dioxane at 10 μM; b) 3D excitation-emission spectra (with a 5 nm step) of **ABM-6** in 1,4-dioxane at 10 μM.

This did however confirm that *N*-functionalisation is possible, which gives the aminomaleimide fluorophores the versatility to be used as a fluorescent tag through either nitrogen, or as a fluorescent linker group between two species of interest.[37,39] A phenyl group could also be directly conjugated to the maleimide through the maleimide nitrogen, however this had the same effect on fluorescence intensity as the conjugation through the amine: fluorescence quenching was observed for **ABM-7**, **ABM-8** and **MAM-4**.

3.4. Conclusions

In conclusion, a library of novel aminomaleimide fluorophores was synthesised. MAMs and ABMs were shown to be highly emissive in the range 400-500 nm with large Stokes shifts (> 100 nm). The fluorescent properties of aminomaleimides were found to depend on the fluorophore's structure: a red-shift was observed for MAMs compared to ABMs, and the fluorescence of aminomaleimides was quenched by the direct conjugation of aromatic rings to the maleimide group. Moreover, the fluorophores' emission wavelength and fluorescence quantum yield showed a dependence on the solvent polarity, and significant red-shifts of the emission maxima and higher quantum yield were observed in aprotic solvents. The consistent lower fluorescent emission observed in protic solvent was attributed to hydrogen bonding between the solvent and the maleimide's carbonyl, altering the electronic structure. This effect could be countered through intramolecular hydrogen bonding, allowing the fluorescent emission of an aminomaleimide in protic environment.

The potential of ABM fluorophores in polymer and nanostructure labelling and its solvent emission dependence is further developed in the following chapters.

3.5. Experimental

3.5.1. Materials and methods

Spectroscopy grade 1,4-dioxane, cyclohexane, and methanol were purchased from VWR. Water for spectroscopy was purified to a resistivity of 18.2 MΩ·cm using a Millipore Simplicity Ultrapure water system. 3,4-Dibromo-1-phenyl-2,5-dihydro-1H-pyrrole-2,5-dione† was synthesised according to the procedure of Muus *et al.*[56] 3-Bromo-2,5-dihydro-1H-pyrrole-2,5-dione† was synthesised according to the procedure of Vanel *et al.*[57] 3-Bromo-1-phenyl-2,5-dihydro-1H-pyrrole-2,5-dione† was synthesised according to the procedure of Martinez-Ariza *et al.*[58] 2,3-Dibutylthiomaleimide (**DTM-1**) was synthesised as previously reported.[35] All other chemicals were purchased from Aldrich, Fluka or Acros and used as received.

^{1}H and ^{13}C NMR spectra were recorded on a Bruker DPX-400, or AV500 spectrometer at room temperature unless otherwise stated. Chemical shifts are given in ppm downfield from the internal standard tetramethylsilane (TMS).

Infrared spectra were recorded (neat) on a PerkinElmer, Spectrum 100 FT-IR Spectrometer.

High Resolution Mass Spectrometry (HR-MS) was conducted on a Bruker UHR-Q-ToF MaXis with electrospray ionisation.

Fluorescence spectra were recorded using an Agilent Cary Eclipse Fluorescence spectrophotometer. UV-vis spectroscopy was carried out on a Perkin Elmer Lambda 35 UV/vis spectrometer or an Agilent Cary 60 UV-Vis Spectrophotometer. Quartz cells with screw caps and four polished sides (Starna) were used for fluorescence and UV-vis measurements.

† Synthesised by Dr Mathew Robin

3.5.2. Specific safety procedures

All work with thiols was carried out in an efficient fume cupboard and on the smallest scale possible. Disposable gloves were used, changed regularly. All materials (gloves, paper towels, glassware) utilised to work with thiol were decontaminated with the thiol killing solution.[59-61]

Sulfide Oxidiser (thiol killing solution):

% by weight: 3% cyclohexane, 82% water, 5% sodium dodecyl sulfate, 10% butan-1-ol, 1 ml of sulfide in 15 ml of microemulsion. Add 5% aqueous sodium hypochlorite solution (undiluted bleach) in 2-fold excess. Takes approximately 15 seconds to kill smell.

3.5.3. Synthetic procedures

3.5.3.1. Aminobromomaleimides (ABMs)

General procedure for the synthesis of ABMs

Reactions were performed according to the protocol established by Awuah and Capretta.[50] All reactions were performed in THF (20 mL) at room temperature with 2,3-dibromomaleimide (1 eq.), sodium carbonate (2.5 eq.) and a small excess of amine (1.05-1.1 eq.). Consumption of 2,3-dibromomaleimide was monitored by TLC, and was complete within 0.5-2 h. The solvent was then evaporated under reduced pressure and the residue was taken up with CH_2Cl_2 (150 mL). The resultant mixture was washed with water (2 × 150 mL), dried with magnesium sulfate and purified via column chromatography on silica gel with petroleum ether/ethyl acetate.

*3.5.3.1.1. 3-Bromo-4-(butylamino)-2,5-dihydro-1H-pyrrole-2,5-dione (**ABM-1**)*

In this case, 2,3-dibromomaleimide (500 mg, 1.96 mmol) and *n*-butylamine (151 mg, 2.06 mmol) were used in the general procedure described above. The product was obtained as a yellow powder (274 mg, 1.11 mmol, 57%) after purification by column chromatography on silica gel using a mixture of 5:1 petroleum ether and ethyl acetate. ^{1}H NMR ($CDCl_3$, 500 MHz) δ 7.75 (br, 1H), 5.51 (br, 1H), 3.65 (q, ^{3}J = 8 Hz, 2H), 1.65 (quin, ^{3}J = 8 Hz, 2H), 1.42 (sex, ^{3}J = 8 Hz, 2H), 0.97 (t, ^{3}J = 8 Hz, 3H); ^{13}C NMR ($CDCl_3$, 125 MHz) δ 167.6, 165.8, 143.7, 69.6, 42.7, 35.6, 19.6, 13.7; FTIR (neat) ν_{max} / cm^{-1} 3336 (H-N of amine), 3145 (H-N of maleimide) 1761 and 1708 (C=O of maleimide), 1630 (C=C of maleimide); HR-MS (MaXis) m/z found 268.9892, calc. 268.9896 ($[C_8H_{11}BrN_2O_2+Na]+$, 100%).

*3.5.3.1.2. 3-Bromo-4-(diethylamino)-2,5-dihydro-1H-pyrrole-2,5-dione (**ABM-2**)*

In this case, 2,3-dibromomaleimide (3.00 g, 11.8 mmol) and diethylamine (0.95 g, 12.9 mmol) were used in the general procedure described above. The product was obtained as a yellow powder (2.11 g, 8.55 mmol, 72%) after purification by column chromatography on silica gel using a gradient from 6:1 to 4:1 of petroleum ether and ethyl acetate. ^{1}H NMR ($CDCl_3$, 400 MHz) δ 7.56 (br, 1H), 3.76 (q, ^{3}J = 7 Hz, 4H), 1.28 (t, ^{3}J = 7 Hz, 6H); ^{13}C NMR ($CDCl_3$, 100 MHz) δ 166.6, 165.5, 144.0, 78.2, 45.8, 14.6; FTIR (neat) ν_{max} / cm^{-1} 3228 (H-N of maleimide) 1756 and 1707 (C=O of maleimide), 1616 (C=C of maleimide); HR-MS (MaXis) m/z found 268.9895, calc. 268.9896 ($[C_8H_{11}BrN_2O_2+Na]+$, 100%).

*3.5.3.1.3. 3-Bromo-4-(isopropylamino)-2,5-dihydro-1H-pyrrole-2,5-dione (**ABM-3**)*

In this case, 2,3-dibromomaleimide (500 mg, 1.96 mmol) and isopropylamine (122 mg, 2.06 mmol) were used in the general procedure described above. The product was obtained as an orange powder (176 mg, 0.76 mmol, 39%) after purification by column chromatography on silica gel using a mixture of 5:1 petroleum ether and ethyl acetate. ^{1}H NMR ($CDCl_3$, 500 MHz) δ 7.86 (br, 1H), 5.33 (br, 1H), 4.41 (m, 1H), 1.30 (d, ^{3}J = 5 Hz, 6H); ^{13}C NMR ($CDCl_3$, 125 MHz) δ 167.8, 166.0, 142.8, 69.6, 44.7, 23.6; FTIR (neat) ν_{max} / cm^{-1} 3322 (H-N amine), 3189 (H-N of maleimide), 1764 and 1708 (C=O of maleimide), 1639 (C=C of maleimide); HR-MS (MaXis) m/z found 254.9738, calc. 254.9740 ([$C_7H_9BrN_2O_2$+Na]+, 100%).

*3.5.3.1.4. 3-Bromo-4-(benzylamino)-2,5-dihydro-1H-pyrrole-2,5-dione (**ABM-4**)*

In this case, 2,3-dibromomaleimide (500 mg, 1.96 mmol) and benzylamine (221 mg, 2.06 mmol) were used in the general procedure described above. The product was obtained as an orange powder (61 mg, 0.22 mmol, 11%) after purification by column chromatography on silica gel using a mixture of 5:1 petroleum ether and ethyl acetate. ^{1}H NMR ($CDCl_3$, 400 MHz) δ 7.36 (m, 5H), 7.11 (br, 1H), 5.60 (br, 1H), 4.86 (d, ^{3}J = 8 Hz, 2H); ^{13}C NMR (CD_3OD, 125 MHz) δ 169.3, 166.5, 157.3, 138.7, 128.3, 127.1, 126.7, 103.22, 45.2; FTIR (neat) ν_{max} / cm^{-1} 3325 (H-N of amine), 3157 (H-N of maleimide) 1772 and 1714 (C=O of maleimide), 1645 (C=C of maleimide); HR-MS (MaXis) m/z found 302.9749, calc. 302.9740 ([$C_{11}H_9BrN_2O_2$+Na]+, 100%).

*3.5.3.1.5. 3-Bromo-4-(phenylamino)-2,5-dihydro-1H-pyrrole-2,5-dione (**ABM-5**)*

In this case, 2,3-dibromomaleimide (500 mg, 1.96 mmol) and aniline (192 mg, 2.06 mmol) were used in the general procedure described above. The product was obtained as an orange powder (103 mg, 0.39 mmol, 19%) after purification by

column chromatography on silica gel using a mixture of 5:1 petroleum ether and ethyl acetate. ^{1}H NMR (CD_3OD, 500 MHz) δ 7.38 (m, 4H), 7.23 (m, 6H); ^{13}C NMR (CD_3OD, 125 MHz) δ 169.3, 166.9, 141.7, 136.3, 128.0, 125.4, 124.6, 79.9; FTIR (neat) ν_{max} / cm^{-1} 3303 (H-N of amine), 3188 (H-N of maleimide) 1766 and 1706 (C=O of maleimide), 1636 (C=C of maleimide); HR-MS (MaXis) m/z found 288.9596, calc. 288.9583 ($[C_{10}H_7BrN_2O_2+Na]+$, 100%).

*3.5.3.1.6. 3-Bromo-4-(butylamino)-1-methyl-2,5-dihydro-1H-pyrrole-2,5-dione (**ABM-6**)*

In this case, 2,3-dibromo-*N*-methylmaleimide (750 mg, 2.79 mmol) and *n*-butylamine (214 mg, 2.93 mmol) were used in the general procedure described above. The product was obtained as a yellow-orange powder (448 mg, 1.72 mmol, 62%) after purification by column chromatography on silica gel using a mixture of 5:1 petroleum ether and ethyl acetate. ^{1}H NMR ($CDCl_3$, 500 MHz) δ 5.46 (br, 1H), 3.63 (q, ^{3}J = 8 Hz, 2H), 3.02 (s, 3H), 1.63 (quin, ^{3}J = 8 Hz, 2H), 1.42 (sex, ^{3}J = 8 Hz, 2H), 0.97 (t, ^{3}J = 8 Hz, 3H); ^{13}C NMR ($CDCl_3$, 125 MHz) δ 168.1, 166.2, 143.3, 69.6, 42.8, 32.7, 24.4, 19.6, 13.7; FTIR (neat) ν_{max} / cm^{-1} 3342 (H-N of amine), 1769 and 1709 (C=O of maleimide), 1647 (C=C of maleimide); HR-MS (MaXis) m/z found 283.0048, calc. 283.0053 ($[C_9H_{13}BrN_2O_2+Na]+$, 100%).

*3.5.3.1.7. 3-Bromo-4-(butylamino)-1-phenyl-2,5-dihydro-1H-pyrrole-2,5-dione (**ABM-7**)*

In this case, 3,4-dibromo-1-phenyl-2,5-dihydro-1H-pyrrole-2,5-dione (150 mg, 0.46 mmol) and *n*-butylamine (35 mg, 0.48 mmol) were used in the general procedure described above. The product was obtained as a yellow-orange powder

(26 mg, 0.08 mmol, 25%) after purification by column chromatography on silica gel using a mixture of 5:1 petroleum ether and ethyl acetate. ^{1}H NMR ($CDCl_3$, 400 MHz) δ 7.44 (m, 2H), 7.34 (m, 3H), 5.57 (br, 1H), 3.70 (q, ^{3}J = 8 Hz, 2H), 1.69 (quin, ^{3}J = 8 Hz, 2H), 1.45 (sex, ^{3}J = 8 Hz, 2H), 0.99 (t, ^{3}J = 8 Hz, 3H);); ^{13}C NMR (CD_3OD, 125 MHz) δ 167.4, 164.5, 144.2, 132.0, 131.6, 128.5, 127.4, 127.2, 126.0, 120.4, 42.1, 32.9, 19.3, 12.8; FTIR (neat) ν_{max} / cm^{-1} 3321 (H-N of amine), 1770 and 1712 (C=O of maleimide), 1649 (C=C of maleimide); HR-MS (MaXis) m/z found 345.0207, calc. 345.0209 ($[C_{14}H_{15}BrN_2O_2+Na]+$, 100%).

*3.5.3.1.8. 3-Bromo-1-phenyl-4-(phenylamino)-1H-pyrrole-2,5-dione (**ABM-8**)*

In this case, 3,4-dibromo-1-phenyl-2,5-dihydro-1H-pyrrole-2,5-dione (150 mg, 0.46 mmol) and aniline (45 mg, 0.48 mmol) were used in the general procedure described above. The product was obtained as a yellow powder (66 mg, 0.19 mmol, 42%) after purification by column chromatography on silica gel using a mixture of 5:1 petroleum ether and ethyl acetate. ^{1}H NMR (CD_3OD, 400 MHz) δ 7.47 (m, 2H), 7.40 (m, 5H), 7.28 (m, 3H); ^{13}C NMR ($CDCl_3$, 125 MHz) δ 166.6, 165.6, 139.9, 135.1, 131.5, 129.2, 128.8, 127.9, 126.6, 125.8, 124.7, 81.2; FTIR (neat) ν_{max} / cm^{-1} 3309 (H-N of amine), 1769 and 1706 (C=O of maleimide), 1647 (C=C of maleimide); HR-MS (MaXis) m/z found 364.9905, calc. 364.9896 ($[C_{16}H_{11}BrN_2O_2+Na]+$, 100%).

3.5.3.2. Monoaminomaleimides (MAMs)‡

General procedure for the synthesis of MAMs

All reactions were performed in THF (20 mL) at room temperature with bromomaleimide (1 eq.), sodium carbonate (2.5 eq.) and a small excess of amine (1.05-1.1 eq.). Consumption of bromomaleimide was monitored by TLC and was

‡ Synthesised and characterised by Dr Mathew Robin

complete within 0.5-2 h. The reaction mixture was filtered, the filtrate collected and the solvent removed under reduced pressure. The resultant residue was then purified via column chromatography on silica gel with petroleum ether/ethyl acetate.

*3.5.3.2.1. 3-(Butylamino)-2,5-dihydro-1H-pyrrole-2,5-dione (**MAM-1**)*

In this case, monobromomaleimide (500 mg, 2.84 mmol) and *n*-butylamine (218 mg, 2.98 mmol) were used in the general procedure described above. The product was obtained as a yellow powder (354 mg, 2.11 mmol, 74%) after purification by column chromatography on silica gel using a mixture of 5:1 petroleum ether and ethyl acetate. ^{1}H NMR ($CDCl_3$, 400 MHz) δ 7.07 (br, 1H), 5.37 (br, 1H), 4.81 (s, 1H), 3.18 (q, ^{3}J = 7 Hz, 2H), 1.63 (m, 2H), 1.41 (m, 2H), 0.96 (t, ^{3}J = 7 Hz); ^{13}C NMR ($CDCl_3$, 100 MHz) δ 172.7, 167.9, 149.9, 85.0, 44.1, 30.5, 20.0, 13.7; FTIR (neat) ν_{max} / cm^{-1} 3311 (H-N of amine), 3187 (H-N of maleimide), 1760 and 1702 (C=O of maleimide), 1624 (C=C of maleimide); HR-MS (MaXis) m/z found 191.0789, calc. 191.0791 ($[C_8H_{12}N_2O_2+Na]+$, 100%).

*3.5.3.2.2. 3-(Diethylamino)-2,5-dihydro-1H-pyrrole-2,5-dione (**MAM-2**)*

In this case, monobromomaleimide (500 mg, 2.84 mmol) and diethylamine (218 mg, 2.98 mmol) were used in the general procedure described above. The product was obtained as a yellow powder (375 mg, 2.23 mmol, 79%) after purification by column chromatography on silica gel using a mixture of 3:1 petroleum ether and ethyl acetate. ^{1}H NMR ($CDCl_3$, 500 MHz) δ 7.68 (br, 1H), 4.80 (d, ^{5}J = 2 Hz, 1H), 3.84 (q, ^{3}J = 7 Hz, 2H), 3.26 (q, ^{3}J = 7 Hz, 2H), 1.23 (t, ^{3}J = 7 Hz, 6H); ^{13}C NMR ($CDCl_3$, 125 MHz) δ 172.3, 167.5, 149.6, 86.8, 47.4, 44.4, 14.8, 11.0; FTIR (neat) ν_{max} / cm^{-1} 3111 (H-

N of maleimide), 1750 and 1681 (C=O of maleimide), 1602 (C=C of maleimide); HR-MS (MaXis) m/z found 191.0790, calc. 191.0791 ($[C_8H_{12}N_2O_2+Na]+$, 100%).

*3.5.3.2.3. 3-(Phenylamino)-2,5-dihydro-1H-pyrrole-2,5-dione (**MAM-3**)*

This compound was synthesised according to the procedure of Bowler et al.[62]

^{1}H NMR ($CDCl_3$, 400 MHz) δ 7.1 (br m, 5H), 5.53 (s, 1H); ^{13}C NMR (CD_3OD, 100 MHz) δ 176.4, 170.4, 145.9, 140.8, 130.5, 125.3, 120.6, 90.0; FTIR (neat) ν_{max} / cm^{-1} 3251 (H-N of aniline), 1769 and 1688 (C=O of maleimide), 1619 (C=C of maleimide); HR-MS (MaXis) m/z found 211.0478, calc. 211.0476 ($[C_{10}H_8N_2O_2+Na]+$, 100%).

*3.5.3.2.4. 3-(Butylamino)-1-phenyl-2,5-dihydro-1H-pyrrole-2,5-dione (**MAM-4**)*

In this case, 3-bromo-1-phenyl-2,5-dihydro-1H-pyrrole-2,5-dione (400 mg, 1.59 mmol) and *n*-butylamine (232 mg, 3.17 mmol) were used in the general procedure described above. The product was obtained as a yellow-green powder (258 mg, 1.06 mmol, 66%) after purification by column chromatography on silica gel using a mixture of 5:1 petroleum ether and ethyl acetate. ^{1}H NMR ($CDCl_3$, 400 MHz) δ 7.44 (t, ^3J = 8 Hz, 2H), 7.36 (m, 2H), 7.32 (t, ^3J = 7 Hz, 1H), 5.50 (br, 1H), 4.97 (s, 1H), 3.24 (q, ^3J = 7 Hz, 2H), 1.67 (m, 2H), 1.44 (m, 2H), 0.98 (t, ^3J = 7 Hz, 3H); ^{13}C NMR ($CDCl_3$, 100 MHz) δ 171.1, 166.3, 149.1, 131.9, 128.9, 127.2, 125.8, 84.1, 44.1, 30.1, 20.0, 13.6; FTIR (neat) ν_{max} / cm^{-1} 3253 (H-N of amine), 1763 and 1698 (C=O of maleimide), 1648 (C=C of maleimide); HR-MS (MaXis) m/z found 267.1105, calc. 267.1104 ($[C_{14}H_{16}N_2O_2+Na]+$, 100%).

3.5.3.3. Monothiomaleimide[§]

*3.5.3.3.1. 3-(Butylsulfanyl)-2,5-dihydro-1H-pyrrole-2,5-dione (**MTM-1**)*

To a solution of monobromomaleimide (400 mg, 2.27 mmol) in methanol (8 mL) was added dropwise a solution of sodium acetate (186 mg, 2.27 mmol) and *n*-butanethiol (204 mg, 2.27 mmol) in methanol (8 mL). After 2 h the solvent was removed under reduced pressure, and the resultant residue dissolved in ethyl acetate and filtered and the filtrate concentrated under reduced pressure. The product was obtained as a yellow powder (317 mg, 1.71 mmol, 75%) after purification by column chromatography on silica gel using a mixture of 4:1 petroleum ether and ethyl acetate. ^{1}H NMR ($CDCl_3$, 400 MHz) δ 7.34 (br, 1H), 6.05 (s, 1H), 2.92 (t, ^{3}J = 7 Hz), 1.75 (m, 2H), 1.49 (m, 2H), 0.97 (t, ^{3}J = 7 Hz); ^{13}C NMR (CD_3OD, 100 MHz) δ 168.8, 167.3, 152.0, 117.5, 31.0, 29.0, 21.4, 12.9; FTIR (neat) ν_{max} / cm^{-1} 3179 (H-N of maleimide), 1768 and 1694 (C=O of maleimide), 1548 (C=C of maleimide); HR-MS (MaXis) m/z found 208.0404, calc. 208.0403 ($[C_8H_{11}NO_2S+Na]+$, 100%).

[§] Synthesised and characterised by Dr Mathew Robin

3.5.4. Fluorophore properties

Quantum yields ($\Phi_{f,x}$) were determined according to a protocol by Resch-Genger and co-workers[51], utilising quinine sulfate dihydrate as a standard in solution in 0.105 M perchloric acid, with a quantum yield of 59% ($\Phi_{f,st}$). Ideally, the solutions (standard and sample) used to measure the quantum yield have an absorbance of 0.1. First, the optimal excitation wavelength is determined and corresponds to the intersect of the sample and standard absorption spectra. The emission spectra of both standard and sample are obtained using the exact same parameters, and the area under the peaks are respectively measured (F_{st}, F_x).

$$\Phi_{f,x} = \Phi_{f,st} \cdot \frac{F_x}{F_{st}} \cdot \frac{f_{st}}{f_x} \cdot \frac{n_x^2(\lambda_{em})}{n_{st}^2(\lambda_{em})} \quad (3.1)$$

In the equation above, n_x and n_{st} correspond to the refractive indices of the solvent of respectively the sample and the standard solutions; f_x and f_{st} are calculated using the equation below, $A(\lambda_{ex})$ being the exact absorbance at the excitation wavelength.

$$f = 1 - 10^{-A(\lambda_{ex})} \quad (3.2)$$

The extinction coefficients (ε_{max}) were determined by measuring the absorbance (A) of solutions at different concentrations (c) and with the Beer-Lambert law: $A = \varepsilon \cdot l \cdot c$, ($l$ is the length of the cuvette), the slope of the plot A vs. c correspond to the extinction coefficient.

Table 3.1. Fluorescence spectroscopy data for ABMs, MAMs, DTM and MTM

molecule	solvent	Φ_f	ε_{max}	$\lambda_{abs,max}$	$\lambda_{ex,max}$	$\lambda_{em,max}$
		%	$10^3 \cdot M^{-1}cm^{-1}$	nm	nm	nm
DTM-1	Cyclohexane	28	5.8	230, 407	232, 405	486
	Dioxane	10	4.9	250, 402	262, 405	504
	Methanol	0.43	4.7	251, 402	250, 402	546
	Water	Not soluble at 0.2 mM				
MTM-1	Cyclohexane	Not soluble at 0.2 mM				
	Dioxane	0.043	4.7	247, 339	n/a	n/a
	Methanol	0.011	4.6	244, 337	n/a	n/a
	Water	Not soluble at 0.2 mM				
ABM-1	Cyclohexane	31	3.7	225, 357	235, 354	442
	Dioxane	38	4.5	229, 367	233, 363	469
	Methanol	1.1	5.5	229, 373	233, 370	514
	Water	Not soluble at 0.2 mM				
ABM-2	Cyclohexane	0.16	7.3	224, 380	232, 379	442
	Dioxane	0.15	6.6	234, 386	233, 381	474
	Methanol	0.054	6.5	236, 392	245, 396	515
	Water	0.037	5.7	231, 410	232, 409	567
ABM-3	Dioxane	35	5.0	229, 364	233, 363	468
ABM-4	Dioxane	34	3.3	231, 362	232, 364	466
ABM-5	Dioxane	0.052	6.7	231, 375	n/a	n/a
ABM-6	Dioxane	20	3.7	240, 376	244, 374	486
ABM-7	Dioxane	0.94	3.7	236, 378	241, 375	493
ABM-8	Dioxane	0.13	4.8	245, 387	n/a	n/a
MAM-1	Cyclohexane	52	5.0	231, 333	231, 334	412
	Dioxane	59	4.9	233, 346	236, 346	450
	Methanol	2.8	5.5	232, 357	233, 355	490
	Water	0.31	5.4	231, 369	231, 365	520
MAM-2	Cyclohexane	Not soluble at 0.2 mM				
	Dioxane	0.43	6.6	238, 367	233, 364	460
	Methanol	0.20	6.6	224, 374	233, 379	500
	Water	0.11	6.4	217, 391	232, 393	535
MAM-3	Dioxane	0.017	9.9	228, 240, 366	n/a	n/a
MAM-4	Dioxane	0.085	2.9	262, 360	n/a	n/a

3.6. References

1. A. B. Mabire, M. P. Robin, W.-D. Quan, H. Willcock, V. G. Stavros and R. K. O'Reilly, *Chem. Commun.*, 2015, **51**, 9733-9736.

2. M. Gao, F. Yu, C. Lv, J. Choo and L. Chen, *Chem. Soc. Rev.*, 2017, **46**, 2237-2271.

3. M. P. Robin and R. K. O'Reilly, *Polym. Int.*, 2015, **64**, 174-182.

4. E. Zhao, J. W. Y. Lam, L. Meng, Y. Hong, H. Deng, G. Bai, X. Huang, J. Hao and B. Z. Tang, *Macromolecules*, 2015, **48**, 64-71.

5. X.-F. Yang, Q. Huang, Y. Zhong, Z. Li, H. Li, M. Lowry, J. O. Escobedo and R. M. Strongin, *Chem. Sci.*, 2014, **5**, 2177-2183.

6. K. Rajagopal, D. A. Christian, T. Harada, A. Tian and D. E. Discher, *International Journal of Polymer Science*, 2010, **2010**.

7. C. Li, Y. Zhang, J. Hu, J. Cheng and S. Liu, *Angew. Chem. Int. Ed.*, 2010, **49**, 5120-5124.

8. H.-A. Klok, S. Becker, F. Schuch, T. Pakula and K. Müllen, *Macromol. Chem. Phys.*, 2002, **203**, 1106-1113.

9. B. Valeur and M. N. Berberan-Santos, *Molecular Fluorescence*, John Wiley & Sons, Incorporated, Somerset, GERMANY, 2013.

10. D. Asanuma, Y. Takaoka, S. Namiki, K. Takikawa, M. Kamiya, T. Nagano, Y. Urano and K. Hirose, *Angew. Chem. Int. Ed.*, 2014, **53**, 6085-6089.

11. J.-T. Hou, W. X. Ren, K. Li, J. Seo, A. Sharma, X.-Q. Yu and J. S. Kim, *Chem. Soc. Rev.*, 2017, **46**, 2076-2090.

12. X.-d. Wang, O. S. Wolfbeis and R. J. Meier, *Chem. Soc. Rev.*, 2013, **42**, 7834-7869.

13. D. Kand, A. M. Kalle and P. Talukdar, *Org. Biomol. Chem.*, 2013, **11**, 1691-1701.

14. M. E. Langmuir, J.-R. Yang, A. M. Moussa, R. Laura and K. A. LeCompte, *Tetrahedron Lett.*, 1995, **36**, 3989-3992.

15. T. O. Sippel, *J. Histochem. Cytochem.*, 1981, **29**, 314-316.

16. J. Youziel, A. R. Akhbar, Q. Aziz, M. E. B. Smith, S. Caddick, A. Tinker and J. R. Baker, *Org. Biomol. Chem.*, 2014, **12**, 557-560.

17. A. Prasanna de Silva, H. Q. Nimal Gunaratne and T. Gunnlaugsson, *Tetrahedron Lett.*, 1998, **39**, 5077-5080.

18. J. Guy, K. Caron, S. Dufresne, S. W. Michnick, Skene and J. W. Keillor, *J. Am. Chem. Soc.*, 2007, **129**, 11969-11977.

19. Y. Chen, C. M. Clouthier, K. Tsao, M. Strmiskova, H. Lachance and J. W. Keillor, *Angew. Chem. Int. Ed.*, 2014, **53**, 13785-13788.

20. F. Gao, H. Chen, S. Xu, Y. Cheng and Y. Ma, *Talanta*, 2013, **116**, 508-513.

21. X. Pan , Z. Liang, J. Li, S. Wang, F. Kong, K. Xu and B. Tang, *Chem. Eur. J.*, 2015, **21**, 2117-2122.

22. N. Wache, A. Scholten, T. Klüner, K.-W. Koch and J. Christoffers, *Eur. J. Org. Chem.*, 2012, **2012**, 5712-5722.

23. X. Guo, X. Zhang, S. Wang, S. Li, R. Hu, Y. Li and G. Yang, *Anal. Chim. Acta*, 2015, **869**, 81-88.

24. Y. Yang, F. Huo, C. Yin, J. Chao and Y. Zhang, *Dyes Pigm.*, 2015, **114**, 105-109.

25. Y. Zhang, F. Huo, C. Yin, Y. Yue, J. Hao, J. Chao and D. Liu, *Sens. Actuators B Chem.*, 2015, **207, Part A**, 59-65.

26. Y. Liu, Y. Liu, W. Liu and S. Liang, *Spectrochim. Acta Mol. Biomol. Spectrosc.*, 2015, **137**, 509-515.

27. R. K. V. Lim and Q. Lin, *Acc. Chem. Res.*, 2011, **44**, 828-839.

28. W. Song, Y. Wang, Z. Yu, C. I. R. Vera, J. Qu and Q. Lin, *ACS Chem. Biol.*, 2010, **5**, 875-885.

29. W. Song, Y. Wang, J. Qu and Q. Lin, *J. Am. Chem. Soc.*, 2008, **130**, 9654-9655.

30. W. Song, Y. Wang, J. Qu, M. M. Madden and Q. Lin, *Angew. Chem. Int. Ed.*, 2008, **47**, 2832-2835.

31. A. Hufendiek, C. Barner-Kowollik and M. A. R. Meier, *Polym. Chem.*, 2015, **6**, 2188-2191.

32. T. Tischer, C. Rodriguez-Emmenegger, V. Trouillet, A. Welle, V. Schueler, J. O. Mueller, A. S. Goldmann, E. Brynda and C. Barner-Kowollik, *Adv. Mater.*, 2014, **26**, 4087-4092.

33. M. Dietrich, G. Delaittre, J. P. Blinco, A. J. Inglis, M. Bruns and C. Barner-Kowollik, *Adv. Funct. Mater.*, 2012, **22**, 304-312.

34. R. K. V. Lim and Q. Lin, *Chem. Commun.*, 2010, **46**, 7993-7995.

35. M. P. Robin, P. Wilson, A. B. Mabire, J. K. Kiviaho, J. E. Raymond, D. M. Haddleton and R. K. O'Reilly, *J. Am. Chem. Soc.*, 2013, **135**, 2875-2878.

36. M. P. Robin, J. E. Raymond and R. K. O'Reilly, *Mater. Horiz.*, 2015, **2**, 54-59.

37. A. B. Mabire, M. P. Robin, H. Willcock, A. Pitto-Barry, N. Kirby and R. K. O'Reilly, *Chem. Commun.*, 2014, **50**, 11492-11495.

38. M. P. Robin and R. K. O'Reilly, *Chem. Sci.*, 2014, **5**, 2717-2723.

39. M. P. Robin, A. B. Mabire, J. C. Damborsky, E. S. Thom, U. H. Winzer-Serhan, J. E. Raymond and R. K. O'Reilly, *J. Am. Chem. Soc.*, 2013, **135**, 9518-9524.

40. M. E. B. Smith, F. F. Schumacher, C. P. Ryan, L. M. Tedaldi, D. Papaioannou, G. Waksman, S. Caddick and J. R. Baker, *J. Am. Chem. Soc.*, 2010, **132**, 1960-1965.

41. M. H. Lauer, R. L. Drekener, C. R. D. Correia and M. H. Gehlen, *Photochem. Photobiol. Sci.*, 2014, **13**, 859-866.

42. K. P. Nacheva, W. A. Maza, D. Z. Myers, F. R. Fronczek, R. W. Larsen and R. Manetsch, *Org. Biomol. Chem.*, 2012, **10**, 7840-7846.

43. K. Onimura, M. Matsushima, M. Nakamura, T. Tominaga, K. Yamabuki and T. Oishi, *J. Polym. Sci., Part A: Polym. Chem.*, 2011, **49**, 3550-3558.

44. H.-d. Xie, L. A. Ho, M. S. Truelove, B. Corry and S. G. Stewart, *J. Fluoresc.*, 2010, **20**, 1077-1085.

45. C.-W. Chiu, T. J. Chow, C.-H. Chuen, H.-M. Lin and Y.-T. Tao, *Chem. Mater.*, 2003, **15**, 4527-4532.

46. W. C. Wu, H. C. Yeh, L. H. Chan and C. T. Chen, *Adv. Mater.*, 2002, **14**, 1072-1075.

47. J. Cui, S. Wang, K. Huang, Y. Li, W. Zhao, J. Shi and J. Gu, *New J. Chem.*, 2014, **38**, 6017-6024.

48. T. L. Smith, *US Pat.*, 4680272, 1987.

49. H. Leismann, G. Marzolph, H.-D. Scharf and M. Behruzi, *Chem. Ber.*, 1983, **116**, 2591-2615.

50. E. Awuah and A. Capretta, *J. Org. Chem.*, 2011, **76**, 3122-3130.

51. C. Würth, M. Grabolle, J. Pauli, M. Spieles and U. Resch-Genger, *Nat. Protocols*, 2013, **8**, 1535-1550.

52. S. H. Kim, J. R. Gunther and J. A. Katzenellenbogen, *Org. Lett.*, 2008, **10**, 4931-4934.

53. L. D. Lavis and R. T. Raines, *ACS Chem. Biol.*, 2008, **3**, 142-155.

54. M. A. Walker, *J. Org. Chem.*, 1995, **60**, 5352-5355.

55. L. Castañeda, Z. V. F. Wright, C. Marculescu, T. M. Tran, V. Chudasama, A. Maruani, E. A. Hull, J. P. M. Nunes, R. J. Fitzmaurice, M. E. B. Smith, L. H. Jones, S. Caddick and J. R. Baker, *Tetrahedron Lett.*, 2013, **54**, 3493-3495.

56. U. Muus, C. Hose, W. Yao, T. Kosakowska-Cholody, D. Farnsworth, M. Dyba, G. T. Lountos, D. S. Waugh, A. Monks, T. R. Burke Jr and C. J. Michejda, *Biorg. Med. Chem.*, 2010, **18**, 4535-4541.

57. R. Vanel, F. Berthiol, B. Bessières, C. Einhorn and J. Einhorn, *Synlett*, 2011, **2011**, 1293-1295.

58. G. Martinez-Ariza, J. Dietrich, F. De Moliner and C. Hulme, *Synlett*, 2013, **24**, 1801-1804.

59. University of Warwick, Department of Chemistry, Handbook 2016, www2.warwick.ac.uk/fac/sci/chemistry/chemintra/safety/handbook/.

60. F. M. Menger and M. J. Rourk, *Langmuir*, 1999, **15**, 309-313.

61. F. M. Menger and A. R. Elrington, *J. Am. Chem. Soc.*, 1991, **113**, 9621-9624.

62. J. T. Bowler, C. R. Clausen, D. J. Blackburn and W. Wu, *Tetrahedron Lett.*, 2014, **55**, 6465-6466.

Chapter 4

CO_2/pH-responsive particles with built-in aminobromomaleimide for fluorescence read-out

4.1. Abstract

A novel fluorescent monomer was synthesised to probe the state of CO_2-responsive cross-linked polymer particles. The fluorescence emission of this aminobromomaleimide-bearing monomer, being sensitive to protic environments, can provide information on the core hydrophilicity of the particles and therefore indicates the swollen state and size of the particles. The core of the particles, synthesised from DEAEMA (*N,N*-diethylaminoethyl methacrylate), is responsive to CO_2 through protonation of the tertiary amines of DEAEMA. The response is reversible and the fluorescence emission can be recovered by simply bubbling an inert gas into the particle solution. Alternate purges of CO_2 and N_2 into the solution of particles allow several on/off fluorescence emission cycles and simultaneous particle swelling/shrinking cycles.

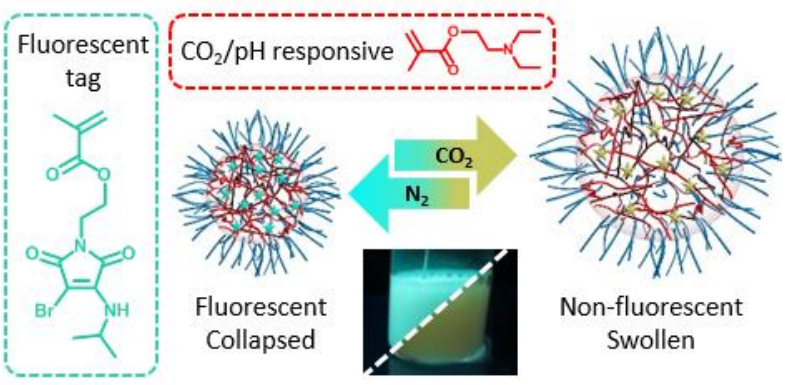

Figure 4.1. Schematic summary of the fluorescent responsive particles.[1]

4.2. Introduction

Stimuli-responsive polymers have received great interest in recent years and have been developed for different applications such as nanotechnology, bio-materials and drug delivery.[2-5] External stimuli such as temperature, pH, CO_2 or light can be utilised to trigger a response and/or change in physical properties.[6-10] Carbon dioxide, a naturally abundant gas and biocompatible, has been more and more recently used as a stimulus for responsive materials. The usage of CO_2-responsive polymers is widely reported to trigger and control self-assembly morphology transitions.[11-14] These responsive polymers are usually synthesised with monomers containing tertiary amine, amidine, guanidine or imidazole functional groups.[15-17] Such functional groups can all be protonated upon a decrease in pH which in turn can be induced by the presence of CO_2. Tertiary amine-containing monomers such as DMAEMA (*N,N*-dimethylaminoethyl methacrylate), DEAEMA and DPAEMA (*N,N*-diisopropylaminoethyl methacrylate) exhibit a pH-responsive behaviour, as they can react with strong and weak acids.[18,19]

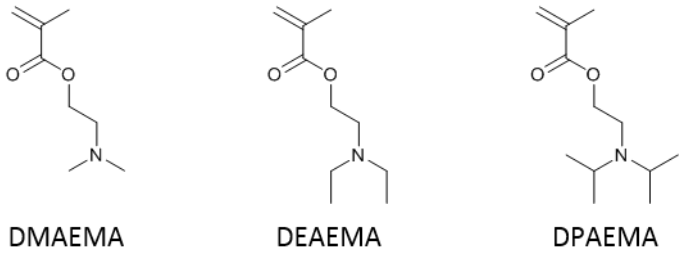

Figure 4.2. Example of tertiary amine-containing monomer structures.

These pH-responsive monomers are also responsive to CO_2 in water, as CO_2 partially dissolves in water to form an equilibrium with carbonic acid, which is a weak acid that can dissociate into HCO_3^-, CO_3^{2-} and H^+, which allows the protonation of the amine monomers, see Scheme 4.1.

$$CO_2(g) + H_2O(aq) \rightleftharpoons H_2CO_3(aq)$$
$$H_2CO_3(aq) \rightleftharpoons H^+(aq) + HCO_3^-(aq)$$

$$-NR_1R_2(aq) + CO_2(g) + H_2O(aq) \rightleftharpoons -NHR_1R_2(aq) + HCO_3^-(aq)$$

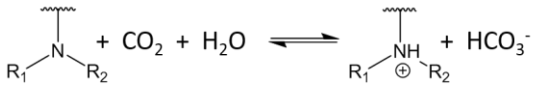

Scheme 4.1. Protonation of a tertiary amine by CO_2 bubbling in water.

The CO_2 response is a reversible process where reversal is carried out by simply bubbling an inert gas (nitrogen or argon) in the solution, which displaces carbonic acid and shifts the equilibrium toward the initial species in solution and thus the initial pH.[20] CO_2-responsive polymer assemblies can also be obtained *via* encapsulation of amine-bearing small molecules into non-responsive systems such as micelles.[21] Further examples of CO_2-responsive materials include the use of CO_2/pH responsive latexes as Pickering emulsifiers, reported by Morse and co-workers for example.[22] The cross-linked latexes were synthesised from DEAEMA, DVB (divinylbenzene) and PEGMA (polyethylene glycol methacrylate) and showed a reversible diameter increase from 230 nm to 590 nm using HCl/KOH or CO_2/N_2 gas purges to change the pH, see Figure 4.3.

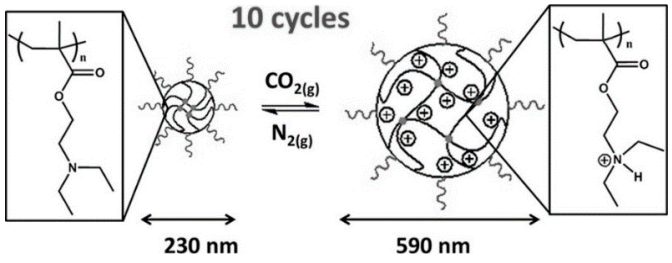

Figure 4.3. CO_2 responsiveness of PEGMA-DEAEMA latexes. Reproduced from reference. [22]

The protonation of the DEAEMA cross-linked core, using HCl or CO_2, increases the core hydrophilicity, which induces a swelling effect. The deprotonation of DEAEMA

via N_2 purging or with addition of KOH decreases the hydrophilicity of the core and results in a reduction of the particle diameter to its original size.

Recently, Chen and co-workers also reported the preparation of CO_2-responsive polymeric microgels which are composed of a DEAEMA core covalently stabilised with PEGA (polyethylene glycol acrylate), cross-linked with EGDMA (ethylene glycol dimethacrylate) or BIS (methylene bis(acrylamide)).[23] The different microgels obtained showed a reversible size increase upon CO_2 and argon bubbling. Depending on the CO_2 concentration, these microgels can reversibly swell, or swell then collapse.

Fluorescent dyes are of key interest owing to their potential use in drug delivery systems.[24-26] Liang and co-workers presented the advantages of a responsive and fluorescence combination for bio-medical applications with the preparation of polymeric nanoparticles that are fluorescent, pH-responsive, and biocompatible for intracellular imaging and drug delivery.[27] We previously reported the synthesis of fluorescently labelled proteins and polymers with a dithiomaleimide moiety; a small functional group that does not affect the polymer or protein scaffold.[28] This fluorescent functional group was also incorporated into an amphiphilic block copolymer which self-assembled into spherical micelles and can be used in nanomedicine.[29] A one-pot emulsion polymerisation synthesis of fluorescent nanogels that were covalently dyed using a dithiomaleimide methacrylate monomer was also reported in our group, see Figure 4.4.[30,31]

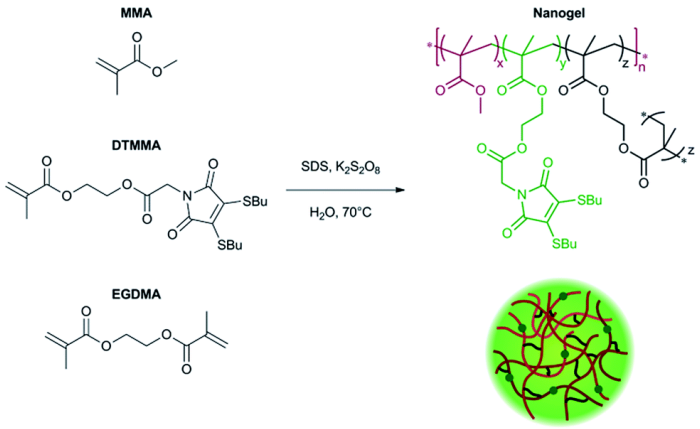

Figure 4.4. Schematic representation of the synthesis of the dithiomaleimide labelled nanogels. Reproduced from reference.[31]

It was also demonstrated these particles do not exhibit self-quenching at high concentration unlike commonly used fluorophores such as Phloxine B. Dithiomaleimides have been previously demonstrated to be highly fluorescent when the maleimide unit is conjugated to an alkyl thiol[32] although dithiomaleimides in the presence of an excess of thiol can undergo substitution, which may result in loss of fluorescence emission properties if substituted with an aromatic thiol.[28,33] To counter this substitution effect and thus the loss of fluorescence, a new class of highly emissive fluorophores, the aminobromomaleimides (ABM), was developed .[34] Their fluorescence properties are environment dependent; in protic solvents a loss of fluorescence can be observed.

This chapter reports the synthesis of fluorescent CO_2-responsive polymeric particles by emulsion polymerisation. A novel ABM functional fluorescent monomer, copolymerised in the particle core, was utilised as a probe of the core hydrophobicity. By simple CO_2 bubbling, the particles become swollen and, as a consequence of the increased hydrophilicity of the particles, their fluorescence drastically decreases. This swelling is reversible by purging the solution with nitrogen and on/off cycles of fluorescence are reproducible with successive CO_2/N_2 purges.

4.3. Results and discussion

4.3.1. Synthesis and characterisation of the monomer

The fluorescent ABM functional group was incorporated into the polymeric particles *via* a novel ABM-functionalised methacrylate monomer. The fluorescent monomer containing the ABM functionality was synthesised in two steps, see Scheme 4.2. First, 2,3-dibromomaleimide methacrylate (DBMMA) was synthesised by alkylation of 2-hydroxyethyl 2-methylprop-2-enoate with 2,3-dibromomaleimide using a modified Mitsunobu reaction procedure reported by Walker.[35] The DBMMA monomer was then functionalised *via* mono-substitution of the bromine with isopropylamine to obtain an aminobromomaleimide methacrylate (ABMMA) (see ^{1}H NMR spectrum in Figure 4.5), following a procedure similar to that used for the synthesis of a library of aminomaleimides, as detailed in chapter 3. Similarly to the small molecules presented in chapter 3, the monomer presents two excitation maxima (λ = 247 nm and λ = 372 nm) for emission maximum (λ = 482 nm) in 1,4-dioxane, see Figure 4.6.

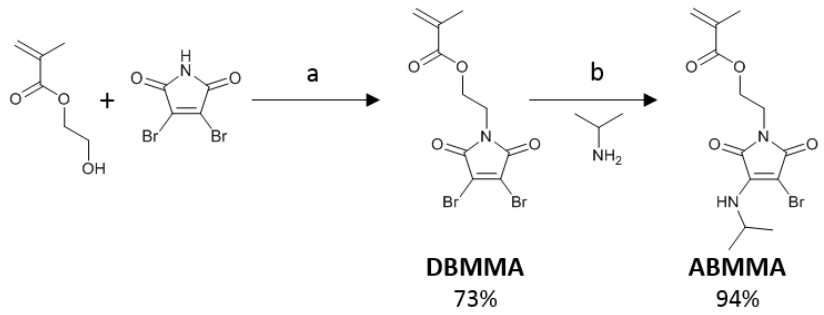

Scheme 4.2. Synthesis of DBMMA and ABMMA. Conditions: (a) PPh_3, diisopropyl azodicarboxylate, 2,2-dimethylpropan-1-ol in THF; (b) Na_2CO_3 in THF.

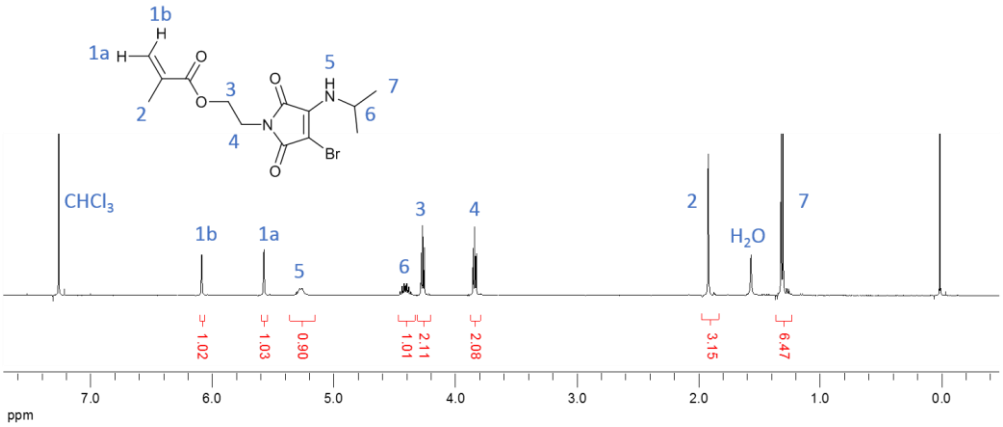

Figure 4.5. ^{1}H NMR spectrum of ABMMA ($CDCl_3$, 400 MHz).

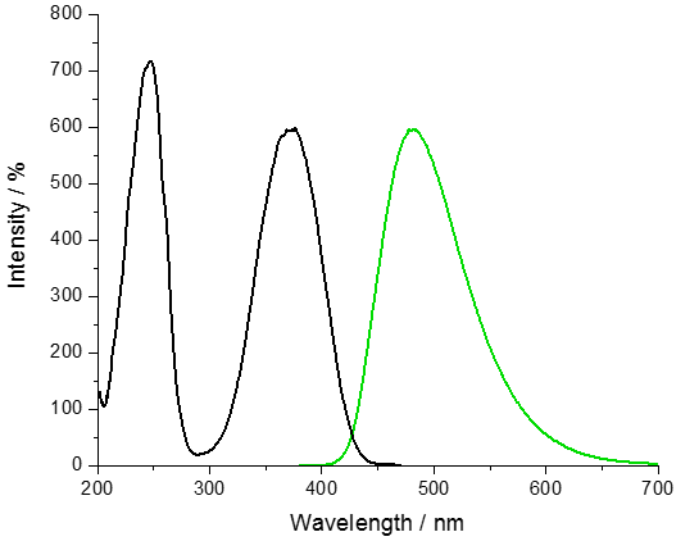

Figure 4.6. Fluorescence emission (green line) and excitation (black line) spectra of ABMMA in 1,4-dioxane at 10^{-5} M; λ_{em} = 486 nm and λ_{ex} = 374 nm.

As it would be expected, the emission and excitation wavelengths are within the same range as the small molecules detailed in chapter 3. For example, the ABM with isopropylamine substituent (**ABM-3**) exhibits excitation maxima at 233 nm and 363 nm for an emission maximum at 468 nm and the ABM with a methyl substituent on the maleimide nitrogen (**ABM-6**) exhibits excitation maxima at 244 nm and 374 nm for an emission maximum at 486 nm.

4.3.2. Synthesis and characterisation of fluorescent responsive particles

Fluorescent responsive particles (FRP) were designed with a tertiary amine-bearing monomer (DEAEMA) and the fluorescent ABMMA monomer, the former allowed a pH response while the latter monomer allowed a fluorescence read-out of the state of the particles. Particles were synthesised *via* emulsion polymerisation in water and the polymerisation was initiated using potassium persulfate (KPS) as the initiator, see Figure 4.7.

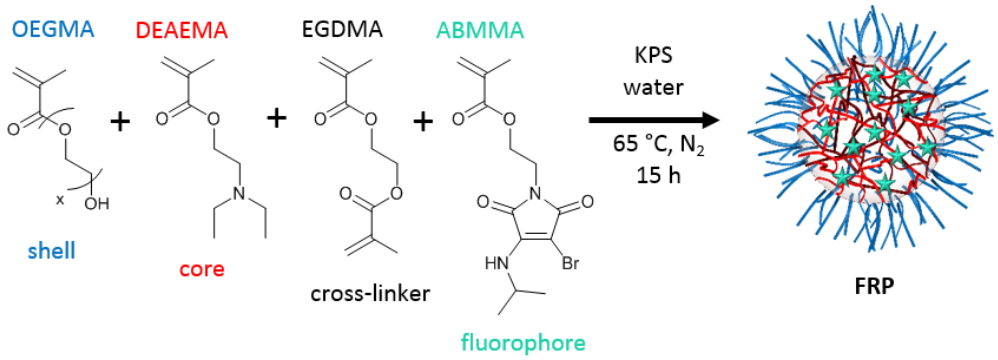

Compound	Variation
DEAEMA	50 to 150 eq. (for 1 eq. of OEGMA360)
EGDMA (cross-linker)	0.5 to 5 wt%
ABMMA (fluorescent)	0 to 2 wt%
KPS (initiator)	1 - 2 wt%

Figure 4.7. Schematic representation of the typical synthesis of fluorescent responsive particles (FRP), and table of the variation of the quantities of co-monomers and initiator.

The emulsion polymerisation procedure consists of emulsifying an insoluble monomer phase in water in the presence of a stabilising amphiphilic compound. In this case, the insoluble core-forming monomer DEAEMA, cross-linker EGDMA, and fluorophore ABMMA were stabilised with OEGMA. The droplets assembled this

way copolymerised to form covalently bound core/shell particles. The tertiary amines of the core-forming block allowed a CO_2-responsive behaviour while the presence of the ABM allowed a built-in fluorescence read-out.

The influence of different parameters such as the cross-linking density, the fluorophore loading, the molecular weight of the stabilising monomer, and the co-monomers ratios were tested to optimise the synthesis of the particles, see Table 4.1. It was observed that the variation of the ratio of the different co-monomers and initiator can affect the formation of particles.

Table 4.1. Different size particles obtained for different monomers and initiator ratios.

OEGMA360 (eq.)	DEAEMA (eq.)	EGDMA (wt%)	KPS (wt%)	ABMMA (wt%)	D_h (nm)	PD	Batch numbers
1	150	1	1	0	185	0.02	**1**
			2	0	160	0.02	**2**
	120	0.5	1	0	530	0.16	**3**
		1	1	0	190	0.07	**4**
				1	230	0.01	**5**
				2	165	0.02	**6**
				4	220	0.03	**7**
			2	0	200	0.03	**8**
			5	0	170	0.04	**9**
		2	1	0	295	0.20	**10**
		5	1	2	175	0.19	**11**
	100	1	1	0	185	0.02	**12**
			2	0	200	0.04	**13**
	85	1	1	0	200	0.02	**14**
	70	1	1	0	260	0.20	**15**
			2	0	145	0.05	**16**
	50	1	1	0	290	0.19	**17**
			2	0	155	0.10	**18**

The data in Table 4.1 showed that the incorporation of the fluorescent ABMMA monomer does not have a consistent impact on the size and dispersity; particles **4**, **5**, **6,** and **7** were of slightly different size but within a 10% error, the dispersity varied between 0.01 and 0.07 but was still low and did not proportionally vary with the quantity of ABMMA.

The amount of initiator did not affect the size of the particles either, particles **4**, **8,** and **9** exhibited the same range of size and the dispersity, as well as particles **12** and **13**, or particles **1** and **2**. A difference in size could be observed between particles **15** and **16**, and **17** and **18**, but in these cases, the dispersity was also affected; a lower dispersity and smaller particles were obtained with 2 wt% of initiator.

It was observed as expected that the cross-linking density affects the particles size and dispersity. For example, 0.5 wt% cross-linking was too low as it formed large and disperse particles (**3**) compared to particles with 1 wt% cross-linking particles (**4**); 2 and 5 wt% cross-linking (respectively **10** and **11**) was too high as it formed particles with a high dispersity (PD > 0.150) in comparison with 1 wt% cross-linking particles (**4**). It seemed that the optimum percentage of cross-linker regarding size and dispersity is 1 wt%.

Variation of the equivalents between DEAEMA and OEGMA360 did not affect the size and dispersity (*ca.* 185 nm, PD < 0.1) of particles synthesised with 150, 120 or 100 equivalents of DEAEMA for 1 equivalent of OEGMA360 (respectively particles **1**, **4**, and **12**). However, for lower number of equivalents (85, 70 or 50; respectively particles **14**, **15**, and **17**) the diameter and the dispersity of the particles obtained were larger as the number of equivalents was smaller.

The synthesis of these different particles (**1-18**) highlighted that intra-particles interactions (larger diameter and dispersity) could be generated by higher cross-linking density, but also by higher OEGMA content (lower number of equivalent of

DEAEMA). However, for higher OEGMA content particles, the size and the dispersity of particles showed a dependence on the initiator amount.

The effect of the OEGMA molecular weight (from 360 Da to 2000 Da) on the particles size and responsive character was also studied (Table 4.2). Changing the molecular weight of the shell monomer OEGMA and keeping the same molar ratio did not affect the particles diameter in a consistent manner. Therefore, it was hypothesised that the density of the shell of the particles changed. These particles were synthesised with 120 equivalents of DEAEMA for 1 equivalent of OEGMA, 1 wt% EGDMA, 1 wt% KPS and 0-2 wt% ABMMA. The hydrodynamic diameter of the different particles in solution in deionised water was measured by dynamic light scattering (DLS) and it was found that the particles were all in the same size range, see Table 4.2 and Figure 4.8 for the DLS measurements of the different particles.

Table 4.2. Characteristics of the different particles synthesised.

Batch name [a]	OEGMA MW (Da)	Fluorescent?	D_h (nm)	PD
RP-360 (4[b])	360	No	190	0.04
RP-500	500	No	240	0.02
RP-950	950	No	230	0.04
RP-2000	2000	No	210	0.02
FRP-360 (7[b])	360	Yes	225	0.03
FRP-2000	2000	Yes	235	0.01

[a] Particle batches named FRP or RP followed by the molecular weight of the OEGMA used (e.g. FRP-360). RP and FRP stand respectively for Responsive Particles and Fluorescent Responsive Particles.

[b] Batch numbers from Table 4.1.

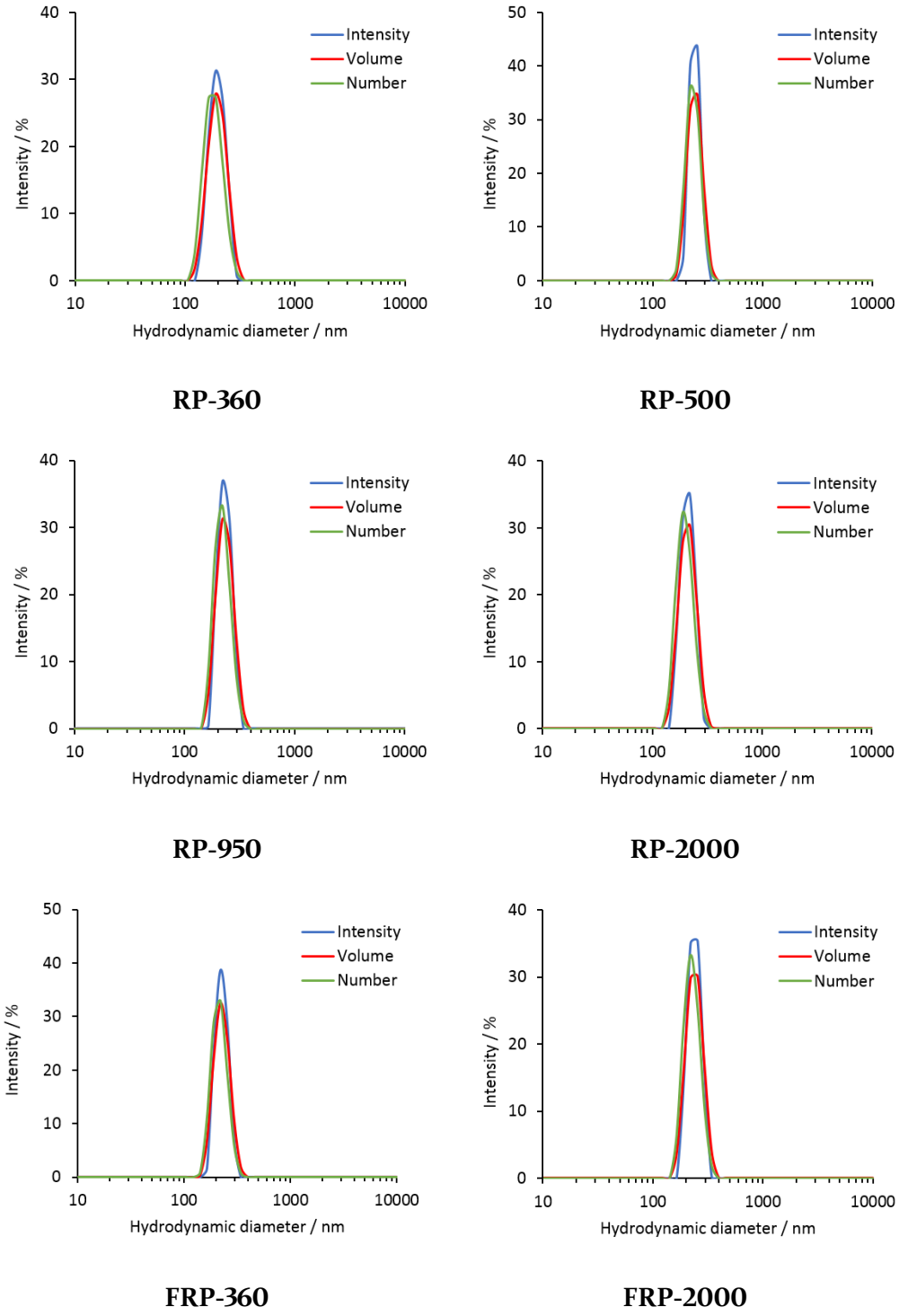

Figure 4.8. DLS data of the different particles synthesised at *ca.* 0.05 mg·mL^{-1}.

The variation of the OEGMA molecular weight or the incorporation of ABMMA did not affect the morphology of the particles and the size range. The different OEGMA utilised changed the density of the shell as the DP was kept the same and the

monomer increased in size. The size of fluorescent particles with different shells (**FRP-360** and **FRP-2000**) was also confirmed by transmission electron microscopy (TEM), see Figure 4.9. The spherical morphology of the particles was confirmed and the average diameter was measured to be 260 nm for particles **FRP-360** and 330 nm for particles **FRP-2000**. The difference between the DLS hydrodynamic diameter and the TEM average diameter could be attributed to the dry state of the TEM technique.[36] Fluorescence spectroscopy was performed on particles containing the fluorescent monomer (**FRP-360** and **FRP-2000**) in solution in deionised water. The particles both presented an emission maximum at 487 nm for an excitation maximum at 375 nm, see Figure 4.10 for emission and excitation spectra of particles **FRP-2000**. Compared to the monomer, only one of the two excitation maxima could be observed for the particles as a consequence of the presence of a scattering peak obscuring the excitation peak.

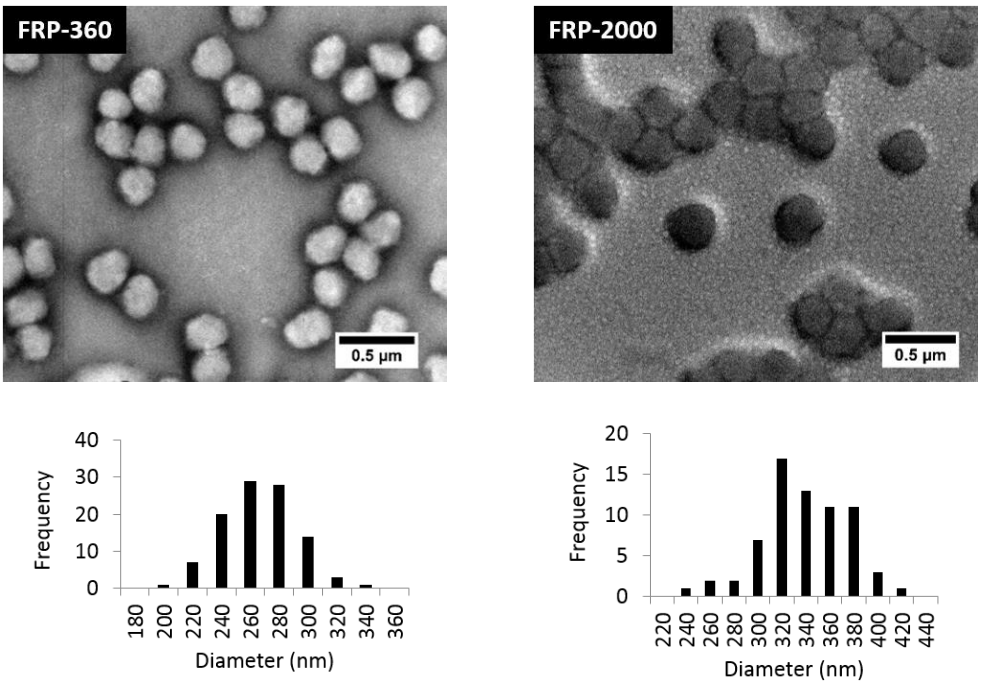

Figure 4.9. TEM images of particles of **FRP-360** and **FRP-2000** stained with uranyl acetate, and the distribution of size observed.*

* TEM images were acquired by Dr Anaïs Pitto-Barry.

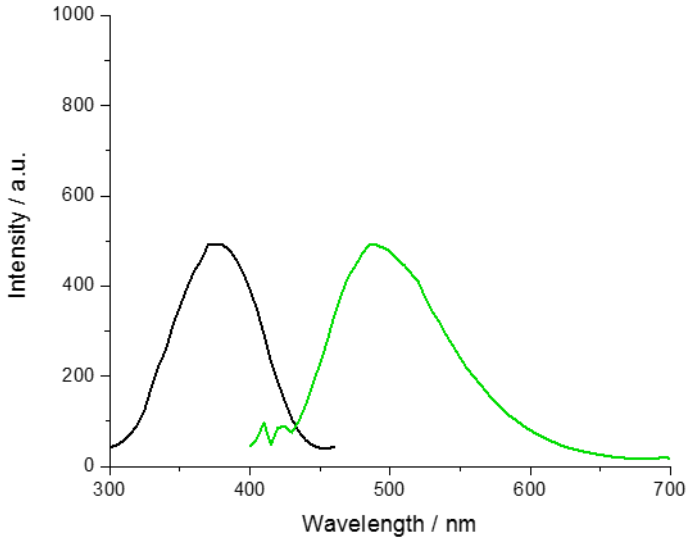

Figure 4.10. Fluorescence emission and excitation spectra for particles **FRP-2000** in water at *ca.* 0.05 mg·mL^{-1}; λ_{em} = 487 nm and λ_{ex} = 375 nm.

4.3.3. Responsiveness experiments

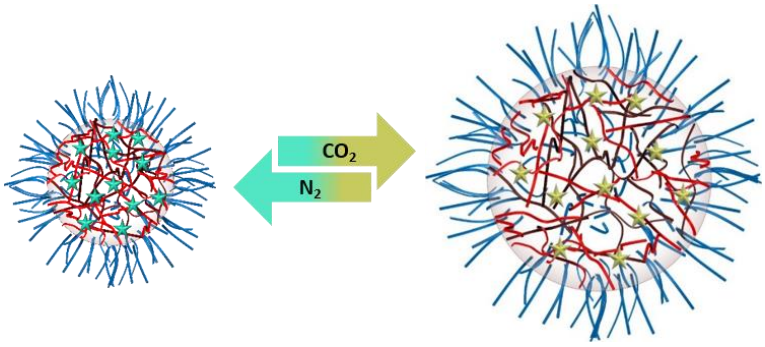

Scheme 4.3. Reversible swelling of a fluorescent responsive particle (FRP).

4.3.3.1. Particle size monitoring

4.3.3.1.1. By DLS

DLS was utilised to monitor changes in the particle diameter in response to bubbling with CO_2. When CO_2 was bubbled in the particles solution, the amines of PDEAEMA present in the core of the particles became protonated and therefore hydrophilic. Owing to their cross-linked structure, the particles swelled and increased in diameter instead of disassembling. A size increase upon CO_2 bubbling for 15 minutes was observed for all the particles, see Figure 4.11. For example, the hydrodynamic diameter of particles **RP-360** increased from 185 nm to 390 nm and particles **RP-2000** presented a diameter increase from 200 nm to 435 nm. As bubbling CO_2 in water changes the pH of the solution, it would have been interesting to control the pH of the different solutions before and after the CO_2 purge.

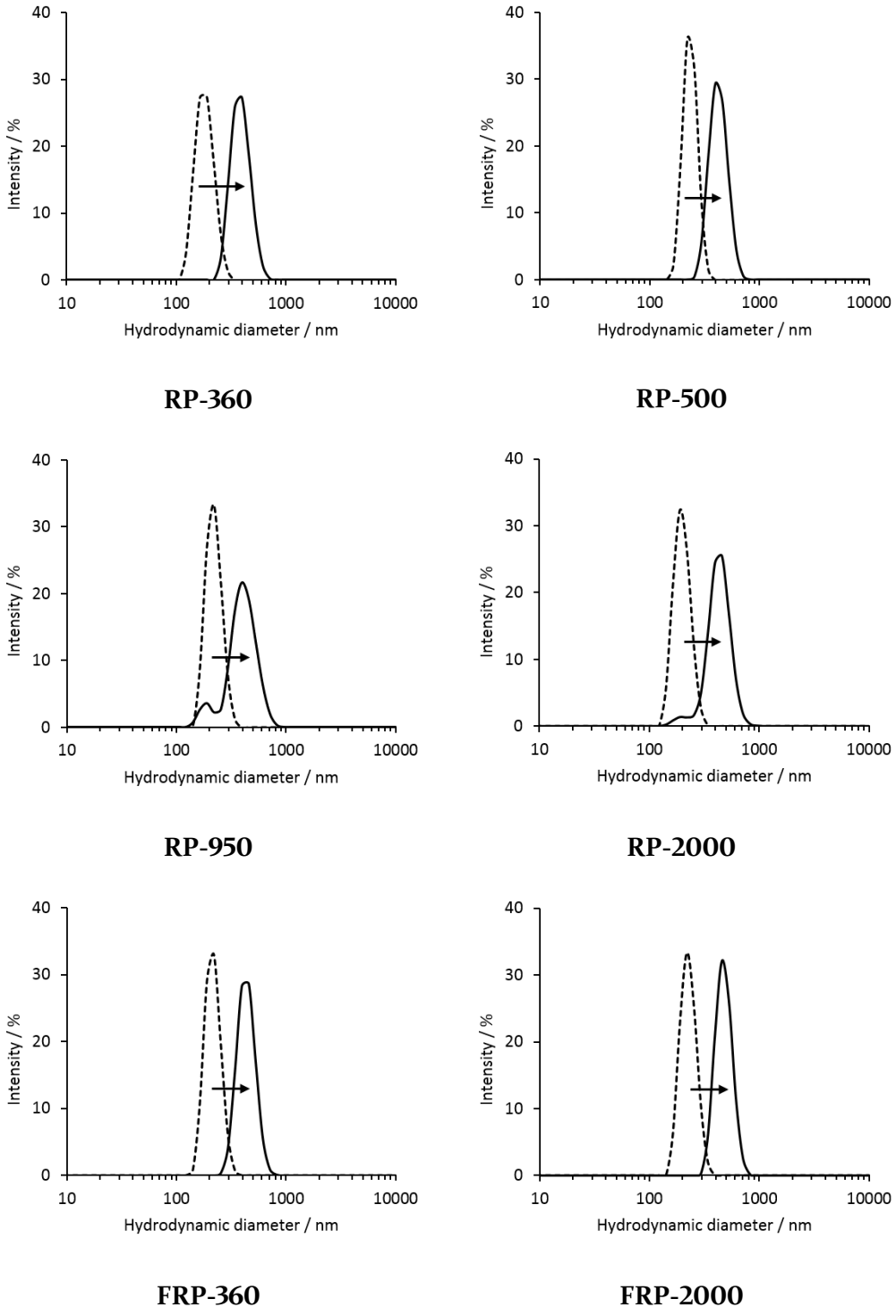

Figure 4.11. DLS data (number distribution) of the particles in water at *ca.* 0.05 mg·mL^{-1}, before (dash line) and after (solid line) CO_2 bubbling. See Table 4.3 for the data details and Figure 4.12 for an example of auto correlation function (**FRP-2000**).

Table 4.3. Hydrodynamic diameter of particles before and after CO_2 bubbling.

Batch name	Before CO_2 bubbling		After CO_2 bubbling	
	D_h (nm)	PD	D_h (nm)	PD
RP-360	190	0.04	405	0.05
RP-500	240	0.02	445	0.10
RP-950	230	0.04	450	0.08
RP-2000	210	0.02	460	0.04
FRP-360	225	0.03	450	0.03
FRP-2000	235	0.01	490	0.02

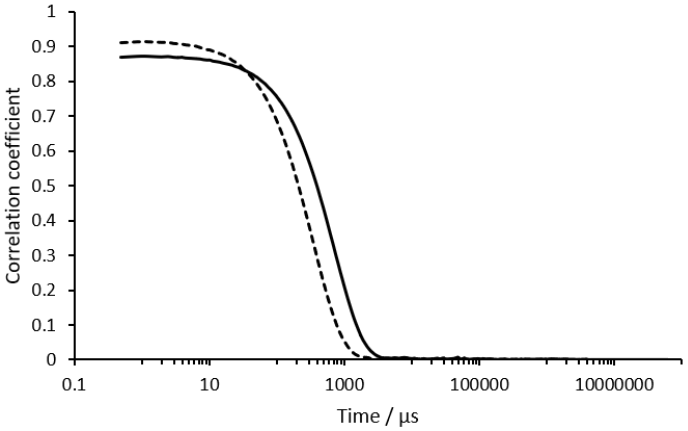

Figure 4.12. Example of auto correlation function for particles before (dash line) and after (solid line) CO_2 bubbling (**FRP-2000**).

4.3.3.1.2. By SAXS[†]

The size increase of the non-fluorescent particles with the small molecular weight OEGMA shell (**RP-360**) was also monitored by small-angle X-ray light scattering (SAXS) with an *in situ* CO_2 purge, see Figure 4.13. The SAXS data showed an increase of the radius of gyration within minutes. Analysis of the SAXS curves over a period of 21 minutes indicated an increase of particle size as well as an increase of the

[†] SAXS experiments and analyses were performed by Dr Anaïs Pitto-Barry.

dispersity. The initial particles could be analysed as spherical micelles with really low core dispersity and some coils accounting for the outer hydrated shell.[37,38] After bubbling CO_2 the dispersity of the core slightly increased (as evidenced by the loss of oscillations in the raw SAXS profiles) and a more pronounced core-shell spherical morphology was observed with an increase of core radius, see Figure 4.13. An initial diameter of 180 nm was observed, and an increase of the diameter was observed upon time: after 2 min of bubbling, 255 nm and after 21 min, 280 nm. The *in situ* analysis was not performed for an extended time as the SAXS profile did not evolve between 10 min 30 s and 21 min, see Figure 4.13.

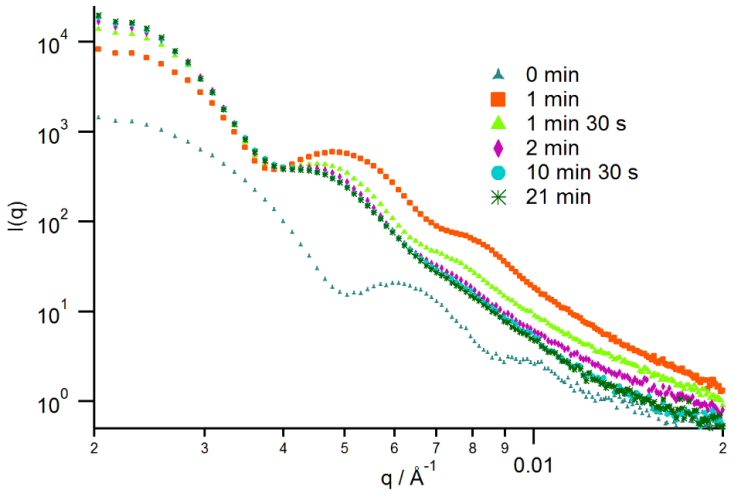

Figure 4.13. *In situ* monitoring by SAXS of particles (**RP-360**) with bubbling CO_2 over 21 min.

4.3.3.2. Fluorescence emission monitoring

As previously demonstrated by our group, the ABM functional group is sensitive to polar protic environments.[34] Thus, the ABM bearing monomer should be able to probe the protonation of its environment. Therefore, the increasing hydrophilicity of the core upon CO_2 bubbling should quench the fluorescence emission of the particles.

Fluorescence emission of the particles **FRP-360** and **FRP-2000** was measured before and after CO_2 bubbling, a drastic decrease of the intensity was observed in both cases. At 487 nm, for **FRP-360** the maximum decreased from 742 a.u. to 168 a.u., see Figure 4.14, and for **FRP-2000** the emission maximum decreased from 810 a.u. to 50 a.u., see Figure 4.15. The decrease in fluorescence emission upon CO_2 bubbling was also observed under a UV lamp (λ = 345 nm), see Figure 4.16.

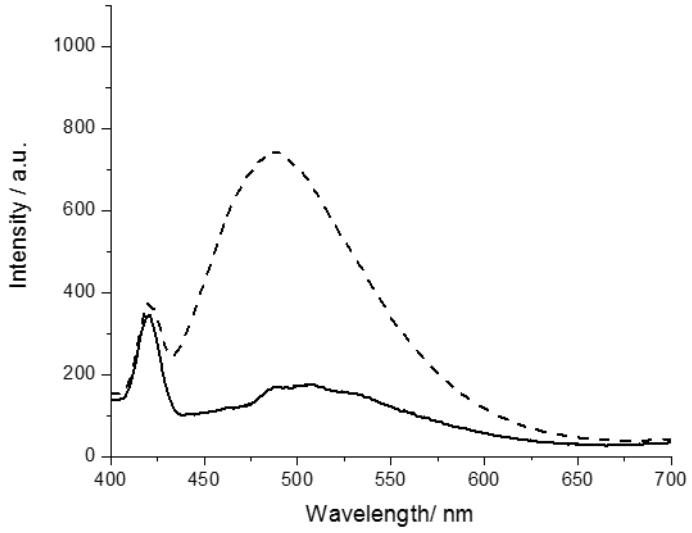

Figure 4.14. Fluorescence emission spectra of particles **FRP-360** in water at *ca.* 0.05 mg·mL^{-1}, before (dash line) and after (solid line) CO_2 bubbling; λ_{ex} = 375 nm.

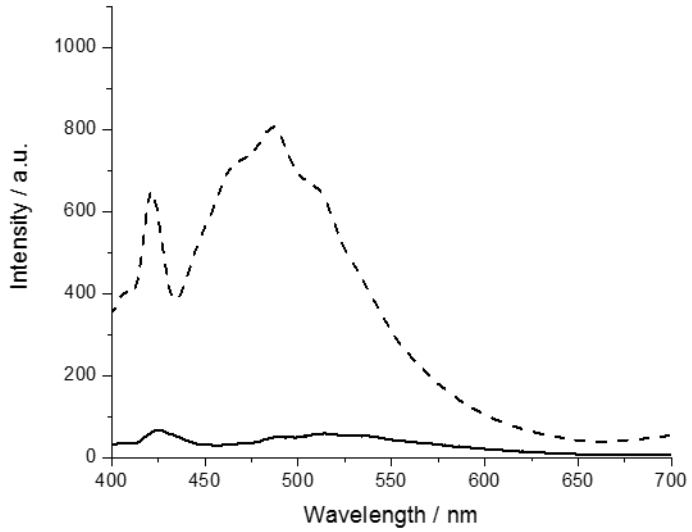

Figure 4.15. Fluorescence emission spectra of particles **FRP-2000** in water at *ca.* 0.05 mg·mL^{-1}, before (dash line) and after (solid line) CO_2 bubbling; λ_{ex} = 375 nm.

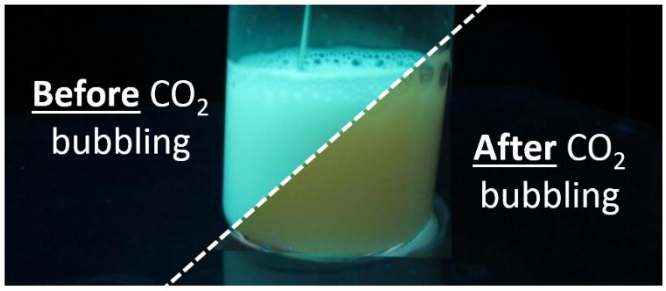

Figure 4.16. Pictures of particles (**FRP-360**) before and after CO_2 bubbling observed under a UV lamp at 345 nm.

4.3.3.3. Reversibility of the system: CO_2/N_2 purge cycles

To test the reversibility of the system, the particles solution was repeatedly purged with successive cycles of CO_2 and N_2 bubbling. Six purge cycles were monitored by DLS and fluorescence spectroscopy (2 extra cycles for fluorescence monitoring). The purging time was kept constant for the entire experiment, CO_2 was bubbled for 15 min and N_2 was bubbled for 30 min. Purge cycles experiments were performed on

fluorescent particles with the denser OEGMA shell (**FRP-2000**). The hydrodynamic diameter and the fluorescence emission at 487 nm of the particles (**FRP-2000**) were measured after each CO_2 or N_2 purge. As shown in Figure 4.17, the size of the particles alternatively increased and decreased six times. The dispersity of the particles also varied upon the different gas purges, see Figure 4.18, however the variation was consistent with the cycles. When CO_2 was bubbled into the particle solution, the particles shrunk and their dispersity decreased.

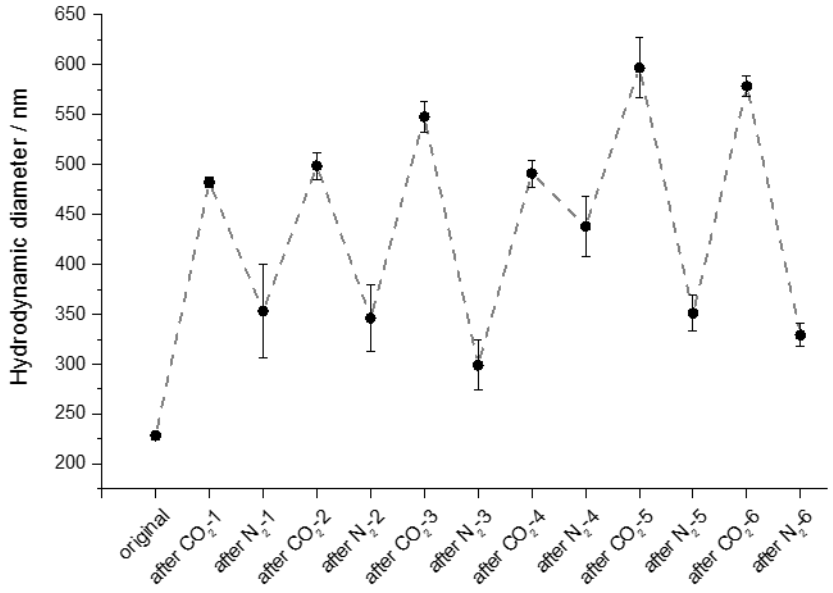

Figure 4.17. Hydrodynamic diameter of the particles in water in water at *ca.* 0.05 mg·mL^{-1}, (**FRP-2000**) measured after each gas purge. Error bars based on standard deviation. Line as a guide for the eye.

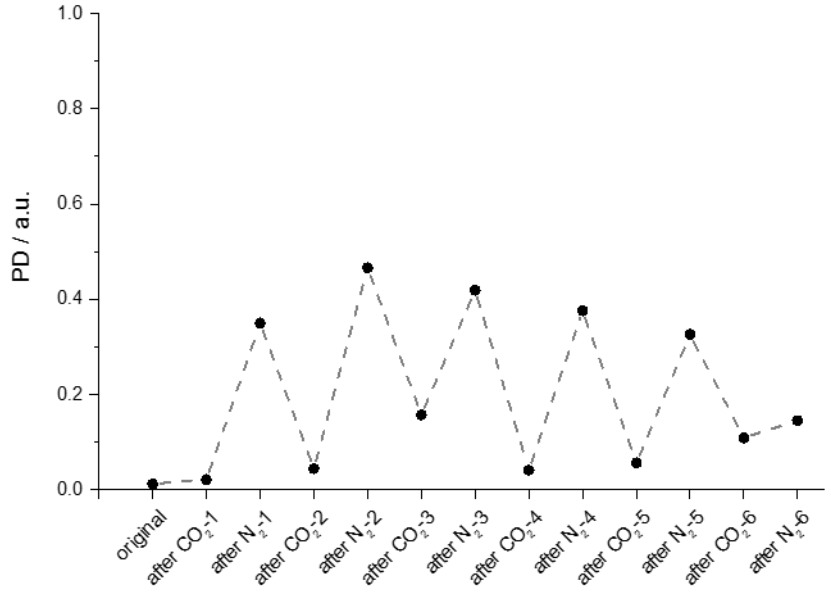

Figure 4.18. Variation of the polydispersity (PD) of the particles (**FRP-2000**) in water at *ca.* 0.05 mg·mL^{-1}, after each gas purge. Line as a guide for the eye.

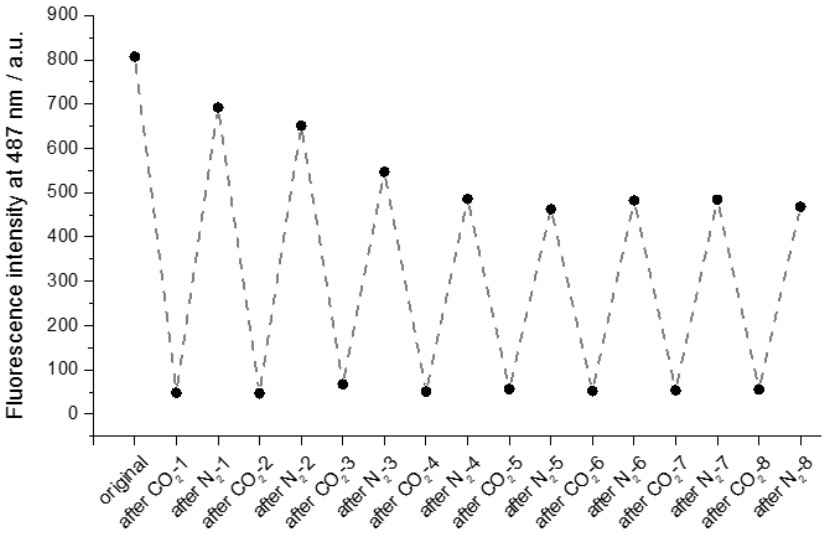

Figure 4.19. Fluorescence emission intensity of the particles in water at *ca.* 0.05 mg·mL^{-1}, (**FRP-2000**) after each gas purge, measured at 487 nm. λ_{ex} = 375 nm. Line as a guide for the eye.

The fluorescence emission intensity was also monitored and was reversibly quenched eight times, see Figure 4.19. The progressive decrease of the maximum

intensity could be explained by an equilibration of the hydration of the system through the first cycles and stays stable from cycle number 4.

The reversibility of the system was also tested on particles with a less dense shell (**RP-360**, **FRP-360**, **RP-500**, **and RP-950**). Despite being able to swell, these particles were unable to collapse upon N_2 bubbling and formed large aggregates. For example, particles **RP-360** exhibited a hydrodynamic diameter of 380 nm after bubbling CO_2, then formed large aggregates upon N_2 bubbling. This solution was subsequently purged with CO_2 and a single population of particles could be observed again with a diameter of 390 nm, see Figure 4.20.

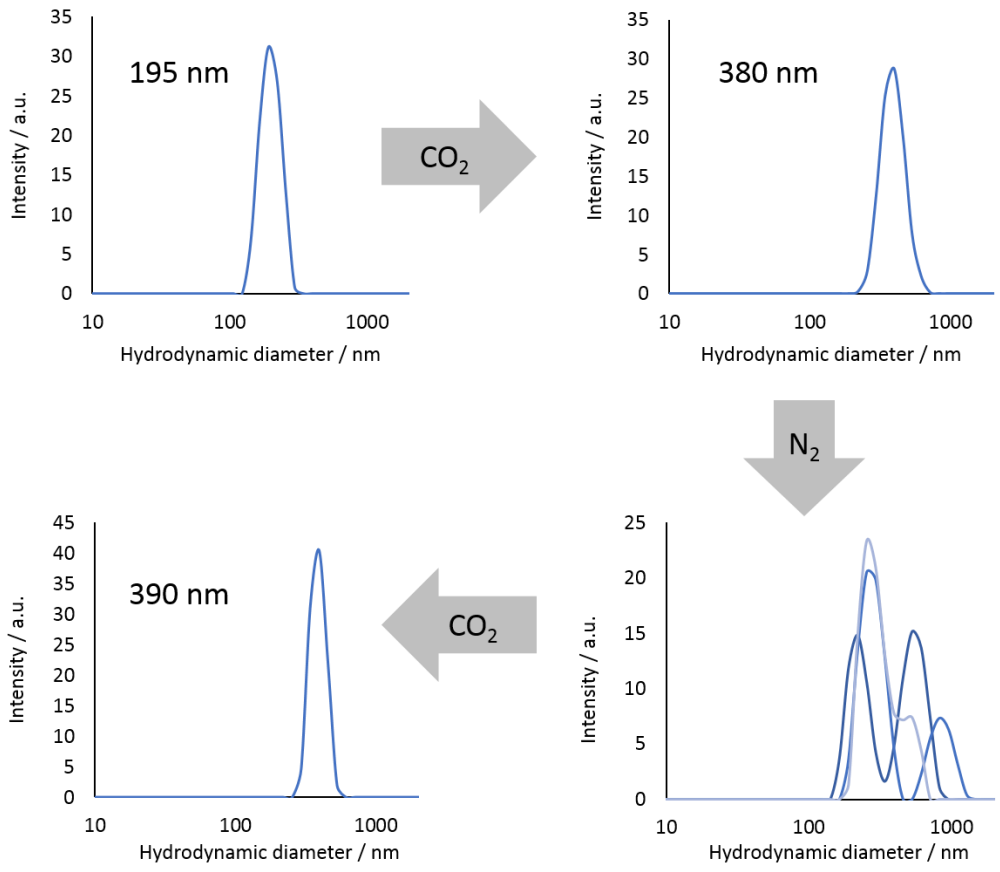

Figure 4.20. DLS data (number distribution) example of irreversible swelling for particles **RP-360** in water at *ca.* 0.05 mg·mL^{-1}. The third graphic shows repeat measurements.

It was hypothesised that the inability to recover the particles' original size could be attributed to the low density of the shell that cannot counter the effect of some core chains irreversibly penetrating the shell during the first protonation. The presence of these hydrophobic chains trapped in the shell when the particles shrink promotes inter-particle interactions, which leads to the formation of uncontrolled large aggregates, see Figure 4.21. The formation of aggregates was significantly reduced with a denser shell made of OEGMA with a molecular weight of 2000 Da (compared to 360 Da used previously). This was also confirmed by the variation of the dispersity shown in Figure 4.18; while the interaction was reduced with the formation of a denser shell, the dispersity still increased upon N_2 bubbling and was reduced when particles were stabilised with CO_2 bubbling (reduction of the pH).

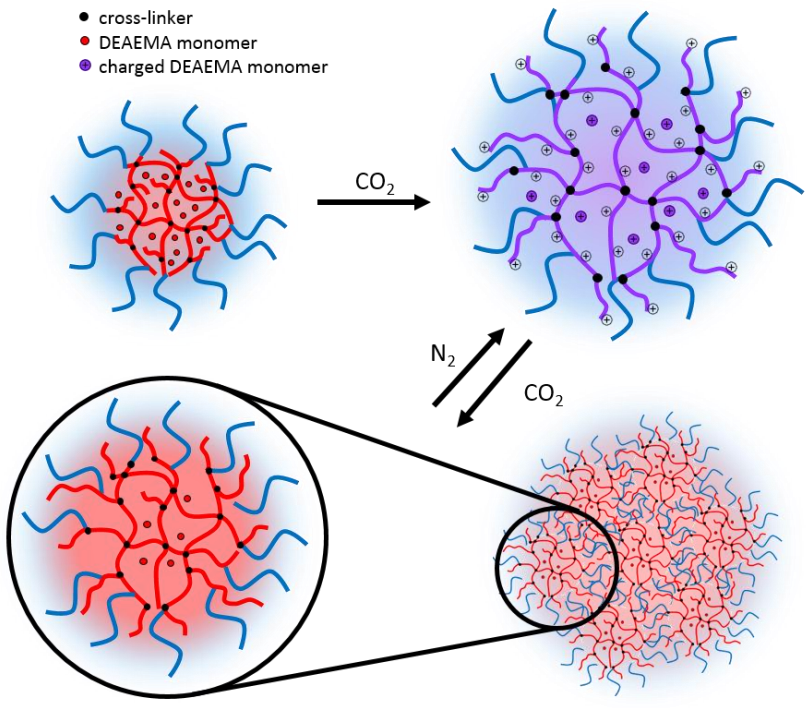

Figure 4.21. Schematic of potential inter-particles interactions.

4.3.3.4. Additional experiments

*4.3.3.4.1. Zeta potential measurements with **RP-360***

In the previous section (Figure 4.21), it was hypothesised that after CO_2 bubbling, particles could be stabilised by charged chains from the core penetrating the shell. The zeta potential of the particles (**RP-360**) in solution was measured before and after bubbling CO_2 and N_2. It was observed that after CO_2 bubbling, the zeta potential was around +30 mV.

It is known that particles with a zeta potential between -30 and +30 mV are less stable than particles with a zeta potential higher than +30 mV or lower than -30 mV, and can form aggregates.[39] One of the factor affecting the zeta potential is the pH of the solution, typically, particles will have a zeta potential higher than +30 mV or lower than -30 mV for low and high pH respectively.

The results obtained were consistent with the theory: particles are more stable after CO_2 bubbling and tend to aggregate after bubbling nitrogen.

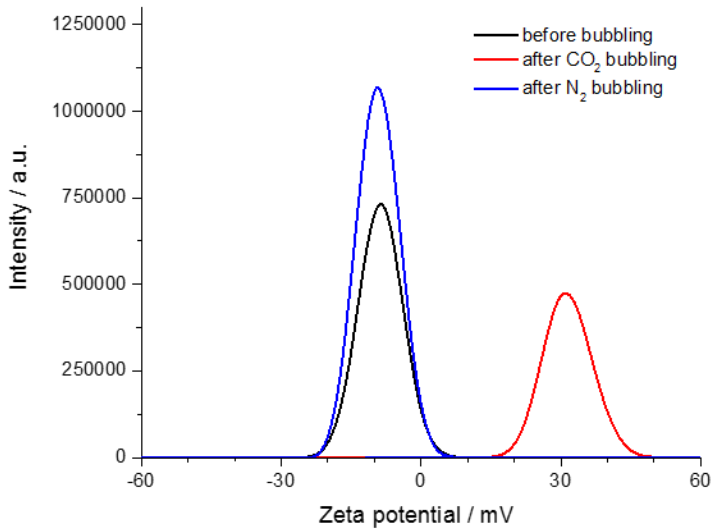

Figure 4.22. Zeta potential distribution for particles solutions in water at *ca.* 0.05 mg·mL^{-1}, before any bubbling, after CO_2 bubbling, and after N_2 bubbling.

*4.3.3.4.2. pH-response with **RP-360***

As mentioned previously in this chapter, these FRP are CO_2/pH-responsive as a consequence of the core composition being mainly DEAEMA. It was shown that particles are responsive to CO_2 *via* monitoring of the particles size upon gas purges. In order to confirm that the response was a result of the protonation of the DEAEMA monomer induced by a change in pH through dissolution of CO_2 in water, the size of the particles was directly measured upon pH change *via* addition of HCl/NaOH solutions (0.1 and 0.05 M). The experiment was realised in different conditions, the first set was performed *via* manual addition of acid/base (see Figure 4.23) and individual measurements of the hydrodynamic diameter, and the second set was obtained through an automated titrator combined with a DLS (see Figure 4.24). The automated system was utilised to refine the data obtained manually by measuring more data points but it required to perform separated measurements (different colour plots in Figure 4.24) for smaller range of pHs.

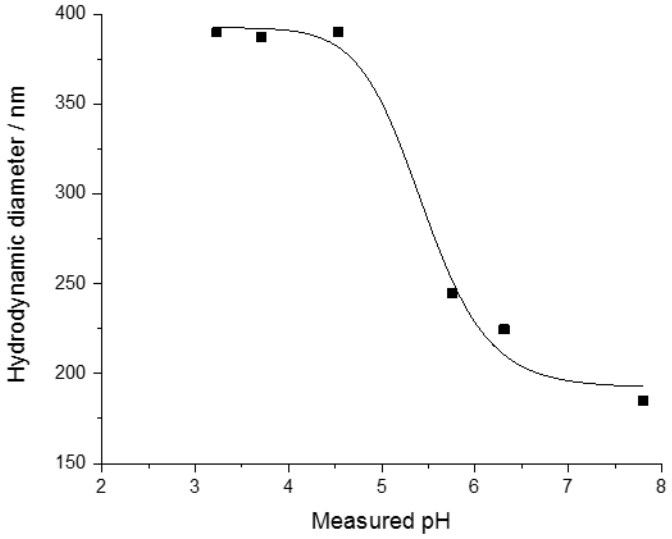

Figure 4.23. Particles size measurements at different pHs (adjusted manually) in water at *ca.* 0.05 mg·mL^{-1}.

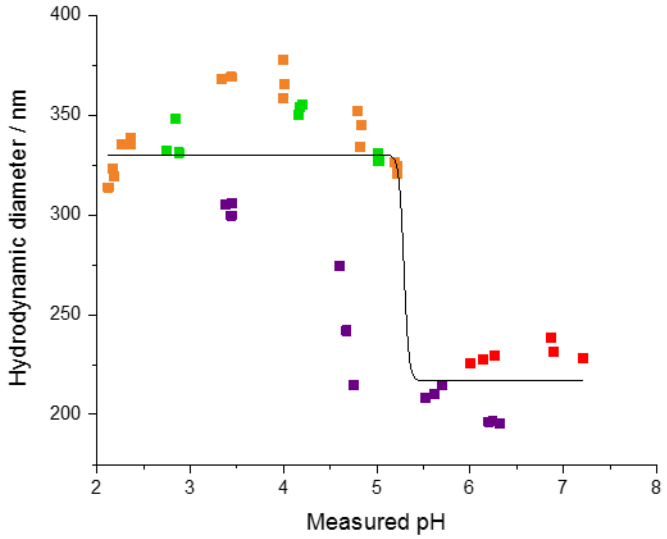

Figure 4.24. Multiple series of particles size measurements at different pHs in water at *ca.* 0.05 mg·mL^{-1}, (auto-titrator coupled to DLS). The different colour plots correspond to different measurements over different ranges of pH: orange and green for pH 2-5.5, purple pH 3-6.5 and red pH 6-7.5.

For both sets of results, a clear change in particle size was observed around pH 5-5.5. For the manual experiment, the diameter changed from 192 nm to 392 nm, and for the automated measurements, the diameter increased from 217 nm to 330nm. These results confirmed the pH-responsive nature of the particles.

*4.3.3.4.3. Temperature-response with **RP-360***

It has previously been shown that a PEGMA-DEAEMA copolymer can exhibit a temperature-responsive behaviour depending on the polymer composition.[40] The particles were therefore tested for temperature response independently from any pH modification: the diameter of the particles was monitored over a range of temperatures from 20 to 90 °C, see Figure 4.25 below. This experiment was performed with particles

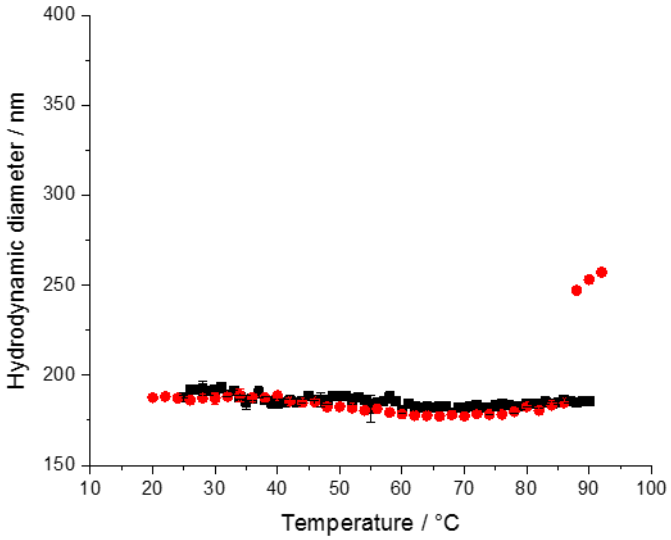

Figure 4.25. Particles size monitored over a range of temperatures 20-90 °C in water at *ca.* 0.05 mg·mL^{-1} (performed in duplicate).

The graph showed the absence of a temperature response, the size of the particles stayed constant between 20 and 90 °C. The three data point around 90 °C could be attributed to bubbles as it is close to the boiling point of water.

4.4. Conclusions

The synthesis of fluorescent responsive particles has been presented. These cross-linked particles were composed of a responsive DEAEMA core cross-linked with EGDMA, and an OEGMA shell. Moreover, the core of these particles was labelled with a novel fluorescent monomer whose synthesis was also presented. This ABM containing methacrylate novel monomer was inspired by the ABM fluorophores presented in chapter 3. The synthesis of the particles *via* free-radical polymerisation allowed the formation of well-defined particles. These particles were analysed by DLS and fluorescence spectroscopy, and found to have a $R_h \approx 200$nm and be emissive in solution in water.

Upon CO_2 bubbling, the DEAEMA got protonated and increased the hydrophilicity of the core, which generate the swelling of the particles (as a consequence of the presence of the cross-linker, the assembly was retained). The consequence of this local change in hydrophobicity was a drastic decrease of the fluorescence emission of the ABM. Thus, the fluorescence intensity could be used to probe the particle core hydrophobicity and particle size. The reversible aspect of this system was obtained after optimisation of the particles composition. It has been demonstrated that the density of the shell can affect the stability and favour aggregation for less dense shell or prevent aggregation for denser shells.

4.5. Experimental

4.5.1. Materials and methods

Dry solvents were obtained by passing over a column of activated alumina using an Innovative Technologies solvent purification system. DEAEMA was filtered through a plug of alumina prior to use and stored at 4 °C. All other chemicals were purchased from Aldrich, Fluka or Acros and used as received.

^{1}H and ^{13}C NMR spectra were recorded on a Bruker DPX-400, or AV300 spectrometer at room temperature unless otherwise stated. Chemical shifts are given in ppm downfield from the internal standard tetramethylsilane (TMS).

Infrared spectra were recorded (neat) on a PerkinElmer, Spectrum 100 FT-IR Spectrometer.

High Resolution Mass Spectrometry (HR-MS) was conducted on a Bruker UHR-Q-ToF MaXis with electrospray ionisation.

Fluorescence spectra were recorded using an Agilent Cary Eclipse Fluorescence spectrophotometer. UV-vis spectroscopy was carried out on a Perkin Elmer Lambda 35 UV/vis spectrometer or an Agilent Cary 60 UV-Vis Spectrophotometer. Quartz cells with screw caps and four polished sides (Starna) were used for fluorescence and UV-vis measurements.

Dynamic Light Scattering (DLS) measurements were performed with a Malvern Zetasizer Nano ZS instrument and analysed with Malvern Zetasizer Software 7.03. All measurements were made in triplicate (with 10 measurements recorded for each run).

Synchrotron small-angle X-ray scattering (SAXS) measurements were carried by Dr Anaïs Pitto-Barry, on the SAXS/WAXS beamline at the Australian Synchrotron facility at a photon energy of 11 keV. The samples in solution were run by using a 1.5

mm diameter quartz capillary. Temperature was held at 25 °C and controlled *via* a water bath connected to a brass block which is part of the sample holder. The measurements were collected at a sample-to-detector distance of 7.323 m to give a q range of 0.02 to 0.14 $Å^{-1}$.

All patterns were normalised to fixed transmitted flux using a quantitative beamstop detector. The scattering from a blank was measured in the same capillary and was subtracted for each measurement. The two-dimensional SAXS images were converted in one-dimensional SAXS profile ($I(q)$ *vs* q) by circular averaging, where $I(q)$ is the scattering intensity. The functions used for the fitting from the NIST SANS analysis package were "Guinier-Porod",[41,42] "Debye",[43] "PolyCoreForm".[44] ScatterBrain[45] and Igor[46] were used to plot and analyse the data. The scattering length density of the solvent and the monomers were calculated using the "Scattering Length Density Calculator" provided by NIST Center for Neutron Research. Limits for q range were applied for the fittings from 0.002 to 0.1 $Å^{-1}$.

The stained transmission electron microscopy (TEM) images were obtained using a JEOL 2000FX or a JEOL 2100 LaB_6 instrument operated at 200 kV. TEM samples were negatively stained by a aqueous solution of uranyl acetate (UA, 2.5 wt%) on formvar/carbon grids (300 Mesh, Cu, Elektron Technology UK LTD). Typically, formvar/carbon grids were cleaned by air plasma from a glow-discharge system (2 min, 20 mA) which also improved the hydrophobicity of the grids. 5 µL of particle solution was added onto the grid and the solution was left to air-dry for 3 h. 5 µL of a 2.5 wt% UA solution was then added onto the grid to stain the particles and was blotted away after 15 s before air-drying.

4.5.2. Synthetic procedures

4.5.2.1. Monomer synthesis

4.5.2.1.1. Synthesis of the dibromomaleimide methacrylate (DBMMA)

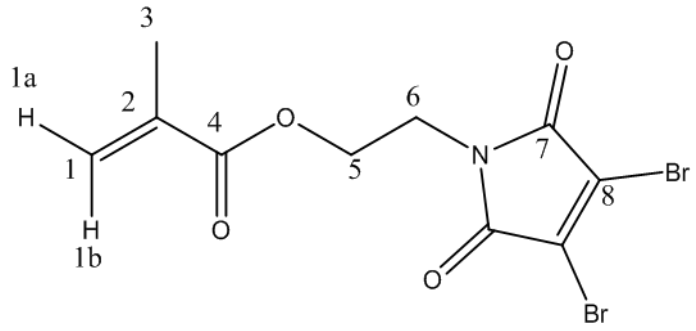

To an oven-dried round-bottom flask under an inert nitrogen atmosphere was added triphenyl phosphine (1.03 g, 1 equiv.) and dry THF (35 mL). The mixture was cooled to -78 °C before the dropwise addition of diisopropyl azodicarboxylate (0.769 mL, 1 equiv.). The mixture was stirred for 5 min before adding 2-hydroxyethyl 2-methylprop-2-enoate (0.475 mL, 1 equiv.), stirred for a further 5 min before adding 2,2 dimethylpropan-1-ol (0.170 g, 0.5 equiv.), and stirred a further 5 min before adding 2,3-dibromomaleimide (1.00 g, 1 equiv.). The reaction was allowed to warm to room temperature while stirring for 18 h. The solvent was removed *in vacuo*, and the crude mixture purified by column chromatography on silica gel using a 1:1 mixture of petroleum ether and dichloromethane, to give the product as a white solid (1.037 g, 73 %). ^{1}H NMR (300 MHz, $CDCl_3$) δ 6.08 (1H, br, H1b), 5.59 (1H, br, H1a), 4.30 (2H, t, $^{3}J_{H\text{-}H}$ = 6.0 Hz, H5), 3.95 (2H, t, $^{3}J_{H\text{-}H}$ = 5.5 Hz, H6), 1.90 (3H, s, H3); ^{13}C NMR (75 MHz, $CDCl_3$) δ 163.1 (C7), 136.2 (C8), 135.2 (C2), 128.9 (C4), 126.0 (C1), 61.0 (C5), 38.0 (C6), 17.6 (C3); FTIR (neat) ν_{max} / cm^{-1} 1720 (C=O of ester), 1633 (C=O of maleimide), 1595 (C=C aromatic), 1170 (C-O of ester); HR-MS (MaXis) *m/z* found 389.8770, calc. 389.8770 ([M+Na]$^{+}$, 100 %).

4.5.2.1.2. Synthesis of (isopropyl)aminobromomaleimide methacrylate (ABMMA)

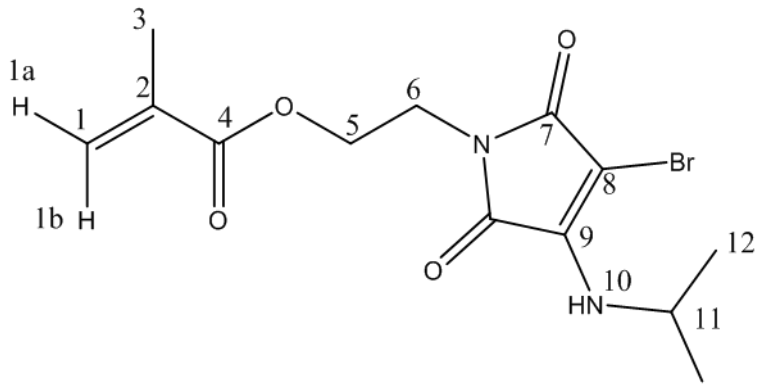

DBMMA (1.00 g, 1 equiv.) was dissolved in THF (50 mL). To the solution, sodium carbonate (0.720 g, 2.5 equiv.) was added and stirred. Isopropylamine (0.250 mL, 1.05 equiv.) was added dropwise to the solution, whereby an immediate colour change of the solution from colourless to yellow and the formation of a white precipitate was observed. Upon complete addition of isopropylamine, the solution was left to stir for 2 h at room temperature. The solvent was removed *in vacuo*, the residue dissolved in CH_2Cl_2 (150 mL), washed with water (2 × 150 mL) and dried with $MgSO_4$. The organic layer was concentrated *in vacuo* and the product purified by column chromatography on silica gel using a 10:1 mixture of petroleum ether and ethyl acetate to yield the product as a yellow-orange solid (0.88 g, 94 %). ^{1}H NMR (400 MHz, $CDCl_3$) δ 6.09 (1H, br, H1b), 5.58 (1H, br, H1a), 5.28 (1H, br, H10), 4.42 (1H, m, H11), 4.27 (2H, t, $^3J_{H\text{-}H}$ = 5.0 Hz, H5), 3.84 (2H, t, $^3J_{H\text{-}H}$ = 6.0 Hz, H6), 1.91 (3H, s, H3), 1.30 (6H, d, $^3J_{H\text{-}H}$ = 6.5 Hz, H12); ^{13}C NMR (75 MHz, $CDCl_3$) δ 166.8 & 166.4 (C4, C8), 165.4 (C7), 141.7 (C9), 135.2 (C2), 125.7 (C1), 61.3 (C5), 44.2 (C11), 36.8 (C6), 23.1 (C12), 17.6 (C3); FTIR (neat) ν_{max} / cm^{-1} 3284 (H-N of isopropylamine), 1710 and 1657 (C=O of maleimide), 1181 (C-O of ester); HR-MS (MaXis) *m/z* found 367.0267, calc. 367.0264 ([M+Na]$^+$,100%); $\lambda_{ex,max}$ (10^{-5} M in 1,4-dioxane at r.t.) 247 nm and 372 nm, $\lambda_{em,max}$ (10^{-5} M in 1,4-dioxane at r.t.) 482 nm.

4.5.2.2. Particles

General procedure for the synthesis of fluorescent particles.

Oligoethylene glycol methacrylate (OEGMA) (0.11 mmol) was first dissolved in 44 mL of water and then ethylene glycol dimethacrylate (EGDMA) (0.126 mmol), and aminobromomaleimide methacrylate (ABMMA) (0.145 mmol) were dissolved in *N,N*-(diethylaminoethyl methacrylate) (DEAEMA) (13.5 mmol) and added dropwise to the solution. The mixture, whilst stirred, was purged with nitrogen for 30 min and further heated at 65 °C for 30 min. The initiator, potassium persulfate (KPS) (0.093 mmol), was dissolved in water (1 mL) and purged with nitrogen before being added to the reaction mixture. The reaction was stirred at 65 °C for 16 h under a nitrogen atmosphere. The particles were purified by exhaustive dialysis (MWCO 3.5 kDa) against water.

*4.5.2.2.1. Responsive and fluorescent responsive particles **1-18***

For all these different batches of particles, OEGMA, MW = 360 Da, Ω-end: OH, was used, and the different ratios between the monomers and initiator were detailed in Table 4.2.

*4.5.2.2.2. Responsive particles with OEGMA360 (**RP-360**)*

In this case, OEGMA, MW = 360 Da, Ω-end: OH (0.04 g), DEAEMA (2.5 g), EGDMA (0.025 g) and KPS (0.025 g) were used in the general procedure.

*4.5.2.2.3. Fluorescent responsive particles with OEGMA360 (**FRP-360**)*

In this case OEGMA, MW = 360 Da, Ω-end: OH (0.04 g), DEAEMA (2.5 g), EGDMA (0.025 g), KPS (0.025 g) and ABMMA (0.09 g) following the general procedure.

*4.5.2.2.4. Responsive particles with OEGMA500 (**RP-500**)*

In this case, OEGMA, MW = 500 Da, Ω-end: CH_3 (0.055 g), DEAEMA (2.5 g), EGDMA (0.025 g) and KPS (0.025 g) were used in the general procedure.

*4.5.2.2.5. Responsive particles with OEGMA950 (**RP-950**)*

In this case, OEGMA, MW = 950 Da, Ω-end: CH_3 (0.105 g), DEAEMA (2.5 g), EGDMA (0.025 g) and KPS (0.025 g) were used in the general procedure.

*4.5.2.2.6. Responsive particles with OEGMA2000 (**RP-2000**)*

In this case, OEGMA, MW = 2000 Da, Ω-end: CH_3, 50 wt% solution in water (0.442 g), DEAEMA (2.5 g), EGDMA (0.025 g) and KPS (0.025 g) were used in the general procedure.

*4.5.2.2.7. Fluorescent responsive particles with OEGMA2000 (**FRP-2000**)*

In this case, OEGMA, MW = 2000 Da, Ω-end: CH3, received as 50 wt% solution in water (0.442 g), DEAEMA (2.5 g), EGDMA (0.025 g), KPS (0.025 g) and ABMMA (0.05 g) were used in the general procedure.

4.5.2.3. General procedure for CO_2/N_2 responsiveness experiments

Carbon dioxide was bubbled into the solution of particles through a needle at a regular flow for 15 min. After characterisation of the solution post-CO2-bubbling, nitrogen was bubbled in the same solution for 30 min, and the resulting solution was characterised. For the different measurements, different solution concentrations were necessary, therefore cycles monitored by fluorescence and light scattering were performed with distinct samples.

4.6. References

1. A. B. Mabire, Q. Brouard, A. Pitto-Barry, R. J. Williams, H. Willcock, N. Kirby, E. Chapman and R. K. O'Reilly, *Polym. Chem.*, 2016, **7**, 5943-5948.

2. M. R. Hill, E. J. MacKrell, C. P. Forsthoefel, S. P. Jensen, M. Chen, G. A. Moore, Z. L. He and B. S. Sumerlin, *Biomacromolecules*, 2015, **16**, 1276-1282.

3. C.-Y. Chen and H.-L. Wang, *Macromol. Rapid Commun.*, 2014, **35**, 1534-1540.

4. P. Theato, B. S. Sumerlin, R. K. O'Reilly and T. H. Epps, *Chem. Soc. Rev.*, 2013, **42**, 7055-7056.

5. I. Cobo, M. Li, B. S. Sumerlin and S. Perrier, *Nat. Mater.*, 2015, **14**, 143-159.

6. B. W. Liu, H. Zhou, S. T. Zhou, H. J. Zhang, A. C. Feng, C. M. Jian, J. Hu, W. P. Gao and J. Y. Yuan, *Macromolecules*, 2014, **47**, 2938-2946.

7. S. Dai, P. Ravi and K. C. Tam, *Soft Matter*, 2008, **4**, 435-449.

8. X. Xiao, S. He, M. Dan, F. Huo and W. Zhang, *Chem. Commun.*, 2014, **50**, 3969-3972.

9. B. A. Abel, M. B. Sims and C. L. McCormick, *Macromolecules*, 2015, **48**, 5487-5495.

10. M. I. Gibson and R. K. O'Reilly, *Chem. Soc. Rev.*, 2013, **42**, 7204-7213.

11. S. Lin and P. Theato, *Macromol. Rapid Commun.*, 2013, **34**, 1118-1133.

12. A. Darabi, P. G. Jessop and M. F. Cunningham, *Chem. Soc. Rev.*, 2016, **45**, 4391-4436.

13. E. Girard, T. Tassaing, J.-D. Marty and M. Destarac, *Chem. Rev.*, 2016, **116**, 4125-4169.

14. Q. Yan and Y. Zhao, *J. Am. Chem. Soc.*, 2013, **135**, 16300-16303.

15. P. Schattling, I. Pollmann and P. Theato, *React. Funct. Polym.*, 2014, **75**, 16-21.

16. Q. Yan, R. Zhou, C. Fu, H. Zhang, Y. Yin and J. Yuan, *Angew. Chem. Int. Ed.*, 2011, **50**, 4923-4927.

17. J. Y. Quek, P. J. Roth, R. A. Evans, T. P. Davis and A. B. Lowe, *J. Polym. Sci., Part A: Polym. Chem.*, 2013, **51**, 394-404.

18. J. Pinaud, E. Kowal, M. F. Cunningham and P. Jessop, *ACS Macro Lett.*, 2012, **1**, 1103-1107.

19. S. Shahalom, T. Tong, S. Emmett and B. R. Saunders, *Langmuir*, 2006, **22**, 8311-8317.

20. Y. Hoshino, K. Imamura, M. Yue, G. Inoue and Y. Miura, *J. Am. Chem. Soc.*, 2012, **134**, 18177-18180.

21. S. Salentinig, P. Jackson and A. Hawley, *Macromolecules*, 2015, **48**, 2283-2289.

22. A. J. Morse, S. P. Armes, K. L. Thompson, D. Dupin, L. A. Fielding, P. Mills and R. Swart, *Langmuir*, 2013, **29**, 5466-5475.

23. Y. Chen, T. Zhao, B. Wang, D. Qiu and N. Ma, *Langmuir*, 2015, **31**, 8138-8145.

24. H. Wang, M. Xu, M. Xiong and J. Cheng, *Chem. Commun.*, 2015, **51**, 4807-4810.

25. M. P. Robin and R. K. O'Reilly, *Polym. Int.*, 2015, **64**, 174-182.

26. J.-K. Y. Tan, J. L. Choi, H. Wei, J. G. Schellinger and S. H. Pun, *Biomater. Sci.*, 2015, **3**, 112-120.

27. S. Li, K. Hu, W. Cao, Y. Sun, W. Sheng, F. Li, Y. Wu and X.-J. Liang, *Nanoscale*, 2014, **6**, 13701-13709.

28. M. P. Robin, P. Wilson, A. B. Mabire, J. K. Kiviaho, J. E. Raymond, D. M. Haddleton and R. K. O'Reilly, *J. Am. Chem. Soc.*, 2013, **135**, 2875-2878.

29. M. P. Robin, A. B. Mabire, J. C. Damborsky, E. S. Thom, U. H. Winzer-Serhan, J. E. Raymond and R. K. O'Reilly, *J. Am. Chem. Soc.*, 2013, **135**, 9518-9524.

30. M. P. Robin and R. K. O'Reilly, *Chem. Sci.*, 2014, **5**, 2717-2723.

31. M. P. Robin, J. E. Raymond and R. K. O'Reilly, *Mater. Horiz.*, 2015, **2**, 54-59.

32. Z.-L. Li, L. Sun, J. Ma, Z. Zeng and H. Jiang, *Polymer*, 2016, **84**, 336-342.

33. A. B. Mabire, M. P. Robin, H. Willcock, A. Pitto-Barry, N. Kirby and R. K. O'Reilly, *Chem. Commun.*, 2014, **50**, 11492-11495.

34. A. B. Mabire, M. P. Robin, W.-D. Quan, H. Willcock, V. G. Stavros and R. K. O'Reilly, *Chem. Commun.*, 2015, **51**, 9733-9736.

35. M. A. Walker, *J. Org. Chem.*, 1995, **60**, 5352-5355.

36. J. P. Patterson, M. P. Robin, C. Chassenieux, O. Colombani and R. K. O'Reilly, *Chem. Soc. Rev.*, 2014, **43**, 2412-2425.

37. D. B. Wright, J. P. Patterson, A. Pitto-Barry, P. Cotanda, C. Chassenieux, O. Colombani and R. K. O'Reilly, *Polym. Chem.*, 2015, **6**, 2761-2768.

38. D. B. Wright, J. P. Patterson, A. Pitto-Barry, A. Lu, N. Kirby, N. C. Gianneschi, C. Chassenieux, O. Colombani and R. K. O'Reilly, *Macromolecules*, 2015, **48**, 6516-6522.

39. *Zeta potential - An introduction in 30 minutes*, Malvern Instrument Limited 2016.

40. G. Gotzamanis and C. Tsitsilianis, *Polymer*, 2007, **48**, 6226-6233.

41. A. Guinier and G. Fournet, *Small-angle scattering of X-rays*, John Wiley & Sons, New York, 1955.

42. O. Glatter and O. Kratky, *Small-Angle X-Ray Scattering*, Academic Press, 1982.

43. R.-J. Roe, *Methods of X-ray and Neutron Scattering in Polymer Science*, Oxford University Press, New York, 2000.

44. P. Bartlett and R. H. Ottewill, *J. Chem. Phys.*, 1992, **96**, 3306-3318.

45. S. T. Mudie, *scatterBrain*, Australian Synchrotron, (v1.15), 2013

46. S. Kline, *J. Appl. Crystallogr.*, 2006, **39**, 895-900.

Chapter 5

Fluorescent glutathione-responsive particles

5.1. Abstract

In this chapter, the development of fluorescent responsive particles was further advanced to include a glutathione (GSH) responsive system. The incorporation of the aminobromomaleimide functionality in the particles' core would allow a read-out of the particles' disassembly. The aminobromomaleimide monomer has been shown to be sensitive to its environment, in polar protic environments the fluorescence is quenched. The proposed particles were cross-linked with a disulfide-based dimethacrylate (DSDMA), which is responsive to glutathione through the reduction of the disulfide bond. In the presence of glutathione, the cross-linked particles would disassemble and therefore the fluorescence of the aminobromomaleimide monomer would be quenched when exposed to the solution.

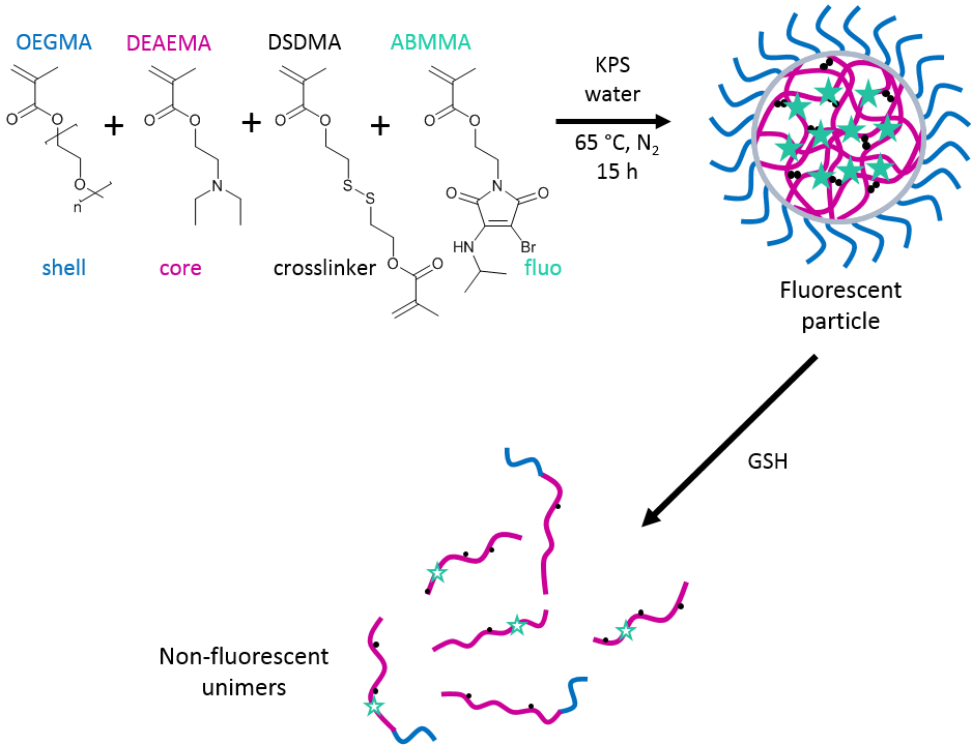

Figure 5.1. Schematic representation of the concept of the project: synthesis of glutathione (GSH) responsive particles with fluorescent read-out.

5.2. Introduction

Along with other responsive systems, redox-responsive polymers have been extensively investigated for drug-delivery applications.[1-12] The natural abundance of the glutathione/glutathione disulfide redox couple in animal cells has encouraged the development of glutathione responsive polymers toward potential drug-delivery applications. *In vivo* studies showed that normal cells exhibit different intra-cellular (1-10 mM) and extra-cellular (1-10 μM) glutathione concentrations, the highest concentration being in the cell.[13] This difference is more significant for cancer cells, which can exhibit a glutathione concentration up to seven-fold higher than normal cells.[13]

Grayson and co-workers presented the synthesis of glutathione-responsive degradable hydrogels,[14] synthesised from (hydroxyethyl)methacrylate (HEMA) and containing a disulfide-based dimethacrylate (DSDMA) cross-linking monomer *via* free radical polymerisation along with an analogous non-responsive nanogel. The DSDMA nanogels exhibited the quick release of a dye in the presence of glutathione at micro-molar concentration. However, when tested for *in vitro* experiments, it appeared that the micro-molar concentration of glutathione was too low to trigger drug release even over a seven day period.

Yang and co-workers presented the synthesis of glutathione, pH, and temperature responsive microgels.[15] Biodegradable poly(vinylcaprolactam) based microgels containing *N,N*-bis(acryloyl) cystamine (BAC) were synthesised with a disulfide containing responsive cross-linker. These microgels were able to encapsulate doxorubicin, and cytotoxicity assays showed the good biocompatibility of these microgels. Upon degradation, triggered by exposure to glutathione, the nanogels effectively released doxorubicin and a good inhibition effect against HeLa cells was observed.

More recently, Yang and co-workers reported a similar poly(oligo(ethylene glycol)methacrylate) (POEGMA) nanogel system utilising the same cystamine-based responsive cross-linker (BAC), see Figure 5.2.[16] These nanogels also exhibited minimal leakage of the doxorubicin, however in the presence of glutathione, effective release of doxorubicin and a good inhibition effect against the HeLA cells were observed.

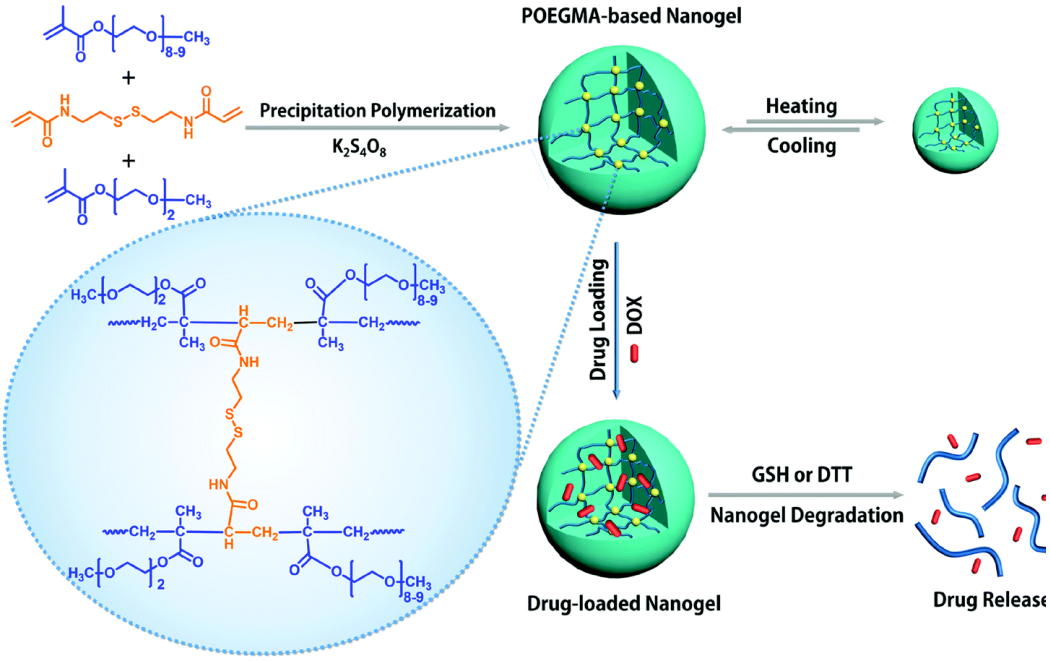

Figure 5.2. Schematic example of the synthesis and response of *N,N*-bis(acryloyl) cystamine containing nanogels; loading and release of doxorubicin. Reproduced from reference.[16]

Whittaker and co-workers synthesised cross-linked star polymers for imaging applications.[9] This polymer, containing 2,2,2-trifluoroethyl methacrylate, could provide a ^{19}F signal for MRI and a disulfide cross-linker was incorporated into the stars to allow the degradation of the contrast agent. The nanogels were shown to degrade upon addition of tris(2-carboxyethyl)phosphine (TCEP), which confirmed the biodegradability of the contrast agent.

These examples show the potential of glutathione-responsive materials for drug-delivery applications. The different concentrations of glutathione inside and outside

the cells and especially with cancer cells provides a straightforward strategy for drug-delivery systems. The use of a glutathione-responsive cross-linker, allowing the disassembly of a polymeric structure upon exposure to high concentration of glutathione could lead to the release of an encapsulated drug.

5.3. Results and discussion

The synthesis of responsive particles was inspired by the particles presented in Chapter 4,[17] however, a different cross-linking monomer was employed. The objective was to utilise a responsive cross-linker that would cleave in the presence of a specific concentration range of glutathione, which would result in the disassembly of the particles and the potential release of an encapsulated drug. The fluorescent functionality present in the core of the particles (fluorescence quenched upon exposure to water) would probe the state of the particles (cross-linked or unimers), therefore give a read-out response on the release of the drug. To achieve this objective, additional parameters needed to be considered for the synthesis of these particles. Firstly, the size of the nanoparticles; to allow the cellular uptake of these particles, their diameter should be below 100 nm, and a low particle size dispersity (PD < 0.1) is necessary.[18-21] Secondly, the particles' response; the particles would have to be responsive and disassemble at an intra-cellular concentration (1 mM) of glutathione, and non-responsive at an extra-cellular concentration (10 μM) of glutathione, allowing the particles to preserve their integrity until they penetrate the cells.

5.3.1. Preliminary tests

The synthesis of the first batch of particles (**1**) was inspired by CO_2-responsive particles synthesised in the previous chapter. The cross-linked core/shell particles (**1**) were composed of oligo(ethylene glycol) methyl ether methacrylate (OEGMA2000, $M_n \approx 2000$ g·mol^{-1}, 1 equivalent) for the hydrophilic shell, *N,N*-diethylaminoethyl methacrylate (DEAEMA, 120 equivalents) and DSDMA (1 wt%) for the cross-linked hydrophobic core, see Figure 5.3. These particles were

synthesised *via* emulsion polymerisation in water, initiated with potassium persulfate (KPS, 1 wt%) at 65 °C under nitrogen atmosphere.

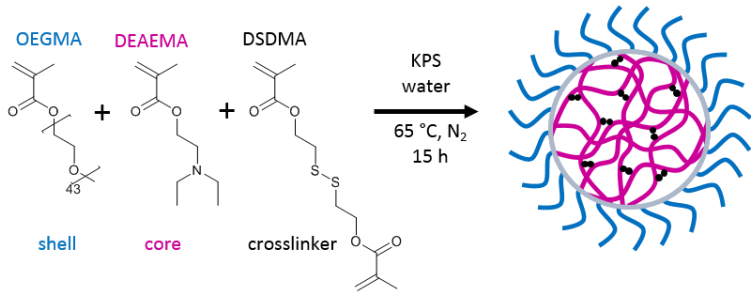

Figure 5.3. Schematic representation of the synthesis of the glutathione-responsive particles (**1**).

The resulting size of these particles was larger than 100 nm, this was expected knowing that the particles synthesised in the previous chapter were 250 nm in diameter. These DSDMA-containing particles (**1**) were 400 nm in diameter with a low dispersity (PD = 0.056), see Figure 5.4.

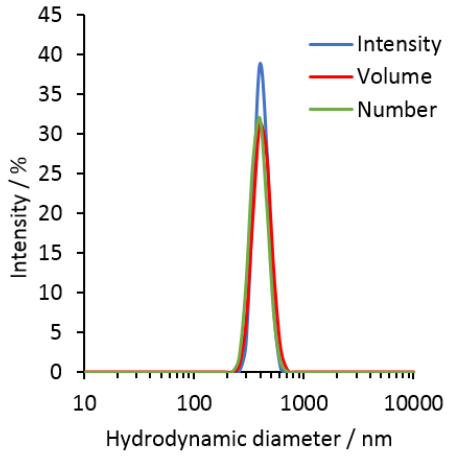

Figure 5.4. DLS data for glutathione-responsive particles (**1**) in water at *ca.* 0.05 mg·mL^{-1}.

As a preliminary test, despite their large diameter, the response of these particles to glutathione was tested. Control experiments with non-responsive particles (**2**,

D_h = 205 nm, PD = 0.03), prepared with the non-responsive cross-linking monomer ethylene glycol dimethacrylate (EGDMA), were also performed. The size of particles in both batches was measured before and after addition of glutathione. Two solutions of glutathione were prepared at 20 mM and 200 µM; when added to the particle samples, the final GSH concentrations of the samples were 1 mM and 10 µM. These concentrations correspond respectively to intra-cellular and extra-cellular concentrations.[13] It was observed that for the 10 µM GSH sample, the particle size of the responsive particles did not change upon addition of GSH up to 6 days after the addition of GSH, see Figure 5.5 and Figure 5.6. However, for the 1 mM GSH sample, a change in particle diameter, from 400 nm to 18 nm, was observed for the responsive particles by DLS, which would correspond to the disassembly of the particles upon addition of GSH, see Figure 5.5 and Figure 5.6. This experiment confirmed that particles were responsive to GSH at a relevant intra-cellular similar concentration and non-responsive at an extra-cellular similar concentration.

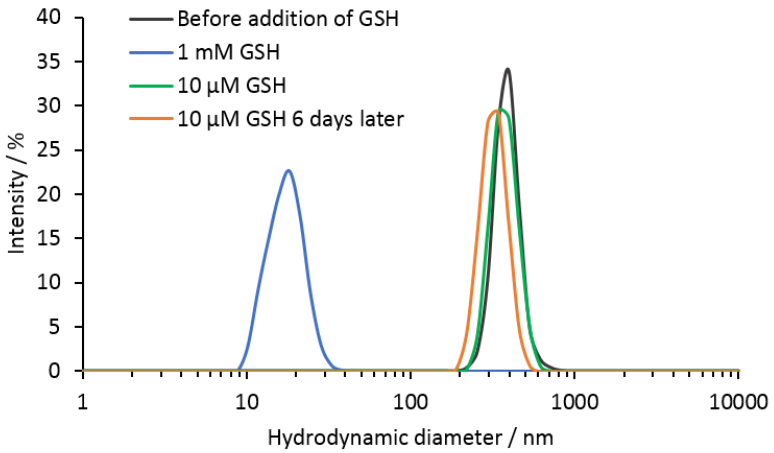

Figure 5.5. DLS data for the responsive particles (**1**) in water at *ca.* 0.05 mg·mL^{-1} before and after the addition of the GSH solutions (1 mM and 10 µM) and 6 days later for 10 µM.

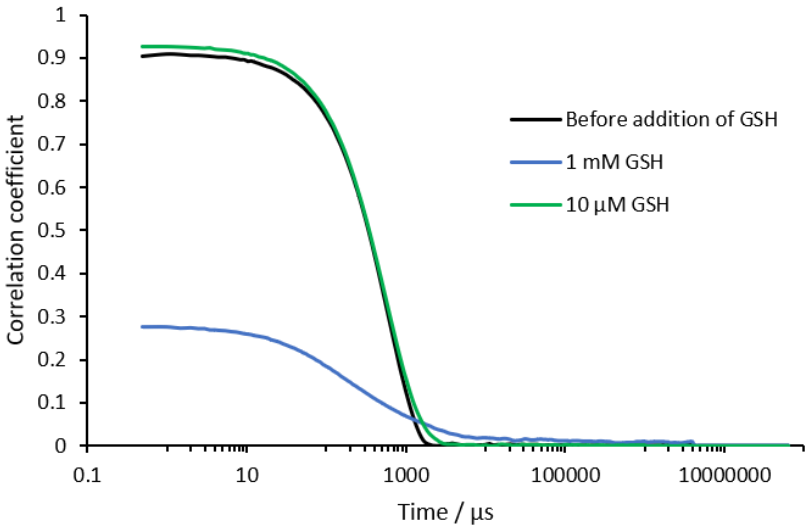

Figure 5.6. Correlation function corresponding to the DLS data for the responsive particles (**1**) in water at *ca.* 0.05 mg·mL^{-1} before and after the addition of the GSH solutions (1 mM and 10 µM).

The equivalent control experiments with the non-responsive particles (**2**) showed, similarly to responsive particles (**1**), an absence of response with 10 µM glutathione, see Figure 5.7 and Figure 5.8. However, with 1 mM, an increase in size can be observed, which could correspond to particles aggregation, see Figure 5.7 and Figure 5.8. These results confirmed that the disassembly observed with the responsive particles (**1**) occurred as a consequence of the presence of the disulphide cross-linker.

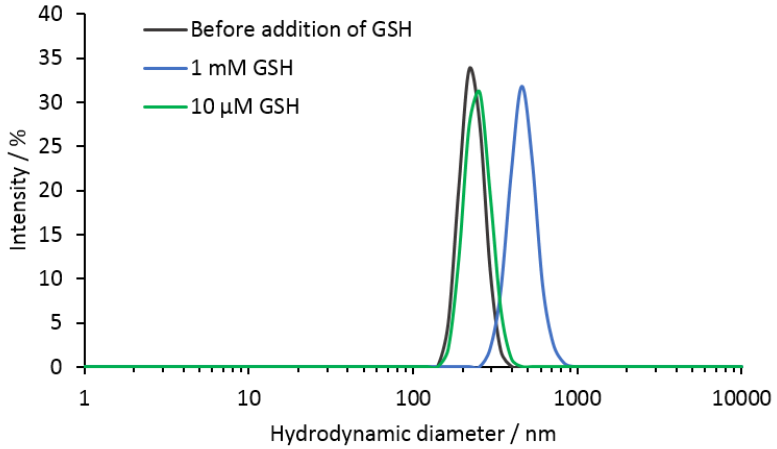

Figure 5.7. DLS data for the non-responsive particles (**2**) in water at *ca.* 0.05 mg·mL^{-1} before and after the addition of the GSH solutions (1 mM and 10 µM).

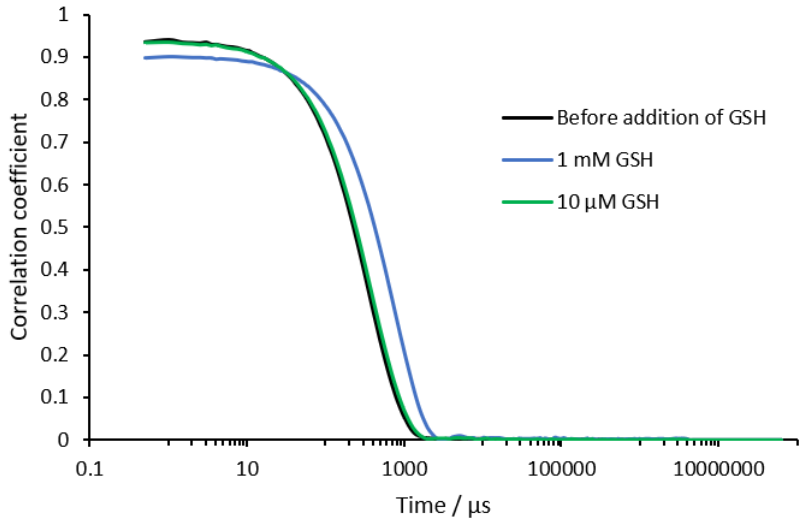

Figure 5.8. Correlation function corresponding to the DLS data for the responsive particles (**2**) in water at *ca.* 0.05 mg·mL^{-1} before and after the addition of the GSH solutions (1 mM and 10 µM).

These experiments confirmed the potential of this particles as GSH-responsive system, however, the size of these particles was too high to allow tests with living cells as the particles would not be able to penetrate the cells. The next objective was to optimise and reduce the size of the glutathione-responsive particles.

5.3.2. Synthesis of fluorescent glutathione-responsive particles

5.3.2.1. Optimisation of the particles synthesis

In order to optimise the size of the particles, different parameters were altered: including the use of different monomers for both the core and shell, and their ratio was varied. The monomers and their ratios were changed in order to increase the hydrophobicity of the core and vary density of the shell; these parameters could both have an effect on particles' size and stability. The synthesis was tested with different percentages of initiator and cross-linker, and different types of stirring were also tested. In this optimisation study, the particles were synthesised without the fluorescent aminobromomaleimide monomer, as it was previously shown in Chapter 4 that the incorporation of this fluorescent monomer does not affect the hydrodynamic diameter of the particles. The different core monomers tested were DEAEMA (as used in Chapter 4), ethyl methacrylate (EMA), and methyl methacrylate (MMA). Different monomers were also tested for the composition of the shell of the particles: oligo(ethylene glycol) methyl ether methacrylate $M_n \approx$ 2000 g·mol^{-1} (OEGMA2000), oligo(ethylene glycol) methacrylate $M_n \approx 360$ g·mol^{-1} (OEGMA360), triethylene glycol methyl ether methacrylate (TEGMA), and di(ethylene glycol) methyl ether methacrylate (DEGMA). Regarding the nature of the cross-linker, the size of the particles was optimised utilising EGDMA instead of DSDMA in the synthesis, as a consequence of the cost difference between the two chemicals. The initiator, potassium persulfate (KPS), and the concentration of monomer in water were kept the constant.

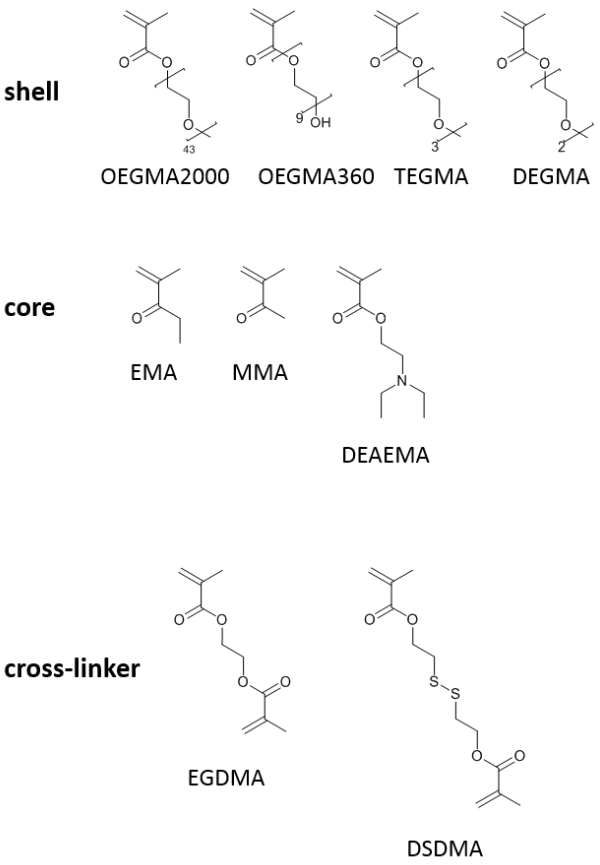

Figure 5.9. Structures of the different monomers utilised in the synthesis of the particles.

Table 5.1. Composition of the different particles presented in this chapter

shell (eq.)				core (eq.)			cross-linker (wt%)		fluorophore (wt%)	initiator (wt%)	Dh (nm)	PD	batch number
OEGMA 2000	OEGMA 360	TEGMA	DEGMA	MMA	EMA	DEAEMA	EGDMA	DSDMA	ABMMA	KPS			
1						120		1		1	400	0.06	**1**
1						120	1			1	205	0.03	**2**
1				120			1			1	n/a	n/a	**3**
1				100			1			1	n/a	n/a	**4**
1				50			1			1	n/a	n/a	**5**
1				40			1			1	n/a	n/a	**6**
1				30			1			1	n/a	n/a	**7**
1				20			1			1	n/a	n/a	**8**
1					120		1			1	n/a	n/a	**9**
1					100		1			1	n/a	n/a	**10**
1					50		1			1	n/a	n/a	**11**
	1					120	1			1	165	0.06	**12**
	1					50	1			1	190	0.02	**13**
		1				120	1			1	410	0.02	**14**
		1				50	1			1	265	0.04	**15**
	1					50	1			5	185	0.02	**16**
		1				50	1			5	115	0.02	**17**
		1				50	1			7	420	0.21	**18**
		1				50	1			10	400	0.02	**19**
			1			50	1			5	155	0.04	**20**
		1				50	2			5	190	0.02	**21**
		1				50	5			5	455	0.05	**22**
		1				50		1		5	95	0.04	**23**
		1				50		1	1	5	140	0.02	**24**

Attempts to reduce the size of the particles were first focused on the composition of the core of the particles. The synthesis of the particles was tested with MMA (particles **3**-**8**), utilising different equivalent ratios of MMA to the shell monomer, OEGMA2000. Monomer ratios ranged from 120 to 20 equivalents of MMA for 1 equivalent of OEGMA2000, with 1 wt% of cross-linker (EGDMA) and 1 wt% of initiator (KPS). Similarly, the synthesis of the particles was tested with EMA (particles **9**-**11**) instead of MMA. The different particle batches obtained were analysed by dynamic light scattering (DLS), all the batches presented similar DLS profiles: high dispersities and multiple populations, see Figure 5.10 for examples of DLS data for MMA and EMA particles (**3** and **9**). It would have been interesting to measure the pH when measuring the size, in order to compare the influence of the variation of the core monomer nature. These results could be attributed to the higher hydrophobicity of PMMA and PEMA compared to PDEAEMA, which could promote the formation of particles aggregates.

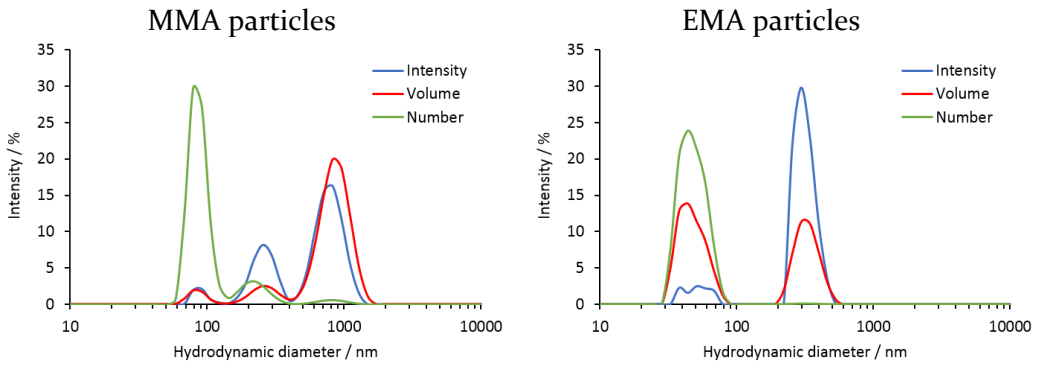

Figure 5.10. Example of DLS data obtained for MMA particles (**3**) or EMA particles (**9**) in water at *ca.* 0.05 mg·mL^{-1}.

Following these unsuccessful experiments, the focus was shifted to the composition of the shell of the particles. As previously observed in Chapter 4, the composition of the shell can have a drastic impact on the particles behaviour. The shell monomer

was changed from OEGMA2000 to OEGMA360 (**12**-**13**) or TEGMA (**14**-**15**), in order to test the effect of the density of the shell on the particles' size, a denser shell would be obtain with OEGMA2000 than with TEGMA as a consequence of a lower number of ethylene oxide units. The different ratios between hydrophobic and hydrophilic monomer were tested to assess the effect on the particles size. Different batches of particles were synthesised with 120 or 50 equivalents of DEAEMA for 1 equivalent of OEGMA360 or TEGMA, with 1 wt% cross-linker and 1 wt% initiator. Particles synthesised with OEGMA360 (**12**-**13**) were of a smaller hydrodynamic diameter (165 nm and 190 nm) compared to the particles synthesised with TEGMA (**14**-**15**; 410 nm and 265 nm) as revealed by DLS analysis. All the particles (**12**-**15**) showed a low dispersity, see Table 5.2. These experiments confirmed that the length of the shell monomer and therefore the shell density can have an impact on the particles' size, however, the particles obtained were too large (> 100 nm).

Table 5.2. Different ratios of DEAEMA to OEGMA360 or TEGMA, and the size of the particles obtained (in water at *ca.* 0.05 mg·mL^{-1}).

Shell monomer	wt% cross-linker	wt% initiator	Number of eq. of DEAEMA	Hydrodynamic diameter (nm)	PD	Batch number
OEGMA360 1 eq.	1	1	120	165	0.06	**12**
			50	190	0.02	**13**
TEGMA 1 eq.	1	1	120	410	0.02	**14**
			50	265	0.04	**15**

As shown in Chapter 4, an increase of the quantity of initiator could contribute to the reduction of the particles' size, therefore, particles were synthesised with 5 wt% of initiator instead of 1 wt%. The particles were synthesised with 50 equivalents of DEAEMA for 1 equivalent of OEGMA360 or TEGMA, with 1 wt% cross-linker and 5

wt% initiator. The particles synthesised with OEGMA360 (**16**) possessed an average hydrodynamic diameter of 185 nm with a low dispersity (PD = 0.02), see Table 5.3. Meanwhile, the particles synthesised with TEGMA (**17**) possessed a diameter of 115 nm with a low dispersity (PD = 0.02), see Table 5.3. This result was the closest to the diameter and dispersity requirements for the particles; particle diameter ≤ 100 nm and a low dispersity (< 0.1). These results confirmed that the shell density can have an impact on the size of the particles.

As an increase in the quantity of initiator reduced particle size for the PDEAEMA particles, higher quantities of initiator were tested: 7 wt% (**18**) and 10 wt% (**19**). Particles were synthesised with 50 equivalents of DEAEMA for 1 equivalent of TEGMA, 1 wt% cross-linker, and 7 wt% or 10 wt% initiator. However, the particles obtained were of diameters of 420 nm (PD = 0.21) and 400 nm (PD = 0.02) respectively, see Table 5.3.

Table 5.3. Different percentages of initiator used for OEGMA360 particles or TEGMA particles, and the size of the particles obtained (in water at *ca.* 0.05 mg·mL^{-1}).

Shell monomer	wt% cross-linker	Number of eq. of DEAEMA	wt% initiator	Hydrodynamic diameter (nm)	PD	Batch number
OEGMA360 1 eq.	1	50	1	190	0.02	**13**
			5	185	0.02	**16**
TEGMA 1 eq.	1	50	1	265	0.04	**15**
			5	115	0.02	**17**
			7	420	0.21	**18**
			10	400	0.02	**19**

For comparable composition, particles synthesised with OEGMA360 (**16**) were 185 nm diameter and particles synthesised with TEGMA (**17**) were 115 nm diameter.

As an improvement in the particle size was observed through the reduction of the number of ethylene glycol units of the shell monomer (from OEGMA2000 with 43 units, and OEGMA360 with 9 units, to TEGMA with 3 units). The synthesis of the particles was tested with a shorter ethylene glycol methacrylate, DEGMA (2 ethylene glycol units) (**20**), the monomer ratios used were 50 equivalents of DEAEMA for 1 equivalent of DEGMA, with 1 wt% cross-linker and 5 wt% initiator. The particles obtained were 155 nm in diameter with a low dispersity (PD = 0.04). In this case, the reduction of the shell monomer length did not further reduce the size of the particles, therefore the use of DEGMA was not further investigated.

Different quantities of cross-linker were also tested, based on the particles synthesised from 50 equivalents of DEAEMA for 1 equivalent of TEGMA, with 1 wt% cross-linker and 5 wt% initiator (**17**). The cross-linking density would be expected to have an impact on the particles' size as it would affect the core compactness. The percentage of cross-linker was increased to 2 wt% (**21**) and 5 wt% (**22**). The size of the particles obtained were 190 nm and 455 nm (PD = 0.05 and PD = 0.02) for 2 wt% and 5 wt% EGDMA respectively, see Table 5.4. It appeared that increasing the quantity of cross-linker did not afford a reduction in the hydrodynamic diameter of the particles. However, the increase in particles' diameter and the consistent low dispersity could indicate inter-cross-linking between particles.

Table 5.4. Different percentages of cross-linker used in TEGMA/DEAEMA particles, and the size of the particles obtained (in water at *ca.* 0.05 mg·mL^{-1}).

Number of eq. of TEGMA	Number of eq. of DEAEMA	wt% initiator	wt% cross-linker	Hydrodynamic diameter (nm)	PD	Batch number
1	50	5	1	115	0.02	**17**
			2	190	0.02	**21**
			5	455	0.05	**22**

In an attempt to improve the particles' size, the synthesis of particles **17** was tested with mechanic stirring utilising an over-head stirrer, however, despite a better shear, the particles obtained were of a larger diameter (420 nm, PD = 0.05).

To conclude, the results of these different tests determined the current optimal conditions to be the one used to obtain particles **17**: 50 equivalents of DEAEMA for 1 equivalent of TEGMA, with 1 wt% cross-linker and 5 wt% initiator, utilising magnetic stirring. As mentioned above, these particles were 115 nm in diameter, with a low dispersity (PD = 0.02) and TEM images confirmed the spherical morphology of the particles (see Figure 5.11 for DLS data and Figure 5.12 for TEM image).

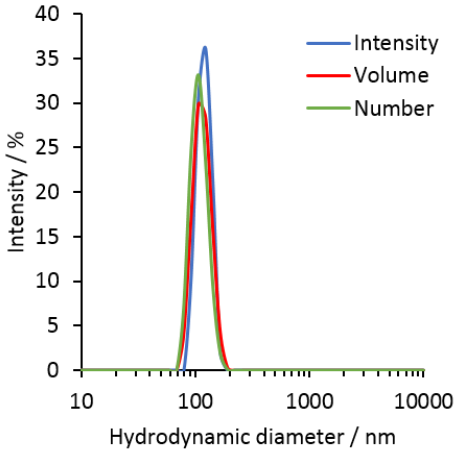

Figure 5.11. DLS data for the optimal DEAEMA/TEGMA/EGDMA particles (**17**), in water at *ca.* 0.05 mg·mL^{-1}.

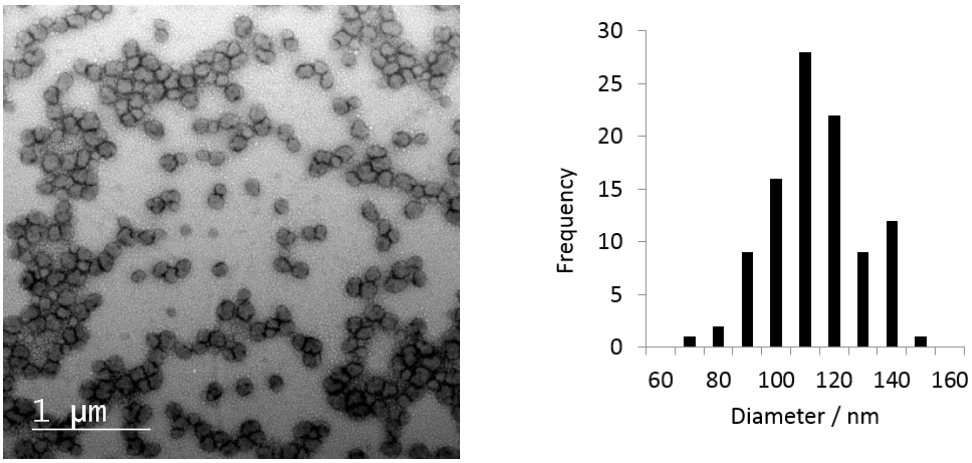

Figure 5.12. TEM image of DEAEMA/TEGMA/EGDMA particles (**17**) stained with uranyl acetate, and the distribution of size observed.

5.3.2.2. Synthesis of DSDMA-containing particles

Following the results of the optimisation, the same particles were synthesised with the glutathione-responsive cross-linker DSDMA instead of EGDMA, with 50 equivalents of DEAEMA for 1 equivalent of TEGMA, 1 wt% DSDMA and 5 wt% initiator (**23**), see Figure 5.13.

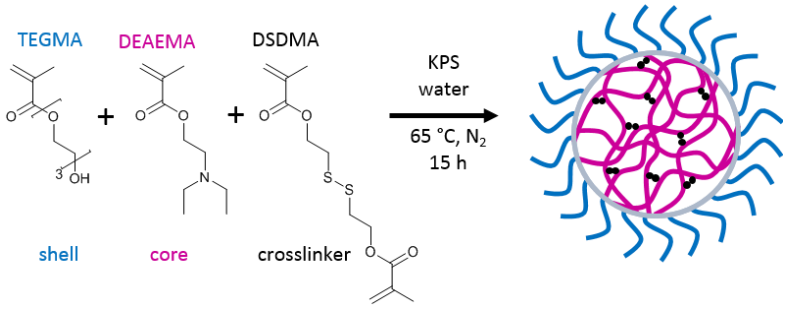

Figure 5.13. Schematic representation of the synthesis of the DSDMA-containing particles (**23**).

These DSDMA cross-linked particles were analysed by DLS and found to have a hydrodynamic diameter of 95 nm with a dispersity of 0.04, and therefore met the particle size requirements defined earlier in this chapter (see Figure 5.14 for DLS data). The spherical morphology was confirmed by TEM (see Figure 5.15), however

the size of the particles observed by TEM appeared to be larger than the size obtained by light scattering, this size difference could be attributed to a drying effect, which could make particles look bigger as they spread upon drying on the TEM grid.

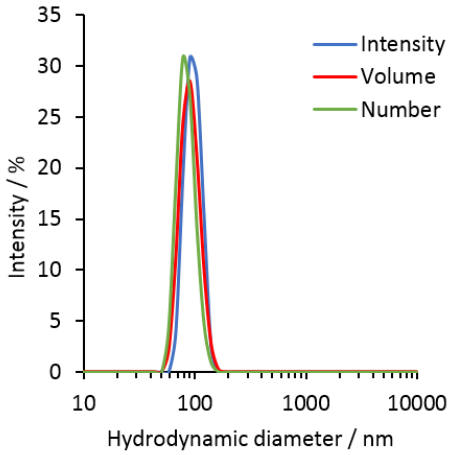

Figure 5.14. DLS data for the DSDMA-containing particles (**23**), in water at *ca.* 0.05 mg·mL^{-1}.

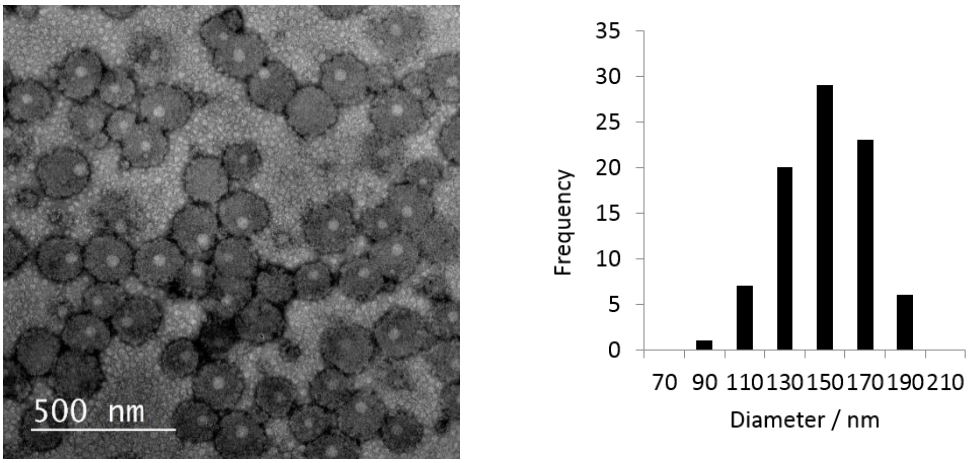

Figure 5.15. TEM image of DSDMA-containing particles (**23**) stained with uranyl acetate, and the distribution of size observed.

5.3.2.3. Synthesis of fluorescent DSDMA-containing particles

Fluorescent DSDMA-containing particles (**24**) were synthesised by emulsion polymerisation following the same protocol as for the DSDMA-containing

particles (**23**), see Figure 5.16. To incorporate the fluorescent monomer ABMMA (aminobromomaleimide methacrylate) into the emulsion polymerisation, it was dissolved into DEAEMA before the mixture was added to the OEGMA solution in water to form the emulsion.

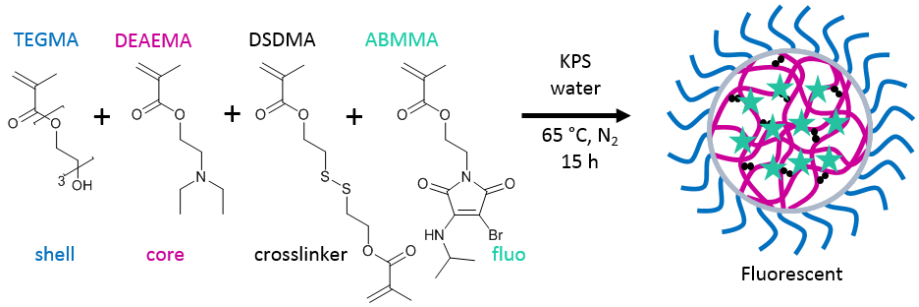

Figure 5.16. Schematic representation of the synthesis of fluorescent DSDMA-containing particles (**24**).

The particles obtained were characterised by DLS, and found to have diameter of 140 nm and a low dispersity (PD = 0.02), see Figure 5.17. The fluorescence emission and excitation spectra were recorded, the emission maximum was found at 482 nm for an excitation maximum at 370 nm, see Figure 5.18.

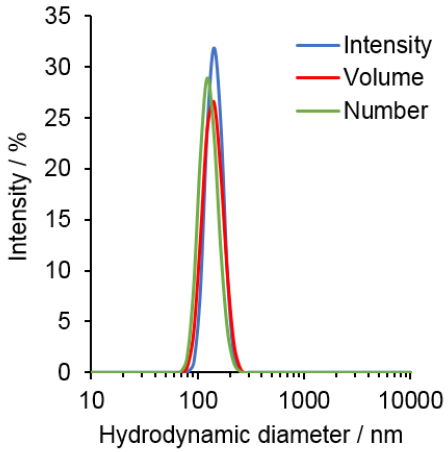

Figure 5.17. DLS data for the fluorescent DSDMA-containing particles (**24**), in water at *ca.* 0.05 mg·mL^{-1}.

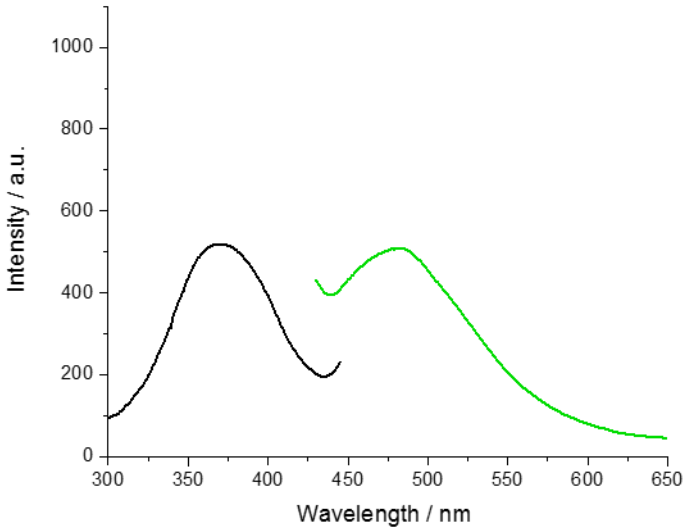

Figure 5.18. Fluorescence emission (green line) and excitation (black line) spectra of the fluorescent DSDMA-containing particles (**24**), in water at *ca.* 0.05 mg·mL^{-1}. λ_{ex} = 375 nm, λ_{em} = 485 nm.

5.3.3. Responsiveness experiments

The DSDMA-containing particles (**23**-**24**) were exposed to glutathione at different concentrations: 1 mM and 10 µM, which respectively correspond to intra-cellular and extra-cellular typical concentrations. A small volume of a concentrated solution of glutathione was added to a solution of particles to obtain the desired final glutathione concentration with a minimised dilution effect on the solution of particles. The DSDMA-containing particles (**23**-**24**) response was monitored by DLS and the response of the fluorescent DSDMA-containing particles (**24**) was also monitored by fluorescence emission.

5.3.3.1. Monitoring of the size of DSDMA-containing particles (23)

According to the preliminary experiment, these DSDMA-containing particles (**23**) would be expected to disassemble upon exposure to 1 mM glutathione. The size of the particles was monitored over time after addition of glutathione. Similarly to the preliminary experiment, in 10 µM glutathione the particles did not exhibit any response, see Figure 5.19.

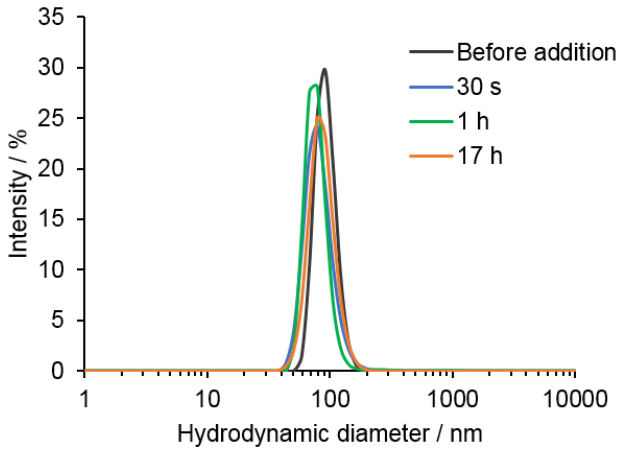

Figure 5.19. DLS data for the DSDMA-containing particles (**23**), in water at *ca.* 0.05 mg·mL^{-1}, with 10 µM GSH monitored over time (number distribution).

However, in 1 mM glutathione, the particles showed a very quick response, within 30 second, the particles size drastically decreased, see Figure 5.20. The disassembly was also confirmed by the lack of scattering, indicating the absence of nanostructure in solution, see Figure 5.20.

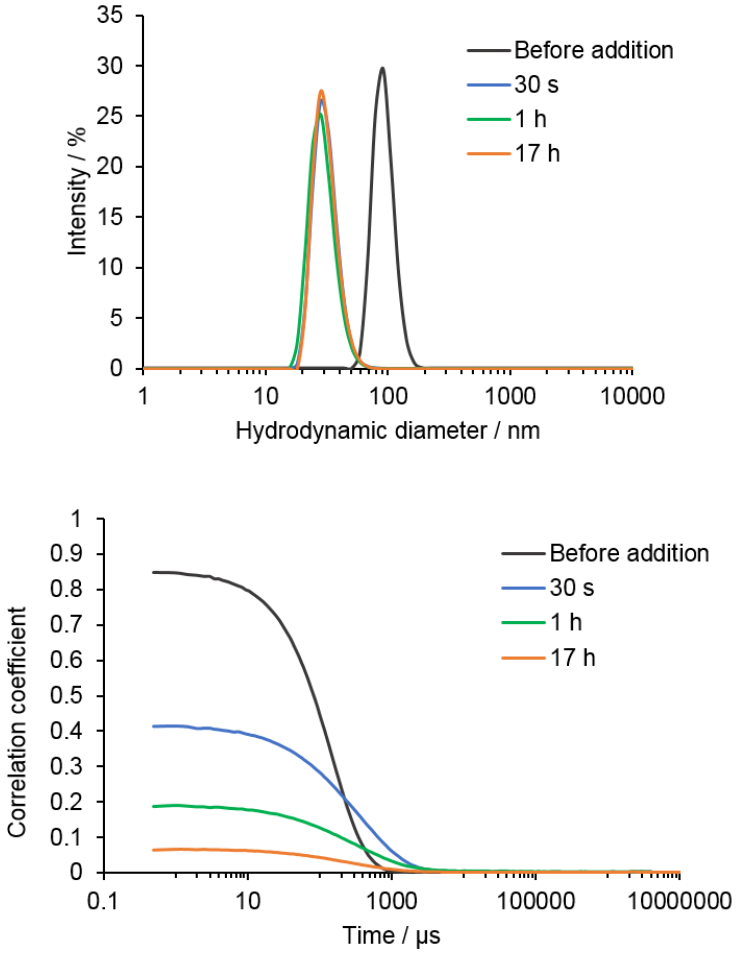

Figure 5.20. DLS data of the DSDMA-containing particles (**23**), in water at *ca.* 0.05 mg·mL^{-1}, with 1 mM GSH monitored over time (number distribution), and corresponding correlation functions.

5.3.3.2. Monitoring of the size and fluorescence emission of the fluorescent DSDMA-containing particles (24)

The size was the fluorescent DSDMA-containing particles (**24**) was monitored and as expected, showed similar results to the non-fluorescent DSDMA-containing

particles (**23**). The DLS data showed a similar absence of response upon exposure to 10 μM glutathione, see Figure 5.21. However, after 17 hours larger nanostructures appeared, which could be a consequence of particles aggregation over time.

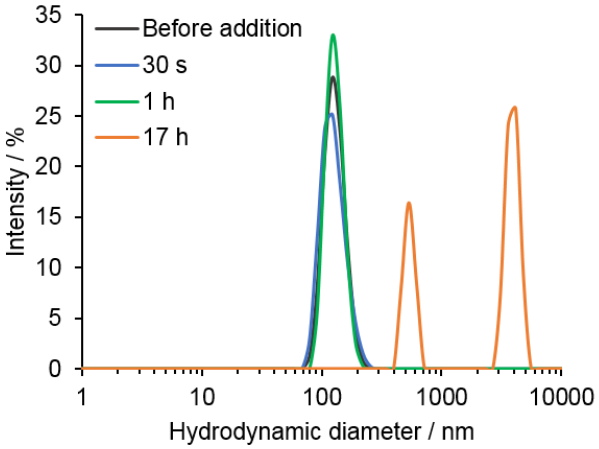

Figure 5.21. DLS data for the fluorescent DSDMA-containing particles (**24**), in water at *ca.* 0.05 mg·mL^{-1}, with 10 μM GSH monitored over time (number distribution).

Similarly to the non-fluorescent particles (**23**), a quick response of fluorescent particles (**24**) exposed to 1 mM glutathione was observed, within 30 second, and a decrease in scattering intensity confirmed the particles disassembly, see Figure 5.22.

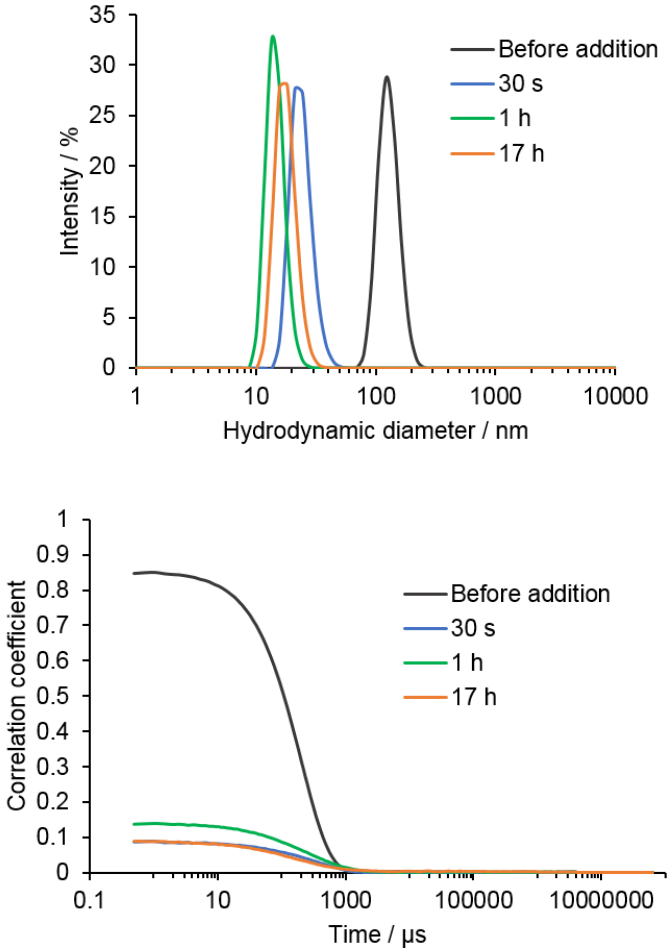

Figure 5.22. DLS data for the fluorescent DSDMA-containing particles (**24**), in water at *ca.* 0.05 mg·mL^{-1}, with 1 mM GSH monitored over time (number distribution) and the corresponding correlation functions.

The fluorescence emission of the fluorescent DSDMA-containing particles (**24**) was monitored over time following the addition of glutathione. As introduced in Chapter 3, the aminobromomaleimide functionality is sensitive to protic environment; the ABM functionality is highly emissive in aprotic environments but the emission is quenched in protic environments as a consequence of hydrogen bonding between the functionality's carbonyls and the solvent. The fluorescent probe ABMMA being located in core of the particles, it is protected from the protic environment, when particles were disassembled upon glutathione addition, the probe would be exposed to the environment, therefore the fluorescence would be quenched. As expected, the

particles with 10 μM glutathione did not show a drastic emission intensity decrease, the minor decrease observed could be the result of the disassembly of a small number of particles, see Figure 5.23. However, particles with 1 mM glutathione showed a quick and drastic emission intensity decrease within 30 second, see Figure 5.24.

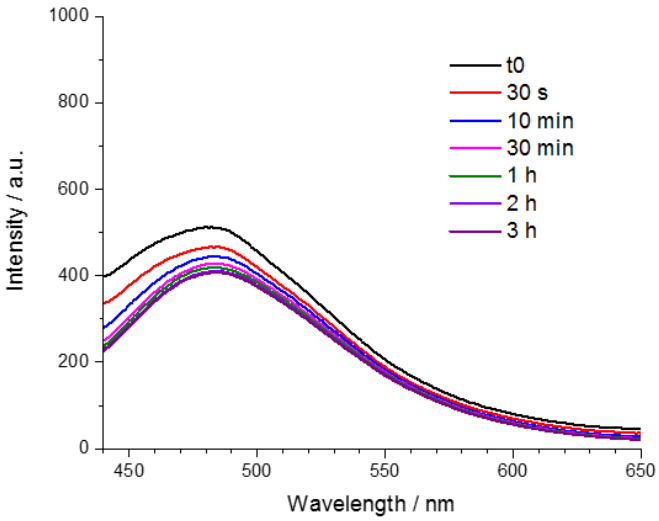

Figure 5.23. Fluorescence emission of fluorescent DSDMA-containing particles (**24**), in water at *ca.* 0.05 mg·mL^{-1}, with 10 μM GSH monitored over time, λ_{ex} = 375 nm.

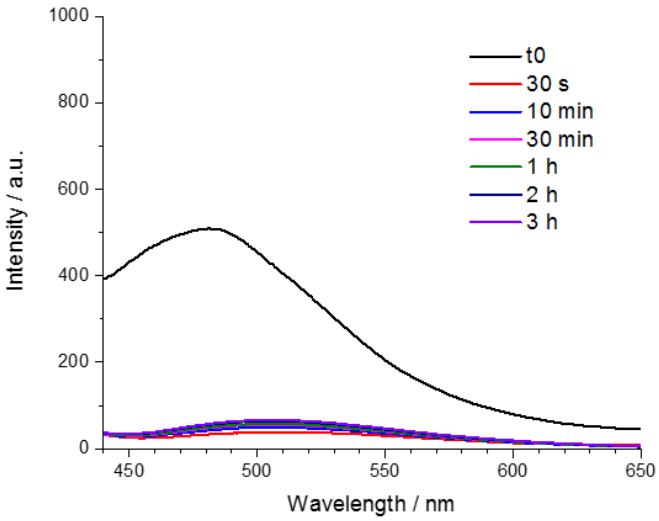

Figure 5.24. Fluorescence emission of fluorescent DSDMA-containing particles (**24**), in water at *ca.* 0.05 mg·mL^{-1}, with 1 mM GSH monitored over time, λ_{ex} = 375 nm.

5.3.4. Sedimentation of the particles

The potential application for this material being drug-delivery related, it was important to be able to purify the particles. However, it was observed that upon purification of the particles *via* dialysis, after several days and dialysate changes, the particles were destabilised and started to sediment. After further investigation, it was found that the stability of the particles was affected by the pH of the particles solution. The pH of the particles solution post-synthesis was basic (pH ≈ 9), following purification *via* dialysis against water, the pH of the solution was progressively neutralised through several dialysate changes. DLS analysis confirmed the formation of aggregates with large particle diameters and a high dispersity, see Figure 5.25. Sedimentation of the purified particles could be observed after being stored on the shelf for several days, see Figure 5.26.

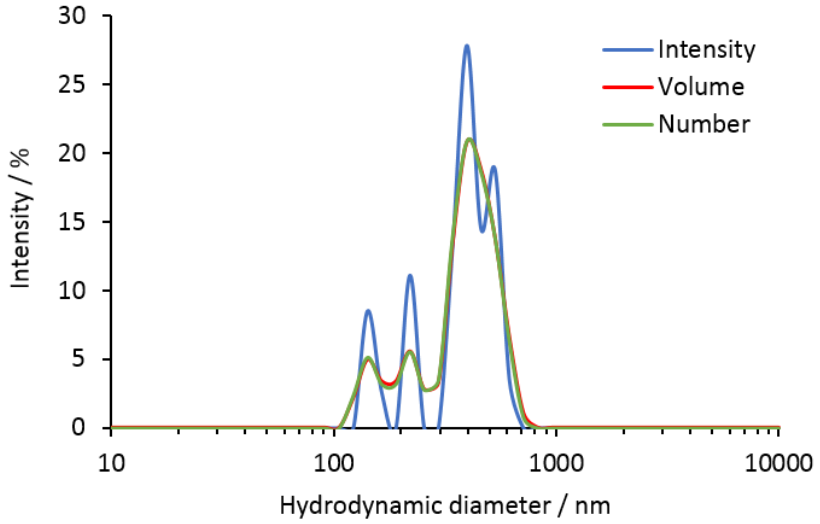

Figure 5.25. DLS data for DSDMA-containing particles (**23**), in water, after dialysis against water (unknown concentration).

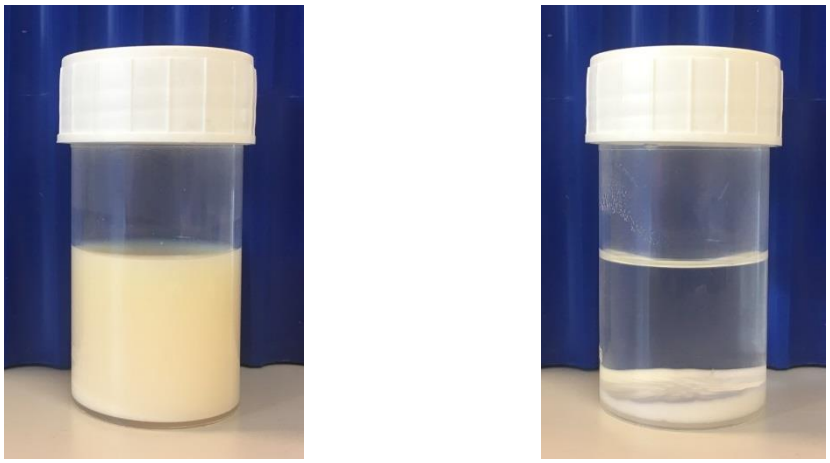

Figure 5.26. Pictures of DSDMA-containing particles (**23**) in water before (left) and after (right) dialysis.

However, TEM images showed particles of a similar shape and dimension before and after dialysis, aggregates were observed in both samples, which could be a result of a drying effect, see Figure 5.27.

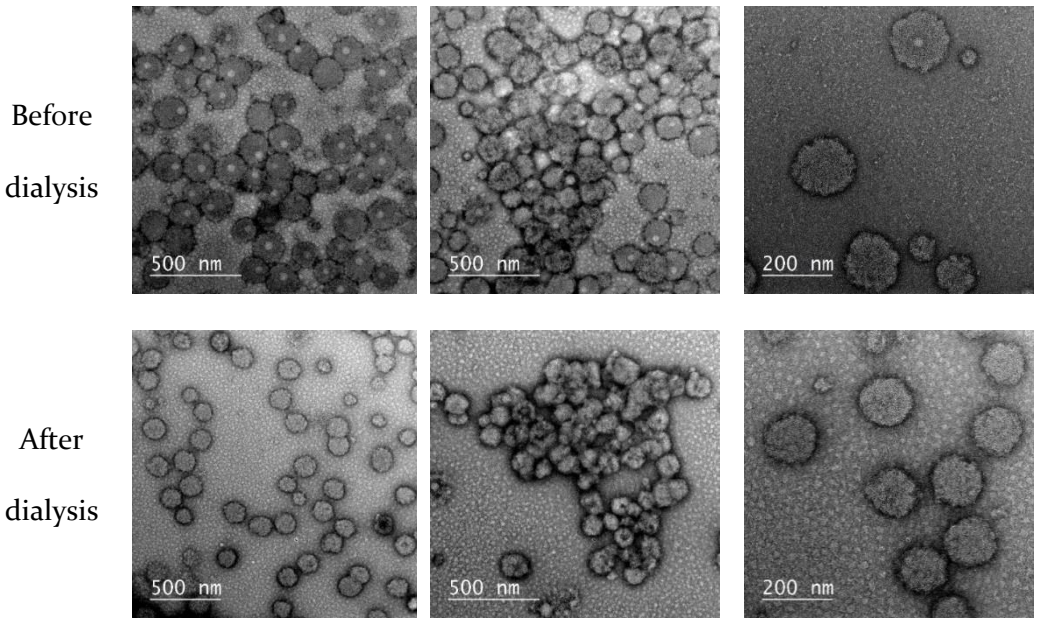

Figure 5.27. TEM images of the DSDMA-containing particles (**23**) before and after dialysis, at different magnifications.

The influence of pH on the stability of the particles was further confirmed through the increase of the pH of the dialysed particle solution to pH 9. The solution appeared to recover stability upon dropwise addition of a 10 mM sodium hydroxide solution, see Figure 5.28. It appeared that after the pH was increased to 9, the hydrodynamic diameter of the particles was reduced, however some aggregates could still be observed by DLS and the dispersity was higher (PD = 0.3) than before purification (PD < 0.1), see Figure 5.29. The instability of the particles could be related to the pH-responsive nature of the core of the particles, as all the particles synthesised with DEAEMA (**1**, **2**, **12**-**24**) exhibited a basic pH at the end of the synthesis, unlike particles synthesised with EMA or MMA (**3**-**11**), which were acidic. The pH at which particles seem to be stable (pH ≈ 9) is not suitable for living cells, therefore, further optimisation of particle synthesis and purification would be required.

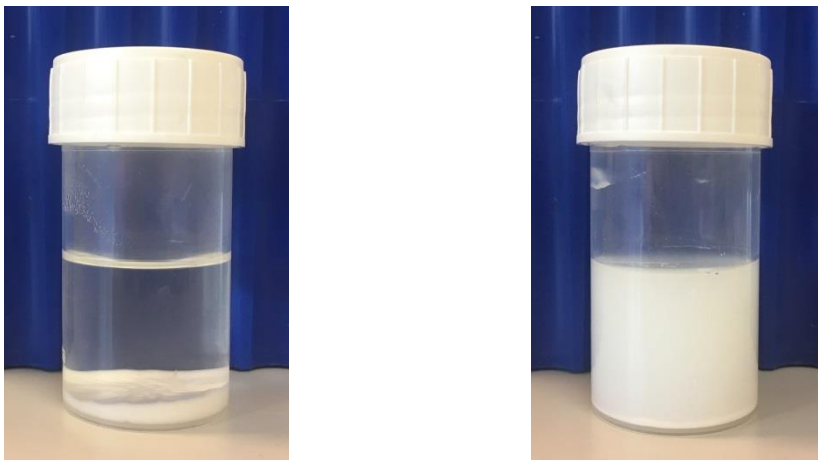

Figure 5.28. Pictures of DSDMA-containing particles (**23**), in water before (left) and after (right) pH increased to 9 *via* addition of NaOH.

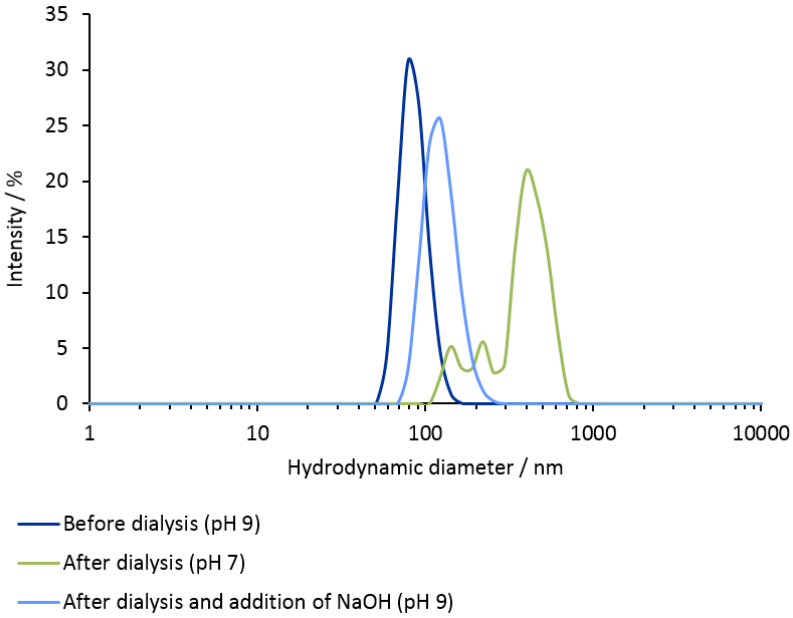

Figure 5.29. DLS data for DSDMA-containing particles (**23**), in water before dialysis (pH 9), after dialysis (pH 7) and after addition of NaOH (pH increased to 9).

5.3.5. Control experiments

Control experiments were performed with particles that are not GSH-responsive and particles that are neither GSH-responsive nor pH-responsive, in order to confirm that GSH only impact on particles is to cleave the particles GSH-responsive cross-linker. The size and the fluorescence intensity of these two batches of particles were measured before and after the addition of GSH for a concentration of 1 mM.

The size and the fluorescence emission of the particles that were not responsive to glutathione were not expected to be affected by GSH. However, it appeared that both fluorescence emission and particles' size were altered by the addition of glutathione.

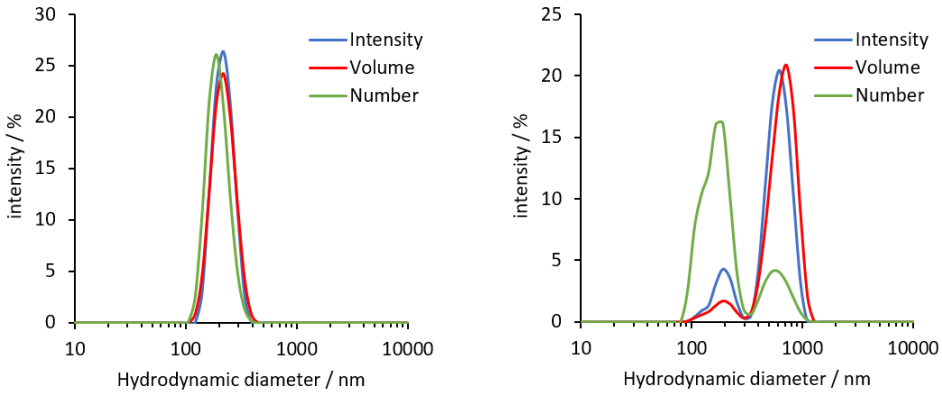

Figure 5.30. DLS data for non-GSH-responsive particles in water at ca. 0.05 g·mL-1 before (left) and after addition of GSH (right).

When glutathione was added to these particles, an increase in diameter of structure and dispersity could be observed, see Figure 5.30. The fluorescence emission of this batch before and after addition of glutathione was measured and a drastic decrease in fluorescence emission intensity was observed (see Figure 5.31) when it was not expected to be changed.

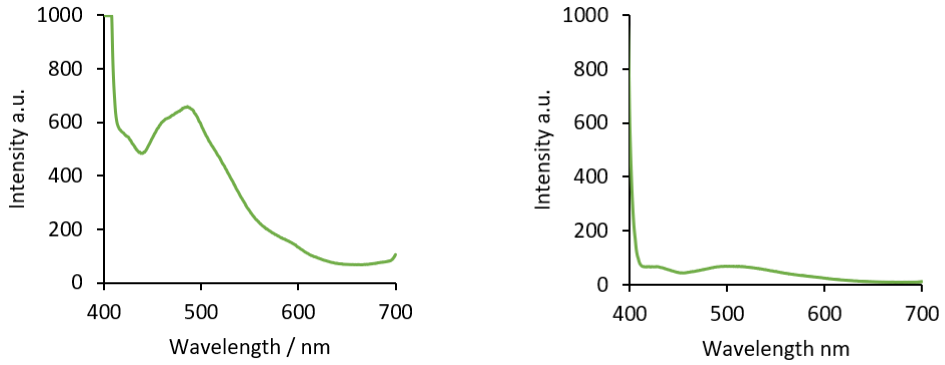

Figure 5.31. Fluorescence emission for non-GSH-responsive particles in water at ca. 0.05 g·mL-1 before (left) and after addition of GSH (right). λ_{ex} = 375 nm.

In an attempt to understand the system, the same measurements were performed with the second batch of particles that are not responsive to GSH and pH. It was observed that particles' diameter increased upon addition of GSH, from 435 nm to 625 nm, see Figure 5.32.

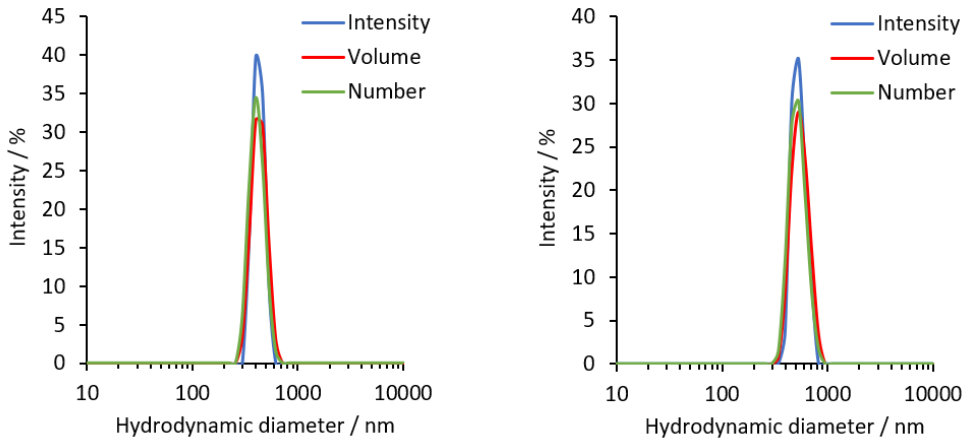

Figure 5.32. DLS data for non-GSH, non-pH-responsive particles in water at ca. 0.05 g·mL-1 before (left) and after addition of GSH (right).

The fluorescence emission of this particle batch was measured before and after the addition of GSH, unlike the previous batch (only non-GSH-responsive) these measurements exhibited a very small decrease in intensity from 320 a.u. to 305 a.u., see Figure 5.33.

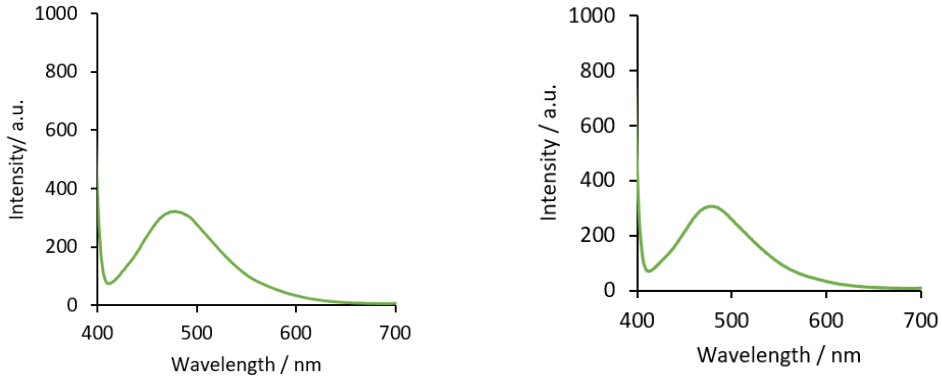

Figure 5.33. Fluorescence emission for non-GSH, non-pH-responsive particles in water at ca. 0.05 g·mL-1 before (left) and after addition of GSH (right). λ_{ex} = 375 nm.

These control experiments highlighted the acidic properties of glutathione and these were contributing in the particles disassembly observed in this chapter. These experiments clearly showed the influence of glutathione on particles that are responsive or not to pH. The pH-responsiveness of the particles probably facilitate the penetration of GSH into the particles core through swelling to then cleave the cross-linker more efficiently.

It also confirmed that the fluorescent probe is not directly affected by the addition of glutathione, therefore, a decrease in fluorescence can indicate a change of the probe's environment. It would have been interesting to monitor the particles' parameters over time.

5.4. Conclusions and future work

In this chapter, the synthesis of fluorescent DSDMA-containing particles and their response to glutathione was presented. It has been shown that DSDMA-containing particles can respond to intra-cellular concentrations of glutathione. The synthesis of the particles was optimised to obtain the desired particles diameter and dispersity. Fluorescent DSDMA-containing particles exhibited a very quick response (30 seconds) to the intra-cellular level of glutathione (1 mM), this response was confirmed by light scattering and fluorescence emission measurements. The fluorescence emission intensity drastically decreased within 30 seconds.

However, despite the successful response of the particles, the current limitations of this system were identified: the particles were only stable at a basic pH, which is not suitable for potential drug-delivery applications. Different parameters could be altered to improve the stability of particles in a neutral pH environment. The first parameter that could be considered is the cross-linking density of the particles, if increased, the core of the particles would be expected to be more compact and less sensitive to pH variations. Another obvious option would be to avoid the use of a pH-responsive monomer; however, it has been shown in the optimisation of the size of the particles that particles with the lowest dispersity were only obtained utilising DEAEMA, which could be attributed to the difference in hydrophobicity of DEAEMA and MMA. The synthesis of the particles could also be attempted using a buffer as the emulsion solvent. Another option would be to use both pH response and GSH-response of this system for a more efficient release.

If stable particles at neutral pH cannot be obtained for drug-delivery applications, these fluorescent DSDMA-containing particles could be used for the detection of glutathione levels. The quenching of the fluorescence emission indicating high level of glutathione could be optimised to detect cancer cells high levels of glutathione.

5.5. Experimental

5.5.1. Materials and methods

DEAEMA, EMA and MMA were filtered through a plug of alumina prior to use and stored at 4 °C. All other chemicals were purchased from Aldrich, Fluka or Acros and used as received.

The magnetic stirrer IKA RCT basic was used to synthesise particles at 1000 rpm.

The mechanic stirrer Stuart SS10 was tested to synthesise a batch of particles at ~ 100 rpm.

The stained transmission electron microscopy (TEM) images were obtained using a JEOL 2000FX or a JEOL 2100 LaB6 instrument operated at 200 kV. TEM samples were negatively stained by an aqueous solution of uranyl acetate (UA, 2.5 wt%) on formvar/carbon grids (300 Mesh, Cu, Elektron Technology UK LTD). Typically, formvar/carbon grids were cleaned by air plasma from a glow-discharge system (2 min, 20 mA) which also improved the hydrophilicity of the grids. 5 µL of particle solution was added onto the grid, which was left to dry for 1 min, then 5 µL of a 2.5 wt% UA solution was added onto the grid to stain the particles and was blotted away after 1 min before air-drying.

Dynamic Light Scattering (DLS) measurements were performed with a Malvern Zetasizer Nano ZS instrument and analysed with Malvern Zetasizer Software 7.03. All measurements were made in triplicate (with 10 measurements recorded for each run).

5.5.2. Synthetic procedures

General procedure for the synthesis of particles by emulsion polymerisation

Oligoethylene glycol methacrylate (OEGMA) was first dissolved in deionised water and then ethylene glycol dimethacrylate (EGDMA) or disulfide-based dimethacrylate (DSDMA), and *N,N*-(diethylaminoethyl methacrylate) (DEAEMA) were added dropwise to the solution. The mixture, whilst stirred, was purged with nitrogen for 30 min and further heated at 65 °C for 30 min. The initiator, potassium persulfate (KPS) was dissolved in water (2 mL) and purged with nitrogen before being added to the reaction mixture to initiate polymerisation. The reaction was stirred at 65 °C for 16 h under a nitrogen atmosphere.

The different equivalents utilised to synthesise the particles are mentioned in the main text where relevant. The different combinations and ratios of monomers, initiator and cross-linker tested in the optimisation of particle synthesis were listed in Table 5.1.

5.5.3. Glutathione addition tests

Two solutions of glutathione in water were prepared at 200 μM and 20 mM.

DLS micro-cuvettes were filled with 570 μL of particle solution and 30 μL of glutathione solution was added, 200 μM solution added to give final GSH concentration of 10 μM or 20 mM solution added to obtain a 1 mM final GSH concentration. The samples were analysed immediately after addition of the glutathione solution.

5.6. References

1. M. Huo, J. Yuan, L. Tao and Y. Wei, *Polym. Chem.*, 2014, **5**, 1519-1528.

2. C.-C. Song, F.-S. Du and Z.-C. Li, *J. Mater. Chem. B*, 2014, **2**, 3413-3426.

3. Y.-C. Wang, F. Wang, T.-M. Sun and J. Wang, *Bioconj. Chem.*, 2011, **22**, 1939-1945.

4. R. Cheng, F. Feng, F. Meng, C. Deng, J. Feijen and Z. Zhong, *J. Control. Release*, 2011, **152**, 2-12.

5. Z. Xu, S. Liu, Y. Kang and M. Wang, *ACS Biomater. Sci. Eng.*, 2015, **1**, 585-592.

6. A. N. Koo, H. J. Lee, S. E. Kim, J. H. Chang, C. Park, C. Kim, J. H. Park and S. C. Lee, *Chem. Commun.*, 2008, **48**, 6570-6572.

7. J. F. Quinn, M. R. Whittaker and T. P. Davis, *Polym. Chem.*, 2017, **8**, 97-126.

8. L. Alfonso and S. Alvaro, *Curr. Top. Med. Chem.*, 2014, **14**, 2662-2671.

9. K. Wang, H. Peng, K. J. Thurecht, S. Puttick and A. K. Whittaker, *Polym. Chem.*, 2014, **5**, 1760-1771.

10. C. Miao, F. Li, Y. Zuo, R. Wang and Y. Xiong, *RSC Advances*, 2016, **6**, 3013-3019.

11. J. A. Syrett, D. M. Haddleton, M. R. Whittaker, T. P. Davis and C. Boyer, *Chem. Commun.*, 2011, **47**, 1449-1451.

12. D. J. Phillips, J. P. Patterson, R. K. O'Reilly and M. I. Gibson, *Polym. Chem.*, 2014, **5**, 126-131.

13. C. V. Smith, D. P. Jones, T. M. Guenthner, L. H. Lash and B. H. Lauterburg, *Toxicol. Appl. Pharmacol.*, 1996, **140**, 1-12.

14. M. Ejaz, H. Yu, Y. Yan, D. A. Blake, R. S. Ayyala and S. M. Grayson, *Polymer*, 2011, **52**, 5262-5270.

15. Y. Wang, J. Nie, B. Chang, Y. Sun and W. Yang, *Biomacromolecules*, 2013, **14**, 3034-3046.

16. Y. Tian, S. Bian and W. Yang, *Polym. Chem.*, 2016, **7**, 1913-1921.

17. A. B. Mabire, Q. Brouard, A. Pitto-Barry, R. J. Williams, H. Willcock, N. Kirby, E. Chapman and R. K. O'Reilly, *Polym. Chem.*, 2016, **7**, 5943-5948.

18. M. Gaumet, A. Vargas, R. Gurny and F. Delie, *Eur. J. Pharm. Biopharm.*, 2008, **69**, 1-9.

19. K. Yin Win and S.-S. Feng, *Biomaterials*, 2005, **26**, 2713-2722.

20. L. Shang, K. Nienhaus and G. U. Nienhaus, *J. Nanobiotechnol.*, 2014, **12**, 5.

21. M. Shilo, A. Sharon, K. Baranes, M. Motiei, J.-P. M. Lellouche and R. Popovtzer, *J. Nanobiotechnol.*, 2015, **13**, 19.

Conclusions and future work

In this thesis, dithiomaleimide and aminomaleimide functionalities were presented as efficient fluorescent probes for responsive polymers. The previously developed chemistry to synthesise dithiomaleimide fluorophores was shown to efficiently produce amine derivatives. A library of aminomaleimides was synthesised, and the investigation of their fluorescent properties was shown to be highly emissive, with high quantum yields in aprotic solvents. Similarly to dithiomaleimides, the emission was found to be drastically decreased in polar protic solvents, and the conjugation of the aromatic substituent with maleimide resulted in a fluorescence emission quenching.

The sensitivity to aromatic substituents and the ability of the dithiomaleimide functionality to undergo a thiol exchange were exploited to switch-off the fluorescence of dithiomaleimide-containing micelles. The fluorescence switch-off occurred as a result of substituting the dithiomaleimide polymer substituents for aromatic substituents, which simultaneously triggered a morphology transition driven by the nature of the polymer end-groups.

It was shown that the aminobromomaleimide functionality could also be used to probe its environment using its sensitivity to protic environments. As the probe was incorporated in the hydrophobic core of the responsive particles, it was able to read-out the behaviour of both CO_2/pH-responsive particles and glutathione-responsive particles. For both particles, a change in their structure could be related to a simultaneous fluorescence emission decrease as a consequence of the modification of the fluorophore's immediate environment. These systems highlight the potential of this functionality to be used as a self-reporting contrast agent.

We believe that this fluorescent aminobromomaleimide probe and its versatile chemistry could be developed for a wide range of applications in polymer chemistry. Some aspects of the aminobromomaleimide chemistry could also be further

investigated. For example, the synthesis of a derivative of dithiomaleimide or aminobromomaleimide that can emit in water would be of great interest for the development of fluorescent hydrogels. Moreover, a higher fluorescent quantum yield and a different emission wavelength range were obtained by changing the structure from dithiomaleimide to aminobromomaleimide, it would be interesting to develop a derivative of these functionalities that could allow the tuning of the emission wavelength.